

Characterization of Slow Pyrolysis Behavior of Live and Dead Vegetation

Elham Amini

A dissertation submitted to the faculty of
Brigham Young University
in partial fulfillment of the requirements for the degree of
Doctor of Philosophy

Thomas H. Fletcher, Chair
Andrew R. Fry
David O. Lignell
David R. Weise

Department of Chemical Engineering
Brigham Young University

Copyright © 2020 Elham Amini

All Rights Reserved

ABSTRACT

Characterization of Slow Pyrolysis Behavior of Live and Dead Vegetation

Elham Amini

Department of Chemical Engineering, BYU

Doctor of Philosophy

Prescribed (i.e., controlled) burning is a common practice used in many vegetation types in the world to accomplish a wide range of land management objectives including wildfire risk reduction, wildlife habitat improvement, forest regeneration, and land clearing. To properly apply controlled fire and reduce unwanted fire behavior, an improved understanding of fundamental processes related to combustion of live and dead vegetation is needed. Since the combustion process starts with pyrolysis, there is a need for more data and better models of pyrolysis of live and dead fuels.

In this study, slow pyrolysis experiments were carried out in a pyrolyzer apparatus and a Thermogravimetric analyzer (TGA) under oxygen free environment in three groups of experiments. In the first group, the effects of temperature (400–800 °C), a slow heating rate (H.R.) (5–30 °C min⁻¹), and carrier gas flow rate (50–350 ml min⁻¹) on yields of tar and light gas obtained from pyrolysis of dead longleaf pine litter in the pyrolyzer apparatus were investigated to find the optimum condition which results in the maximum tar yield. In the second group of experiments, 14 plant species (live and dead) native to forests in the southern United States, were heated in the pyrolyzer apparatus at the optimum condition. A gas chromatograph equipped with a mass spectrometer (GC–MS) and a gas chromatograph equipped with a thermal conductivity detector (GC–TCD) were used to study the speciation of tar and light gases, respectively. In the third group of experiments, the slow pyrolysis experiments for all plant species (live and dead) were carried out in the TGA at 5 different heating rates ranged from 10 to 30 °C min⁻¹ to study the kinetics of pyrolysis.

The results showed that the highest tar yield was obtained at a temperature of 500 °C, heating rate of 30 °C min⁻¹, and sweep gas flow rate of 100 ml min⁻¹. In addition, the tar composition is dominated by oxygenated aromatic compounds consisting mainly of phenols. The light gas analysis showed that CO and CO₂ were the dominant light gas species for all plant samples on a dry wt% basis, followed by CH₄ and H₂. The kinetics of pyrolysis was studied using one model-free method and three model-fitting methods. First, the model-free method of Kissinger-Akahira-Sunose (KAS) was used to calculate the rates of pyrolysis as a function of the extent of conversion. The results showed that different plant species had different rates at different conversions. Then, three model fitting methods were used to find the kinetic parameters to potentially provide a single rate for each plant species. The results showed that the simple one-step model did not fit the one-peak pyrolysis data as well as the distributed activation energy model (DAEM) model. The multiple-reaction DAEM model provided very good fits to the experimental data where multiple peaks were observed, even at different heating rates.

Keywords: slow pyrolysis, live vegetation, biomass, light gas, tar, pyrolysis temperature, heating rate, fuel type, pyrolysis kinetics, TGA, iso-conversional methods, model-fitting methods, DAEM

ACKNOWLEDGEMENTS

I would like to give my appreciation to all of those who have been influential in helping me with this dissertation. First, my advisor, Dr. Thomas H. Fletcher, for all of his support intellectually, technically, financially, and for guiding me with patience to complete this project. I would like to express my appreciation for my committee members, Dr. Fry, Dr. Lignell, and Dr. Weise, for their advice and encouragement during this project.

I also express my appreciation to the U.S. Forest Service, especially Dr. David Weise for the technical and financial support. I also thank the undergraduate students, Joel Howarth, Jonathan DeYoung, Nathan Johnson, Matt Belingheri, and Blake Billings for helping me during the experiments and data analysis. I would like to thank Dr. Mark Dietenberger for providing precious data and Kevin Cole for helping to construct the setup and his technical support.

Finally, I would also like to thank my husband and love of my life, Dr. Mohammad Saeed Safdari, for helping and encouraging me during the experiments and for always showing how proud he is of me. The last word goes to my family, especially my parents, for the way they raised me, stood by me, and encouraged me to pursue my dreams.

This research was supported by DOD/EPA/DOE Strategic Environmental Research and Development Program, Project RC-2640, funded through contract 16-JV-11272167-024, administered by the USDA Forest Service PSW Research Station.

TABLE OF CONTENTS

List of Tables	vii
List of Figures	viii
1 Introduction	1
2 Literature Review	4
2.1 Biomass.....	4
2.2 Cellulose, Hemicellulose, and Lignin.....	5
2.3 Live and Dead Fuel.....	7
2.4 Pyrolysis of Biomass, Parameters, and Products.....	8
2.5 Mechanism of Biomass Conversion by Pyrolysis	11
2.6 Kinetic Parameters Estimation from TGA Data	13
2.7 Previous Pyrolysis Research on Forest Fuels	18
2.8 Summary of Literature Review.....	19
3 Objective and Tasks.....	20
3.1 Objective	20
3.2 Tasks	20
4 Description of Experiments.....	22
4.1 Plant Characteristics.....	22
4.2 Summative Analysis	23
4.3 Proximate and Ultimate Analysis	23
4.4 Experimental Setup and Procedure.....	26
4.4.1 Pyrolyzer.....	26
4.4.2 Experimental Procedure in the Pyrolyzer.....	27
4.4.3 TGA-DSC.....	28
4.4.4 Tar and Gas Analysis.....	29
4.5 Statistical Analysis.....	30
4.6 Root Mean Square Error (RMSE) and Mean Absolute Error (MAE)	30
4.7 Correlation Coefficient	30
5 Effect of Operating Parameters on Pyrolysis Product Yields.....	32
5.1 The Optimum Operating Condition.....	32
5.2 Comparison with Literature	35
5.3 Summary and Conclusion.....	36
6 Slow Pyrolysis of Plant Species Using the Pyrolyzer Apparatus.....	38

6.1	Pyrolysis Product Yields.....	38
6.2	Light Gas Analysis.....	40
6.3	Tar Characterization.....	43
6.3.1	Functional Group Distribution in Tar.....	51
6.4	Summary and Conclusion.....	52
7	Pyrolysis Kinetics Obtained from Iso-Conversional Methods.....	54
7.1	TGA Results.....	54
7.2	The Effect of Heating Rate.....	63
7.3	Analysis of Activation Energy Using the KAS Method.....	64
7.4	Kinetic Parameters for the Drying Zone for All Plant Species.....	69
7.5	Kinetic Parameters for the Major Pyrolysis Zone for All Plant Species.....	70
7.6	Comparison of Activation Energies for Different Biomass.....	83
7.7	The Effect of Aging on Activation Energy.....	84
7.8	Summary and Conclusion.....	89
8	Pyrolysis Kinetics Obtained from Model-Fitting Methods.....	91
8.1	Pyrolysis Completion Temperature.....	91
8.2	Simple One-Step Model.....	94
8.3	Distributed Activation Energy Model (DAEM).....	97
8.3.1	Single-Reaction DAEM Model.....	97
8.3.2	Multiple-Reaction DAEM Model.....	101
8.4	Comparison between Three Models.....	113
8.5	Correlation between Activation Energies and the Main Components Content....	116
8.6	Summary and Conclusion.....	118
9	Summary and Conclusion.....	120
9.1	Yields of Pyrolysis Products.....	120
9.2	Light Gas Species Analysis.....	121
9.3	Tar Species Analysis.....	121
9.4	TGA Results.....	122
9.5	Kinetic Analysis Based on KAS Method.....	122
9.6	Kinetic Analysis Based on Model-Fitting Methods.....	123
9.7	Correlation Between Activation Energies and the Main Components Content ...	123
9.8	Recommendations for Future Work.....	123
	References.....	125
	Appendix A. The Yields of Tar Components as Ar, ArO, Non-Ar, and N-Contain.....	139

Appendix B.	All Identified Tar Components	141
Appendix C.	The Distribution of the Most Prevalent Components in Tar.....	147
Appendix D.	TG and DTG Curves	154
Appendix E.	Regression Lines Used in the KAS Method	162
Appendix F.	TG and DTG Curves Resulted from the Simple One-Step Model	172
Appendix G.	TG and DTG Curves Resulted from the Single-Reaction DAEM Model .	182
Appendix H.	TG and DTG Curves Resulted from the Multiple-Reaction DAEM	192
Appendix I.	RMSE and MAE Values for All Model Fitting Methods	202

LIST OF TABLES

Table 2-1: Yield of products for different types of degradation processes.....	9
Table 4-1: List of plants used in pyrolysis experiments	22
Table 4-2: The summative analysis of live plant species	24
Table 4-3: Proximate and ultimate analysis of plant species	25
Table 5-1: Comparative studies for pyrolysis of different biomass.....	37
Table 6-1: Pyrolysis products variation for live and dead plant species.....	40
Table 6-2: The most prevalent components observed in tar	46
Table 7-1: The mass loss % during different reaction zones for all plant species.....	59
Table 7-2: Activation energies and pre-exponential factors for drying zone using KAS.....	71
Table 7-3: Activation energies and pre-exponential factors for pyrolysis zone using KAS	76
Table 7-4: Kinetic analysis results obtained from pyrolysis of different samples from literature	85
Table 8-1: The kinetic parameters obtained from the simple one-step model.....	96
Table 8-2: Kinetic parameters obtained from the single-reaction DAEM model.....	100
Table 8-3: The kinetic parameters obtained from the multiple-DAEM-reaction model	107
Table 8-4. RMSE and MAE values corresponding to the simulated datasets in figure 8-7	115
Table 8-5: The normalized values of cellulose, hemicellulose and lignin contents	116
Table 8-6: The correlation coefficients between main components and activation energies	118
Table B-1: All identified tar components from pyrolysis of all plant species	141
Table I-1: The RMSE and MAE values corresponding to the DTG curves for live plants.....	202
Table I-2: The RMSE and MAE values corresponding to the DTG curves for dead plants	203

LIST OF FIGURES

Figure 1-1: Heat transfer mechanisms in heterogeneous fuel beds for prescribed fires.....	2
Figure 2-1: Composition of the plant biomass.....	5
Figure 2-2: Pathways involved in the primary mechanisms of biomass components conversion	12
Figure 4-1: Schematic of the pyrolyzer used for generating char and tar.....	26
Figure 5-1: Effect of pyrolysis operating condition on conversion and product yields.....	33
Figure 6-1: Pyrolysis product distributions of plant species on a daf basis.....	39
Figure 6-2: Composition of light gases obtained from pyrolysis of: a) live and b) dead plants...	41
Figure 6-3: Gas chromatogram of tar obtained at 500 °C for pyrolysis of longleaf pine litter.	44
Figure 6-4: The yields of tar components as Ar, ArO, Non-Ar, and N-containing compounds...	44
Figure 6-5: The distribution of most prevalent components in tar obtained from pyrolysis	49
Figure 6-6: Total volatile yields from slow pyrolysis experiments in pyrolyzer and ASTM.....	51
Figure 6-7: Functional groups distribution in tar for live and dead plants	52
Figure 7-1: TG/DTG curves of pyrolysis of a) live saw palmetto b) dead saw palmetto.....	55
Figure 7-2: DTG curves of dead little bluestem grass and dead inkberry	61
Figure 7-3: Temperature range of maximum mass loss rates during pyrolysis.....	62
Figure 7-4: TG (a) and DTG (b) curves of pyrolysis of live saw palmetto	63
Figure 7-5: Regression lines used to obtain apparent activation energies using the KAS	65
Figure 7-6: Activation energy distribution for pyrolysis of LBSG based on the KAS method....	66
Figure 7-7: DTG curves for major pyrolysis zones of live and dead little bluestem grass.....	70
Figure 7-8: Distribution of pyrolysis rates as a function of conversion based on the KAS	80
Figure 7-9: Distribution of pyrolysis rates (live vs. dead) as function of conversion using KAS	83
Figure 7-10: Activation energies for pyrolysis of different types of biomass	84

Figure 7-11: Activation energy distribution for pyrolysis of LLPF, DLPF, and pine straw	87
Figure 7-12: DTG curves for major pyrolysis zones of LLPF, DLPF, and pine straw	88
Figure 8-1: The completion temperature for all live plant species at heating rates.....	92
Figure 8-2: The pyrolysis completion temperature for live vs. dead plant samples.	93
Figure 8-3: Comparison of simple one-step model curve-fit with TG and DTG curves.....	95
Figure 8-4: Comparison of best-fit single-reaction DAEM model with TGA and DTG data.....	99
Figure 8-5: DTG pyrolysis curves at a heating rate of 30 °C min ⁻¹	104
Figure 8-6: TG and DTG curves resulted from experimental and multiple-reaction DAEM	106
Figure 8-7: Comparison of best-fit model fitting methods	114
Figure 8-8: Scatterplots of activation energy vs. the corresponding component.....	117
Figure A-1: The yields of tar components as Ar, ArO, Non-Ar, and N-contain components	140
Figure D-1: TG and DTG curves for all live and dead plant species.	161
Figure E-1: Regression lines used to obtain apparent activation energies using the KAS.	171
Figure F-1: Comparison of best-fit simple one-step model with TGA and DTG data.	181
Figure G-1: Comparison of best-fit single-reaction DAEM model with TGA and DTG.....	191
Figure H-1: Comparison of best-fit multiple-reaction DAEM model with TGA and DTG data	201

1 INTRODUCTION

Wildland fire is an important component of many American ecosystems. Wildland fires can have necessary ecological influences in many North American ecosystems or can dangerously affect life, property and natural resources. These hazards decrease with the proper application of controlled burning.

Controlled burning is an intended application of fire to forest fuels under specific conditions to obtain a variety of objectives such as reducing hazardous fuel, site preparation for seeding and planting, wildland habitat management, control of insects, diseases, and weeds, and bio-diversity maintenance (Wade and Lunsford, 1989; Fernandes and Botelho, 2003; Ferguson et al., 2013). Controlled burning consumes smaller plants and decreases combustible materials, the potential for ignition and fire propagation in the fuel bed (Ferguson et al., 2013). Fuel bed pyrolysis and ignition determine fire ignition and propagation rates in both wildland fires and prescribed burning, but the details of solid fuel reaction under wildland fire conditions remain poorly understood. Solid fuel samples degrade at high temperatures through pyrolysis and combustion. The heat transfer process in combustion of heterogeneous fuel beds for prescribed fires is shown in Figure 1-1. This figure shows that the fuel bed is composed of two parts: a lower region for horizontal dead fuels and an upper region for vertical live fuels. The flame from the horizontal dead fuels is a heat source for the pyrolysis of vertical live fuels. Pyrolysis strongly depends on

the solid fuel particle temperature, which is a function of the heat transfer from the flame to the unburned live fuels. As solid fuels are heated, water in the surface layers evaporates, then pyrolysis occurs, followed by combustion of the volatiles and remaining solid (often called char).

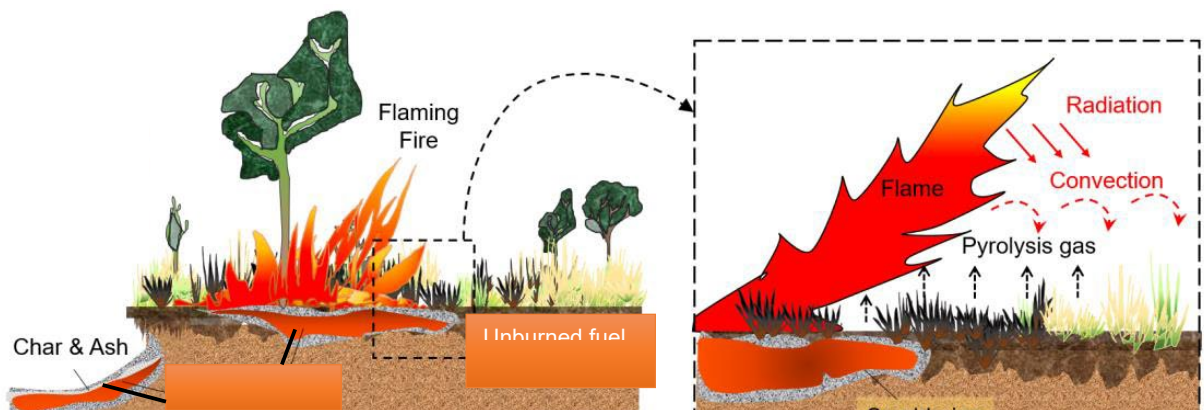


Figure 1-1: Heat transfer mechanisms in heterogeneous fuel beds for prescribed fires (Lin et al., 2019).

Pyrolysis of biomass, such as dead and dried vegetation, as well as wood, has been explored in detail (Bradbury et al., 1979; DiBlasi, 1994; Diebold, 1994; Rao and Sharma, 1998; Babu, 2008), especially for power systems. However, there is a lack of research in the field of pyrolysis of live fuels to support wildland fire research. Many fire models assume the fuel bed as homogenous, with properties taken from wet dead fuels, in some instances with higher heat content, and do not consider properties of live vegetation. However, subsequent research has shown this assumption to be in error (Safdari et al., 2018a) and new models are being developed (Lamorlette et al., 2018).

As part of a project measuring and modeling pyrolysis at different fuel scales, the focus of this research is to provide fundamental information about slow pyrolysis of live and dead plant species all of which are native to the forests of the southeastern United States. Studying pyrolysis

at low heating rates is needed for understanding the behavior of preheating and/or smoldering (Figure 1-1), as well as providing data to evaluate pyrolysis models over a wider range of heating rates. Knowledge gained from the larger project will hopefully improve our understanding of wildland fires and ability to model wildland fire (open burning). Pyrolysis of biomass is also important for many other industrial applications involving biomass utilization. The results of present work can help improve controlled fire application to accomplish desired fire effects and limit potential escapes by helping help modelers improve descriptions of the fundamental processes related to slow pyrolysis in heterogeneous fuel beds of live and dead fuels. In this project, the fundamentals of pyrolysis of live and dead fuels at slow heating rates and low temperatures are investigated. Also, the pyrolysis of different plant species and kinetic parameters are studied.

This dissertation is classified into nine chapters. Chapter 2 contains a literature review which discusses biomass in general, differences between live and dead fuel, pyrolysis of biomass, pyrolysis mechanisms and parameters, kinetic parameters of pyrolysis, and previous pyrolysis research on live fuels. Next, the objective and tasks of the research are explained in Chapter 3. The description of the experiments are discussed in chapter 4. The characterization of pyrolysis product and species yields are presented in Chapters 5-6. The kinetics of slow pyrolysis are presented in Chapters 7, along with analysis using an iso-conversional model. The kinetic data are analyzed with simple first-order and other models in Chapter 8. Finally, the summary and conclusion are presented in Chapter 9.

2 LITERATURE REVIEW

Much of the literature on biomass and biomass pyrolysis has focused on wood and agricultural wastes, supporting the burning biomass for power or using the pyrolysis products for chemicals. Very little research has focused on pyrolysis of live vegetation that pertains to wildland fire. Therefore, much of this literature review pertains to biomass in general, with only the last section pertaining to pyrolysis of live (and dead) forest fuels. The literature review contains the following sections: (1) a general description of biomass; (2) cellulose, hemicellulose, and lignin (3) live and dead fuels; (3) biomass pyrolysis; (4) mechanisms of biomass conversion by pyrolysis; (5) kinetic parameters estimation from TGA data and (6) previous pyrolysis research on forest fuels.

2.1 Biomass

Biomass is a combination of hydrocarbon material consisting of carbon, hydrogen and oxygen, with small amounts of nitrogen and sulfur. Biomass includes different natural and derived materials, such as woody wastes, sawdust, agricultural residues, bio-solids, woody and herbaceous species, grass, aquatic plants, etc. (Sharma et al., 2015). The nature and the chemical composition of the biomass polymers differ significantly with types of biomass (Pasangulapati et al., 2012). Figure 2-1 illustrates the main components of a plant's biomass. Cellulose (around 50% on dry basis), hemi-cellulose (20–40% (in non-woody biomass on dry basis and 10–30% in wood) and lignin (10–40% in non-woody and 20–40% in wood) are the three main groups of

lignocellulose materials in biomass. The ratio of these three components changes with the type of biomass, the part of the plant sampled, and biomass characteristics (Yu et al., 2017). These components mainly consist of alkanes, aromatics, esters, alcohols and ketones groups with different oxygen-containing structures (Yang et al., 2007). Cellulose, hemicellulose and lignin make up structural carbohydrates. Other than lignocelluloses, there are some low molecular weight inorganic (such as Si, Ca, Mg, etc.) and organic substances. Extractives are organic components in biomass and include resins, alcohols, fatty acids, and phenolic components (Zabaniotou, 1999; Sharma et al., 2015; Nomanbhay et al., 2017). Live fuels also contain structural carbohydrates, non-structural carbohydrates, lipids, proteins, and sugars (Jolly et al., 2014; Jolly and Butler, 2015; Jolly and Johnson, 2018; Matt et al., 2020), which may impact combustion. Dead fuels have been found to have fewer extractives than live fuels; the amount varies among species (Countryman, 1982).

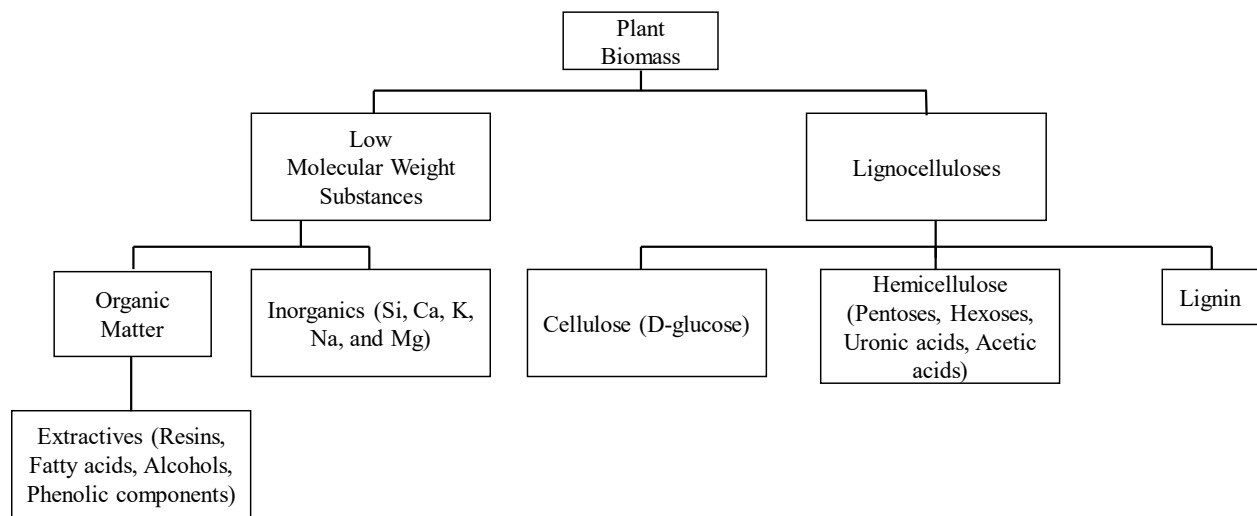


Figure 2-1: Composition of the plant biomass (Nomanbhay et al., 2017).

2.2 Cellulose, Hemicellulose, and Lignin

Cellulose is the major structural polymer of a plant cell wall, which usually exists as long

fibers called microfibrils. Cellulose is a linear polysaccharide made of anhydro-D-glucose monomeric units with a β -(1 \rightarrow 4)-linkage. This bonding feature allows the microfibril structure to develop very strong intra-molecular and inter-molecular hydrogen bonding. Microfibrils are usually fixed on a matrix that contains hemicellulose and lignin (Perez et al., 2002; Pasangulapati et al., 2012).

Hemicellulose is a branched polysaccharide consisting of different sugar monomers such as xylose, mannose, glucose, galactose and arabinose and uronic acids. Unlike cellulose which forms microfibrils, hemicellulose can form hydrogen bonds with cellulose and lignin, and hence they are called “cross linking glucans”. Hemicellulose has a low thermal stability and differs in composition and structure. The dehydration of hemicellulose occurs at low temperatures (less than 280 °C) and depolymerization occurs at higher temperatures. Depolymerization results in volatile organics, furans, levoglucosenone, levoglucosan and other anhydrohexoses while dehydration yields water soluble acids, char, gases, water and anhydride fragments (Perez et al., 2002; Van de Velden et al., 2010).

Lignin is one of the main components present in woody biomass, and is the strengthening component of the cell wall. Lignin is the cementing substance that provides elasticity and mechanical strength to the wood. Lignin is a phenolic macromolecule which has high degree of cross-linking between the phenylpropane units. This nature of cross-linking makes lignin more thermally stable than hemicellulose and cellulose, and produces more char and aromatic components. Lignin has a very complex structure which depends on the plant species. The pyrolysis of lignin yields different products such as catechols, vanillins, and aromatic carbohydrates due to the diversity of the lignin structure. Low temperatures (less than 573 °C) favor dehydration, while higher temperatures lead to the formation of a diversity of lignin monomers. The monomers are decomposed at the temperatures above 773 °C and enter the vapor

phase. (Demirbaş, 2000; Perez et al., 2002; Van de Velden et al., 2010; Pasangulapati et al., 2012).

2.3 Live and Dead Fuel

The fuel beds of wildland fires are heterogeneous in nature, contain different fuel components, and have a mixture of live and dead fuels (Weise and Wright, 2014). These characteristics affect heat transfer, air flow, the combustion process and fire propagation. The burning behavior is different for live and dead fuels (Prince and Fletcher, 2014). Fires that occur in the living crowns of woody shrubs and trees are often the most uncontrollable and unpredictable (Byram, 1959; McAllister et al., 2012).

Living vegetation burns readily when moisture content decreases and large fires can occur when moisture content approaches seasonal minimums. Live and dead fuels can be mainly distinguished by the moisture content. Fuels with no metabolic activity are dead and typically have moisture contents (m_{H_2O}/m_{dry}) less than 30-35% because of fiber saturation. Living plants (fuels) actively regulate water, whereas dead foliar fuels absorb/desorb water passively and typically may have an amount of moisture greater than 35% only if the water on the leaf surface is absorbed into the cell cavities (Viney, 1991). This feature distinguishes wet dead fuel from live fuel (McAllister et al., 2012). The water absorbed in the cell walls of wet dead fuel may be vaporized by heating the fuel. However, in live fuel, unevaporated water may explode rapidly and causes the cell walls to burst. A noticeable amount of moisture may remain in the fuel during ignition (Engstrom et al., 2010; Pickett et al., 2010).

In addition to moisture content, ash content and density differ between live and dead vegetation. Live fuels tend to have higher ash content and higher density than dead fuels. Density of dead fuel is found to be about 90 percent of that of live fuel (Countryman, 1982). Density of

the fuel affects the ease of ignition and burning rate of wildland fires. Fuels with low density need shorter ignition time for a given amount of heat. In a small experimental fire, the fire spread rate decreased as fuel density increased (Fons, 1946; Countryman, 1982). Dead and live fuels burn differently and have different effects on fires and flames (Dimitrakopoulos et al., 2010). Energy is required to evaporate moisture from the fuel particle, which delays ignition. Moisture may also cause the flame temperature to decrease and therefore slows the heating of the solid. Live fuels can affect the direction and rate of spread of wildland fires (Ferguson et al., 2013).

A considerable number of large fires in the United States occurs in live fuels with significant amounts of moisture (Ferguson et al., 2013). Using a live fuel moisture time series and large fire history, Dennison and Mortiz (2009) presented a strong evidence that for a moisture content above 79% large fires did not occur, but when the moisture content of live fuels decreased below 79% and 77%, respectively, large fires occurred in the Los Angeles and Santa Monica areas.

The effects of moisture on live vegetation combustion has been studied, but there is not sufficient research on the role of moisture on pyrolysis. The pyrolysis time in a thermally thick regime increases with the amount of moisture content (Ferguson et al., 2013). In a similar manner, fires which occurred in fuel stands with high moisture content were found to have lower char heights than in stands with lower moisture content (Beringer et al., 2003; Ferguson et al., 2013), indicating less severe burning behavior.

2.4 Pyrolysis of Biomass, Parameters, and Products

Pyrolysis is the thermal decomposition of material that occurs prior to combustion without requiring O₂ (Antonakou et al., 2006; Dhyani and Bhaskar, 2017). Pyrolysis occurs along several pathways and affects the major components of biomass, which are cellulose, hemicellulose, and lignin (Haykiri-Acma et al., 2010).

Depending on the environmental conditions, biomass pyrolysis processes can be classified into three main categories (Table 2-1): slow pyrolysis (slow heating rates, temperatures less than 500 °C residence time greater than 20 s), moderate pyrolysis (temperatures of 500 °C and residence time of 10–20 s), and fast pyrolysis (fast heating rates, temperatures greater than 500 °C, and residence time less than 2 s) (Dhyani and Bhaskar, 2017).

There are two main steps for pyrolysis of solid fuel: primary and secondary pyrolysis. Primary pyrolysis occurs at relatively low temperatures, as the solid fuel decomposes to volatile gases and char, and produces light gases (such as CO, CO₂, H₂O, and H₂), tar, char, and mineral ash. Secondary pyrolysis is a process when the products of primary pyrolysis, especially tar, undergo further reactions at higher temperatures and longer residence times. Secondary pyrolysis reactions generally occur at temperatures above 500 °C for biomass tar (Lewis and Fletcher, 2013)

Table 2-1: Yield of products for different types of degradation processes (Sharma et al., 2015)

Mode	Conditions	Liquid (%)	Char (%)	Gas (%)
Fast	Temperature ~ 500°C, short vapor residence time ~ 1 s	75	12	13
Moderate	Temperature~500°C, moderate vapor residence time ~ 10-20 s	50	20	30
Slow	Temperature ~ 500°C, very long vapor residence time ~ 5-30 min	30	35	35

Biochar is generally high in carbon content and is the solid product of pyrolysis process. Tar is defined as the volatile species that will condense to solid or liquid when cooled to room temperature. Tar is a complex mixture consisting of a variety of organic components from different chemical groups such as aromatics, hydrocarbons, aliphatic compounds, and oxygenated compounds (Imam and Capareda, 2012; Isahak et al., 2012). The organic compounds

can be divided into low-polarity components (organic layer) and high-polarity components (water soluble) according to their water solubility. These components can be categorized as ketones, acids, phenols, aldehydes, ethers, hydrocarbons, esters, sugars, etc. (Bridgwater et al., 1999; Isahak et al., 2012; Jahirul et al., 2012; Lazzari et al., 2016; Dhyani and Bhaskar, 2017). The composition of tar predominantly depends on the type of feedstock, and the tar yield can exceed 70 wt% on dry basis (Dhyani and Bhaskar, 2017; Luo et al., 2017).

The yields of pyrolysis products depend on heating rate, temperature, fuel type, and fuel properties. There has been quite a bit of research on biomass pyrolysis, studying the effects of these parameters (DiBlasi, 1994; Ceylan and Topcu, 2014; Chen et al., 2015c; Ansah et al., 2016; Ozsin and Putun, 2017). The lower pyrolysis temperatures and low heating rates favor the production of char. Higher pyrolysis temperatures, high heating rates, and long residence times lead to the formation of gas products. Studies have shown that the highest tar yields are obtained at a reaction temperature around 500°C, high heating rates, and short vapor residence times for minimizing secondary reactions (Horne and Williams, 1996; Bridgwater et al., 1999; McKendry, 2002; Onay and Kockar, 2003; Imam and Capareda, 2012; Papari and Hawboldt, 2015; Luo et al., 2017).

Tar characteristics, product distribution, and gas composition reveal the interaction between hemicellulose, cellulose, and lignin (Raveendran et al., 1996; Yang et al., 2006). It has been reported that many of the components in tar are primary products of lignin degradation (280 – 500 °C) during pyrolysis (Aysu and Küçük, 2014). The presence of phenolic hydroxyl and methoxy groups in chemical structure of lignin makes it highly reactive. In general, phenols are mainly produced from the degradation of lignin which is a rich source of phenolic components; furans, ketones and carboxylic acids are thought to come from cellulose and hemicellulose degradation (Uçar and Karagöz, 2009; Aysu and Küçük, 2014; Chen et al., 2016). In addition,

decomposition of lignin leads to the formation of aromatic carbons, since lignin contains aromatic rings in its chemical structure (Farag et al., 2014).

Hemicellulose has a random amorphous structure with little strength which makes it highly activated in thermal decomposition. Generally, pyrolysis of hemicellulose (200 – 280 °C) mainly produces acids and furfural (Aysu and Küçük, 2014; Chen et al., 2016). In contrast, cellulose has a well-ordered structure with long polymer chains of glucose which make it thermally stable. Cellulose pyrolysis leads to a high tar yield (Chen et al., 2016), but not necessarily aromatic compounds. Furans, cyclopentanone, and linear carbonyls are mainly formed by depolymerization and fragmentation of active cellulose (240 - 350 °C) (Chen et al., 2016). Three primary transformations processes occur when biomass is heated. The first process is the drying process (up to about 130 °C). In this process, the moisture of the large porous network of the biomass dries up completely. The second process occurs between 180 and 400 °C and is called pyrolysis or devolatilization. In this process, the light volatiles and tar are released. The third process, which occurs in a wide-temperature range (extending to about 720 °C), is called the char formation phase (Lapuerta et al., 2004; Chen et al., 2006; Costa et al., 2016; Ozsın and Putun, 2017).

2.5 Mechanism of Biomass Conversion by Pyrolysis

Heating the biomass breaks different chemical bonds within the polymers which results in the releasing of volatile components and reaction rearrangement within the matrix of the residue. These reactions are called primary mechanisms. After the formation of volatile compounds, some of them which are unstable undergo additional conversions referred to as secondary reactions (Hosoya et al., 2007; Van de Velden et al., 2010; Huang et al., 2012; Collard and Blin, 2014).

The main component of biomass are biopolymers. Depending on the nature of the broken

chemical bonds, the primary conversion of biopolymers can be described by three main pathways: char formation, depolymerization and fragmentation (Figure 2-2). As the plant material is exposed to high temperature, first moisture content decreases, then during primary pyrolysis, the plant constituents (i.e., hemicellulose, cellulose, lignin, etc.) break down and form primary pyrolysis products (Gomez-Barea and Leckner, 2010). Char consists of a solid residue which has an aromatic polycyclic structure. The formation of benzene rings and the combination of these rings in a polycyclic structure are the main steps of this pathway (Collard and Blin, 2014). Depolymerization occurs when the bonds between the monomer units of the polymers break. During depolymerization the degree of polymerization of the chains decreases until the produced molecules become volatile. These molecules are condensable at room temperature and are most frequently found in the liquid fraction (Collard and Blin, 2014).

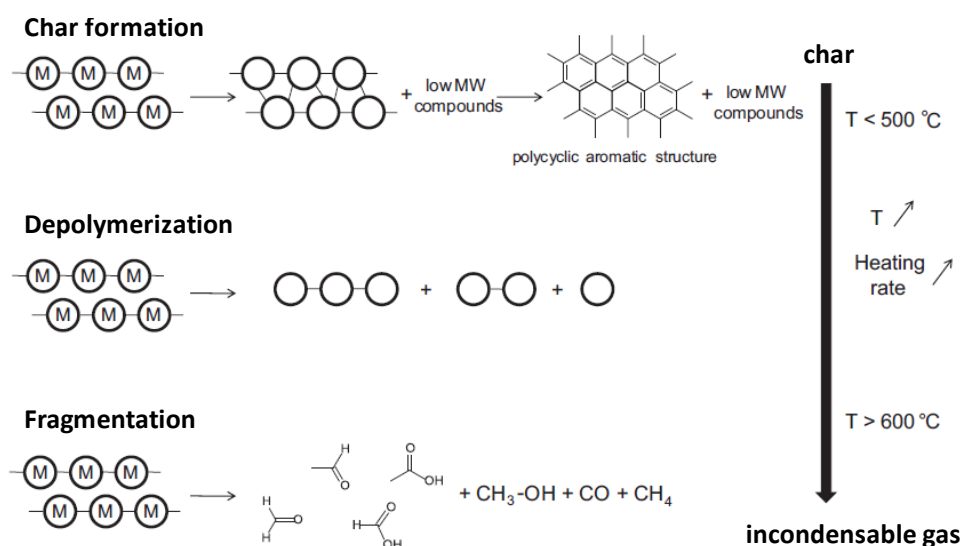


Figure 2-2: Pathways involved in the primary mechanisms of biomass components conversion (M: monomer; MW: molecular weight) (Collard and Blin, 2014).

Fragmentation results in the linkage of many covalent polymer bonds even within the monomer units, and forms the noncondensable gases and a diversity of small chain organic

components which are condensable at room temperature (Collard and Blin, 2014). The released volatile components can undergo secondary reactions such as recombination or cracking when they are not stable under the reactor temperature conditions.

Cracking reactions result in the breaking of chemical bonds within the volatile components and formation of lower MW (molecular weight) molecules (Collard and Blin, 2014). The products obtained from the fragmentation and cracking reactions are similar, because the breaking of the same chemical bonds can undergo either within the volatile components or within the polymer. As a result, it is difficult to recognize which pathway is responsible of producing low MW components.

2.6 Kinetic Parameters Estimation from TGA Data

Studying the thermal decomposition of natural fuels and finding the kinetic parameters are very important in understanding fire behavior, natural fuel combustion modeling and fire propagation (Chen et al., 2006). A commonly-used technique to study the kinetic characteristics of complex reactions is Thermogravimetric Analysis, or TGA. In TGA, the kinetic results are not significantly affected by mass and heat transfer limitations (Banon et al., 2016).

Thermogravimetric/differential thermogravimetry (TG/DTG) experiments can be either isothermal or non-isothermal. During the isothermal method, the sample is heated up as quickly as possible to the reaction temperature. The sample should be held at that temperature while recording the mass vs. time. The activation energy and the kinetic frequency factor can be determined by plotting the rate constant from different experiments of multiple temperatures against the inverse temperature on a log plot.

Non-isothermal methods which involve heating a sample at constant heating rates and measuring the weight with respect to temperature or time must generally be used for pyrolysis,

because pyrolysis almost always starts during the heating period (Kök and Pamir, 1999; Engstrom et al., 2010; Du et al., 2014; Bai et al., 2015). In the case of a constant heating rate, time and temperature are related through:

$$T = \beta \cdot t + T_0 \quad (2-1)$$

where t is time, β is the heating rate, T is the temperature, and T_0 is the initial temperature.

There are various ways to determine activation energy after a mass versus time curve has been generated using TGA; these varying methods result in different activation energy results. Reduction methods first linearize the collected data and then determine kinetic parameters from the slope of the linearized equation, including activation energy, reaction order, and pre-exponential factors. Other researchers have developed methods where linearization of an equation is avoided (Hillier et al., 2010; Hillier and Fletcher, 2011). It is often assumed that the pyrolysis reaction is a first-order global reaction with an Arrhenius form of the rate constant:

$$\frac{dm}{dt} = -A \exp\left(\frac{-E}{RT}\right) m \quad (2-2)$$

where T is the temperature of the sample, E is the activation energy, A is the pre-exponential factor, and m is the mass. Equation 2-2 is often changed to be in terms of conversion or normalized mass. Equation 2-3 represents a special case of a more general n^{th} order equation:

$$\frac{dm}{dt} = -A \exp\left(\frac{-E}{RT}\right) m^n \quad (2-3)$$

Distributed activation energies or parallel reactions may also be used to describe pyrolysis rates (Hillier and Fletcher, 2011; Richards and Fletcher, 2016). These kinetic equations are not actual explanations of the elementary reaction mechanism but are useful engineering applications. Typically, there are two categories of methods used for the utilization of non-isothermal data in order to determine the kinetic parameters that appear in equation 2-2. The first method linearizes the data by dividing by the mass and then taking either the log10 or the natural

log of both sides of the equation. This equation is shown in Equation 2-4 and is called the derivative method.

$$\ln\left(-\frac{dm}{dt}\right) = \ln(A) - \frac{E}{RT} \quad (2-4)$$

Equation 2-4 is shown in a linear form that when the left side of the equation is plotted on the y-axis vs. $1/T$ on the x-axis; the resulting graph will be a straight line when the reaction is first order. The slope of this straight line is the activation energy, and the intercept is the pre-exponential factor. There are two problems with this method; first is the fact that the estimation of the derivative is usually imprecise. The second problem lies in the fact that the pre-exponential factor is desensitized by taking the log of its value. This means that when the intercept is found, small errors will be magnified when the pre-exponential factor is determined.

Many other researchers employ an integral method when determining kinetic parameters.

$$\int_{m_0}^m \frac{dm}{m} = \int_0^t -A \exp\left(\frac{-E}{RT}\right) dt \quad (2-5)$$

$$m = m_0 \cdot \exp\left(\int_0^t -A \exp\left(\frac{-E}{RT}\right) dt\right) \quad (2-6)$$

Integral solutions approximate the right-hand side of Equation 2-6 with a linear form to fit the mass versus temperature model so that activation energy and pre-exponential factor can be determined (Hillier and Fletcher, 2011).

Although TGA experiments seem simple, they have several difficulties in practice, especially for pyrolysis experiments. Non-isothermal analysis begins with the temperature much lower than the reaction temperature. For example, the analysis can start at room temperature and heat the sample at a constant heating rate through the temperature region of the reaction (Hillier et al., 2010). Equation 2-2 is then fit to the curve of mass loss using the temperature at each time. The problem with non-isothermal analysis arises from Equation 2-2 due to the Arrhenius form; there is no analytical solution of the integral when T changes with time.

There are two classes of methods which have been developed to formulate the mathematical expression that describes solid fuel decomposition: (a) the model-fitting method and (b) the iso-conversional method (model-free method) (Vyazovkin and Wight, 1999; White et al., 2011; Kongkaew et al., 2015). In the model-fitting method, there are different reaction models (such as the reaction order model, the diffusion model, and the power law model) which are proposed to describe the decomposition process of solid fuels. The assumed form of reaction model is used to determine the kinetic parameters. Generally, the decomposition mechanism and the corresponding reaction models vary with the type of solid fuels and pyrolysis conditions. Obtaining a correct mechanistic reaction model for the decomposition process of any solid fuel is difficult, and perhaps impossible. That is why the model-fitting methods produce uncertain values of kinetic parameters (Vyazovkin and Wight, 1999). In addition, model fitting methods obtain a single value of the activation energy for an overall process. This value is an average value that does not characterize changes in the mechanism of the reaction and kinetics with the degree of conversion. However, the iso-conversional method does not have the aforementioned disadvantages, because it does not make any assumptions about the model of the reaction and allows the activation energy to be found as a function of the degree of conversion. However, iso-conversional models may not be as useful in large fire simulations since the activation energy changes with conversion and perhaps heating rate. There are different iso-conversional methods such as Friedman, Flynn-Wall-Ozawa (FWO) (Flynn and Wall, 1966), Kissinger-Akahira-Sunose (KAS) (Kissinger, 1957), and Starink (1996) methods that have been successfully used for the kinetic analysis of the pyrolysis process of different solid materials (Yuan et al., 2017).

The most-used approach to simply determine kinetics from TGA data is the single-step global model coupled with different iso-conversional methods. However, the difference in decomposition of the biomass components makes the biomass pyrolysis process extremely

complex. Therefore, a multi-step reaction model is more suitable than a single-step model to simulate pyrolysis of solid fuels (such as biomass and coal). The distributed activation energy model (DAEM) is a multi-step reaction model which is also a commonly used model in kinetic studies of biomass pyrolysis (Goyal et al., 2008; Soria-Verdugo et al., 2013; Bai et al., 2015; Hu et al., 2017). In the single-step model, the rate of conversion can be described as Equation 2-7 (Hu et al., 2017).

$$\frac{d\alpha}{dt} = k(T)f(\alpha) \quad (2-7)$$

where α is conversion; t is the reaction time; $k(T)$ is the Arrhenius reaction constant which is dependent on temperature; and $f(\alpha)$ is the reaction mechanism model which is dependent on conversion (α). Conversion (α) is defined as:

$$\alpha = \frac{m_0 - m_t}{(m_0 - m_f)} \quad (2-8)$$

where m_0 , m_t and m_f are the initial, instantaneous and final mass of pyrolysis process. By considering a constant heating rate, β ($\beta = dT/dt$, $^{\circ}\text{C min}^{-1}$), the reaction rate equation for biomass pyrolysis becomes (Hu et al., 2017):

$$\frac{d\alpha}{dT} = \frac{A}{\beta} \exp\left(-\frac{E}{RT}\right) f(\alpha) \quad (2-9)$$

The equations of Friedman, Starink, KAS (Kissinger–Akhira–Sunose), and the simplified DAEM are given as Equations 2-10 – 2-13, respectively (Gao et al., 2001; Lapuerta et al., 2004; Chen et al., 2006; Bai et al., 2015; Costa et al., 2016; Yurdakul, 2016):

$$\ln\left(\beta \frac{d\alpha}{dT}\right) = \ln(Af(\alpha)) - \frac{E}{RT} \quad (2-10)$$

$$\ln\left(\frac{\beta}{T^{1.8}}\right) = \text{constant} - 1.0037 \frac{E}{RT} \quad (2-11)$$

$$\ln\left(\frac{\beta}{T^2}\right) = \text{constant} - \frac{E}{RT} \quad (2-12)$$

$$\ln\left(\frac{\beta}{T^2}\right) = \ln\left(\frac{AR}{E}\right) - 0.6075 - \frac{E}{RT} \quad (2-13)$$

The slope of the regression lines $\ln\left(\beta \frac{d\alpha}{dT}\right)$, $\ln\left(\frac{\beta}{T^{1.8}}\right)$ and $\ln\left(\frac{\beta}{T^2}\right)$ vs. $\frac{1}{T}$ for Friedman, Starink, KAS and DAEM methods, respectively can give the activation energy under the same amount of conversion at different heating rates (Bai et al., 2015). The Kissinger method is another non-isothermal model-free method which can be represented as follows:

$$\ln\left(\frac{\beta}{T_m^2}\right) = \ln\left(\frac{AR}{E}\right) - \frac{E_a}{RT_m} \quad (2-14)$$

where β is heating rate, and T_m is the peak temperature of DTG curve. The slope of the plot of $\ln\left(\frac{\beta}{T_m^2}\right)$ versus $\frac{1}{T_m}$ gives E_a .

One other model that has been widely used to find the kinetic parameters of thermal degradation is the Coats-Redfern model which is defined as Equation 2-15 (Costa et al., 2016):

$$\ln\left[\frac{(-\ln(1-\alpha))}{T^2}\right] = \ln\left[\left(1 - \frac{2RT}{E}\right) \frac{AR}{\beta E}\right] - \frac{E}{RT} \quad (2-15)$$

where α is the mass loss rate, β is the heating rate ($^{\circ}\text{C min}^{-1}$), and $\ln\left[\left(1 - \frac{2RT}{E}\right) \frac{AR}{\beta E}\right]$ is the pre-exponential factor. The activation energy can be obtained by plotting $\ln\left[\frac{(-\ln(1-\alpha))}{T^2}\right]$ vs. $\frac{1}{T}$ (Costa et al., 2016).

2.7 Previous Pyrolysis Research on Forest Fuels

Valuable research in the field of forest fuels pyrolysis has been conducted in the past few decades (Philpot, 1970; Duvvuri et al., 1975; Susott, 1980; Tihay and Gillard, 2011). However, characterization of pyrolysis products and the difference between the pyrolysis behavior of live and dead fuels were not investigated in detail. During wildland fires, slow heating rate pyrolysis exists in pre-heating and/or smoldering zones, while high heating rate pyrolysis occurs in the flame region. A comprehensive research study was conducted by Safdari (2018) regarding high heating rate pyrolysis of live and dead vegetation. During Safdari's research, the fast pyrolysis of 14 plant

species native to the southern United States was studied using a flat-flame burner (FFB). The yield of pyrolysis products (tar, char and light gases) and their characterization were studied and were compared with the results obtained from current research (Safdari et al., 2019, 2020).

The results of this current study, combined with previous research (Safdari, 2018), can be used to investigate reactions that occur during slow and fast pyrolysis and subsequent combustion of both live and dead plants. The data are vital to find the heat release associated with slow and fast pyrolysis of live and dead vegetation. The combined results of both research projects can ultimately help modelers come up with more accurate models to predict prescribed burning behavior and fire propagation.

2.8 Summary of Literature Review

Many valuable studies have been performed during the past few decades regarding the pyrolysis and combustion of biomass (dead and dried plants). However, there is not sufficient study in understanding the pyrolysis of live wildland fuels, characterization of their pyrolysis products and rate of pyrolysis. The research described in this dissertation helps to improve understanding in the areas which have received little attention in this field. These areas include: (1) the effects of pyrolysis fuel type, fuel condition (i.e., live and dead), temperature, and heating rate on the yields and the compositions of pyrolysis products from pyrolysis of wildland fuels; and (2) the effects of pyrolysis fuel type, fuel condition (i.e., live and dead), temperature, and heating rate on the kinetic parameters and rates of slow pyrolysis of live and dead plant species. The results of this dissertation will help to provide a better understanding of the fundamental processes related to the pyrolysis and eventual combustion of wildland fuels.

3 OBJECTIVE AND TASKS

3.1 Objective

The main objective of this work was to provide fundamental information about slow pyrolysis of 14 plant species native to the forests of the southern United States. These plant species were chosen since they were commonly burned fuels in prescribed fires. The effect of plant type and plant condition (live and dead) on the yield and the characterization of the pyrolysis products was investigated. An additional objective was to find the kinetic parameters and pyrolysis rates using an appropriate model.

This research is part of a large project with collaboration of 12 academic and governmental organizations (Weise et al., 2018); the results of the current work combined with the results of the other groups will be used by other investigators to improve the understanding of the behavior of wildland fires and prediction of fire propagation.

3.2 Tasks

The specific tasks that will help to achieve these objectives are:

- 1- Develop a system to collect tars and gases from slow pyrolysis of live and dead vegetation.
- 2- Quantitatively measure the pyrolysis products from Task 1 and analyze them. Find the optimum operating condition that maximizes the yield of tar.

- 3- Measure the yields of pyrolysis products for live and dead fuels for different plant species and describe any differences.
- 4- Measure the pyrolyzed species to see if there is a difference between the tar and light gas components obtained from the slow pyrolysis of live and dead fuels for different plant species.
- 5- Determine the kinetics of slow pyrolysis reactions of live and dead vegetation for different plant species using both model-free and fixed-model rate equation forms.
- 6- Find the correlation between activation energies obtained from task 5 and main components of plant species

In order to accomplish the tasks, a pyrolyzer apparatus and a TGA were used for studying slow pyrolysis products and kinetics of pyrolysis, respectively. Both the pyrolyzer and TGA were operated under inert conditions at five different heating rates of 10 – 30 °C min⁻¹. The proximate and ultimate analysis were performed for each plant species. The pyrolysis of both live and dead plants was studied. A gas chromatograph equipped with a mass spectrometer (GC-MS) and a gas chromatograph equipped with a thermal conductivity detector (GC-TCD) were used to study the speciation of tar and light gases, respectively.

4 DESCRIPTION OF EXPERIMENTS

4.1 Plant Characteristics

Table 4-1 lists the 14 plant species used in pyrolysis experiments, which were classified into three growth types: shrub, tree, and grass (note that longleaf pine litter is the same species as longleaf pine foliage).

Table 4-1: List of plants used in pyrolysis experiments

Common name	Scientific name	Growth form	Leaf shape
Darrow's blueberry	<i>Vaccinium darrowii</i> Camp "Rosa's Blush"	Shrub	Elliptical
Dwarf palmetto	<i>Sabal minor</i> (Jacq.) Pers.	Shrub	Palmate
Fetterbush	<i>Lyonia lucida</i> (Lam.) K. Koch	Shrub	Elliptical
Inkberry	<i>Ilex glabra</i> (L.) A. Gray	Shrub	Elliptical
Little bluestem	<i>Schizachyrium scoparium</i> (Michx.) Nash	Grass	Linear
Live oak	<i>Quercus virginiana</i> Mill.	Tree	Elliptical
Longleaf pine foliage	<i>Pinus palustris</i> Mill.	Tree	Linear
Longleaf pine litter (pine straw)	<i>Pinus palustris</i> Mill.	Tree	Linear
Saw palmetto	<i>Serenoa repens</i> (W. Bartram) Small	Shrub	Palmate
Sparkleberry	<i>Vaccinium arboreum</i> Marshall	Shrub	Elliptical
Swamp bay	<i>Persea palustris</i> (Raf.) Sarg.	Shrub	Elliptical
Water oak	<i>Quercus nigra</i> L.	Tree	Elliptical
Wax myrtle	<i>Morella cerifera</i> (L.) Small	Shrub	Elliptical
Wiregrass	<i>Aristida stricta</i> Michx.	Grass	Linear
Yaupon	<i>Ilex vomitoria</i> Aiton 'Schelling Dwarf'	Shrub	Elliptical

These plant species were selected since they are commonly burned in prescribed fires. The plants were grown in a nursery and then express-mailed to the combustion laboratory at Brigham

Young University (BYU) as live plants. These plants were kept alive with sufficient sunlight and regular watering. Plants are generally considered dead when metabolic activity ceases. For the dead plant experiments in this work, plants were left for a minimum of one week to completely dry and reach a moisture content less than 10%.

It was not possible to conduct a study of aging for all dead samples. However, longleaf pine litter was studied, which is dead longleaf pine needles that have aged for several months. The pyrolysis products of live longleaf pine needles, freshly dried (and hence dead) longleaf pine needles, and longleaf pine litter were measured to study the effect of aging.

4.2 Summative Analysis

The summative component analysis was measured by the University of Wisconsin Forage Laboratory and the results are presented in Table 4-2 (Matt et al., 2020). The “Other” category includes lipids, glucose, fructose, pectin, protein, starch, phenols, minerals and silicates. Note that many plants were analyzed to have over 50% of the mass in the “Other” category on a dry basis, which is much different than wood and other commonly-studied biomass. Typical ash contents (shown later) were in the 2-3 wt% range. Therefore, the main components generally assumed in most biomass research (i.e., hemicellulose, cellulose, and lignin) only comprise 41 to 76% of the mass of these live plants based on this analysis.

4.3 Proximate and Ultimate Analysis

The moisture content of plant samples was determined by placing a 5-gm sample in a Computrac MAX 1000 moisture analyzer (H.R. = 100 °C min⁻¹). The ultimate and proximate analysis (see Table 4-3) were performed by the University of Wisconsin Forage Laboratory using ASTM D5291 and ASTM D7582 procedures, respectively.

Table 4-2: The summative analysis of live plant species

Common name	Hemicellulose ^a (%)	Cellulose ^a (%)	Lignin ^a (%)	Other ^a (%)
Darrow's blueberry	N/A ^b	N/A	N/A	N/A
Dwarf palmetto	18	28	17.1	36.9
Fetterbush	6.9	16.6	30.3	46.2
Inkberry	5.4	11.1	25	58.5
Little bluestem	21.5	31.3	21.2	26
Live oak	10.9	19.2	23.7	46.2
Longleaf pine foliage	15	19	23.5	42.5
Longleaf pine litter	N/A	N/A	N/A	N/A
Saw palmetto	18.6	11	29.8	40.6
Sparkleberry	N/A	N/A	N/A	N/A
Swamp bay	10.5	18.3	32.9	38.3
Water oak	5.8	15.7	25.3	53.2
Wax myrtle	10.5	17.6	28.1	43.8
Wiregrass	22.8	34.8	18.7	23.7
Yaupon	7.3	8.8	25.2	58.7

^a Dry basis^b Means not available

Table 4-3: Proximate and ultimate analysis of plant species

Common name	MC ¹	Proximate analysis ²			Ultimate analysis ³						
		Ash	VM	FC	C	H	N	S	O	LHV	HHV
Darrow's blueberry	104	2.85	n.a. ⁴	n.a.	n.a.	n.a.	n.a.	n.a.	n.a.	n.a.	n.a.
Dwarf palmetto	188.46	2.93	87.18	9.89	47.36	5.93	2.14	0.66	43.91	19.04	20.61
Fetterbush	128.33	2.14	76.00	21.85	54.36	5.81	0.80	0.12	38.91	19.00	20.57
Inkberry	135.11	1.83	78.71	19.46	54.63	6.42	0.87	0.11	37.97	20.94	22.52
Live oak	136.20	2.71	78.67	18.62	49.57	6.01	2.30	0.15	41.97	18.21	19.81
Little bluestem	239.44	2.20	83.00	14.8	51.22	5.66	2.22	0.15	40.75	17.63	19.09
Longleaf pine foliage	180.07	1.84	78.22	19.94	51.37	3.00	1.21	0.11	44.31	19.26	20.11
Longleaf pine litter	15.33	1.77	76.89	21.33	52.31	6.09	2.31	0.06	39.23	19.59	21.10
Saw palmetto	160.53	1.65	75.16	23.19	49.49	58.00	0.90	0.17	43.96	19.09	20.56
Sparkleberry	118.96	3.10	76.55	20.35	52.49	7.71	0.74	0.16	38.90	18.96	20.90
Swamp bay	118.21	1.74	78.24	20.01	52.48	6.11	1.36	0.17	39.88	20.50	22.10
Water oak	127.23	2.92	78.22	18.86	50.06	5.57	1.47	0.10	42.80	18.23	19.96
Wax myrtle	143.94	2.32	75.58	22.09	50.65	5.44	2.31	0.14	41.46	19.98	21.36
Wiregrass	114.32	2.00	80.06	17.94	47.42	6.34	3.31	0.25	42.68	17.74	19.34
Yaupon	167.24	4.33	82.41	13.26	51.34	6.28	1.46	0.18	40.74	19.79	21.43

¹ MC (moisture content wt% dry basis) of sample used in experiment at BYU

² VM (volatile material), FC (fixed carbon). Values are wt% dry-ash free. ASTM D7582

³ C, H, N, S, O – values are % dry mass; LHV – low heating value, HHV – high heating value (kJ g⁻¹, dry-ash free basis). ASTM D5291, D4239, E71

⁴ Means not available

The O content was determined by difference from the sum of the C, H, N, and S elements in the ultimate analysis. Both low (LHV) and high heating values (HHV) were determined.

4.4 Experimental Setup and Procedure

This section details the different techniques and experimental apparatuses used in this work.

4.4.1 Pyrolyzer

The pyrolyzer reactor used in the present study is shown in Figure 4-1.

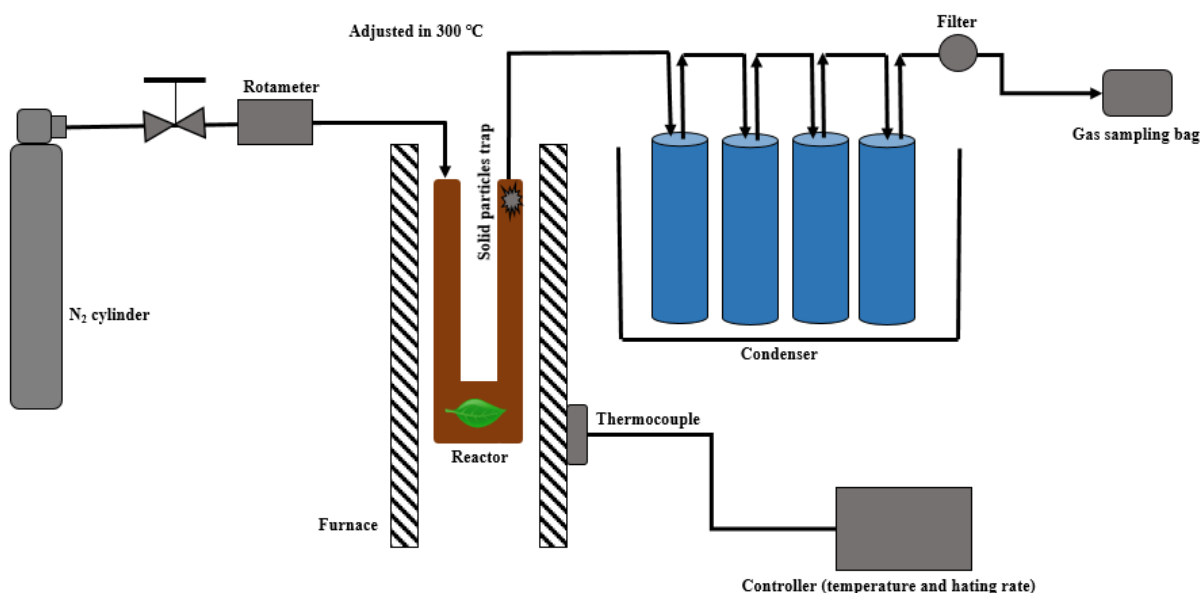


Figure 4-1: Schematic of the pyrolyzer used for generating char and tar.

This reactor was previously used by Hillier et al. (2013) and was modified for the present study. The reactor was heated externally by an electric furnace at a constant heating rate to a selected final temperature. The temperature of the furnace was controlled by a thermocouple connected to the controller. The reactor was made from $\frac{3}{4}$ in. stainless steel tubing with a U-like

shape. Gas condensers were constructed by packing fine glass wool into test tubes and using rubber stoppers to close the top. The stoppers had two holes drilled into them through which ¼ in. stainless steel tubing was tightly fitted. The gases entered the test tubes and passed through the glass wool before exiting. The four condensers were placed in an ice bath filled with dry ice to aid condensation. The inlet and outlet tubes were made of ¼ in. stainless steel tubing. The inlet tubes inside of the heater were connected to a nitrogen (carrier gas) cylinder and were served to preheat the gases. The inlet N₂ stream was not heated since the temperature of the N₂ gas reached the furnace temperature before entering the pyrolysis zone because (1) the N₂ flow rate was low and (2) the inlet N₂ tube was long enough. The outlet of the heater, which was covered by heating tape (heated up to 300 °C) to avoid any possible condensation of organic vapors before entering the ice bath, was designed to allow for thermocouple access. A filter holder with filter paper was placed after the condensers to verify that tars did not travel downstream. The non-condensable gases coming out from the outlet of condensers were collected in a gas sampling bag for transfer to gas analysis devices.

Before the pyrolysis experiment, nitrogen gas purged through the reactor for 10 minutes to create an oxygen-free environment inside the reactor.

4.4.2 Experimental Procedure in the Pyrolyzer

The pyrolysis experiments were conducted in the pyrolyzer apparatus by first weighing the u-shaped portion of the reactor. Second, a quantity of glass wool was fitted to the exit region of the reactor as a particle filter. For each pyrolysis experiment, approximately two grams of sample were placed in the reactor. Whole leaves were folded (not cut) to fit into the reactor, with little or no stem material. Two groups of experiments were performed. In the first group, three sets of experiments were conducted with dead longleaf pine litter to find the optimum operating

condition to obtain the highest tar yield. The first set of experiments was conducted with heating rates of 5, 10, 15, 20, 25, and 30 °C min⁻¹ to a final temperature of 500 °C under constant flow rate of nitrogen at 100 ml min⁻¹, to investigate the effect of heating rate. The second set of experiments was conducted with a heating rate of 30 °C min⁻¹ to final temperatures of 400, 500, 600, 700, and 800 °C, under nitrogen flow rate of 100 ml min⁻¹, to study the effect of temperature. The third set of experiments was conducted to determine the effect of sweep gas flowrate on product yields, with nitrogen flow rates of 50, 100, 200, 250, 300, and 350 ml min⁻¹ to a final temperature of 500 °C with a heating rate of 30 °C min⁻¹. Three separate experiments were conducted at each heating rate, temperature, and sweep condition to determine repeatability.

The second group of experiments was performed at the optimum heating rate, temperature, and sweep gas flow rate for all 14 plant species (live and dead) to find the yields of light gas, tar, and char. Light gas and tar were subsequently analyzed for species composition. Three separate experiments were conducted for each species at this optimum condition to determine repeatability. For each experiment, furnace temperature was held for a minimum of 1 hour at the final temperature until no further release of gas was observed. The yield of char and liquid products were determined by weighing the reactor and the tar collection tubes before and after the experiment. The gas yield was calculated by difference.

4.4.3 TGA-DSC

The slow pyrolysis experiments were conducted using a TGA-DSC Mettler Toledo in a helium atmosphere with a flow rate of 50 ml min⁻¹ (Rahmati et al., 2018). For each experiment, approximately 6 mg of sample was loaded into the platinum 30 µl crucible. The TGA apparatus heated the sample from ambient temperature to 800 °C using linear heating rates of 10, 15, 20, 25, and 30 °C min⁻¹. To eliminate diffusion and heat transfer problems and ensure kinetic control,

small particle sizes (0.5 – 1 mm) were used (Becidan et al., 2007). Mass loss and derivative mass loss were measured continuously during the heating.

4.4.4 Tar and Gas Analysis

Tar was removed from the glass wool and the sides of the test tubes using dichloromethane (DCM) as solvent. Water was removed from the tar/DCM solution by adding about 2 g anhydrous CaSO_4 powder. The decanted DCM/tar solution was analyzed off-line by an HP 5890 gas chromatograph (GC) equipped with an HP 5972 mass spectrometer (MS), and a Rxi®-1ms capillary column (60 m \times 0.25 mm \times 1.0 μm). Helium was used as a carrier gas with a constant flowrate of 2 ml min^{-1} . The temperature of the oven was held at 50 $^{\circ}\text{C}$ for 5 min, then increased to 310 $^{\circ}\text{C}$ with a rate of 10 $^{\circ}\text{C min}^{-1}$ and was held at this temperature for 5 min. 1 μL of sample with a split ratio of 10 was injected (i.e., 1/10 of the sample goes through the column) (Safdari et al., 2016). The area under each peak represents the mole fraction of a component in the tar. These tar results must be viewed as semi-quantitative, since the system response for each tar molecule to relate moles to peak area was not determined, due to the large number (> 200) of peaks.

The light gas analysis was carried out in a ThermoFisher Scientific Trace 1310 gas chromatograph (GC) equipped with a thermal conductivity detector (TCD) and Chrompack Molsieve5A (25 m \times 0.32 mm \times 30 μm) and TracePLOT TG-Bond Q (30 m \times 0.32 mm \times 10 μm) columns (Fazlollahi et al., 2017; Safdari et al., 2018b). Calibration standards for CO , CO_2 , CH_4 , and H_2 were used to make the light gas analysis quantitatively accurate. C_2H_6 and C_3H_8 were also run through the GC/TCD system to identify the retention times for the peaks for these species, but the peak heights for these species were so low in the pyrolysis experiments that detailed calibration was not performed.

4.5 Statistical Analysis

For statistical analysis, the ANOVA (Analysis of Variance) data analysis tool in Microsoft Excel 2017 was used. All the results of this study are the average of three replications, and the error bars represent the $\pm 95\%$ confidence intervals for three experiments. The 95% confidence intervals ($\alpha = 0.05$) using the t-value table are calculated as follows:

$$\mu = \bar{x} \pm t \times \left(\frac{s}{\sqrt{n}} \right) \quad (4-1)$$

where \bar{x} is the average value of the replications, s is standard deviation, n is the number of replications, t is the t-value which is equal to 2.92.

4.6 Root Mean Square Error (RMSE) and Mean Absolute Error (MAE)

To compare the predicted values from model fitting methods and experimental data obtained from slow pyrolysis of all live and dead plant species in TGA, the root mean square error (RMSE) and mean absolute error (MAE) values were calculated as follows:

$$RMSE = \sqrt{\frac{\sum_{i=1}^n (P_i - E_i)^2}{n}} \quad (4-2)$$

$$MAE = \frac{1}{n} \sum_{i=1}^n |P_i - E_i| \quad (4-3)$$

where P is the predicted value from the model, E is the experimental data, and n is the number of employed experimental data points (Torres-Garcia and Brachi, 2019).

4.7 Correlation Coefficient

The correlation coefficient measures the direction and strength of a linear relationship between two variables on a scatterplot. The following formula was used to calculate the linear relationship values between cellulose, hemicellulose and lignin content and the corresponding activation energy values of each plant species:

$$r = \frac{1}{n-1} \cdot \sum \left(\frac{x_i - \bar{x}}{s_x} \right) \left(\frac{y_i - \bar{y}}{s_y} \right) \quad (4-2)$$

where r is correlation coefficient, n is the number of plant species, x_i is hemicellulose, cellulose and lignin content of each plant species, \bar{x} is mean of x_i values, s_x is standard deviation of x_i values, y_i is activation energy, \bar{y} is mean of y_i values, s_y is standard deviation of y_i values.

5 EFFECT OF OPERATING PARAMETERS ON PYROLYSIS PRODUCT YIELDS⁵

In this chapter, the effect of temperature, heating rate and sweep gas flow rate on product yields obtained from pyrolysis of longleaf pine litter was studied and an optimum operating condition which results in the highest tar yield was determined. The resulting tar yields were then compared with literature values.

5.1 The Optimum Operating Condition

The effect of pyrolysis temperature, heating rate, and sweep gas flowrate on product yields obtained from pyrolysis of longleaf pine litter was studied. The results are presented in Figure 5-1. In the first set of experiments, the effect of heating rate on pyrolysis product yields at a temperature of 500 °C was studied. The heating rates explored were between 5 and 30 °C min⁻¹. The highest heating rate explored was 30 °C min⁻¹ to ensure that the sample temperature in the TGA and the pyrolyzer would be the same as the furnace temperature. In addition, in real wildland fire the heating rates in the smoldering and preheating zones are generally lower than 30 °C min⁻¹. From Figure 5-1a, it can be seen that increasing the heating rate from 5 °C min⁻¹ to 30 °C min⁻¹ slightly increased the tar yield from 49.1 wt% to 51.5 wt% and decreased the char yield from 30.5 wt% to 24.1 wt%. The results of this study show that the change in heating rate had only a small effect on tar yield at these slow heating rates, but a greater impact on char yield.

⁵ The results of this chapter were published in Fuel (Amini et al., 2019)

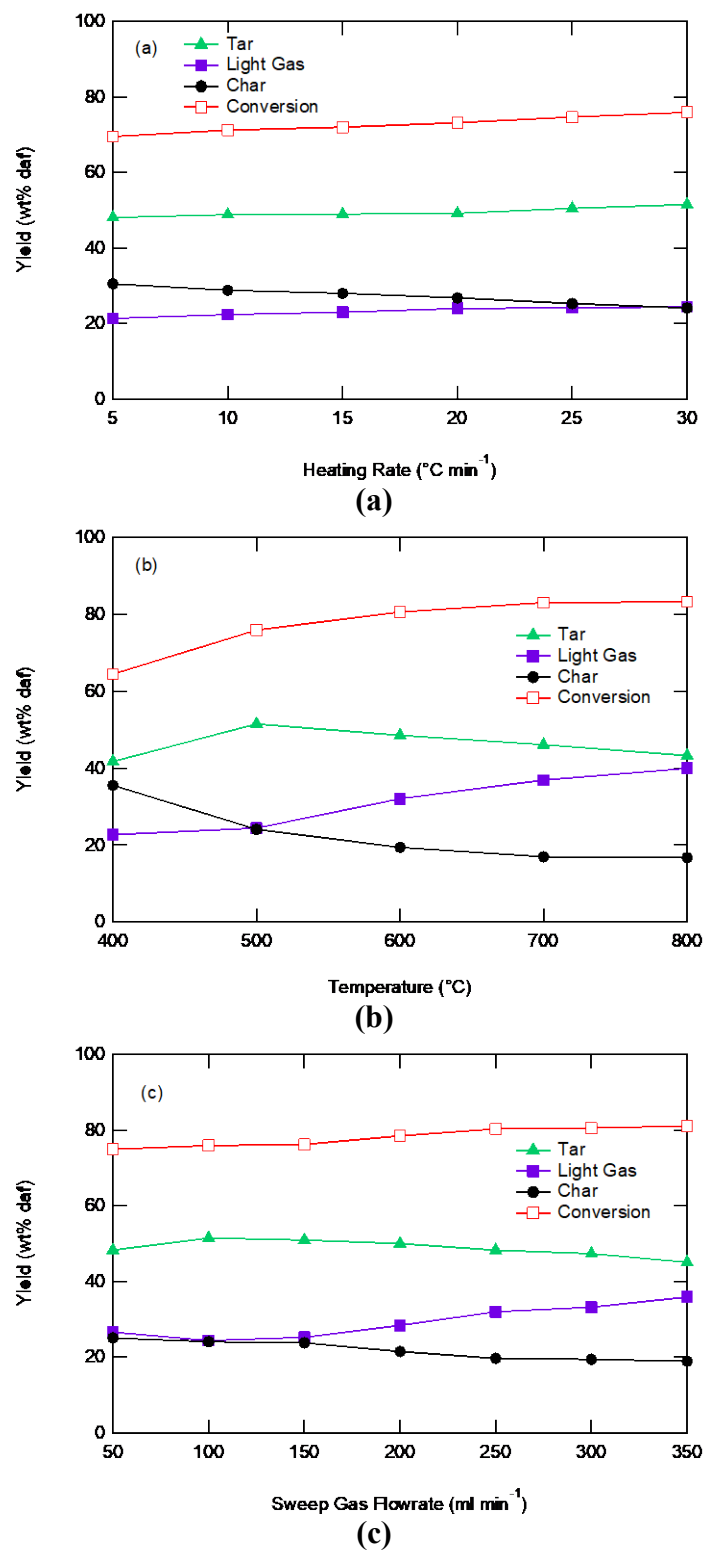


Figure 5-1: Effect of pyrolysis: a) heating rate, b) temperature, and c) sweep gas flowrate on conversion and product yields (daf).

In the second set of experiments, the effect of temperature on pyrolysis product yields was investigated, as shown in Figure 5-1b, which shows that biomass conversion increases with increasing temperature due to extra energy inputs available to break the biomass bonds (Akhtar and Saidina Amin, 2012). As temperature is increased from 400 to 500 °C, the tar yield increased from 41.7 wt% to 51.5 wt% at a heating rate of 30 °C min⁻¹. The highest tar yield was obtained at 500 °C for a heating rate of 30 °C min⁻¹. Beyond 500 °C, increasing the temperature negatively affected the tar yield. When temperature is increased from 500 °C to 800 °C, tar yields decreased from 51.5 wt% to 43.2 wt%. The most probable reason for a decreasing yield of tar at temperatures above 500 °C is the secondary cracking of volatiles at higher temperatures (Kar, 2011; Isahak et al., 2012; Morali et al., 2016). As seen from Figure 5-1b, the char yield decreased from 35.5 wt% to 16.7 wt%, with increasing temperature at a heating rate of 30 °C min⁻¹ from 400 °C to 800 °C that could be either due to greater primary decomposition of dead longleaf pine litter at higher temperatures or through secondary decomposition of char residue (Pütün et al., 2005; Chen et al., 2015a; Krishna et al., 2016). The increased temperature leads to an increased yield of gases from 22.7 wt% to 40.0 wt%. due to secondary cracking of pyrolysis vapors (Pütün et al., 2005; Chen et al., 2015a; Krishna et al., 2016).

The third set of experiments was performed to study the effect of sweep gas flow rate on conversion and product yields by conducting the pyrolysis experiments with different nitrogen gas flow rates (50 – 350 ml min⁻¹) at a temperature and a heating rate of 500 °C and 30 °C min⁻¹, respectively (Figure 5-1c). The maximum tar yield of 51.5 wt% was obtained at a flow rate of 100 ml min⁻¹. The conversion and tar yield were increased with increasing sweep gas flowrate from 50 to 100 ml min⁻¹ and reached the maximum value at 100 ml min⁻¹. Beyond 100 ml min⁻¹, increasing the sweep gas flowrate decreased the tar yield. In contrast the char and gas yields,

initially decreased with increasing the nitrogen gas flowrate from 50 to 100 ml min⁻¹, reaching the minimum values at 100 ml min⁻¹, and then increased with increasing the flowrate. The flowrate of sweep gas affects the residence time of the vapor phase obtained from pyrolysis. The role of sweep gas is to help the products to leave the hot zones quickly and minimize the secondary reactions such as thermal cracking, recondensation and repolymerization and maximize the yield of tar (Demiral et al., 2012; Hu et al., 2013). However, higher flow rates lead to decreases in liquid product yields and increases in gaseous product yields due to either inadequate cooling or fast exit of pyrolysis vapors from cooling zones (Hu et al., 2013; Aysu and Küçük, 2014).

In this study, it was found that pyrolysis temperature has the most important effect on product yields. A temperature of 500 °C, heating rate of 30 °C min⁻¹, and sweep gas flowrate of 100 ml min⁻¹ was the optimum condition to produce the highest amount of tar from slow pyrolysis of dead longleaf pine litter. However, the heating rate of 30 °C min⁻¹ is only optimum for the range tested and it is possible that higher tar yields could be obtained at higher heating rates. The standard deviation for these data was less than 5%, showing excellent data reproducibility.

5.2 Comparison with Literature

The range of tar yields obtained in this study (41.7 – 51.5 wt%) for longleaf pine litter are in the range of tar yields that have been reported in the literature (23.3 – 55.17 wt%) for different kinds of biomass in general (Özbay et al., 2008; Uzun et al., 2010; Abnisa et al., 2011; Demiral et al., 2012; Hu et al., 2013; Aysu and Küçük, 2014; Shadangi and Mohanty, 2014; Chen et al., 2015a; Majhi et al., 2015; Bordoloi et al., 2016; Morali et al., 2016; Varma and Mondal, 2017), and specifically with the maximum tar yield of 43.8% reported by Varma and Mondal (Varma and

Mondal, 2017) for pine needles. Table 5-1 represents the optimum operation conditions reported in the literature for maximum tar yields from different types of biomass.

5.3 Summary and Conclusion

In this chapter, results were shown for the slow pyrolysis experiments of longleaf pine litter conducted in the pyrolyzer at different temperatures, heating rates, and sweep gas flow rates to find an optimum operating condition to obtain the highest tar yield. The main conclusions are listed as follow:

- 1- The change in heating rate had only a small effect on tar yield at these slow heating rates, but a greater impact on char yield.
- 2- Among the pyrolysis operating parameters, temperature had the most important effect on product yields.
- 3- A temperature of 500 °C, heating rate of 30 °C min⁻¹, and sweep gas flowrate of 100 ml min⁻¹ was the optimum condition to produce the highest amount of tar from slow pyrolysis of dead longleaf pine litter.

Table 5-1: Comparative studies for pyrolysis of different biomass to obtain maximum tar yield

Biomass	Reactor	Temperature (°C)	Heating rate (°C min ⁻¹)	N ₂ flow rate (ml min ⁻¹)	Wt% tar	Reference
Apricot pulps	Fixed-bed reactor	550	5	100	23.3 ^a	Özbay et al. (2008)
Pine needles	Semi-batch	550	50	100	43.8 ^b	Varma and Mondal (2017)
<i>Ferula orientalis L.</i>	Fixed-bed reactor	500	50	100	45.2 ^c	Aysu and Küçük (2014)
Blue-green algae blooms	Fixed-bed reactor	500	-	100	54.9 ^b	Hu et al. (2013)
Corn cob	Fixed-bed reactor	500	40	100	26.4 ^a	Demiral et al. (2012)
Bamboo	Laboratory-scale pyrolysis reactor	500	10	70	36.5 ^b	Chen et al. (2015a)
<i>Jatropha curcas</i> cake	Fixed-bed reactor	550	5	100	45.0 ^b	Majhi et al. (2015)
Tea waste	Fixed-bed reactor	500	300	200	29.6 ^b	Uzun et al. (2010)
Karanja seed	Semi batch reactor	550	-	50	55.1 ^b	Shadangi and Mohanty (2014)
microalgae <i>Scenedesmus dimorphus</i>	Fixed-bed reactor	500	40	100	36.6 ^b	Bordoloi et al. (2016)
hornbeam (<i>Carpinus betulus L.</i>) sawdust	Fixed-bed reactor	550	30	100	35.2 ^a	Morali et al. (2016)
Palm Shell	Fluidized-bed reactor	500	-	2000	47.3 ^b	Abnisa et al. (2011)

^a dry, ash-free basis^b Basis is not mentioned in the literature^c ash-free basis, including water

6 SLOW PYROLYSIS OF PLANT SPECIES USING THE PYROLYZER APPARATUS⁶

This chapter provides the results from the slow pyrolysis experiments for live and dead plant species using the pyrolyzer apparatus. The optimum pyrolysis operating condition with a temperature of 500 °C, heating rate of 30 °C min⁻¹ and sweep gas flowrate of 100 ml min⁻¹ found in the first group of experiments was used to determine the pyrolysis products yields for all live and dead plant species (as explained in chapter 5).

6.1 Pyrolysis Product Yields

The distribution of pyrolysis products (tar, light gas, and char) depends on several factors such as plant species, reactor configuration, operating conditions, etc. Figure 6-1 illustrates the product yields for live and dead plant species, respectively, obtained at the optimum tar yield condition. The results are the average of three experiments expressed on a dry, ash-free (daf) basis. The 95% confidence intervals for these data are shown as error bars in Figure 6-1, showing excellent data reproducibility.

As shown in Table 6-1, Tar yields varied between 44.4 wt% and 54.1 wt% for live plants, and 45.1 – 55.1 wt% for dead plant species (daf basis). The yields of light gas were in the range of 19.8 – 29.1 wt% for live plant species, and 18.8 – 30.4 wt% for dead plants. Char yields varied from 23.1 wt% to 28.2 wt% for live plant species, and between 23.2 – 28.3 wt% for dead plants.

⁶ The results of this chapter were published in Fuel (Amini et al., 2019)

The highest amount of tar was obtained from pyrolysis of dwarf palmetto (live and dead), with a yield of 54.1 wt% (daf).

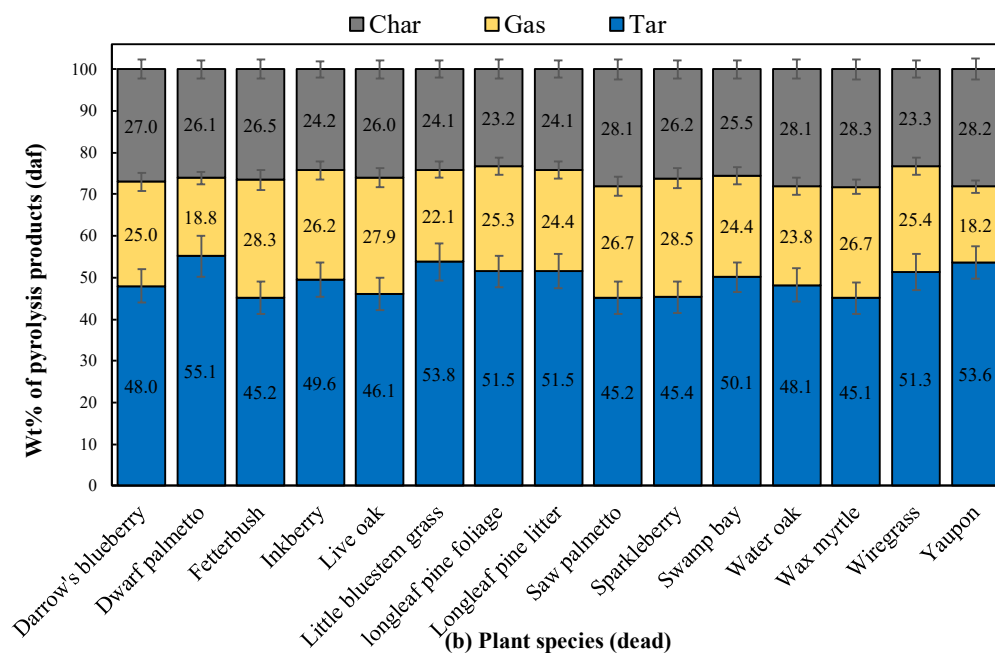
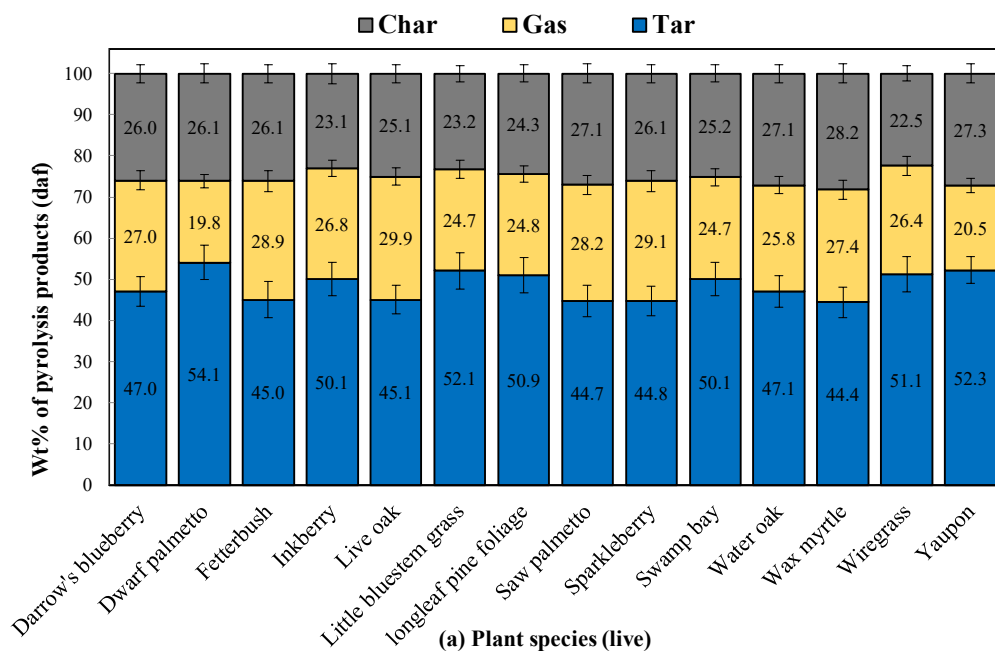


Figure 6-1: Pyrolysis product distributions of (a) live and (b) dead plant species on a daf basis. Error bars represent the 95% confidence intervals based on three samples.

Table 6-1: Pyrolysis products variation for live and dead plant species

Pyrolysis products (daf)	Live (wt%)	Dead (wt%)
Tar	44.4 - 54.1	45.1 - 55.1
Gas	19.8 - 29.1	18.8 - 30.4
Char	23.1 - 28.2	23.2 - 28.3

The results showed that the pyrolysis products yields from live and dead plant samples of the same species differed only slightly, and the plant species appears to be more important than live vs. dead samples for pyrolysis product distribution. Similar results were obtained by (Safdari, 2018) which studied the distribution of the fast pyrolysis products of the same plant species. This information is important for wildland fire modelers which previously assumed the fuel beds of the wildland fires as homogenous and did not consider different types of plant species.

6.2 Light Gas Analysis

Figure 6-2 represents the light gas compositions on a dry wt% (H₂O-free) basis resulting from slow pyrolysis of plant samples (live and dead) at the optimum operating condition of 500 °C with a heating rate of 30 °C min⁻¹ and sweep gas flowrate of 100 ml min⁻¹. The 95% confidence intervals for these data are shown as error bars in Figure 6-2, showing excellent data reproducibility. Despite slight differences due to type of plant, the gas composition for all plant species were similar and mainly consist of CO, CO₂, H₂, and CH₄. Gas species with higher carbon number (e.g., C₂H₆, C₃H₈, etc.) were not observed within the detection limits of the GC-TCD instrument (500 ppm). CO was the dominant compound in the light gases on a wt% dry basis, followed by CO₂, CH₄, and H₂ for both live and dead plant species. For live plant samples, CO yield ranged from 47.2 wt% for dwarf palmetto to 57.6 wt% for longleaf pine foliage.

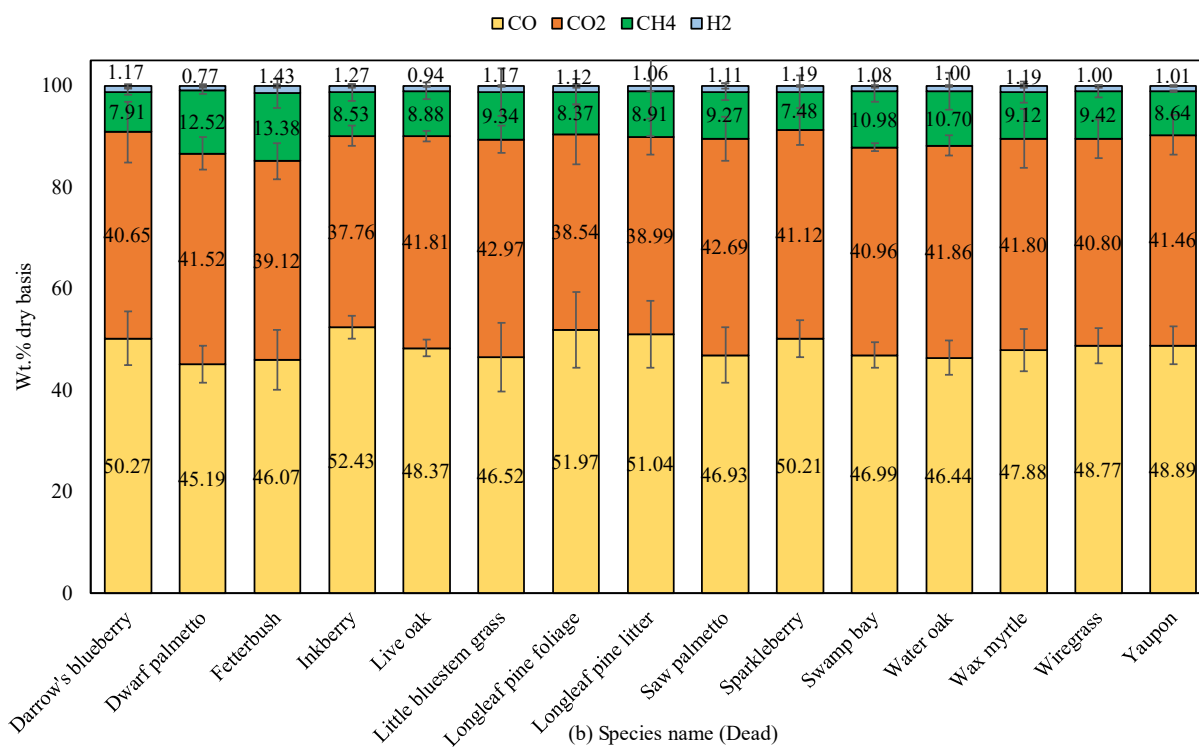
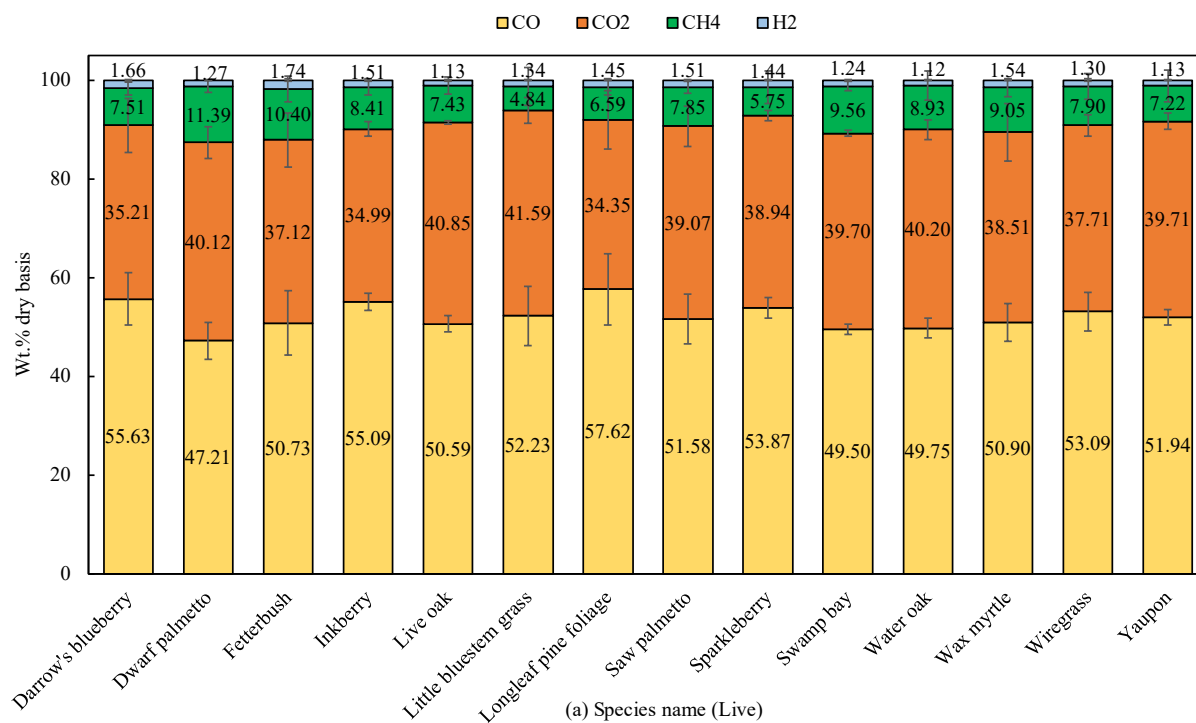


Figure 6-2: Composition of light gases (dry basis) obtained from pyrolysis of: a) live and b) dead plants. Error bars represent the 95% confidence intervals based on three samples.

For dead plant samples, the yield of CO was between 45.2 wt% for dwarf palmetto and 52.4 wt% for inkberry. On average, the CO yield for live samples was 3.8 wt% (absolute) higher than the corresponding dead samples. The largest statistical difference in carbon monoxide composition between live and dead samples ($P < 0.05$) was observed in the little bluestem grass (5.7 wt% on an absolute basis), followed by longleaf pine foliage (5.6 wt%) and Darrow's blueberry (5.4 wt%).

CO₂ was the second most dominant light gas composition which varied between 34.4 wt% and 41.6 wt% for live plants, and 37.8 wt% and 43.0 wt% for dead plants. On average, the CO₂ yield for live samples was 2.5 wt% (absolute) lower than the corresponding dead samples. Darrow's blueberry demonstrated the largest statistical difference in carbon dioxide composition (5.4 wt%) between live and dead samples ($P < 0.05$). Longleaf pine foliage (4.2 wt%) and saw palmetto (3.6 wt%) had the next largest statistical differences ($P < 0.05$) in CO₂ composition between live and dead samples.

CH₄ yield varied from 4.8 wt% to 11.4 wt% for live plants and from 6.6 to 13.4 wt% for dead plants. On average, the CH₄ yield for live samples was 1.6 wt% (absolute) lower than the corresponding dead samples. The little bluestem grass showed the highest statistical difference in methane composition (4.5 wt%) between live and dead samples ($P < 0.05$).

The yield of H₂ ranged between 1.1 and 1.7 wt% for live plants and between 0.8 and 1.2 wt% for dead plants. On average, the H₂ yield for live samples was 0.3 wt% (absolute) higher than the corresponding dead samples. The largest statistically differences ($P < 0.05$) between live and dead plant samples were observed in Dwarf palmetto (0.5 wt%), Darrow's blueberry (0.48 wt%), and saw palmetto (0.4 wt%). From a combustion prospective, the difference in weight fraction of H₂ was minor among all the live or dead plant species. The results of this study are

supported by biomass pyrolysis literature where similar gas components were reported (Encinar et al., 2000; Uçar and Karagöz, 2009; Fu et al., 2011; Varma and Mondal, 2017). The main gas products from pyrolysis are formed from specific functional groups (Yang et al., 2007). For example, the cracking and reforming of the carbonyl $C=O$, ether $C-O-C$, and carboxylic acid ($COOH$) are likely to produce CO , CO_2 at temperatures below $600\text{ }^{\circ}C$, and the formation of CH_4 is mainly due to the fracture of $O-CH_3$ groups (Chen et al., 2016). The chemical structure of biomass components affects the chemical composition of the light gas products. For example, hemicellulose displays a higher CO_2 yield due to higher carboxyl content, and cellulose pyrolysis leads to a higher CO yield, mainly because of thermal cracking of carbonyl and carboxyl. The release of H_2 and CH_4 are mainly attributed to the pyrolysis of lignin (Chen et al., 2014; Dhyani and Bhaskar, 2017).

For longleaf pine, no significance differences in weight fractions of the major light gas components were observed between the dead sample and pine straw, showing that aging did not affect the light gas composition yields. Based on the results of the light gas analysis, it may be acceptable to consider an average light gas composition (dry basis) for live or dead plant species. Similar results were obtained from the fast pyrolysis of the same plant species (Safdari, 2018).

6.3 Tar Characterization

A typical GC-MS chromatogram of tar obtained from pyrolysis of longleaf pine litter at the optimum condition is given in Figure 6-3. This is one example of more than 90 tar analysis experiments performed. Tars obtained from the slow pyrolysis of live and dead plant species in the pyrolyzer apparatus were a complex mixture of C_5 - C_{20} organic aromatic (Ar), non-aromatic (Non-Ar), oxygenated aromatic (ArO), and some N-containing components. As an example, the yields of tar components categorized as Ar, ArO, Non-Ar, and N-contain compounds for

Darrow's blueberry and dwarf palmetto are presented in Figure 6-4. The results for all plant species are presented in Appendix A (Figure A-1). As shown in Figure 6-4 and Figure A-1, ArO compounds were the most prevalent species in tar obtained from pyrolysis of all live and dead plant samples.

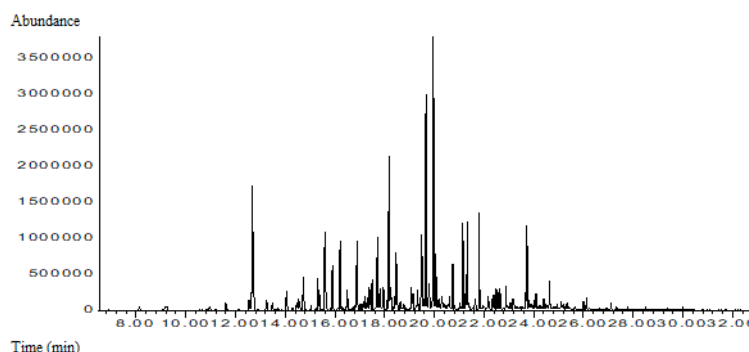


Figure 6-3: Gas chromatogram of tar obtained at 500 °C for pyrolysis of longleaf pine litter.

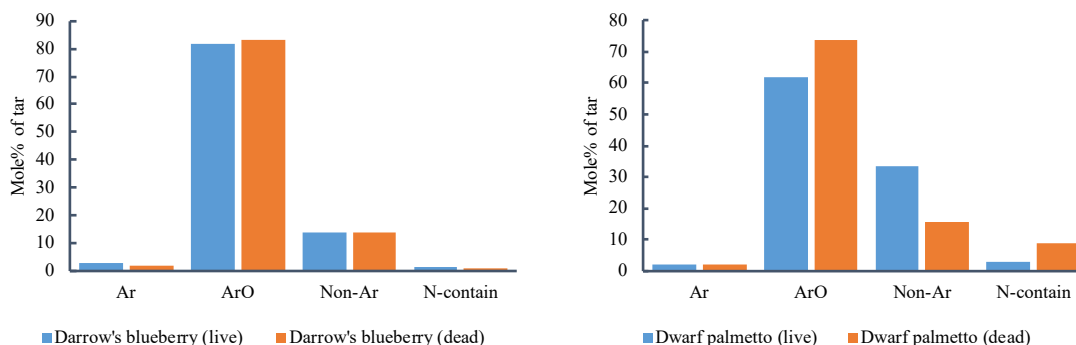


Figure 6-4: The yields of tar components categorized as Ar, ArO, Non-Ar, and N-containing compounds for live and dead Darrow's blueberry and dwarf palmetto.

The majority of aromatic compounds were one-ring aromatics with OH attachments. As expected, plants from the same family have similar behavior in the formation of tar compounds. For example, the slow pyrolysis of dead saw palmetto and dead dwarf palmetto both formed more ArO compounds than live samples. In contrast, tar obtained from slow pyrolysis of dead water

oak and dead live oak both contained less ArO compounds than live samples. More than 200 compounds were identified in tars obtained from slow pyrolysis of all plant species (live and dead); the most prevalent components are listed in Table 6-2. All identified tar components are presented in Appendix B (Table B-1).

Phenolic compounds, such as phenol, 1,2-benzenediol, and 2-methyl phenol which all belong to the ArO group, are the most prevalent species in tar (Table 6-2). The other components belong to aldehyde, ketone, alcohol, furan, acid, and phenyl groups. Single-ring aromatics with OH attachments were the most dominant components observed in the tar obtained from live and dead samples at these conditions. Very few multi-ring components were observed. Due to the moderate temperature (500 °C) and the fact this temperature corresponded to the maximum tar yield at slow heating rates, the tar species observed seem to be primary pyrolysis products, without being influenced by further “secondary” pyrolysis reactions in the gas phase. As an example, the distribution of the most prevalent components in tar obtained from pyrolysis of longleaf pine is shown in Figure 6-5. The results for all other plant species are presented in Appendix C (Figure C-1). The 95% confidence intervals for these data are shown as error bars in Figure 6-5 and Figure C-1, showing excellent data reproducibility.

Tar analysis results revealed that tar composition was different for different plant species. For example, phenol ranged from 1.9 mol% in dead longleaf pine litter to 38.7 mol% in dead dwarf palmetto. Dead saw palmetto and dead dwarf palmetto, which are from the same family, had very high phenol yields of 33.7 mol% and 38.7 mol%, respectively. A considerable difference in phenol composition in tar was observed for dead longleaf pine foliage and dead longleaf pine litter. While dead longleaf pine foliage had a phenol composition of 18.8 mol%, tar obtained from pyrolysis of longleaf pine litter contained only 1.9 mol% phenol.

Table 6-2: The most prevalent components observed in tar

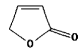
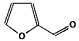
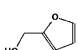
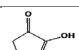
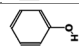
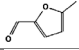
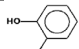
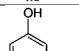
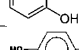
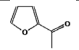
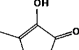
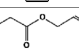
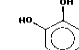
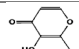
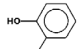
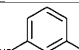
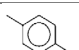
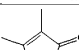
#	Peak retention time (min)	Component	M.F.	Chemical class	Functional group	Structure
1	13.665	2(5H)-Furanone	C ₄ H ₄ O ₂	ArO	Ketone	
2	12.681	Furfural	C ₅ H ₄ O ₂	ArO	Aldehyde	
3	13.251	2-Furanmethanol	C ₅ H ₆ O ₂	ArO	Alcohol	
4	14.72	2-Cyclopenten-1-one, 2-hydroxy-	C ₅ H ₆ O ₂	ArO	Ketone	
5	15.893	Phenol	C ₆ H ₆ O	ArO	Phenol	
6	15.597	2-Furancarboxaldehyde, 5-methyl-	C ₆ H ₆ O ₂	ArO	Aldehyde	
7	19.29	1,2-Benzenediol	C ₆ H ₆ O ₂	ArO	Phenol	
8	20.599	1,3-Benzenediol	C ₆ H ₆ O ₂	ArO	Phenol	
9	20.632	1,4-Benzenediol	C ₆ H ₆ O ₂	ArO	Phenol	
10	14.147	Ethanone, 1-(2-furanyl)-	C ₆ H ₆ O ₂	ArO	Ketone	
11	16.872	2-Cyclopenten-1-one, 2-hydroxy-3-methyl-	C ₆ H ₈ O ₂	ArO	Ketone	
12	17.415	Propanoic acid, 2-propenyl ester	C ₆ H ₁₀ O ₂	Non-Ar	Acid	
13	22.397	1,2,3-Benzenetriol	C ₆ H ₆ O ₃	ArO	Phenol	
14	18.461	Maltol (Larixic acid)	C ₆ H ₆ O ₃	ArO	Acid	
15	17.387	Phenol, 2-methyl-	C ₇ H ₈ O	ArO	Phenol	
16	16.971	Phenol, 3-methyl-	C ₇ H ₈ O	ArO	Phenol	
17	17.3	Phenol, 4-methyl-	C ₇ H ₈ O	ArO	Phenol	
18	16.779	2-Cyclopenten-1-one, 2,3-dimethyl-	C ₇ H ₁₀ O	ArO	Ketone	

Table 6-2 Continued

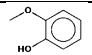
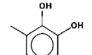
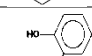
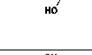
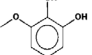
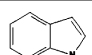
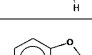
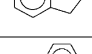

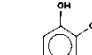
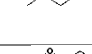
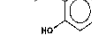
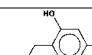
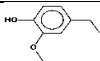
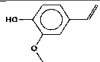
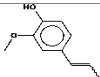
#	Peak retention time (min)	Component	M.F.	Chemical class	Functional group	Structure
19	17.739	Phenol, 2-methoxy-	C ₇ H ₈ O ₂	ArO	Phenol	
20	20.312	1,2-Benzenediol, 3-methyl-	C ₇ H ₈ O ₂	ArO	Phenol	
21	20.721	1,2-Benzenediol, 4-methyl-	C ₇ H ₈ O ₂	ArO	Phenol	
22	20.579	1,2-Benzenediol, 3-methoxy-	C ₇ H ₈ O ₃	ArO	Phenol	
23	21.001	Indole	C ₈ H ₇ N	N-Contain	Benzenoid	
24	19.666	Benzofuran, 2,3-dihydro-	C ₈ H ₈ O	ArO (2r)	Furans	
25	18.909	Phenol, 4-ethyl-	C ₈ H ₁₀ O	ArO	Phenol	
26	19.949	2-Methoxy-5-methylphenol	C ₈ H ₁₀ O ₂	ArO	Phenol	
27	19.534	Phenol, 2-methoxy-4-methyl-	C ₈ H ₁₀ O ₂	ArO	Phenol	
28	19.515	1,3-Benzenediol, 4-ethyl-	C ₈ H ₁₀ O ₂	ArO	Phenol	
29	22.551	1,2-Benzenediol, 4-ethyl-	C ₈ H ₁₀ O ₂	ArO	Phenol	
30	19.251	1,3-Benzodioxole, 2-methoxy-	C ₈ H ₈ O ₃	ArO	Phenyl	
31	21.727	Phenol, 2,6-dimethoxy-	C ₈ H ₁₀ O ₃	ArO	Phenol	

Table 6-2 Continued

#	Peak retention time (min)	Component	M.F.	Chemical class	Functional group	Structure
32	20.894	Phenol, 4-ethyl-2-methoxy-	C ₉ H ₁₂ O ₂	ArO,	Phenol	
33	21.387	2-Methoxy-4-vinylphenol	C ₉ H ₁₀ O ₂	ArO	Alcohol	
34	23.284	Phenol, 2-methoxy-4-(1-propenyl)-	C ₁₀ H ₁₂ O ₂	ArO	Phenol	

The results showed that dead longleaf pine foliage and dead longleaf pine litter yield different tar compositions at these experimental conditions and that metabolic process associated with foliage weathering once the needles have been cast are likely causes for the difference.

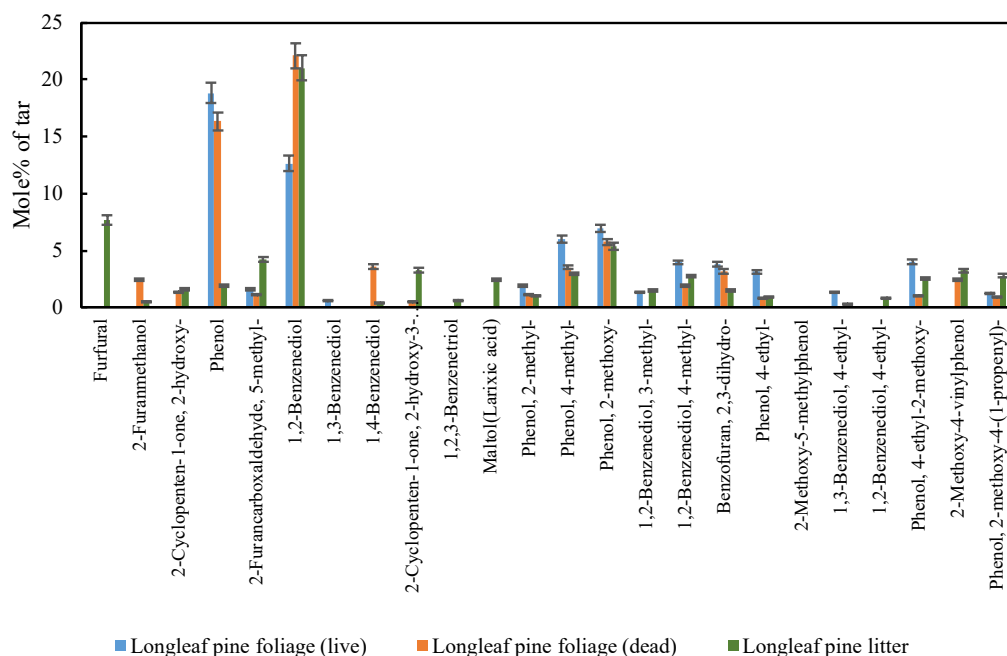


Figure 6-5: The distribution of most prevalent components in tar obtained from pyrolysis of plant species. Error bars represent the 95% confidence intervals based on three samples.

There are quite a few minor tar species with mole fractions less than 5 mol%. Some of these minor species (and occasionally major species) are only observed in the pyrolysis products from live samples, while others are only observed from dead samples. For example, tars from live water oak consisted of furfural (8 mol%), maltol (larixic acid) (1.5 mol%), 2-methyl phenol (1.4 mol%), 2-methoxy 5-methyl phenol (2.8 mol%), and 4 ethyl-1,3- benzenediol (0.8 mol%), none of which were observed in the tars from the dead water oak. However, 1,2,3 benzenetriol (1.1 mol%) and 2,3 dihydrobenzofuran (3.1 mol%) were only observed in the tars from dead water oak. Similar minor changes in tar species between live and dead samples were observed for other plant species.

It is not clear how these relatively minor changes in tar species between live and dead plant species will change the combustion characteristics.

It has been reported that many of the components in biomass tar are primary products of lignin degradation (280 – 500 °C) during pyrolysis (Aysu and Küçük, 2014). The presence of phenolic hydroxyl and methoxy groups in chemical structure of lignin makes it highly reactive. In general, phenols are mainly produced from the degradation of lignin which is a rich source of phenolic components; furans, ketones and carboxylic acids are thought to come from cellulose and hemicellulose degradation (Uçar and Karagöz, 2009; Aysu and Küçük, 2014; Chen et al., 2016). In addition, decomposition of lignin leads to the formation of aromatic carbons, since lignin contains aromatic rings in its chemical structure (Farag et al., 2014). Hemicellulose has random amorphous structure with little strength which makes it highly activated in thermal decomposition. Generally, pyrolysis of hemicellulose (200-280 °C) mainly produces acids and furfural (Aysu and Küçük, 2014; Chen et al., 2016). In contrast, cellulose has a good ordered structure with long polymer of glucose which make it thermally stable. Cellulose pyrolysis leads to a high tar yield (Chen et al., 2016), but not necessarily aromatic compounds. Furans, cyclopentanone, and linear carbonyls are mainly formed by depolymerization and fragmentation of active cellulose (240 - 350 °C) (Chen et al., 2016).

The volatiles yields obtained in this study are compared with the ASTM proximate analysis (reported by Safdari, et al., (2018a) (Figure 6-6). It can be seen that, for most plant species the total volatiles yield from the ASTM analysis is a few absolute percentage points higher than the yields from the pyrolyzer apparatus due to the higher temperature (750 °C) of the ASTM analysis method. However, the 500 °C condition used in the pyrolyzer apparatus minimized secondary reactions of tar species, which was the aim of the present experiments.

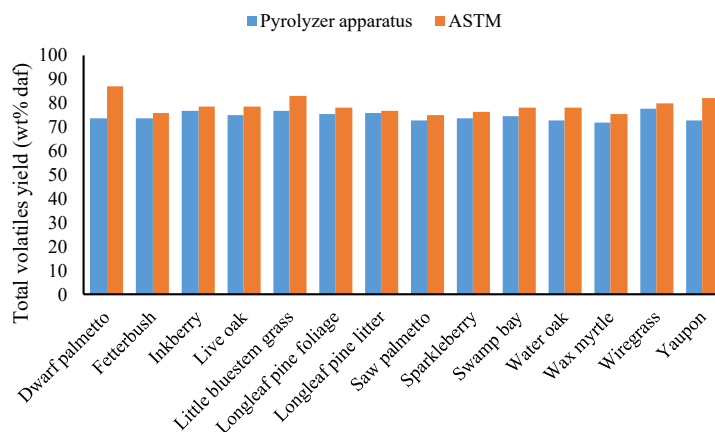


Figure 6-6: Total volatile yields obtained from slow pyrolysis experiments in pyrolyzer apparatus and ASTM analysis.

6.3.1 Functional Group Distribution in Tar

Figure 6-7 shows the functional groups distribution in tar obtained from slow pyrolysis of four plant species, which are representative of palmetto-type, grass, broadleaf, and needle-like species. Phenols are the most prevalent components in tar obtained from pyrolysis of all plant types, ranging from 56.9 wt% for live dwarf palmetto to 70.5 wt% for live longleaf pine. Ketones, aldehydes, and acids comprised a significant amount of the tars from all plant species, ranging between 4.7 – 19.2 wt%, 1.2 – 8.70 wt%, and 5.1 – 12.0 wt%, respectively. Moreover, furans comprised 4.3 wt% and 8.1 wt% of live longleaf pine (needle-like species) and dead little bluestem (grass).

Differences between the distribution of functional groups in tar for live and dead plant samples were small. For example, tar obtained from the pyrolysis of live and dead longleaf pine contained 70.5 and 68.2 mol% phenols, respectively. Aldehydes comprised 6.0 mol% of the tar obtained from pyrolysis of live longleaf pine foliage vs. about 2.7 mol% from dead longleaf pine foliage. In contrast, large differences were observed in the functional group distribution in tars obtained from pyrolysis of different plant species. For live longleaf pine (needle-like species),

the tar contained more than 70 mol% phenolic compounds vs. 58.2 mol% phenolic compounds in tar from live Inkberry (broadleaf species).

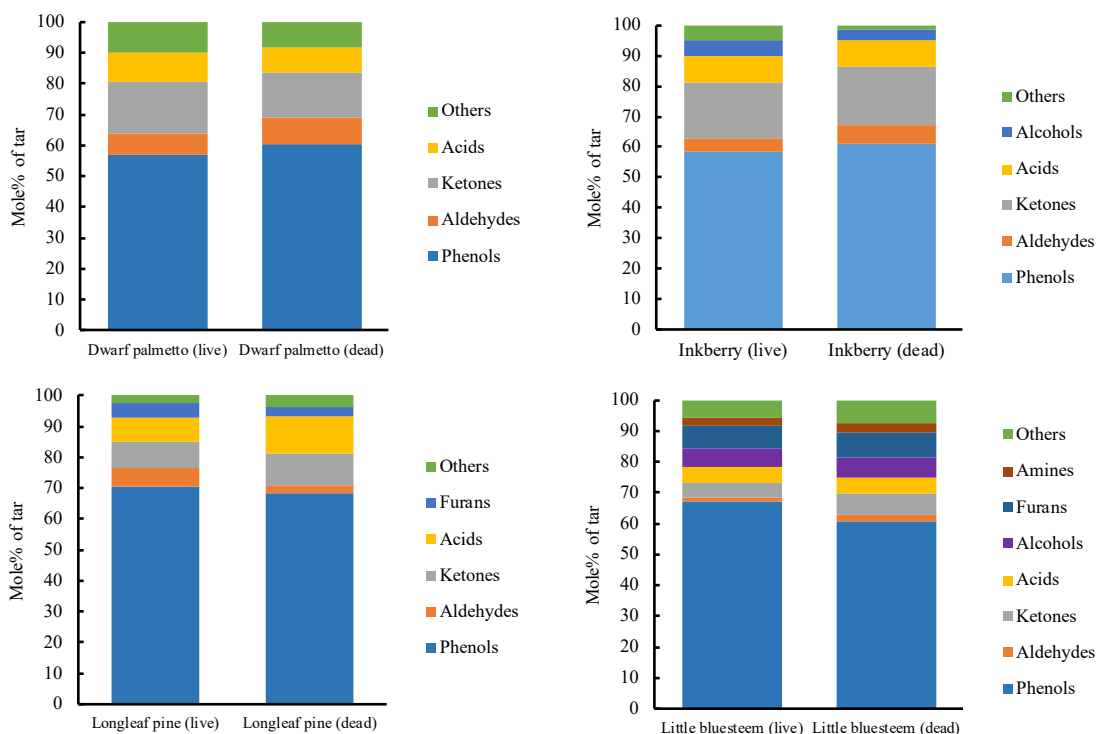


Figure 6-7: Functional groups distribution in tar for live and dead plants.

6.4 Summary and Conclusion

In this chapter, the slow pyrolysis experiments were performed for all live and dead plant species in the pyrolyzer at optimum operating condition. The yield of pyrolysis products as well as analysis of tar and light gas characterization were studied. The main conclusions are listed as follow:

- 1- Tar and gas species are the primary pyrolysis products, without being influenced by further secondary pyrolysis reactions in gas phase due to moderate temperature (500 °C).
- 2- CO was the dominant light gas species for all plant samples on a dry, wt% basis,

followed by CO₂, CH₄ and H₂. Live plant species had slightly higher weight fractions of CO and H₂ (average differences of 3.8 and 0.3 wt% absolute, respectively) than corresponding dead samples, but slightly lower weight fractions of CO₂ and CH₄ (average differences of 2.5 and 1.6 wt% absolute, respectively).

- 3- Tar and light gas yields from live and dead plant samples of the same species differed only slightly.
- 4- The plant species appears to be more important than live vs. dead samples for tar species formed as well as for pyrolysis product distribution and light gas analysis.
- 5- Tar and light gas yields ranged between 44.4 – 54.1 wt% (daf) and 23.1 – 28.2 wt% (daf) for live plant samples, respectively.
- 6- The main constituents identified in the tar obtained from the slow pyrolysis of live and dead plant samples were oxygenated aromatics (ArO), which were mainly phenolic compounds (-OH).
- 7- Single-ring aromatics with OH attachments were the most prevalent compounds observed in the tar obtained from live and dead samples at these conditions. Very few multi-ring compounds were observed.
- 8- No significant differences between the distribution of functional groups in tar were observed for live and dead plant samples for a given plant species. In contrast, there were significant differences in the functional groups distribution in tars obtained from pyrolysis of different plant species.
- 9- Based on the product distributions observed in these experiments, differences in the fire behavior of live and dead fuels should be largely due to moisture content, since only small differences were observed in pyrolysis product distributions and tar components.

7 PYROLYSIS KINETICS OBTAINED FROM ISO-CONVERSIONAL METHODS⁷

In this chapter, first, the time-dependent mass-loss characterization of the all plant species (live and dead) at a heating rate of 30 °C min⁻¹ was studied. Second, the model-free method of KAS was used to calculate the kinetic parameters for all live and dead plant species, describing both the water evaporation and thermal devolatilization mechanisms. Third, the rate of pyrolysis was calculated for all live and dead plant species. The effect of aging on the activation energy was also studied using naturally-abscised foliage with a long drying time.

7.1 TGA Results

Over the entire temperature range, the pyrolysis of biomass contains two main stages after the drying process: (a) decomposition of the majority of the biomass and (b) subsequent minor amounts of devolatilization (Ozsin and Putun, 2017). Biomass pyrolysis (especially woody biomass) can be normally explained by degradation of three main components, namely cellulose, hemicellulose and lignin. However, foliar materials like leaves contain significant amounts of other compounds, such as lipids, glucose, protein, fructose, pectin, etc. (Fourty et al., 1996; Safdari, 2018; Matt et al., 2020). In addition, it has been reported that inorganic components and minor extractives affect degradation behavior by having some catalytic effects on pyrolysis of

⁷ The results of this chapter were published in the Journal of Analytical and Applied Pyrolysis (Amini et al., 2019b)

biomass (Meng et al., 2015; Ozsin and Putun, 2017). Sample TGA analyses during the pyrolysis process of live saw palmetto and dead saw palmetto at a heating rate of $30\text{-}^{\circ}\text{C min}^{-1}$ are presented in Figure 7-1. The TG and DTG curves for all other plant species are presented in Appendix D (Figure D-1).

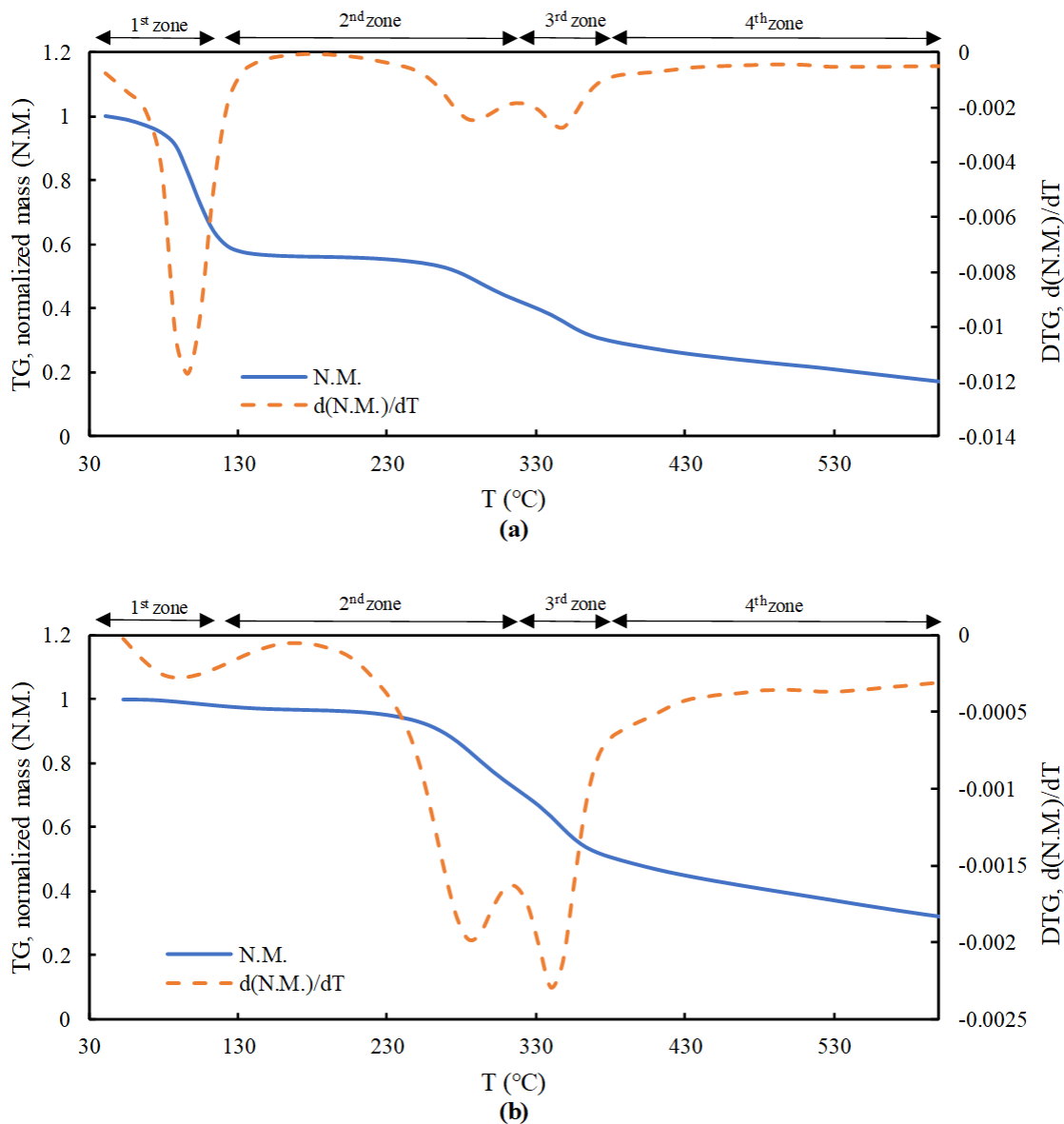


Figure 7-1: TG/DTG curves of pyrolysis of a) live saw palmetto b) dead saw palmetto with a heating rate of $30\text{ }^{\circ}\text{C min}^{-1}$.

Mass remaining was normalized by the initial mass on the left-hand axis, and the derivative of the normalized mass is shown on the right-hand axis. Four major zones were identified in Figure 7-1 based on the derivative curve. According to Figure 7-1, both live and dead saw palmetto consisted of four zones.

The first zone (30 – 160 °C) is the drying zone where live saw palmetto and dead saw palmetto lost 44 and 3.3 wt% of the total mass, respectively. The mass release in this zone is thought to be due mainly to moisture evaporation, possible degradation of light organic components, and hydrolysis of some extractives (White et al., 2011; Balogun et al., 2014; Mehmood et al., 2017; Ozsin and Putun, 2017). Free water and bound water are two types of water distributed in biomass. Bound water has strong bonding force with the materials, whereas free water has a weak bonding force. By increasing the temperature, biomass first loses the free water before about 90 °C and then the bound water starts to evaporate. At temperatures around 160 °C, most of the water is removed and the mass loss of biomass is very small (Chen et al., 2013). Treatments of water evaporation include heat transfer-limited models, equilibrium models, chemical rate models, and mass transfer models (Chan et al., 1985; Lu et al., 2008; Prince, 2014). For simplicity, and for comparative purposes, the moisture release in the TGA experiments is treated here as a first-order chemical rate with an Arrhenius rate coefficient.

The next two zones (250 – 430 °C) are fast devolatilization zones where active pyrolysis occurred and the sample lost a large portion of weight, as indicated by two significant mass-loss peaks (shown in derivative curve). Similar results were reported for sabal palmetto, where the highest mass loss occurred at medium temperatures (300 – 400 °C) (Buessing and Goldfarb, 2012). The 4th zone is the slow degradation zone. The data shown in Figure 7-1 (as well as data from all other plant species studied here) are consistent with reports that active pyrolysis of

biomass at slow heating rates varying between $5 - 50\text{ }^{\circ}\text{C min}^{-1}$ occurs at temperatures above $200\text{ }^{\circ}\text{C}$ (Nassar, 1985; Ramajo-Escalera et al., 2006; Bonelli et al., 2007; Radhakumari et al., 2016) and below $450\text{ }^{\circ}\text{C}$ (Munir et al., 2009; White et al., 2011).

The DTG peaks of live and dead samples are similar in position and height except for the first peak representing the mass loss due to evaporation. Note the change in scale of the right-hand axis. The difference in the height of the first peak is due to the different moisture content of live and dead samples. Similar peak heights and locations in zones 2 and 3 indicate that the live and dead samples of saw palmetto do not differ in volatiles content. These TGA results are consistent with results from Amini et al. (2019) that the gas and tar yields were similar for live and dead samples of each of the 14 plant species studied.

In the second zone ($250 - 320\text{ }^{\circ}\text{C}$), the mass loss on a dry basis ($24.1\text{ wt}\%$ for LSP and $25\text{ wt}\%$ for DSP) may be partially attributed to the hemicellulose decomposition (Damartzis et al., 2011). However, the weight loss in this zone for both live and dead samples was higher than the hemicellulose content of saw palmetto ($18.6\text{ wt}\%$ dry basis) due to possible degradation of lignin which has a wider range of degradation temperature ($100 - 800\text{ }^{\circ}\text{C}$) (Ma et al., 2015). Hemicellulose has a lower thermal stability than cellulose because it is a mixture of different polymerized monosaccharides (xylose, glucose, galactose, mannose, arabinose, etc.) with a lower degree of polymerization. Ma et al. (2015) showed that the main hemicellulose degradation occurred at temperatures from 185 to $325\text{ }^{\circ}\text{C}$. However, the mass loss in this zone for both the live and dead samples may also be due to possible degradation of lignin, which has a wider range of degradation temperature ($100 - 800\text{ }^{\circ}\text{C}$), and degradation of other constituents such as lipids, glucose, protein, fructose, pectin, minerals, etc. (Damartzis et al., 2011; Ma et al., 2015).

In the third zone ($320 - 430\text{ }^{\circ}\text{C}$) in Figure 7-1, a mass loss of $26.3\text{ wt}\%$ and $25\text{ wt}\%$ (dry

basis) occurred for the live and dead samples, respectively, which may be due to the decomposition of both cellulose and lignin (Damartzis et al., 2011). Cellulose is a high-molecular component with long linear chain composed of d-glucosyl group, and has a partly crystalline structure made of ordered microfibrils (Lopez-Velazquez et al., 2013). This structure makes the thermal degradation of cellulose more difficult than hemicellulose (Yang et al., 2004; Ma et al., 2015).

During the last zone, namely the slow degradation zone with a long tail (400 – 604 °C), the mass loss of 19.5 wt% (dry basis) for the live sample and 16.4 wt% (dry basis) for the dead sample may be attributed to lignin degradation (Damartzis et al., 2011).

The main difference between pyrolysis of LSP and DSP is related to the first zone, namely the drying zone which occurred at temperatures between 30 – 160 °C. However, a small difference in the temperature range as well as the amount of mass loss during the zones were observed. Detailed information concerning the mass loss during each zone for all plant species (live and dead) is presented in Table 7-1.

Similar to saw palmetto, Darrow's blueberry (DB), swamp bay (SB), live oak (LO), water oak (WO), and wire grass (WG) showed a four-zone reaction process. The pyrolysis process of inkberry consisted of four zones. The pyrolysis of dwarf palmetto (DP), pine straw, longleaf pine foliage (LPF), and little bluestem grass (LBG) were two-zone processes. Figure 7-2 shows the DTG curves of pyrolysis of dead little bluestem grass (DLBG) and dead inkberry (DI) at a heating rate of 30 °C min⁻¹ as examples of plant species with three-zone and five-zone reaction process. The results showed that different plant species have different mass loss behavior. However, the pyrolysis rates for live and dead pyrolysis rates for a given plant species are almost the same.

Table 7-1: The mass loss % during different reaction zones for all plant species (live and dead) at heating rate of 30 °C min⁻¹

Scientific name	Common name		Zone 1 ^a	Zone 2 ^b	Zone 3 ^b	Zone 4 ^b	Zone 5 ^b
<i>Aristida stricta</i> Michx.	Wiregrass	Live	62.7	28.0	35.7	7.5	–
		Dead	6.5	28.1	33.7	7.2	–
<i>Ilex glabra</i> (L.) A. Gray	Inkberry	Live	51.3	40.4	13	15.7	4.6
		Dead	4.5	43.8	12.9	12.1	4.1
<i>Ilex vomitoria</i> Aiton ‘Schelling Dwarf’	Yaupon	Live	48.4	24.3	33.6	12.9	–
		Dead	4.5	28.2	39.7	13.1	–
<i>Lyonia lucida</i> (Lam.) K. Koch	Fetterbush	Live	69.4	24.5	32.4	13.2	–
		Dead	5.3	29.1	38.6	13.4	–
<i>Morella cerifera</i> (L.) Small	Wax myrtle	Live	54.7	18.9	24.9	21.4	–
		Dead	5.3	17.7	33.9	14.2	–
<i>Persea palustris</i> (Raf.) Sarg.	Swamp bay	Live	53.0	48.5	28.8	–	–
		Dead	6.9	52.8	15.8	–	–
<i>Pinus palustris</i> Mill.	Longleaf pine foliage	Live	66.5	59.3	11.3	–	–
		Dead	3.8	60.2	12.2	–	–
<i>Pinus palustris</i> Mill.	Longleaf pine litter	Naturally-abscised	4.7	61.3	12	–	–
<i>Quercus nigra</i> L.	Water oak	Live	52	28.9	26.6	15.3	–
		Dead	4.7	28.1	30.2	13.5	–
<i>Quercus virginiana</i> Mill.	Live oak	Live	49.4	20	32.3	13.3	–
		Dead	5.5	24.9	29.9	12.5	–
<i>Sabal minor</i> (Jacq.) Pers.	Dwarf palmetto	Live	61.1	55.4	16.6	–	–
		Dead	5.4	59.2	15.5	–	–
<i>Schizachyrium scoparium</i> (Michx.) Nash	Little bluestem grass	Live	65.1	59.5	9.9	–	–
		Dead	8.3	58.1	9.6	–	–

Table 7-1 Continued

Scientific name	Common name		Zone 1 ^a	Zone 2 ^b	Zone 3 ^b	Zone 4 ^b	Zone 5 ^b
<i>Serenoa repens</i> (W. Bartram) Small	Saw palmetto	Live	44	24.1	26.4	19.5	—
		Dead	3.3	25	25	16.4	—
<i>Vaccinium arboreum</i> Marshall	Sparkleberry	Live	54.4	19.8	27.4	13.3	—
		Dead	8.2	18.4	29.4	12.9	—
<i>Vaccinium darrowii</i> Camp “Rosa’s Blush”	Darrow’s blueberry	Live	70.9	35.3	25.9	11.9	—
		Dead	5.8	37.2	26.5	9.1	—

^a wt% of total mass

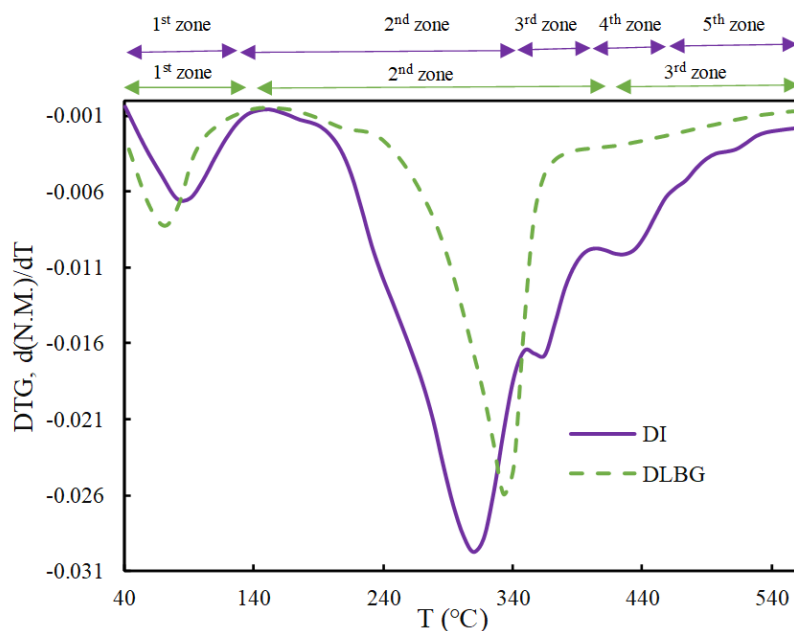


Figure 7-2: DTG curves of dead little bluestem grass (DLBG), and dead inkberry (DI) at the heating rate of 30 °C min⁻¹.

Comparing the DTG curves of pine straw with live and dead LPF revealed very similar mass loss behavior (see Table 7-1), indicating that the aging does not affect the amount of mass loss of a particular plant species (on a dry, ash-free basis). Figure 7-3 shows the variation of the peaks of the mass loss rate curves vs. temperature for the pyrolysis zones of all the plant species. The peaks represent the highest mass loss rate during the corresponding zone of pyrolysis. According to Figure 7-3a, for live samples, the first peaks occurred at a temperature range between 247 and 302 °C, and the second peaks occurred at temperatures ranging from 333 to 364 °C. Between live samples, little bluestem grass and wire grass had the highest mass loss rates, with DTG peaks values of -0.0085 and -0.0081 °C⁻¹ at temperatures of 333 and 340 °C, respectively. These rates were significantly different (and statistically significant with $P < 0.5$) than the maximum rates of the other species.

For dead samples, as shown in Figure 7-3b, the first peaks occurred at temperatures ranging

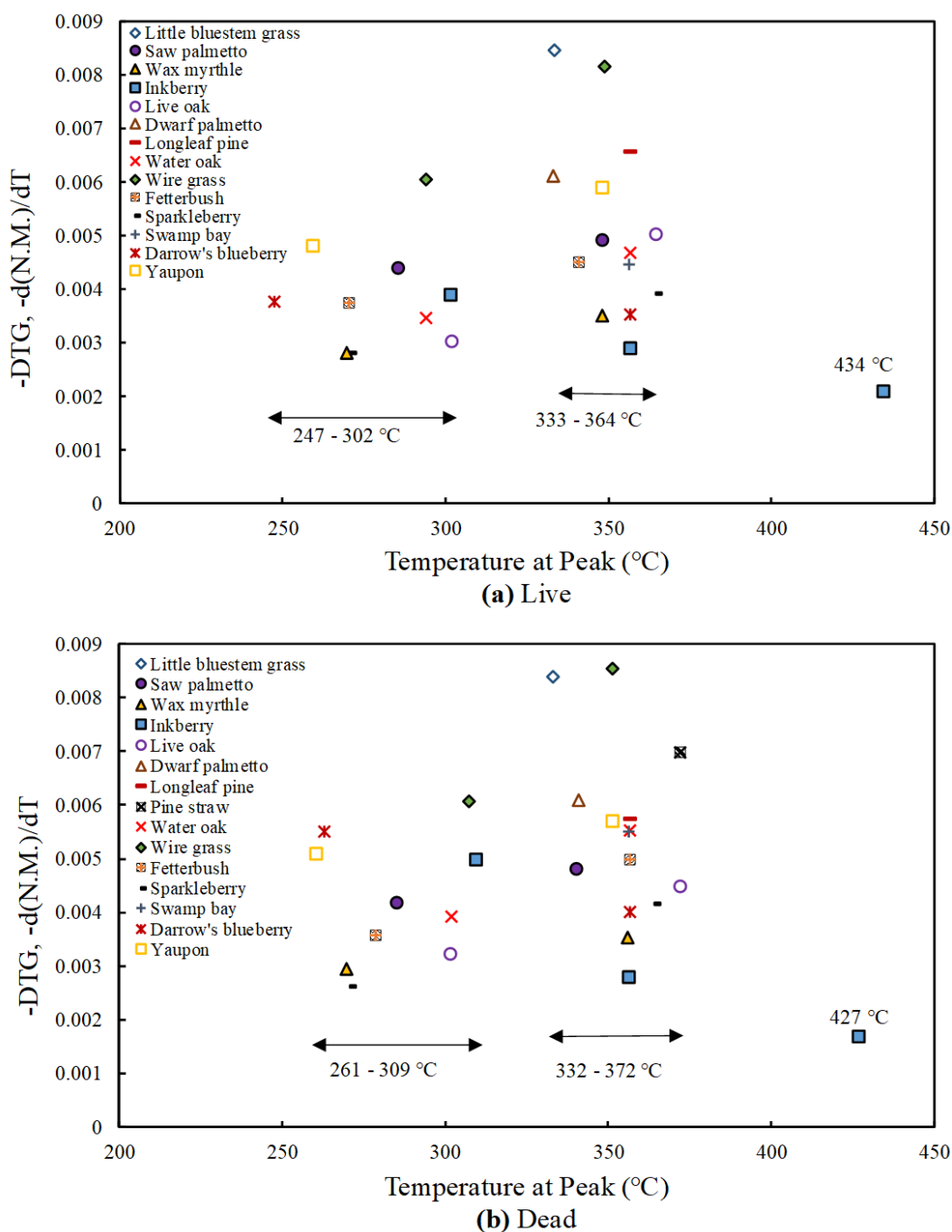


Figure 7-3: Temperature range of maximum mass loss rates during pyrolysis of all plant species.

from 261 to 309 °C, and the second peaks occurred in a temperature range between 332 and 372 °C. Inkberry was the only species that had the third peak (i.e., four-zone pyrolysis reaction, but the fourth zone did not have a peak). Between dead samples, wire grass and little bluestem

grass had the highest mass loss rate with DTG peaks values of -0.0085 and -0.0084 $^{\circ}\text{C}^{-1}$ at temperatures of 352 and 333 $^{\circ}\text{C}$, respectively, which was similar to observations for the live samples.

7.2 The Effect of Heating Rate

As an example of the change in pyrolysis rate vs. heating rate, the TG/DTG curves of pyrolysis of live saw palmetto at heating rates of 10 , 15 , 20 , 25 , and 30 $^{\circ}\text{C min}^{-1}$ are presented in Figure 7-4.

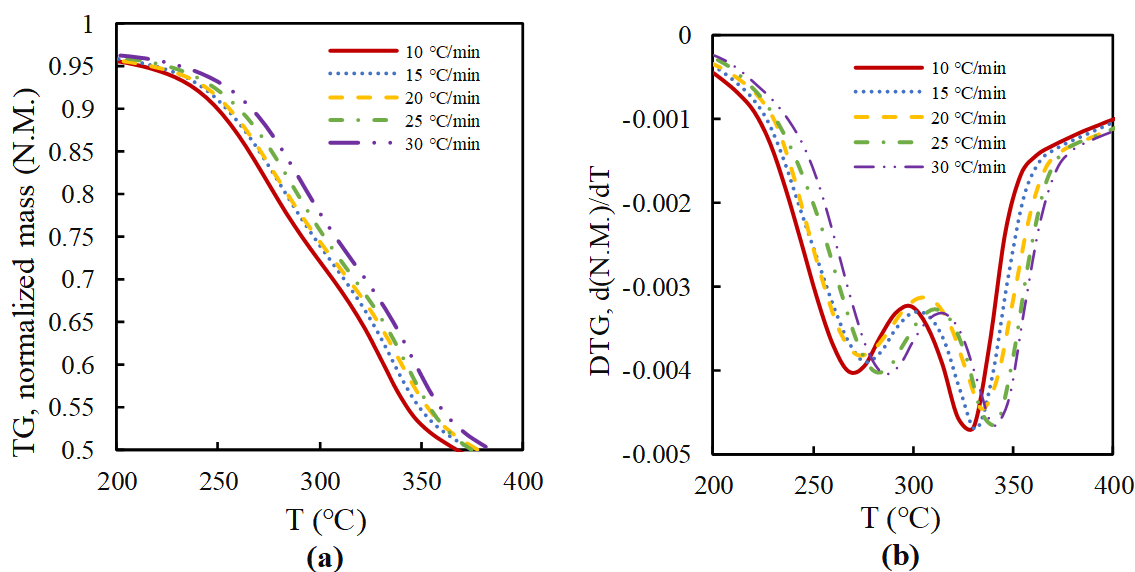


Figure 7-4: TG (a) and DTG (b) curves of pyrolysis of live saw palmetto at heating rates of 10 , 15 , 20 , 25 , and 30 $^{\circ}\text{C min}^{-1}$.

The mass release before 150 $^{\circ}\text{C}$ was excluded and the mass was renormalized to consider the process related to sample decomposition during the major pyrolysis zone and not water evaporation. As seen from Figure 7-4, the mass loss pattern (i.e., the general shape and number of peaks) and the maximum pyrolysis rate were the same at all heating rates, which indicates that the heating rate did not affect the degradation chemistry (Maia and de Moraes, 2016; Mehmood

et al., 2017). In addition, a shift in the temperatures of maximum mass loss rate points in both TG and DTG curves was observed. During pyrolysis at high heating rates, the reaction time is shorter and therefore the sample decomposes at a higher temperature (Ma et al., 2015; Banon et al., 2016). This shift in pyrolysis temperature with heating rate is a common occurrence for biomass and other solid fuels (Anthony et al., 1975; Vamvuka et al., 2003; Hu et al., 2007; Damartzis et al., 2011; Hillier and Fletcher, 2011; Cortés and Bridgwater, 2015; Ozsin and Putun, 2017; Dhaundiyal et al., 2018). The actual increase in overall mass loss with increasing heating rate, as shown in Figure 7-4a, was relatively small at any given temperature below about 500 °C. The same behavior of changes in pyrolysis rate and temperatures at peak rates was observed for all plant species.

7.3 Analysis of Activation Energy Using the KAS Method

To investigate the effect of conversion on apparent activation energy during the drying zone and the major pyrolysis zone, nine levels of conversion varying between 10% to 90% were used at five different heating rates of 10, 15, 20, 25, and 30 °C min⁻¹. The model-free KAS method was used to estimate apparent activation energies for all plant species (live and dead). The temperature was recorded for each specified conversion for a given heating rate, and then plotted in a way to regress the activation energy. As an example, Figure 7-5 illustrates the regression lines of live little bluestem grass and dead little bluestem grass for the drying and the major pyrolysis zones based on the KAS method. The regression lines of all other plant species for the drying and the major pyrolysis zones based on KAS method are presented in Figure E-1. The apparent activation energies for nine conversion degrees were calculated by the KAS method for the drying and for the major pyrolysis zones for both the live and dead samples. The correlation coefficients observed at all conversion degrees (0.1 – 0.9) ranged from 0.94 to 0.99.

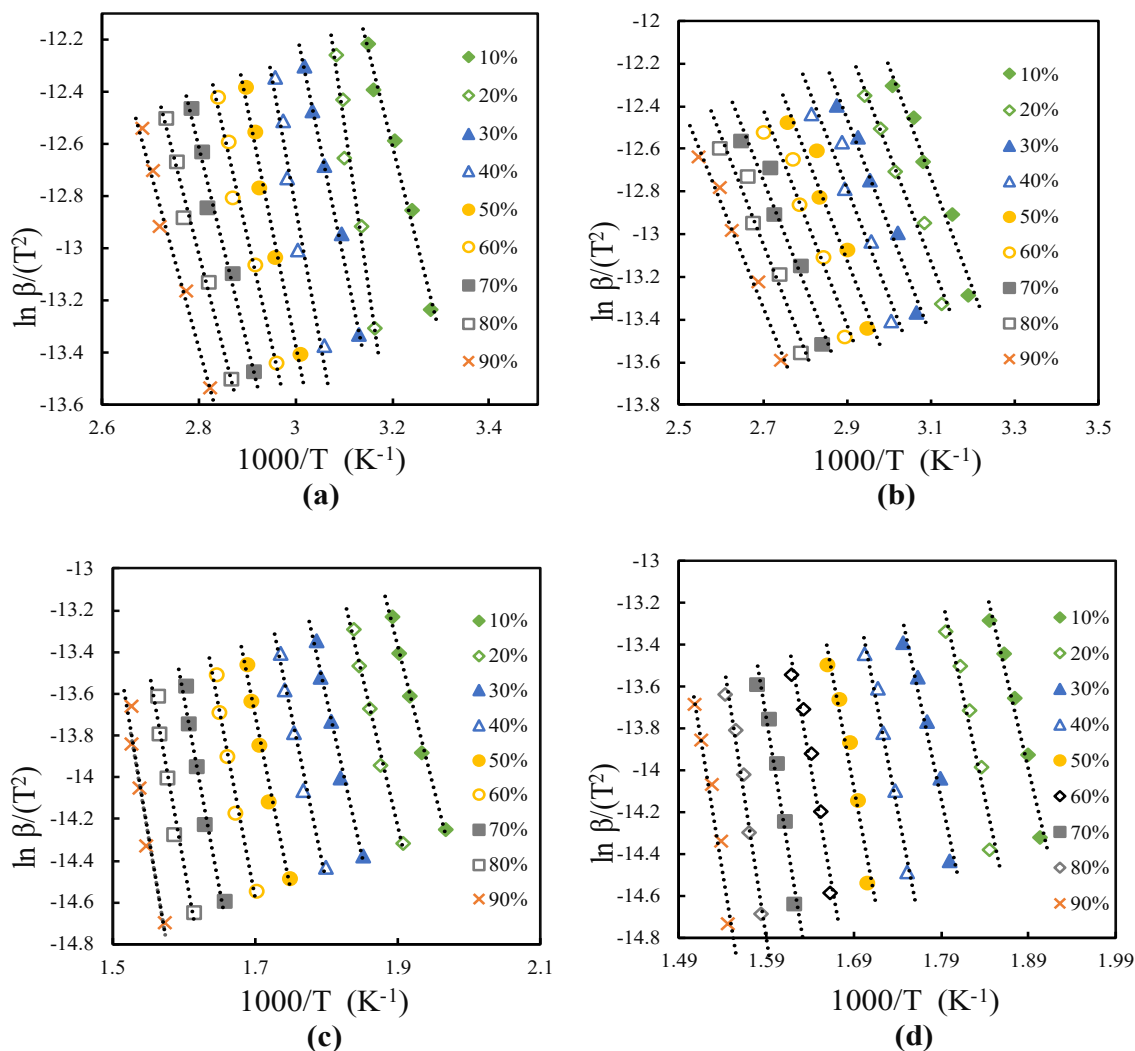


Figure 7-5: Regression lines used to obtain apparent activation energies using the KAS method for pyrolysis of little bluestem grass. (a) drying phase (live) (b) drying phase (dead) (c) major pyrolysis zone (live) (d) major pyrolysis zone (dead).

Figure 7-6 illustrates the dependence of activation energies on the degree of conversion based on the KAS method. The 95% confidence intervals (based on 3 repeats) are shown as error bars in Figure 7-6, showing excellent reproducibility of data. The results showed that there is a strong dependency of activation energy on the degree of conversion for the both the drying and major pyrolysis zones. Note that the error bars for the activation energies are smaller than ± 2 kJ mol⁻¹.

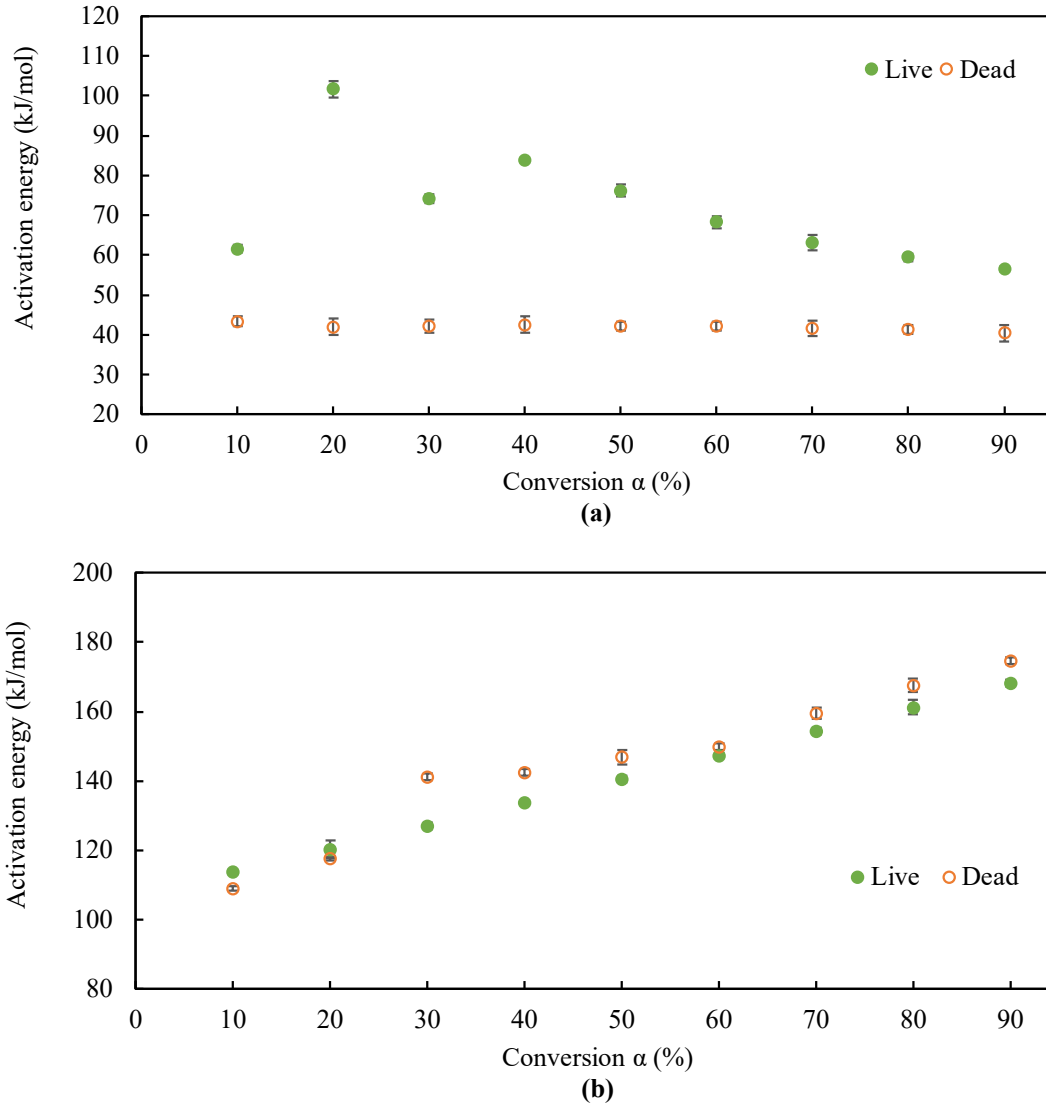


Figure 7-6: Activation energy distribution for pyrolysis of live and dead little bluestem grass during (a) drying and (b) major pyrolysis zones based on the KAS method. The 95% confidence intervals are presented as error bars.

According to Figure 7-6a, calculated activation energies in the drying zone of the live samples varied significantly with conversion. In contrast, the calculated activation energies remained almost steady for the drying zone of dead samples (Figure 7-6a). These results showed that the dependency of activation energy on conversion degree during the drying zone of the pyrolysis process may be related to the moisture content of the sample. This result was somewhat unexpected since small samples and low heating rates were used, which should have minimized

heat and mass transfer effects. For the major pyrolysis zone, activation energy values showed an increasing trend with extent of conversion for both the live and dead samples (Figure 7-6b). Since these were constant heating rate experiments, the temperature also increased with increasing extent of conversion. Increasing activation energy with increasing temperature can be contributed to parallel reaction routes with different activation energies (Lu et al., 2013; Ma et al., 2015; Hu et al., 2017). Bonds in the macromolecular structure with lower activation energies are broken first, followed by bonds with higher activation energies.

For the first region in Figure 7-6b, $10\% < \alpha < 30\%$ (corresponding to the temperature range 185-238 °C), the activation energies had the lowest values and increased from 113.7 to 127.0 kJ mol⁻¹ for the live samples and from 109.0 to 141.2 kJ mol⁻¹ for the dead samples, all based on the KAS method. The lower activation energies at the beginning of pyrolysis can be attributed to several reasons. First, at the beginning of the major pyrolysis process, the decomposition started easily on the sites, which are weakly linked to the linear polymeric chain of the hemicellulose, whose decomposition requires low energy. Then, after these weaker bonds break, random scission of linear chains leads to increases in activation energy (Ma et al., 2015).

In the range of $\alpha=30-80\%$ (equivalent to the temperature range of 238 – 420 °C), the activation energy increased from 127.0 to 161.2 kJ mol⁻¹ and from 141.2 to 167.5 kJ mol⁻¹ (based on the KAS method) for the live and dead samples, respectively. Based on woody biomass pyrolysis studies, cellulose degradation occurs in this region. In the range of $\alpha=80-90\%$ ($T > 420$ °C), the highest activation energies based on the KAS method (168.1 and 174.7 kJ mol⁻¹, respectively for the live and dead samples) were obtained, which may correspond to the degradation of some of the lignin (Vamvuka et al., 2003; Yang et al., 2004; Ma et al., 2015). In the lower temperature range, the weak-linked sites in the lignin's three-dimensional structure can

be broken. However, parts of three-dimensional structure of lignin break at higher temperature ranges and require the highest energy (Chen et al., 2013; Ma et al., 2015). Hence, the lignin may decompose partially in each of these three regions. The solid remaining after pyrolysis is called char, which comprises approximately 30 wt% of the initial dry, ash-free mass of the plant in these experiments (Amini et al., 2019). The apparent activation energy corresponds to the minimum energy required for breaking the chemical bonds between atoms and starting a reaction. Therefore, the higher value of apparent activation energy means that the reaction is slower and starts with more difficulty. The average activation energy for the drying zone (71.7 kJ mol^{-1}) obtained from the KAS method is higher for live sample (42.0 kJ mol^{-1} was obtained for the dead sample).

The average activation energy value obtained from the KAS method for the drying zone of pyrolysis of LLBG is 71.7 kJ mol^{-1} which is higher than the corresponding value for DLBG (42.0 kJ mol^{-1}). Therefore, more energy is required to release moisture for the live sample, and that the moisture release for the live samples was slower. This difference in activation energy for moisture release could be due to a physiological reason that live plants have mechanisms to try to hold moisture (Prince and Fletcher, 2014). Comparing the results of this study with literature shows that the activation energies obtained in this study for little bluestem grass from the KAS model were higher than the reported activation energies for different biomass obtained from drying kinetic models. The activation energies obtained from drying kinetic models were in the range of $5\text{-}30 \text{ kJ mol}^{-1}$ for different biomass reported in the literature (Li and Kobayashi, 2005; AntonioVega-Gálvez et al., 2010; Cai and Chen, 2010; Chen et al., 2012; Chen et al., 2013). The activation energies for drying zone can be affected by factors such as type of biomass, calculation method, kinetic models, and experimental condition. Beside these factors, the higher activation

energy for little bluestem grass seems to show that most of the water in this plant sample is bound water which needs more energy to evaporate (Kovalov et al., 2017). For the major pyrolysis zone, the average activation energies obtained for live and dead samples using the KAS method were not significantly different (140.7 and 145.4 kJ mol⁻¹, respectively). This shows that drying does not significantly affect the pyrolysis rate of LBG on a dry basis. This result also can be seen from the DTG curves of LLBG and DLBG, which are presented in Figure 7-7, for a heating rate of 30 °C min⁻¹ as an example. These curves were normalized to remove the portion of the mass release attributed to moisture evaporation. According to this figure, the DTG curves of live and dead samples almost overlapped. In addition, the peak of DTG curves occurred at almost the same temperature of 335 °C. This similarity in the pyrolysis rates of live vs. dead samples was observed for most of the plant species.

7.4 Kinetic Parameters for the Drying Zone for All Plant Species

Kinetic parameters at different conversions for all plant species (live and dead), based on the KAS method, are presented in Table 7-2 for the drying zone. For live samples, average activation energies were in the range of 71.7– 111.0 kJ mol⁻¹. Little bluestem grass had the lowest average activation energy with a value of 71.7 kJ mol⁻¹. The highest average activation energy with a value of 110.3 kJ mol⁻¹ were obtained from pyrolysis of wax myrtle. For dead samples, average activation energies were in the range of 36.7 – 95.3 kJ mol⁻¹. The lowest average activation energy with a value of 36.7 kJ mol⁻¹ was obtained from pyrolysis of pine straw. Fetterbush had the highest average activation energy with a value of 95.3 kJ mol⁻¹. The 95% confidence intervals for average activation energies were between 0.1 and 2.1 and between 0.3 and 2.1 for live and dead samples, respectively. All 95% confidence interval values are reported in Table 7-2.

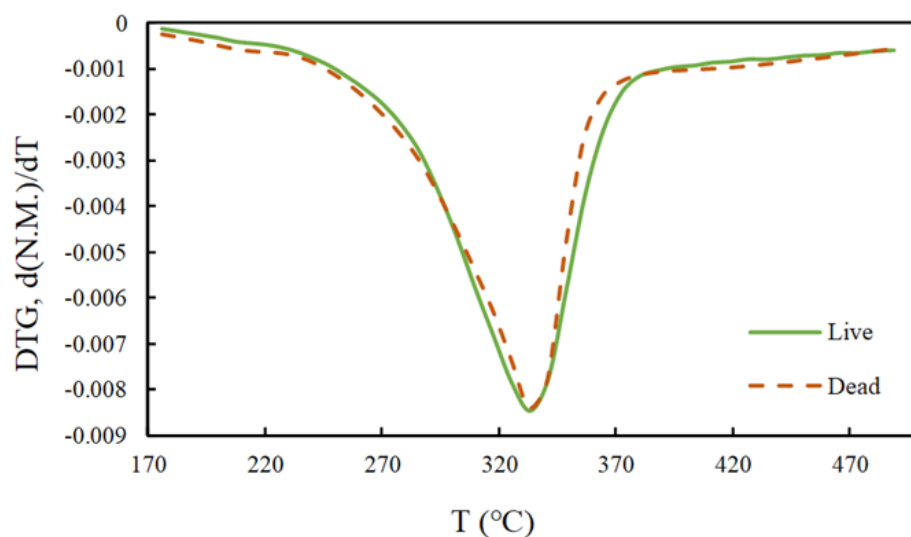


Figure 7-7: DTG curves at 30 °C min⁻¹ for major pyrolysis zones of live and dead little bluestem grass. These curves were normalized to be on a moisture-free basis.

For the all plant species, live samples with higher moisture content had higher activation energies during drying stage than dead samples. Among all plant species, wax myrtle exhibited the largest statistically difference ($P < 0.05$) in average activation energy value (64.8 kJ mol^{-1} , absolute) between the live and dead samples. Swamp bay and little bluestem grass also had large difference in average activation energy for live vs. dead samples (38.5 and 29.7 kJ mol^{-1} , respectively). Sparkleberry had the lowest difference in average activation energy value (4.0 kJ mol^{-1}) based on KAS method between live and dead samples.

7.5 Kinetic Parameters for the Major Pyrolysis Zone for All Plant Species

Table 7-3 represents kinetic parameters at different conversions for all plant species (live and dead), based on the KAS method for the major pyrolysis zone. For live samples, average activation energies were in the range of $120.8 - 232.9 \text{ kJ mol}^{-1}$. Yaupon had the lowest average activation energy with a value of $120.8 \text{ kJ mol}^{-1}$. The highest average activation energy with a value of $232.9 \text{ kJ mol}^{-1}$ were obtained from pyrolysis of saw palmetto.

Table 7-2: Activation energies (E^a) and pre-exponential factors ($\text{Log}_{10}A^b$) at different conversions for all plant species (live and dead), representing needle, grass, palmetto, and broadleaf species based on the KAS method for the drying zone (the 95% confidence intervals are reported in parenthesis)

Darrow's blueberry					Dwarf palmetto			
Conversion	Live		Dead		Live		Dead	
(%)	$\text{Log}_{10} A$	E	$\text{Log}_{10} A$	E	$\text{Log}_{10} A$	E	$\text{Log}_{10} A$	E
10	12.82(0.02)	109.4(2.4)	15.4(0.08)	93.9(2.1)	11.47(0.24)	92.5(2.4)	11.60(0.35)	93.3(2.1)
20	9.15(0.08)	109.1(2.0)	15.4(0.01)	71.3(1.8)	11.31(0.23)	90.4(2.3)	10.20(0.09)	83.3(1.4)
30	15.34(0.27)	114.7(2.5)	16.2(0.03)	108.4(2.4)	11.05(0.07)	88.5(2.1)	9.90(0.17)	81.1(1.1)
40	13.43(0.23)	104.4(1.9)	14.5(0.08)	97.0(2.6)	10.77(0.20)	86.7(2.0)	9.60(0.19)	79.1(1.0)
50	11.92(0.05)	96.0(1.7)	13.0(0.04)	88.0(1.6)	10.52(0.26)	85.1(1.8)	9.32(0.18)	77.3(0.9)
60	10.72(0.20)	89.0(1.8)	11.8(0.10)	80.8(1.8)	10.27(0.27)	83.5(1.9)	9.82(0.25)	80.7(0.8)
70	9.74(0.13)	83.2(2.3)	10.9(0.16)	74.8(1.6)	10.04(0.25)	82.2(2.2)	9.53(0.31)	78.9(1.3)
80	8.94(0.51)	78.3(1.6)	10.0(0.04)	69.8(1.5)	9.82(0.28)	81.0(2.3)	9.28(0.29)	77.2(1.5)
90	14.32(0.03)	74.1(0.9)	9.4(0.03)	65.6(1.4)	9.71(0.14)	79.8(1.4)	9.69(0.28)	79.9(1.6)
Average		95.3(2.1)		83.3(1.9)		85.0(2.1)		81.2(2.0)
Fetterbush					Inkberry			
Conversion	Live		Dead		Live		Dead	
(%)	$\text{Log}_{10} A$	E	$\text{Log}_{10} A$	E	$\text{Log}_{10} A$	E	$\text{Log}_{10} A$	E
10	17.92(0.22)	129.5(1.6)	19.56(0.24)	135.5(1.6)	14.85(0.39)	113.7(1.9)	11.63(0.31)	93.5(2.4)
20	16.81(0.37)	122.4(2.7)	17.17(0.38)	120.7(2.6)	14.23(0.12)	110.4(2.1)	8.17(0.08)	71.1(1.5)
30	15.47(0.19)	114.0(1.4)	14.92(0.19)	107.0(1.4)	14.00(0.53)	108.3(3.7)	10.05(0.39)	82.6(3.2)
40	14.61(0.61)	107.8(0.8)	13.43(0.61)	97.4(1.1)	13.63(0.21)	105.7(1.3)	8.19(0.21)	70.3(1.2)
50	13.53(0.05)	102.3(0.4)	11.93(0.05)	89.4(0.3)	12.74(0.17)	100.0(1.2)	8.54(0.11)	72.2(0.95)
60	13.01(0.35)	99.8(2.7)	11.08(0.35)	84.6(2.3)	12.11(0.22)	96.2(1.5)	8.21(0.15)	69.8(1.2)
70	12.32(0.38)	95.6(2.8)	10.19(0.39)	79.2(2.4)	11.78(0.19)	94.2(1.9)	8.09(0.04)	69.1(0.3)
80	12.68(0.44)	91.4(1.3)	9.38(0.44)	74.1(2.5)	11.72(0.35)	93.9(2.4)	8.79(0.26)	73.6(1.9)
90	12.08(0.90)	87.4(0.14)	8.72(0.02)	69.5(0.4)	11.22(0.31)	90.4(2.5)	9.09(0.25)	75.7(2.1)
Average		105.5(1.3)		95.3(1.4)		101.4(0.7)		75.3(0.5)
Live oak					Little bluestem grass			
Conversion	Live		Dead		Live		Dead	
(%)	$\text{Log}_{10} A$	E	$\text{Log}_{10} A$	E	$\text{Log}_{10} A$	E	$\text{Log}_{10} A$	E
10	8.90(0.24)	120.2(2.1)	13.00(0.34)	99.4(2.6)	7.73(0.2)	61.5(1.1)	7.13(0.19)	43.5(1.2)
20	15.15(0.13)	109.3(2.1)	12.08(0.12)	93.0(2.0)	14.57(0.50)	101.3(2.9)	8.15(0.21)	42.2(0.9)
30	13.71(0.53)	103.0(3.5)	11.23(0.44)	87.8(3.4)	10.00(0.37)	75.6(2.6)	9.74(0.38)	42.6(2.5)

Table 7-2 Continued

Conversion	Live oak				Little bluestem grass			
	Live		Dead		Live		Dead	
	Log ₁₀ A	E	Log ₁₀ A	E	Log ₁₀ A	E	Log ₁₀ A	E
40	12.51(0.42)	96.5(0.9)	10.49(0.47)	83.3(1.5)	11.39(0.38)	86.3(1.4)	10.86(0.50)	42.4(1.1)
50	11.51(0.15)	88.4(1.1)	9.85(0.13)	79.5(1.0)	9.94(0.13)	76.3(1.0)	10.09(0.13)	42.2(1.4)
60	10.67(0.19)	82.6(1.3)	9.30(0.16)	76.2(1.3)	8.47(0.15)	67.6(1.0)	8.21(0.10)	41.6(0.9)
70	9.98(0.05)	78.9(0.4)	8.83(0.36)	73.3(0.4)	7.66(0.04)	62.7(1.3)	8.47(0.12)	41.3(1.6)
80	9.40(0.28)	77.2(2.0)	8.41(0.26)	70.8(1.9)	7.25(0.2)	60.5(1.6)	7.53(0.22)	41.9(1.1)
90	8.93(0.25)	72.9(2.0)	8.11(0.22)	68.5(1.9)	6.64(0.19)	56.5(1.6)	11.50(0.32)	40.4(1.1)
Average		92.1(0.4)		81.6(0.3)		71.7(0.1)		42.1(0.7)
Conversion	Longleaf pine				Pine straw			
	Live		Dead		Live		Dead	
	Log ₁₀ A	E	Log ₁₀ A	E	Log ₁₀ A	E	Log ₁₀ A	E
10	11.21(0.59)	87.1(3.8)	9.97(0.65)	77.0(2.8)	6.40(0.26)		55.0(2.5)	
20	11.25(0.10)	86.7(3.2)	9.19(0.23)	72.1(4.0)	6.94(0.22)		47.6(2.3)	
30	11.15(0.49)	86.1(4.7)	7.68(0.13)	61.5(2.3)	6.10(0.26)		41.8(1.9)	
40	9.92(0.23)	78.8(1.4)	7.53(0.39)	56.7(3.2)	5.20(0.07)		37.3(1.6)	
50	10.90(0.63)	85.2(4.7)	6.92(0.34)	52.4(1.8)	5.81(0.3)		33.5(1.8)	
60	10.33(0.62)	81.9(2.9)	5.34(0.10)	47.9(2.6)	4.47(0.22)		32.1(0.5)	
70	10.03(0.47)	79.5(4.3)	4.81(0.27)	46.1(2.4)	4.08(0.16)		29.0(1.3)	
80	9.31(0.25)	76.8(5.0)	4.45(0.09)	42.5(2.2)	4.78(0.21)		28.0(2.5)	
90	8.95(0.58)	74.7(4.1)	4.23(0.05)	41.2(1.5)	4.74(0.23)		26.2(0.9)	
Average		81.9(1.7)		55.3(0.3)			36.7(0.6)	
Conversion	Saw palmetto				Sparkleberry			
	Live		Dead		Live		Dead	
	Log ₁₀ A	E	Log ₁₀ A	E	Log ₁₀ A	E	Log ₁₀ A	E
10	7.61(0.79)	61.5(1.1)	5.62(0.15)	53.9(1.4)	14.15(0.37)	106.2(1.8)	9.00(0.24)	126.1(3.3)
20	14.53(1.04)	101.3(2.5)	5.71(0.15)	53.7(1.2)	13.75(0.45)	103.0(2.6)	9.38(0.24)	112.4(2.5)
30	9.81(0.56)	75.6(2.6)	5.88(0.23)	53.5(3.2)	13.23(0.50)	99.9(3.5)	9.61(0.38)	101.7(6.2)
40	11.39(0.38)	86.3(1.4)	5.73(0.26)	52.4(1.3)	12.72(0.443)	96.8(1.6)	9.79(0.44)	93.3(2.4)
50	9.94(0.13)	76.3(1.0)	5.70(0.1)	52.3(1.8)	12.23(0.16)	93.9(1.1)	9.93(0.13)	86.4(3.0)
60	8.66(0.41)	67.6(1.0)	5.55(0.34)	50.4(0.5)	11.74(0.21)	91.2(1.4)	10.04(0.6)	80.7(3.6)
70	7.78(0.36)	62.2(1.4)	5.45(0.08)	50.9(2.6)	11.30(0.52)	88.7(1.9)	10.15(0.15)	75.9(3.9)
80	7.25(0.21)	60.5(1.6)	5.58(0.17)	51.4(1.3)	10.91(0.33)	86.3(2.3)	10.26(0.31)	71.9(1.9)

Table 7-2 Continued

Saw palmetto					Sparkleberry			
Conversion	Live		Dead		Live		Dead	
	Log ₁₀ A	E	Log ₁₀ A	E	Log ₁₀ A	E	Log ₁₀ A	E
90	6.72(0.48)	56.5(1.6)	5.31(0.15)	50.3(1.4)	10.59(0.30)	84.1(2.3)	10.38(0.29)	68.4(1.9)
Average		72.0(0.7)		52.1(0.5)		94.5(0.6)		90.8(0.7)
Swamp bay					Water oak			
Conversion	Live		Dead		Live		Dead	
	Log ₁₀ A	E	Log ₁₀ A	E	Log ₁₀ A	E	Log ₁₀ A	E
10	6.71(0.17)	106.1(1.8)	14.18(0.37)	57.6(1.5)	11.74(0.60)	90.5(3.9)	6.80(0.29)	60.9(1.8)
20	6.78(0.30)	102.6(2.6)	13.58(0.35)	57.6(1.3)	11.06(0.57)	84.6(2.2)	6.92(0.04)	59.5(3.1)
30	6.95(0.26)	101.8(3.5)	13.42(0.52)	57.7(3.5)	10.67(0.45)	82.1(2.9)	6.94(0.42)	60.1(3.5)
40	6.85(0.22)	99.7(1.6)	12.60(0.57)	56.6(1.4)	9.92(0.50)	78.8(1.9)	6.78(0.37)	58.2(1.7)
50	6.78(0.09)	94.0(1.2)	12.24(0.16)	56.6(1.9)	9.24(0.12)	73.7(0.9)	6.66(0.17)	58.3(2.0)
60	6.61(0.11)	90.2(1.4)	11.62(0.71)	55.4(2.5)	8.61(0.13)	69.8(1.1)	6.58(0.42)	56.7(2.6)
70	6.66(0.31)	87.4(2.0)	11.19(0.17)	55.4(2.9)	8.30(0.38)	66.7(2.2)	6.35(0.09)	57.1(3.3)
80	6.73(0.20)	87.7(2.3)	11.13(0.33)	55.8(1.5)	7.70(0.30)	66.6(1.7)	6.40(0.19)	56.4(1.5)
90	6.61(0.18)	84.2(2.3)	10.60(0.30)	54.8(1.5)	7.53(0.21)	62.7(3.2)	6.11(0.13)	54.4(2.8)
Average		94.9(1.0)		56.4(0.9)		75.1(1.0)		58.0(0.8)
Wax myrtle					Wire grass			
Conversion	Live		Dead		Live		Dead	
	Log ₁₀ A	E	Log ₁₀ A	E	Log ₁₀ A	E	Log ₁₀ A	E
10	10.50(0.54)	139.9(6.2)	16.72(0.71)	51.7(1.5)	19.27(0.3)	136.1(2.8)	13.90(0.35)	101.5(2.1)
20	11.63(0.59)	134.0(3.4)	16.04(0.10)	56.4(2.5)	16.88(0.53)	122.7(1.9)	15.35(0.06)	107.0(3.5)
30	12.37(1.11)	110.6(4.4)	11.70(0.60)	48.0(2.8)	16.56(0.40)	117.9(2.5)	12.89(0.51)	93.9(1.9)
40	12.82(0.64)	105.4(1.7)	10.61(0.66)	44.0(1.3)	15.10(0.44)	107.3(1.2)	12.78(0.43)	91.9(1.6)
50	13.22(0.17)	120.9(1.5)	13.38(0.34)	42.2(1.9)	13.28(0.10)	97.9(2.5)	11.65(0.18)	91.4(2.6)
60	13.49(0.42)	99.5(1.9)	10.43(0.71)	39.6(2.1)	12.08(0.24)	90.5(2.1)	11.12(0.41)	84.7(2.2)
70	14.32(0.66)	104.9(4.8)	10.52(0.16)	40.2(2.3)	11.69(0.18)	86.9(0.9)	10.49(0.09)	80.7(2.0)
80	14.61(1.14)	92.3(2.4)	8.45(0.54)	47.9(1.3)	10.43(0.25)	85.4(1.3)	10.22(0.25)	79.0(1.9)
90	15.16(0.42)	91.5(4.7)	8.54(0.20)	46.0(2.4)	10.35(0.17)	80.7(2.4)	9.30(0.10)	77.3(2.3)
Average		111.0(1.1)		46.2(0.8)		102.8(0.6)		89.7(0.6)

Table 7-2 Continued

Conversion	Yaupon			
	Live		Dead	
	Log ₁₀ A	E	Log ₁₀ A	E
10	13.50(0.69)	101.2(4.5)	7.79(0.33)	60.9(1.8)
20	11.15(0.80)	84.6(2.2)	8.91(0.06)	60.1(1.7)
30	10.67(0.45)	82.1(2.9)	8.94(0.54)	60.1(3.5)
40	9.92(0.50)	78.5(1.3)	9.76(0.53)	58.0(2.1)
50	9.24(0.12)	73.2(2.0)	9.64(0.25)	58.2(2.0)
60	8.61(0.13)	69.8(1.1)	10.59(0.67)	56.7(2.6)
70	8.27(0.30)	66.7(2.2)	10.31(0.15)	57.1(3.3)
80	7.70(0.30)	66.6(1.7)	11.39(0.66)	56.4(1.5)
90	7.53(0.21)	63.1(2.4)	11.03(0.24)	54.4(2.8)
Average		76.2(1.1)		58.0(0.9)

^a kJ mol⁻¹

^b s⁻¹

For dead samples, average activation energies were in the range of 130.4 – 210.9 kJ mol⁻¹. The lowest average activation energy with a value of 130.4 kJ mol⁻¹ was obtained from pyrolysis of yaupon. Saw palmetto had the highest average activation energy with a value of 210.9 kJ mol⁻¹. Among all plant species, wax myrtle exhibited the largest difference in average activation energy value (42.0 kJ mol⁻¹) between the live and dead samples. Darrow's blueberry also had a large difference in average activation energy for live vs. dead samples (29.2 kJ mol⁻¹). Longleaf pine foliage had the lowest difference in average activation energy value (0.1 kJ mol⁻¹) based on KAS method between live and dead samples. The 95% confidence intervals for average activation energies were between 0.3 and 1.5 and between 0.6 and 2.2 for live and dead samples, respectively. All 95% confidence interval values are reported in Table 7-3.

A similar pyrolysis kinetics study was done on three Mediterranean plants of *Cistus creticus* (CC), *Myrtus communis* (MC) and *Genista corsica* (GC) which are often involved in wildland fires. The TGA experiments were performed on oven-dried samples (24 hr at 70 °C). Using the KAS method, three heating rates of 10, 20, and 30 °C min⁻¹ and nine degrees of conversion between 10 – 90% were considered. The resulting average activation energies for the Mediterranean plants were in the range of activation energies obtained from the current study. The average activation energies were 155.2, 215.1, and 185.3 kJ mol⁻¹ for GC, MC, and CC, respectively (Tihay and Gillard, 2011).

Figure 7-8 shows the distribution of pyrolysis rates for the major pyrolysis zone as a function of conversion for all live plant species. A similar decreasing trend of pyrolysis rates was observed for all plant species after conversion of 20%. Different plant species had different rates at different conversions. During the sample decomposition, the highest rates were observed at the beginning of the pyrolysis between $\alpha=10 - 20\%$, for all samples.

Table 7-3: Activation energies (E^a) and pre-exponential factors ($\text{Log}_{10} A^b$) at different conversions for all plant species (live and dead), representing needle, grass, palmetto, and broadleaf species based on the KAS method for the major pyrolysis zone (the 95% confidence intervals are reported in parenthesis)

Darrow's blueberry					Dwarf palmetto			
Conversion	Live		Dead		Live		Dead	
	$\text{Log}_{10} A$	E	$\text{Log}_{10} A$	E	$\text{Log}_{10} A$	E	$\text{Log}_{10} A$	E
10	8.87(0.23)	113.0(1.9)	10.04(0.43)	125.7(3.3)	9.67(0.26)	128.6(2.2)	9.42(0.4)	128.8(3.4)
20	9.26(0.52)	117.5(4.2)	10.72(0.28)	133.5(4.6)	10.09(0.25)	135.7(4)	10.57(0.25)	140.5(2.5)
30	9.69(0.36)	124.6(4.5)	11.56(0.69)	142.8(5.2)	10.90(0.31)	143.4(5.2)	11.11(0.66)	146.0(3.9)
40	9.86(0.33)	129.9(2.1)	11.96(0.54)	150.0(3.8)	11.35(0.39)	150.9(1.4)	11.40(0.51)	150.5(4.8)
50	9.95(0.13)	129.2(3.6)	12.75(0.48)	159.6(2.1)	11.62(0.15)	150.4(4.2)	12.30(0.66)	160.0(2.1)
60	9.90(0.03)	133.0(2.0)	12.92(0.1)	165.2(1.1)	11.95(0.60)	155.7(2.4)	13.24(0.16)	172.7(1.2)
70	10.20(0.05)	136.6(3.6)	13.55(0.2)	177.3(5.3)	12.22(0.15)	160.7(4.3)	14.29(0.21)	189.5(6.2)
80	10.64(0.31)	144.9(3.8)	14.42(0.61)	187.5(5.0)	12.18(0.51)	163.3(4.3)	16.83(0.82)	218.5(5.7)
90	10.58(0.35)	146.2(5.3)	14.63(0.63)	195.7(5.4)	12.32(0.54)	166.6(4.8)	16.52(0.71)	222.2(2.7)
Average		130.5(0.7)		159.7(1.2)		150.6(0.9)		169.8(1.1)
Fetterbush					Inkberry			
Conversion	Live		Dead		Live		Dead	
	$\text{Log}_{10} A$	E	$\text{Log}_{10} A$	E	$\text{Log}_{10} A$	E	$\text{Log}_{10} A$	E
10	10.95(0.29)	134.5(2.3)	11.90(0.50)	145.4(3.8)	8.34(0.23)	111.5(1.9)	8.17(0.35)	110.9(2.9)
20	11.42(0.28)	143.2(4.2)	12.52(0.29)	153.4(2.7)	8.78(0.22)	118.3(3.5)	8.71(0.20)	116.3(2.1)
30	12.35(0.35)	152.9(5.5)	13.45(0.80)	163.6(4.4)	9.59(0.28)	125.7(4.5)	9.46(0.56)	123.2(4.5)
40	12.92(0.45)	162.5(1.5)	13.80(0.62)	171.0(5.5)	10.02(0.35)	132.9(1.3)	9.77(0.48)	128.6(4.1)
50	13.27(0.17)	163.8(4.5)	14.56(0.78)	180.6(2.4)	10.33(0.14)	133.8(5.0)	10.42(0.56)	135.4(1.8)
60	13.70(0.69)	171.6(2.6)	14.88(0.77)	185.9(2.7)	10.67(0.54)	139.0(2.1)	10.71(0.55)	139.0(2.0)
70	14.09(0.17)	179.3(4.8)	15.46(0.23)	200.7(5.9)	10.99(0.13)	144.4(3.9)	11.21(0.17)	149.6(4.4)
80	15.00(0.63)	191.5(5.1)	16.13(0.76)	208.5(4.5)	11.70(0.49)	153.6(4.1)	11.77(0.58)	155.1(3.3)
90	15.16(0.67)	199.6(4.8)	16.66(0.71)	224.4(2.7)	11.83(0.52)	159.4(3.8)	12.24(0.52)	166.7(2.0)
Average		166.5(0.7)		181.5(0.9)		135.4(0.6)		136.1(0.6)
Live oak					Little bluestem grass			
Conversion	Live		Dead		Live		Dead	
	$\text{Log}_{10} A$	E	$\text{Log}_{10} A$	E	$\text{Log}_{10} A$	E	$\text{Log}_{10} A$	E
10	9.48(0.26)	126.2(2.2)	10.69(0.45)	140.7(3.7)	8.65(0.23)	113.7(1.9)	8.51(0.36)	115.6(0.7)
20	9.93(0.24)	133.9(3.9)	11.08(0.26)	145.4(2.6)	9.08(0.22)	120.3(2.4)	9.43(0.22)	124.2(1.6)
30	10.81(0.31)	142.5(3.2)	11.73(0.70)	151.4(5.5)	9.91(0.29)	127.0(3.6)	10.18(0.61)	133.2(1.0)

Table 7-3 Continued

Conversion	Live oak				Little bluestem grass			
	Live		Dead		Live		Dead	
	Log ₁₀ A	E	Log ₁₀ A	E	Log ₁₀ A	E	Log ₁₀ A	E
40	11.26(0.39)	150.4(2.5)	11.81(0.58)	155.5(5.0)	9.33(0.32)	133.8(1.3)	10.66(0.53)	142.6(2.9)
50	11.59(0.15)	151.7(4.1)	12.30(0.66)	160.8(2.1)	9.60(0.13)	140.6(2.2)	11.51(0.62)	152.4(2.0)
60	11.95(0.60)	158.1(2.4)	12.34(0.64)	161.9(2.4)	9.93(0.50)	147.5(2.2)	11.98(0.63)	162.6(2.3)
70	12.31(0.15)	164.5(4.4)	12.62(0.19)	171.1(5.0)	10.23(0.12)	154.3(4.1)	12.68(0.19)	173.2(3.5)
80	13.07(0.55)	175.0(4.6)	12.93(0.64)	173.9(3.8)	10.86(0.46)	161.2(4.3)	10.67(0.53)	177.9(3.8)
90	13.22(0.58)	181.9(4.4)	13.14(0.56)	183.1(2.2)	10.98(0.48)	168.1(2.7)	11.04(0.47)	178.1(3.1)
Average		153.8(0.5)		160.4(0.8)		140.7(0.3)		145.4(1.0)
Conversion	Longleaf pine				Pine straw			
	Live		Dead		Live		Dead	
	Log ₁₀ A	E	Log ₁₀ A	E	Log ₁₀ A	E	Log ₁₀ A	E
10	10.60(0.19)	121.1(1.7)	11.64(0.35)	135.8(2.6)	13.26(0.26)		163.5(2.9)	
20	11.30(0.25)	137.9(2.6)	12.26(0.30)	143.7(3.3)	13.58(0.23)		166.6(2.5)	
30	11.89(0.31)	156.9(3.9)	12.73(0.47)	150.2(5.7)	14.04(0.46)		172.7(2.6)	
40	12.43(0.29)	169.5(1.9)	13.15(0.53)	158.8(3.9)	14.49(0.44)		176.9(3.3)	
50	12.93(0.24)	162.3(2.7)	13.54(0.80)	166.7(2.9)	14.90(0.14)		185.2(4.7)	
60	13.43(0.34)	172.8(3.9)	13.91(0.35)	176.4(4.1)	14.96(0.65)		187.8(2.6)	
70	14.36(0.45)	186.3(2.9)	14.26(0.19)	184.4(3.9)	15.34(0.16)		194.3(5.1)	
80	14.43(0.30)	198.7(3.7)	14.61(0.41)	191.3(4.8)	15.75(0.35)		200.8(4.1)	
90	14.96(0.29)	200.3(4.0)	14.98(0.39)	199.5(5.1)	15.79(0.33)		202.7(4.5)	
Average		167.3(1.1)		167.4(1.6)				183.4(1.4)
Conversion	Saw palmetto				Sparkleberry			
	Live		Dead		Live		Dead	
	Log ₁₀ A	E	Log ₁₀ A	E	Log ₁₀ A	E	Log ₁₀ A	E
10	16.58(0.45)	197.9(3.4)	14.98(0.63)	180.0(4.8)	10.53(0.28)	134.6(2.3)	9.02(0.24)	120.9(3.2)
20	16.89(0.23)	210.3(1.6)	15.52(0.36)	187.5(3.4)	10.73(0.35)	136.0(3.5)	9.26(0.26)	124.9(2.7)
30	18.12(0.53)	223.0(1.8)	16.43(0.98)	198.4(2.7)	10.85(0.40)	141.1(4.9)	9.75(0.38)	130.8(3.4)
40	18.59(0.64)	230.6(3.8)	17.56(0.87)	203.6(5.9)	10.77(0.36)	144.3(2.4)	9.69(0.44)	130.9(3.3)
50	18.82(0.25)	227.6(3.6)	17.27(0.92)	211.5(2.8)	10.63(0.14)	141.9(1.8)	9.94(0.13)	135.2(4.7)
60	19.15(0.97)	238.1(3.7)	17.35(0.91)	214.0(3.1)	10.42(0.19)	141.7(2.2)	9.94(0.61)	135.8(3.7)
70	19.39(0.23)	244.4(5.7)	17.73(0.26)	227.8(4.1)	10.61(0.49)	142.5(3.2)	10.04(0.15)	142.4(4.8)
80	20.29(0.86)	259.6(4.2)	18.14(0.89)	231.3(5.0)	10.68(0.32)	148.5(3.9)	10.46(0.31)	145.3(1.9)

Table 7-3 Continued

Saw palmetto					Sparkleberry			
Conversion	Live		Dead		Live		Dead	
	Log ₁₀ A	E	Log ₁₀ A	E	Log ₁₀ A	E	Log ₁₀ A	E
90	20.18(0.89)	264.9(3.5)	18.38(0.79)	244.0(3.0)	10.49(0.29)	147.7(4.1)	10.39(0.29)	147.2(4.1)
Average		232.9(0.6)		210.8(1.0)		142.0(1.2)		134.8(1.6)
Swamp bay					Water oak			
Conversion	Live		Dead		Live		Dead	
	Log ₁₀ A	E	Log ₁₀ A	E	Log ₁₀ A	E	Log ₁₀ A	E
10	8.84(0.23)	121.0(2.1)	9.42(0.25)	126.6(3.3)	9.17(0.24)	114.7(2.0)	8.27(0.22)	110.5(2.9)
20	7.17(0.35)	103.4(2.6)	9.88(0.26)	133.1(2.9)	9.75(0.32)	119.1(3.0)	8.78(0.23)	116.9(2.5)
30	8.27(0.31)	116.4(4.0)	10.66(0.41)	142.6(2.4)	10.20(0.38)	126.8(4.4)	9.54(0.37)	124.9(4.3)
40	9.21(0.31)	129.6(2.1)	10.85(0.49)	144.3(3.7)	10.47(0.35)	133.0(2.2)	9.74(0.44)	128.3(3.3)
50	10.20(0.12)	138.8(1.8)	11.39(0.15)	151.9(5.3)	10.64(0.14)	134.0(1.7)	10.29(0.14)	135.8(4.7)
60	11.12(0.22)	151.3(2.3)	11.69(0.72)	155.2(3.6)	10.73(0.19)	136.9(2.1)	10.57(0.65)	139.0(2.6)
70	12.60(0.58)	166.3(3.8)	12.11(0.18)	161.1(3.1)	11.21(0.52)	140.7(3.2)	10.97(0.16)	147.1(5.1)
80	14.10(0.58)	189.5(5.0)	12.89(0.38)	173.9(4.5)	11.57(0.34)	149.6(3.9)	11.70(0.35)	157.2(4.1)
90	15.32(0.43)	205.8(3.1)	13.09(0.36)	178.9(5.0)	11.59(0.32)	151.6(4.2)	11.91(0.33)	162.2(4.5)
Average		146.9(1.2)		151.9(1.8)		133.5(1.2)		135.6(1.4)
Wax myrtle					Wire grass			
Conversion	Live		Dead		Live		Dead	
	Log ₁₀ A	E	Log ₁₀ A	E	Log ₁₀ A	E	Log ₁₀ A	E
10	10.76(0.28)	135.6(2.3)	15.15(0.40)	174.5(2.8)	11.47(0.30)	150.6(2.6)	11.14(0.29)	146.6(3.9)
20	11.58(0.37)	142.9(3.6)	15.79(0.41)	180.8(3.7)	12.06(0.39)	154.0(2.2)	11.32(0.30)	150.0(3.3)
30	12.30(0.46)	154.3(5.4)	16.98(0.66)	192.5(4.2)	12.53(0.47)	163.8(5.7)	11.88(0.46)	156.7(2.6)
40	12.82(0.43)	164.2(2.7)	17.22(0.78)	199.5(3.4)	12.81(0.43)	170.6(2.8)	11.77(0.53)	154.3(3.9)
50	13.22(0.17)	167.6(2.1)	18.06(0.24)	213.1(4.4)	12.99(0.17)	169.9(4.1)	12.65(0.17)	164.7(5.8)
60	13.52(0.24)	173.5(2.7)	18.46(1.13)	218.5(2.9)	13.07(0.23)	173.5(2.7)	13.23(0.81)	167.9(4.1)
70	14.32(0.66)	180.7(4.1)	19.04(0.28)	227.9(4.2)	13.64(0.63)	177.5(4.0)	12.78(0.19)	162.5(3.9)
80	14.95(0.44)	194.6(5.1)	20.19(0.60)	237.7(4.1)	14.07(0.42)	188.1(4.9)	13.93(0.41)	182.0(4.8)
90	15.16(0.42)	199.6(5.6)	20.40(0.57)	246.6(4.1)	14.09(0.39)	190.1(5.3)	13.84(0.39)	182.7(5.1)
Average		168.1(1.5)		210.1(2.2)		170.9(1.5)		163.1(1.6)

Table 7-3 Continued

Conversion	Yaupon			
	Live		Dead	
	Log ₁₀ A	E	Log ₁₀ A	E
10	7.19(0.19)	97.5(1.7)	7.80(0.21)	104.3(2.8)
20	7.82(0.25)	102.8(2.6)	8.33(0.22)	111.1(2.4)
30	8.36(0.31)	110.9(3.9)	9.09(0.35)	116.1(5.0)
40	8.71(0.29)	117.9(1.9)	9.34(0.42)	123.1(3.1)
50	8.99(0.12)	120.5(1.5)	9.87(0.13)	130.7(4.6)
60	9.19(0.16)	124.7(1.9)	10.18(0.62)	134.7(3.2)
70	9.73(0.45)	129.8(2.9)	10.57(0.16)	142.1(3.8)
80	10.17(0.30)	139.8(3.7)	11.30(0.33)	153.0(4.0)
90	10.33(0.29)	143.4(4.0)	11.53(0.32)	158.2(4.4)
Average		120.8(1.1)		130.4(1.1)

^a kJ mol⁻¹

^b s⁻¹

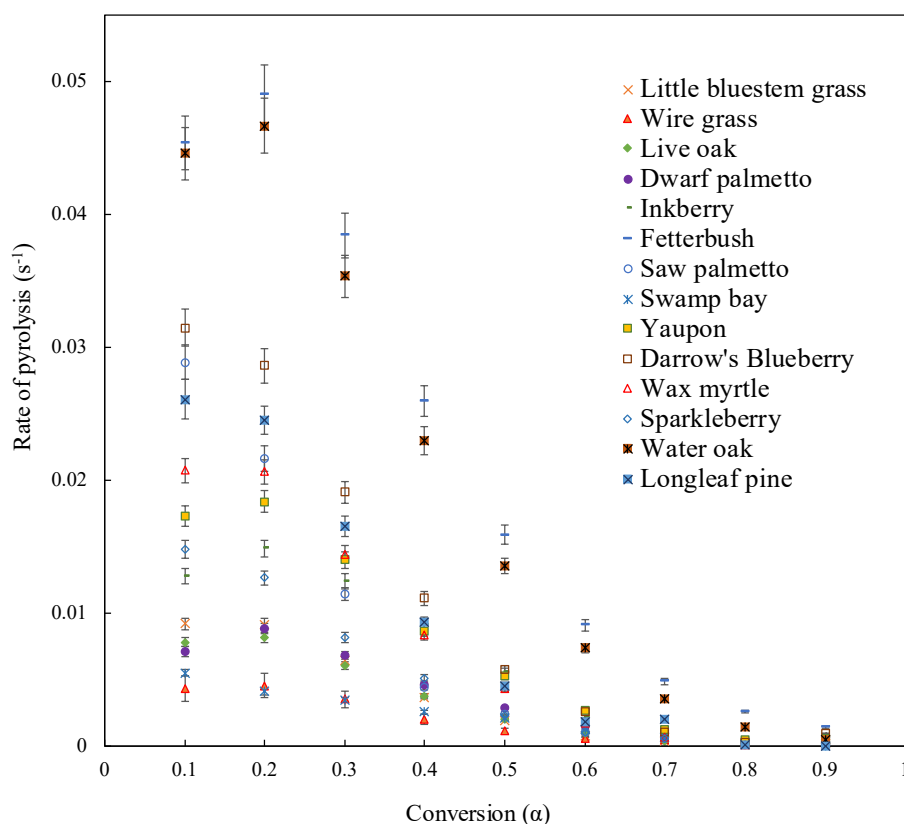
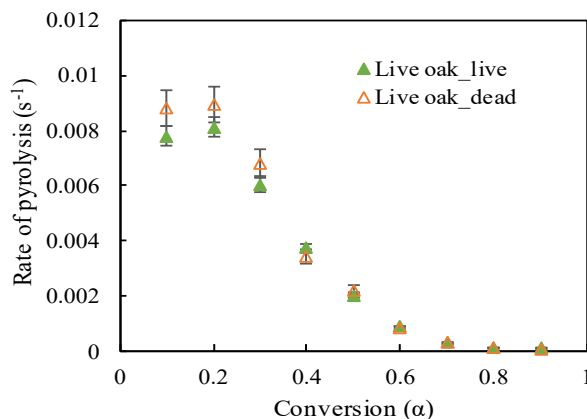
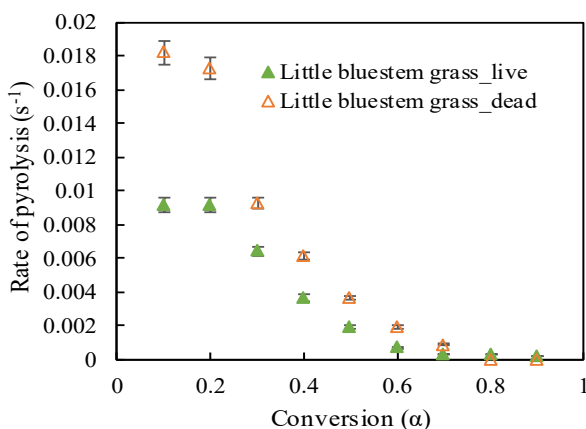
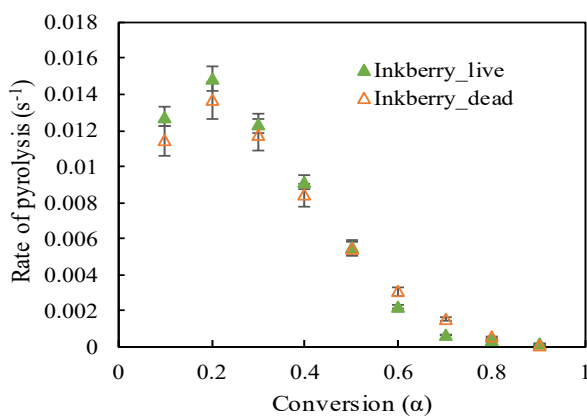
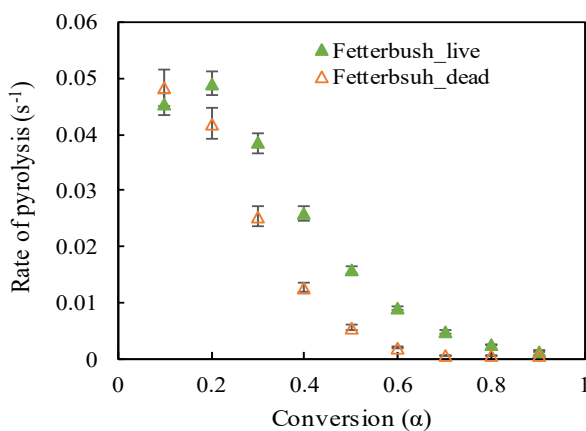
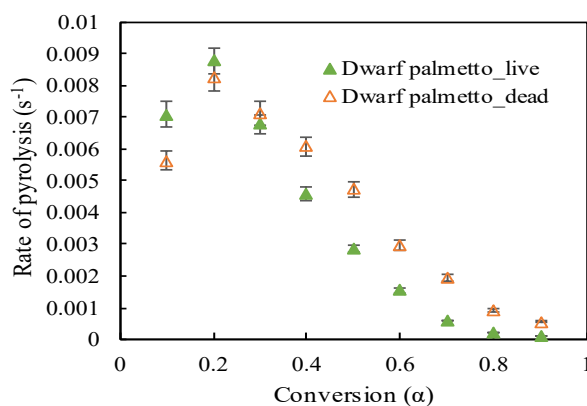
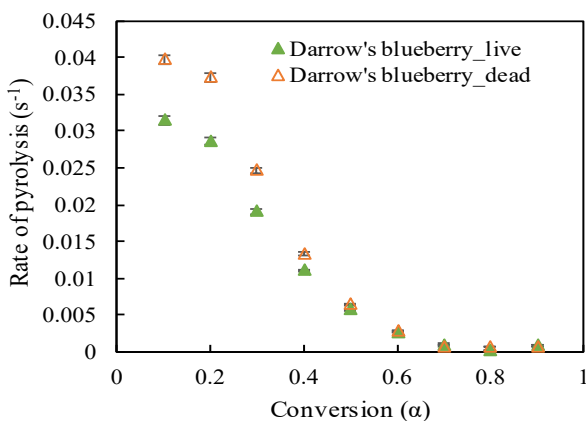


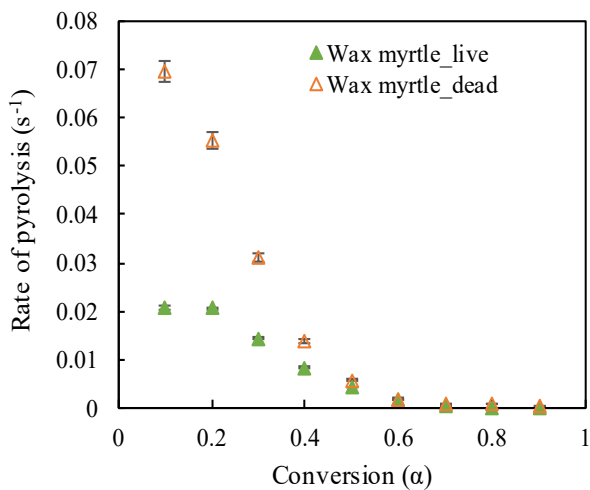
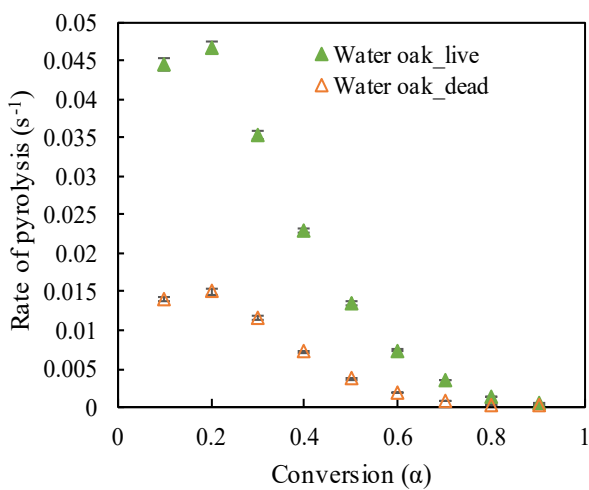
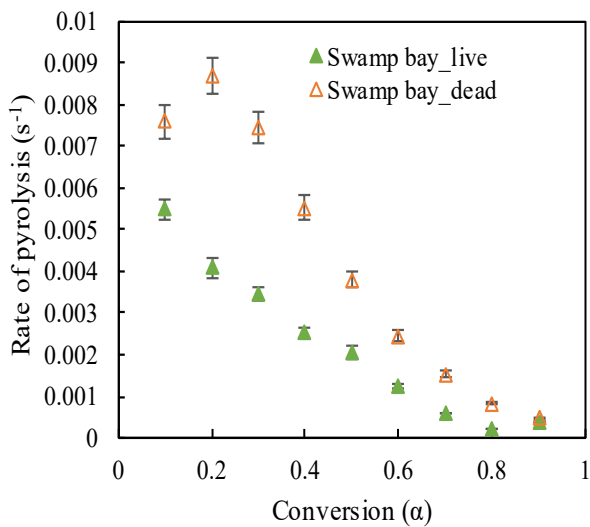
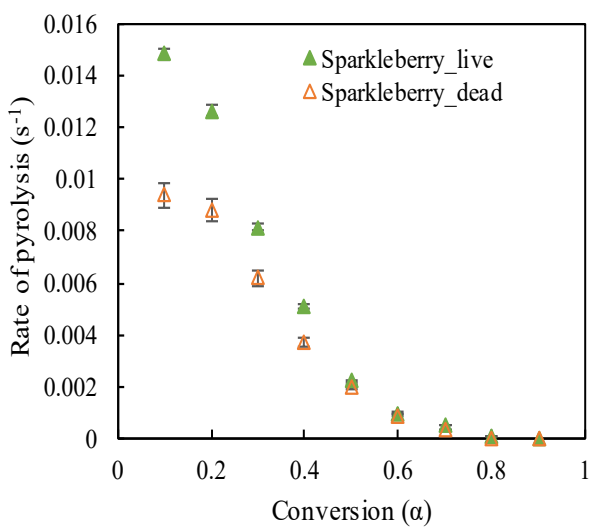
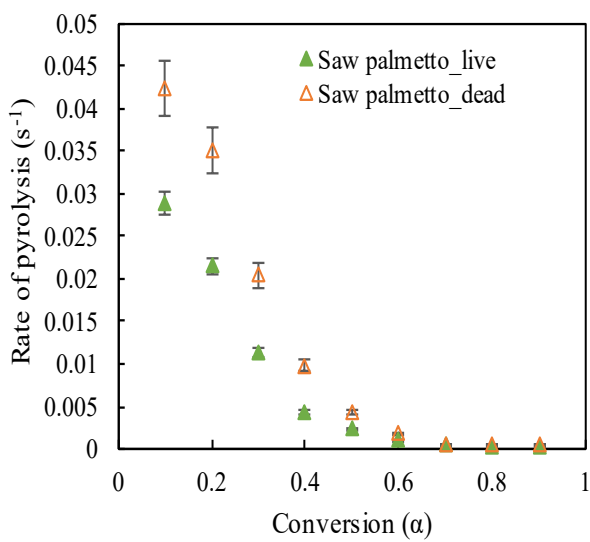
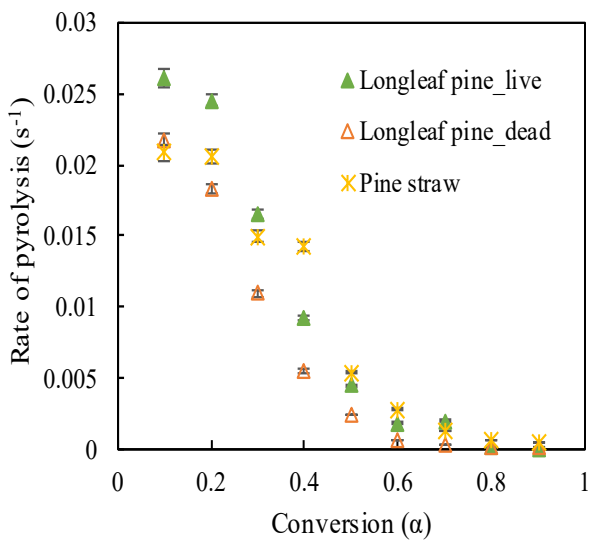
Figure 7-8: Distribution of pyrolysis rates as a function of conversion based on the KAS method for all plant species at 300 °C. Error bars represent the 95% confidence intervals based on three samples.

Between $\alpha=80 - 90\%$, the rates of pyrolysis became very low and approached zero. Fetterbush and water oak had the highest rates at each extent of conversion between all plant species. Wire grass and swamp bay had the lowest pyrolysis rates at each extent of conversion. The highest pyrolysis rate was observed for fetherbush with a rate of 0.045 s^{-1} at conversion of 20%.

Figure 7-9 shows a comparison of the rates as function of conversion at 300 °C for live and dead samples. As conversion increased, live and dead samples exhibited a decreasing trend of pyrolysis rates for all plant species. All the graphs of rates as function of conversion for both live and dead samples approached near zero at higher conversion of $\alpha=80 - 90\%$. For inkberry,

yaupon, and live oak the pyrolysis rates as a function of conversion for live and dead samples almost overlapped. Pyrolysis rates of live and dead samples of Dwarf palmetto, Darrow's blueberry, fetterbush, longleaf pine, and wire grass were close to each other at different conversions, but did not seem to overlap.





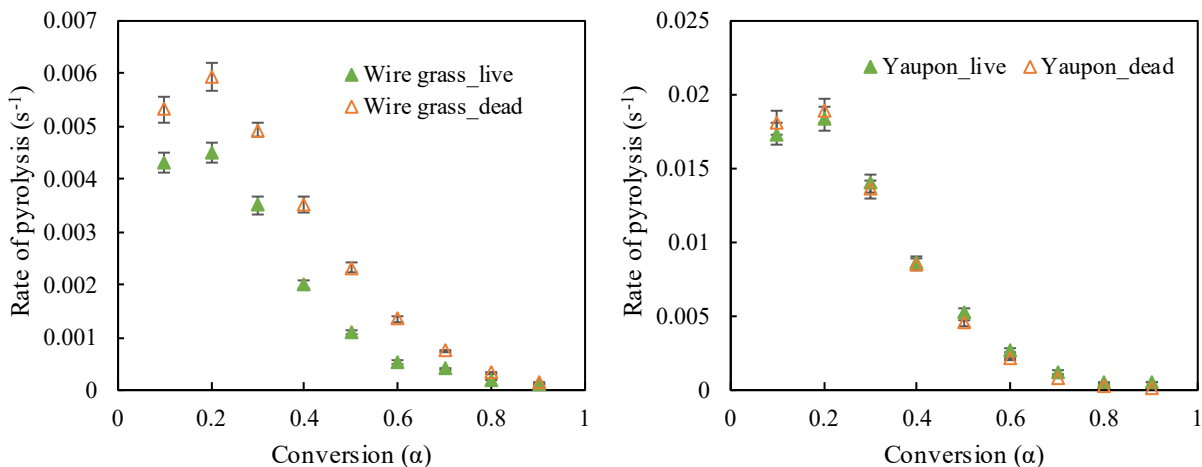


Figure 7-9: Distribution of pyrolysis rates as a function of conversion based on the KAS for live and dead samples of all plant species at 300 °C. Error bars represent the 95% confidence intervals based on three samples.

For little bluestem grass, saw palmetto, swamp bay, sparkleberry, water oak, and wax myrtle, the rates of pyrolysis were significantly different between live and dead samples, especially at lower conversions.

7.6 Comparison of Activation Energies for Different Biomass

Different biomass samples have different decomposition characteristics and activation energies due to their different chemical compositions. To compare the results of this study with other biomass pyrolysis research, activation energies obtained from different biomass samples reported in the literature using iso-conversional models are summarized in Table 7-4 (Hu et al., 2007; Damartzis et al., 2011; Gai et al., 2013; Balogun et al., 2014; Kongkaew et al., 2015; Ma et al., 2015; Yuan et al., 2015; Ozsin and Putun, 2017; Dhaundiyal et al., 2018).

Figure 7-10 shows a comparison of the pyrolysis activation energies from the live plants in this study with different types of biomass reported in the literature (Hu et al., 2007; Damartzis et al., 2011; Gai et al., 2013; Balogun et al., 2014; Kongkaew et al., 2015; Ma et al., 2015; Yuan et

al., 2015; Ozsin and Putun, 2017; Dhaundiyal et al., 2018). For this figure, the biomass was classified into eight groups: palmetto, grass, broadleaf, straw, needle, nut, wood, and shells. The average activation energies obtained in this study for palmetto, grass, broadleaf, and needle types (190, 155, 149, and 167 kJ mol⁻¹, respectively) were very close to the average activation energies obtained for different types of straw (155 kJ mol⁻¹) reported in the literature.

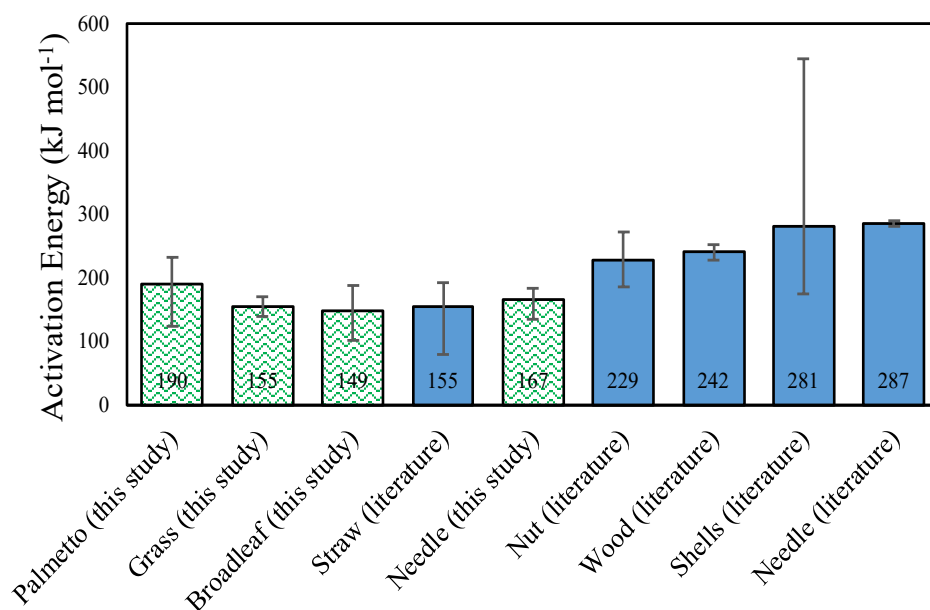


Figure 7-10: Activation energies for pyrolysis of different types of biomass (green pattern columns are obtained from this study and the blue ones are reported in the literature).

7.7 The Effect of Aging on Activation Energy

The kinetic analysis of pyrolysis of live longleaf pine foliage (LLPF), dead longleaf pine foliage (DLPF) and pine straw were investigated to study the effect of aging on activation energies as well as the dependence of activation energies on degree of conversion for both drying and major pyrolysis zones. Figure 7-11 illustrates the dependency of activation energies on the degree of conversion based on the KAS method. The 95% confidence intervals are shown as error bars in this figure, representing excellent data reproducibility.

Table 7-4: Kinetic analysis results obtained from pyrolysis of different biomass samples from literature for the major pyrolysis zone

Biomass	β^a (°C min ⁻¹)	α (%)	Kinetic method	E _a (kJ mol ⁻¹)	A (min ⁻¹)	Reference
Chestnut shell	5-40	10-90	KAS Starink FWO	175.2 175.5 175.9	-	(Ozsin and Putun, 2017)
Cherry stone	5-40	10-90	Starink FWO KAS	272.2 268.5 272.4	-	(Ozsin and Putun, 2017)
Grape seed	5-40	10-90	Starink FWO KAS	187.1 186.9 187.3	-	(Ozsin and Putun, 2017)
<i>Tectona grandis</i>	5-35	15-85	Starink FWO	253.2 253.2	7.1×10^{21}	(Balogun et al., 2014)
Palm kernel shell	10-40	0.9-87	KAS FWO	231-545 227-529	-	(Ma et al., 2015)
Cardoon stems	5-30	20-80	KAS FWO	224.5 229.7	1.8×10^{19} 5.7×10^{17}	(Damartzis et al., 2011)
Cardoon leaves	5-30	20-80	KAS FWO	350.0 242.0	3.0×10^{31} 7.3×10^{28}	
Corn Straw	5-40	20-80	Starink	129	-	(Gai et al., 2013)

Table 7-4 Continued

Biomass	β^a ($^{\circ}\text{C min}^{-1}$)	α (%)	Kinetic method	E_a (kJ mol^{-1})	A (min^{-1})	Reference
Rice husk	5-40	20-80	Starink	79	-	(Gai et al., 2013)
<i>Parthenium hystrophorus</i>	5-20	0.5-70	FWO KAS Kissinger	145.8 145.4 148.0		(Dhaundiyal et al., 2018)
Rice straw	5-15	10-80	FWO KAS Kissinger	192.6 193.6 172.6	1.3×10^{22} 6.9×10^{15} 1.5×10^{11}	(Kongkaew et al., 2015)
Pine needle	5-20	20-75	FWO KAS	291.5 281.5	-	(Yuan et al., 2015)
Rice straw	2.5-10	14-81	Ozawa	158	5.4×10^7	(Hu et al., 2007)
Rice husk	2.5-10	14-81	Ozawa	184	8.3×10^6	
Cotton straw	2.5-10	14-81	Ozawa	177	9.6×10^{12}	
Maize straw	2.5-10	14-81	Ozawa	159	3.2×10^6	
Camphor branch	2.5-10	14-81	Ozawa	190	2.4×10^7	

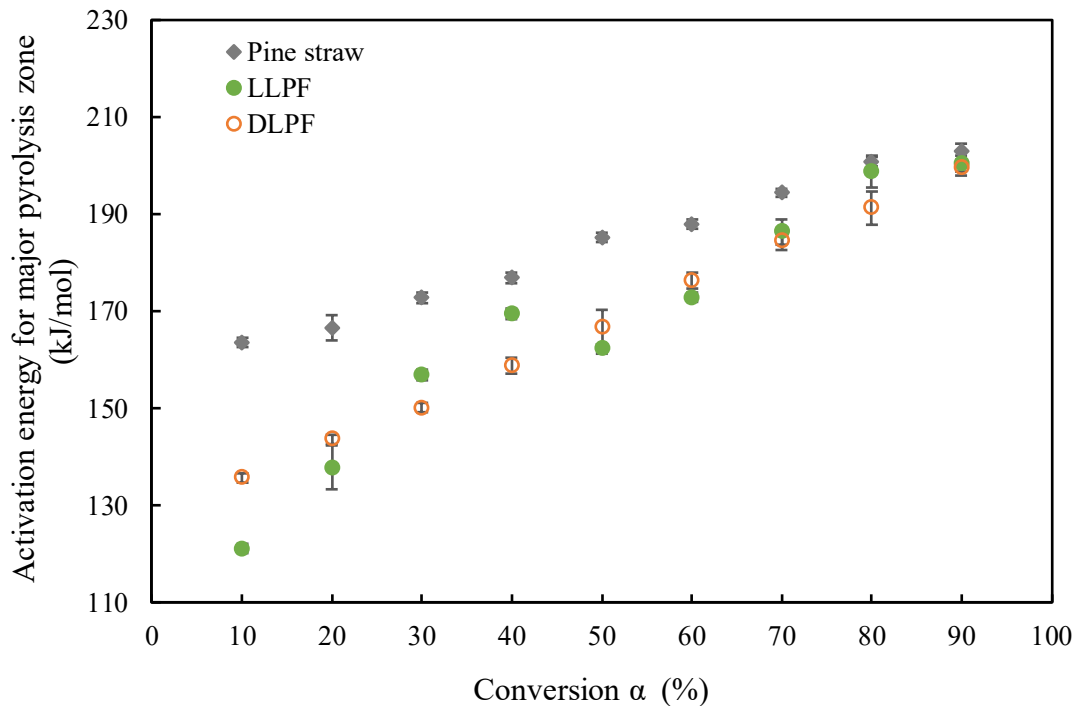


Figure 7-11: Activation energy distribution for pyrolysis of live and dead longleaf pine foliage, and pine straw during major pyrolysis zone based on the KAS method. Error bars represent the 95% confidence intervals from three samples.

According to this figure, the activation energy increased almost linearly with conversion in the major pyrolysis zone for LLPF and DLPF. This might be attributed to the parallel reaction routes with different activation energies. Similar to LLPF and DLPF, activation energies also increased almost linearly with conversion for pine straw, but not at the same rate of increase as the LLPF and DLPF samples. This shows that the aging did not affect the reaction routes of a pyrolysis process, but did affect the actual rates. For the drying zone, the average activation energy was higher for LLPF (82 kJ mol^{-1}) than those for DLPF (55 kJ mol^{-1}) and pine straw (36 kJ mol^{-1}). These results revealed that a sample with higher moisture content needs higher activation energy which means that the reaction occurs slowly. Comparing DLPF and pine straw showed that the pine straw had the lowest activation energy for drying and consequently fastest moisture release reaction.

For the major pyrolysis zone, the average activation energy for LLPF was 167 kJ mol^{-1} based on the KAS method. This value was 167 kJ mol^{-1} for DLPF. This shows that, similar to LBG, the activation energies for the live and dead samples in the major pyrolysis zone were not significantly different. For pine straw, the activation energy based on the KAS method was 183 kJ mol^{-1} which was higher than that for DLPF.

The higher activation energy for pyrolysis zone of pine straw revealed that the aging affects the reaction and the minimum energy requirement for pyrolysis process. The longer drying time made the pyrolysis process slower. This result also can be described with DTG curves of LLPF, DLPF, and pine straw. According to Figure 7-12, the peak of DTG curve for pine straw shifted toward higher temperature, which shows that the pyrolysis of pine straw is slower than LPF. This shift in peak temperature could be attributed to the lower amount of extractives in pine straw which have catalytic effects during pyrolysis (Ozsin and Putun, 2017). For LLPF and DLPF, the peak of DTG curves occurs at almost the same temperature. This result is similar to the results obtained from pyrolysis of LBG.

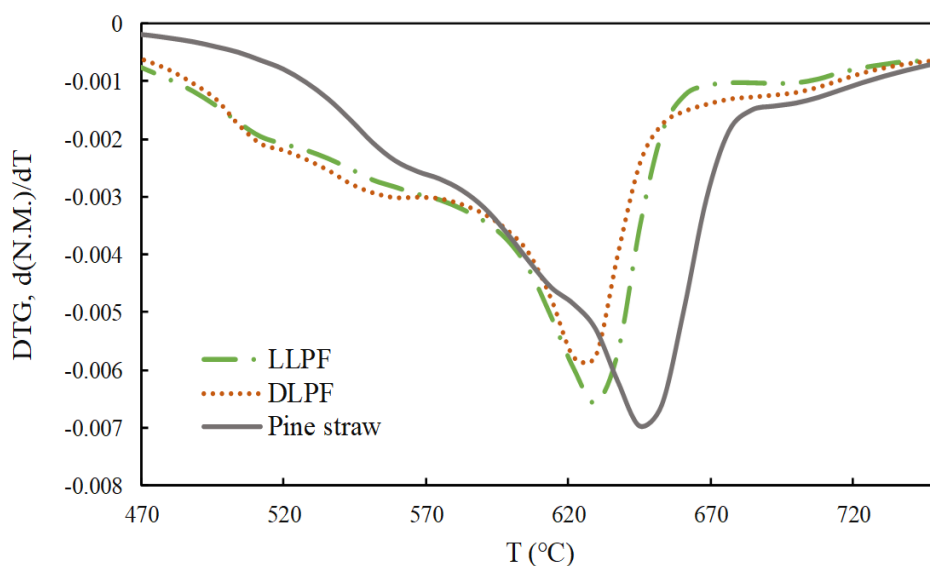


Figure 7-12: DTG curves for major pyrolysis zones of LLPF, DLPF, and pine straw for 30 °C min^{-1} .

7.8 Summary and Conclusion

In this chapter, slow pyrolysis experiments of 14 live and dead plant species native to the forests in the southern United States were conducted in a TGA. The iso-conversional method of KAS at five different heating rates ranged from 10 to 30 °C min⁻¹ was used to calculate the average activation energy and pre-exponential factor for all plants. The conclusions from this research are:

- 1- The condition of the plant (live vs. dead) did not affect the number of pyrolysis peaks or zones of a particular plant species.
- 2- The heating rate did not affect the number of the peaks of DTG curve for a plant species. The mass loss pattern was same at all heating rates except for a shift in the temperature of the peak mass loss rates. In addition, the maximum pyrolysis rate increased slightly with increasing heating rate.
- 3- The live samples with higher moisture contents had higher activation energies during the drying zone.
- 4- The iso-conversion analysis of activation energies as a function of the extent of conversion showed similar trends for both live and dead samples of a given plant species.
- 5- The distribution of pyrolysis rate as a function of conversion was studied for all live and dead plant species. The results showed that different plant species had different rates at different conversions. During the sample decomposition, the highest rates were observed at the beginning of the pyrolysis between $\alpha=10-20\%$, for all samples. Between $\alpha=80-90\%$, the rate of pyrolysis became very low and approached zero.
- 6- The average activation energies obtained in this study for palmetto, grass, broadleaf,

and needle types (190, 155, 149, and 167 kJ mol⁻¹, respectively) were very close to the average activation energies obtained for straw (154 kJ mol⁻¹) reported in the literature.

- 7- Aging affected the reaction and the minimum energy requirement for pyrolysis process. The aging made the pyrolysis process slower and led to higher activation energy values. However, aging did not influence the trend of activation energy distribution increasing with degree of conversion.
- 8- For some of the species, the pyrolysis rates were significantly different between live and dead samples.

In this chapter, the rates of pyrolysis were calculated as a function of the extent conversion. However, in the next chapter, the kinetic parameters for all plant species will be calculated by model-fitting methods of multiple heating rates to potentially provide a single rate for each plant species (live and dead), which can be more easily used in detailed wildland fire models.

8 PYROLYSIS KINETICS OBTAINED FROM MODEL-FITTING METHODS

The characterization of pyrolysis products and the dependence of the kinetic parameters on the degree of conversion using iso-conversional methods for all the plant species were studied in previous chapters. The main aim of this chapter is to present single kinetic parameters for the entire pyrolysis process which can be used by wildland fire modelers. The model forms explored here are the simple one-step model and the single and multiple reaction distributed activation energy models (DAEM). The mass loss and derivative mass loss data were fitted simultaneously at three heating rates of 10, 20, and 30 °C min⁻¹ to find kinetic parameters for these model forms.

8.1 Pyrolysis Completion Temperature

The completion temperature has been extensively used by many researchers to characterize pyrolysis and combustion properties of solid fuels (M.Vleeskens and N.Nandi, 1986; El-Sayed and Mostafa, 2014; Mishra and Mohanty, 2018). The temperature where the normalized rate of decomposition decreases consistently to less than 1%/min is defined as the completion temperature (El-Sayed and Mostafa, 2014). The pyrolysis completion temperature was determined for both the live and dead plant species at all three heating rates of 10, 20, and 30 °C-min⁻¹; the results for the live samples are presented in Figure 8-1. The pyrolysis completion temperature varied between 381 and 473 °C, with little bluestem grass having the lowest completion temperature and inkberry having the highest. The pyrolysis completion temperature

may possibly be related to the propensity of the plant species to burn; plant species with low pyrolysis completion temperatures would finish burning earlier in a fire scenario.

The effect of heating rate on completion temperature is also shown in Figure 8-1; increasing heating rate increases the completion temperature. For example, increasing heating rate from 10 to 30 °C min⁻¹ increased the completion temperature from 458 to 473 °C and from 361 to 381 °C for inkberry and little bluestem grass, respectively. Pyrolysis at higher heating rates occurs in shorter reaction times which results in the decomposition of sample at higher temperature (Ma et al., 2015; Banon et al., 2016). It is expected that the completion temperature will continue to rise at higher heating rates.

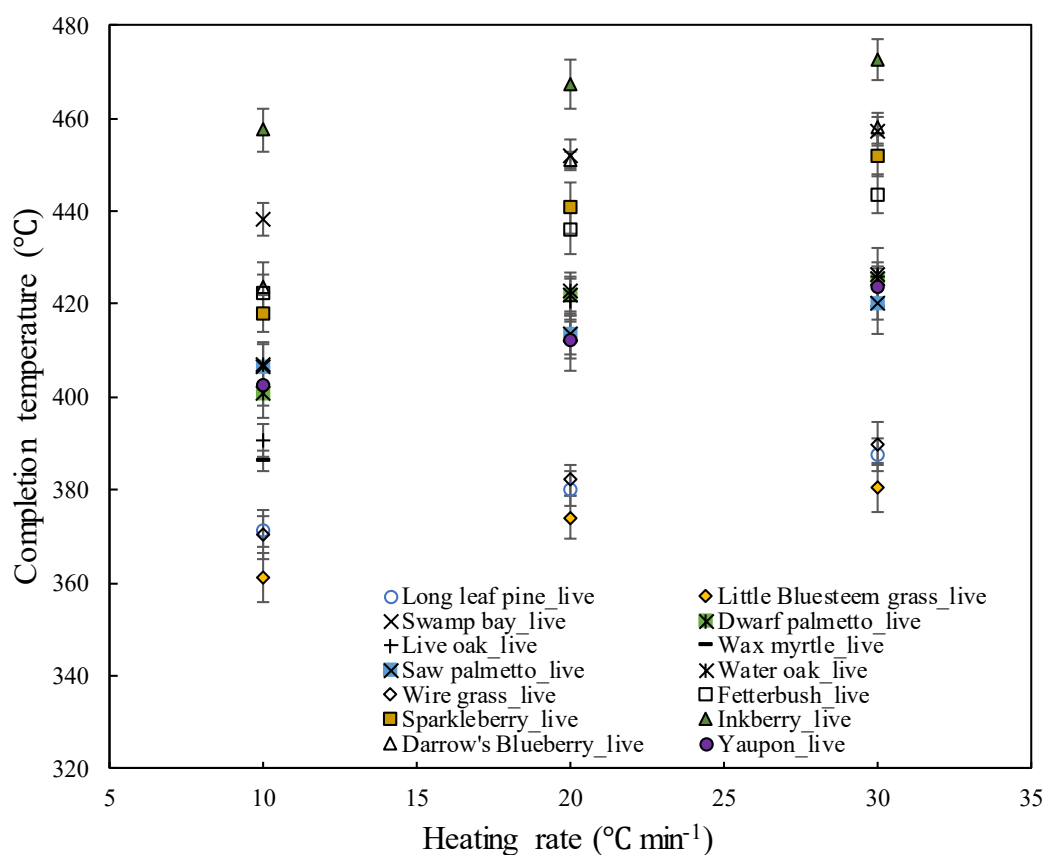


Figure 8-1: The completion temperature for all live plant species at heating rates of 10, 20, and 30 °C min⁻¹. Error bars represent the 95% confidence intervals based on three samples.

The completion temperature was also compared between live and dead samples (Figure 8-2). Little bluestem grass, yaupon, and fetterbush had almost the same completion temperature between live and dead samples. Most of the species such as live oak, water oak, wax myrtle, sparkleberry, wire grass, inkberry, Darrow's blueberry, and saw palmetto had higher completion temperature for live samples, showing that these species became more combustible after drying enough to die. For longleaf pine, swamp bay, and dwarf palmetto, the completion temperature was higher for dead samples, showing that these plant species may have become slightly less combustible after drying. Comparing the results for longleaf pine revealed that, aging increased the completion temperature and made the fuel less combustible. This could be caused by lower amount of extractives in pine straw, which pyrolyze at low temperatures and have been reported to have catalytic effects on pyrolysis (Ozsin and Putun, 2017).

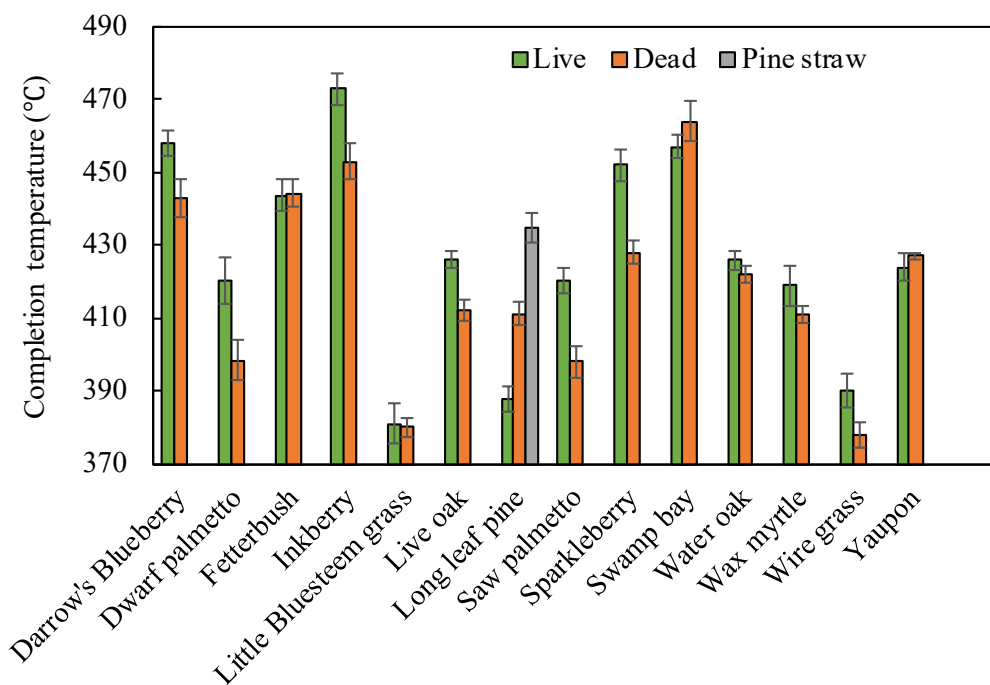
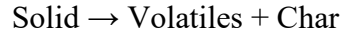


Figure 8-2: The pyrolysis completion temperature for live vs. dead plant samples. Error bars represent the 95% confidence intervals based on three samples.

8.2 Simple One-Step Model

Biomass pyrolysis is often described by the following simple reaction:



Biomass pyrolysis depends on the conversion, residual mass, and temperature. The simple one-step model is based on the Arrhenius reaction form. Many researchers have used this model in their computational fluid dynamics (CFD) codes (Chaos et al., 2011; Boateng and Mtui, 2012; Xue et al., 2012). The model is as follows:

$$\frac{dV}{dt} = A \exp\left(-\frac{E}{RT}\right) (V_{\infty} - V) \quad (8-1)$$

where A and E are Arrhenius kinetic coefficients, t is time, T is the particle temperature, R is the Arrhenius constant, V is the normalized mass of volatiles, and V_{∞} is the final value of V.

Using one set of coefficients for each reaction, the cumulative mass and the derivative of the mass from all heating rates of 10, 20, and 30 °C min⁻¹ were fitted simultaneously to the experimental data. Representative curve-fits of the TGA and DTGA single peak and multiple peak pyrolysis data for live little bluestem grass and live water oak using the simple one-step model are presented in Figure 8-3. The curve-fits for other plant species are presented in Appendix F (Figure F-1). Based on the fits curve for the both single and multiple peak data, this simple model did not accurately predict the pyrolysis reaction and can only be considered as an approximate method.

The values of activation energies and pre-exponential factors for the pyrolysis zone (first peak after the drying zone) of each plant species were determined using the combined data from the experiments at three constant heating rates of 10, 20, and 30 °C min⁻¹, and the results are presented in Table 8-1. For live samples, activation energies obtained from the simple one-step model were in the range of 47.7 – 76.9 kJ mol⁻¹. Yaupon had the lowest activation energy with a

value of $47.7 \pm 2.8 \text{ kJ mol}^{-1}$. The highest activation energy with a value of $76.9 \pm 2.1 \text{ kJ mol}^{-1}$ were obtained from pyrolysis of saw palmetto. For dead samples, activation energies were in the range of 47.1 - 76.6 kJ mol^{-1} . The lowest activation energy for dead samples ($47.1 \pm 2.4 \text{ kJ mol}^{-1}$) was obtained from pyrolysis of yaupon. Dead saw palmetto had the highest activation energy ($76.6 \pm 1.2 \text{ kJ mol}^{-1}$) of all the dead samples.

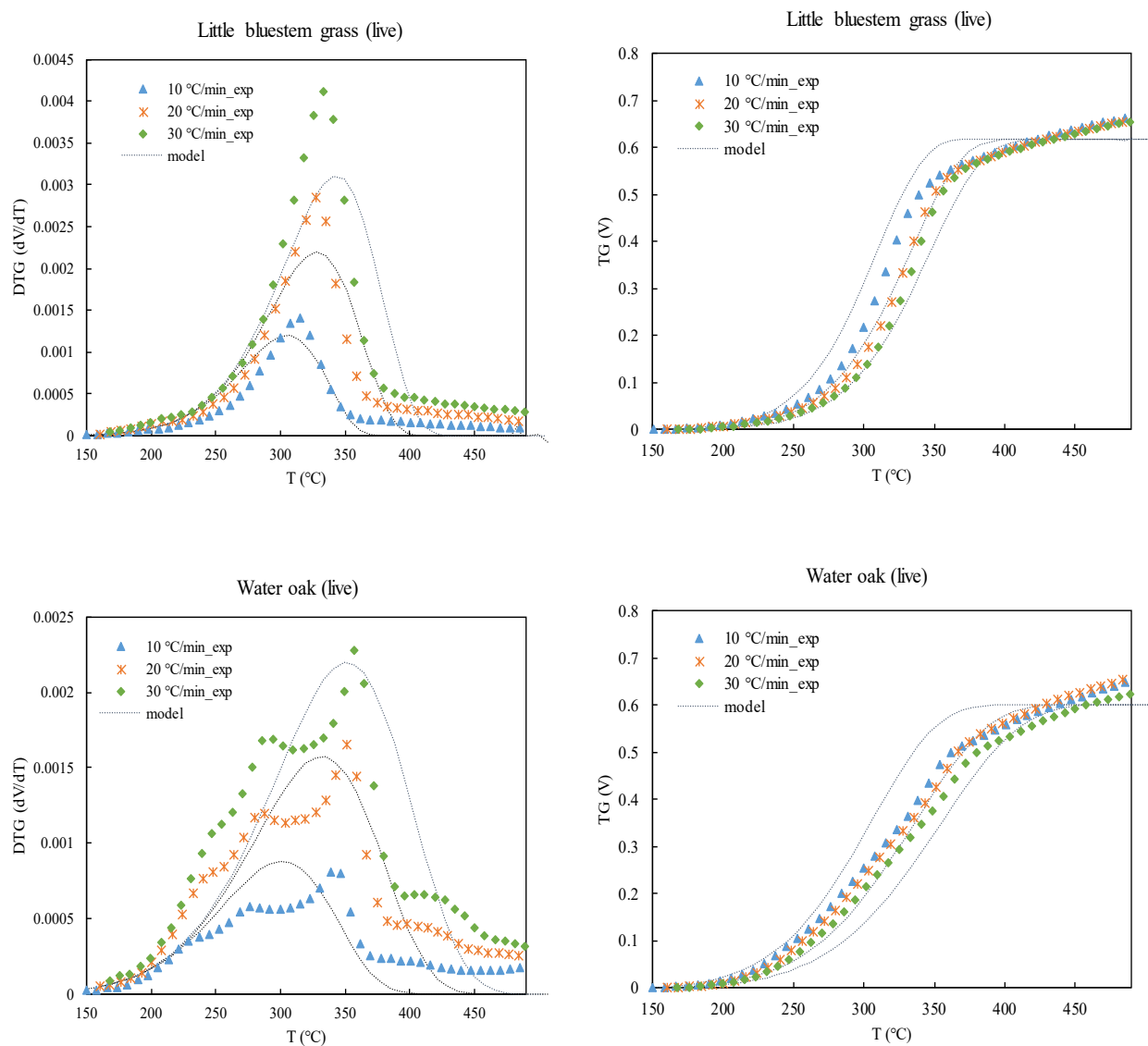


Figure 8-3: Comparison of simple one-step model curve-fit with TG and DTG curves for live little bluestem grass and water oak at the heating rates of 10, 20, and 30 °C min⁻¹.

Table 8-1: The kinetic parameters (mean values of three replicates) obtained from the simple one-step model for each plant species (the 95% confidence intervals are reported in the parentheses)

Species	E _a (kJ mol ⁻¹)		Log ₁₀ A (s ⁻¹)		V _∞ (normalized)	
	Live	Dead	Live	Dead	Live	Dead
Darrow's blueberry	50.2(4.4)	51.0(4.6)	2.23(0.47)	1.87(0.25)	0.62(0.02)	0.62(0.03)
Dwarf palmetto	54.3(4.2)	59.3(6.7)	4.29(0.86)	3.55(0.93)	0.62(0.04)	0.63(0.02)
Fetterbush	59.9(4.3)	61.6(4.2)	2.18(0.31)	2.41(0.20)	0.60(0.03)	0.61(0.04)
Inkberry	50.6(4.4)	53.5(4.5)	1.89(0.09)	2.64(0.41)	0.60(0.03)	0.61(0.01)
Live oak	51.8(4.5)	55.3(3.7)	2.86(0.20)	2.75(0.09)	0.55(0.04)	0.56(0.06)
Little bluestem grass	58.2(3.9)	60.1(7.4)	4.39(0.30)	4.16(0.11)	0.60(0.04)	0.60(0.01)
Longleaf pine foliage	65.2(5.3)	61.6(5.7)	2.49(0.01)	2.29(0.02)	0.63(0.04)	0.61(0.03)
Longleaf pine litter	-	70.7(7.2)	-	4.29(0.13)	-	0.64(0.03)
Saw palmetto	76.9(3.5)	76.6(2.0)	3.47(0.23)	3.25(0.14)	0.55(0.03)	0.55(0.05)
Sparkleberry	53.2(4.6)	55.6(4.8)	2.15(0.12)	2.51(0.25)	0.56(0.-3)	0.56(0.01)
Swamp bay	54.1(5.6)	58.4(7.2)	2.83(0.22)	2.82(0.14)	0.61(0.06)	0.59(0.02)
Water oak	50.6(3.9)	52.9(4.9)	2.42(0.11)	3.23(0.12)	0.60(0.03)	0.60(0.02)
Wax myrtle	66.7(5.3)	66.4(1.8)	2.40(0.12)	2.20(0.17)	0.50(0.02)	0.51(0.02)
Wire Grass	74.6(5.1)	72.2(2.2)	4.54(0.11)	4.45(0.27)	0.66(0.03)	0.67(0.03)
Yaupon	47.7(3.1)	47.1(4.0)	2.37(0.15)	2.59(0.13)	0.58(0.02)	0.57(0.03)

Among all plant species, dwarf palmetto exhibited the largest statistically difference in activation energy value (5 kJ mol^{-1} , absolute) between the live and dead samples ($P < 0.05$), which is less than a 10% difference from the live sample value. Wax myrtle and saw palmetto had the lowest difference in activation energy value (0.3 kJ mol^{-1}) based on simple one-step model between live and dead samples (less than 0.5% of the live value).

8.3 Distributed Activation Energy Model (DAEM)

The DAEM method was originally proposed by Vand (1943) and has been applied to different complex reactions (Anthony et al., 1975; Fletcher et al., 1992; Shen et al., 2011; Soria-Verdugo et al., 2013; Richards and Fletcher, 2016; Xiong et al., 2016). This model assumes that the decomposition of biomass occurs through a variety of reactions that have a range of activation energies. The activation energy distribution function representing the range of activation energies is usually taken to be a Gaussian distribution. In this study, two forms of DAEM were used: (1) the single-reaction DAEM model, and (2) the parallel-reaction DAEM model, both models using the series reaction formulation (Fletcher et al., 1992).

8.3.1 Single-Reaction DAEM Model

The single-reaction DAEM model consists of one first-order reaction with a distributed activation energy defined by a Gaussian shape. A mean and standard deviation of the activation energy must be specified along with a single pre-exponential factor. The original formulations of the DAEM model used parallel reaction rates, so that all activation energies could participate in the reaction at any time (Vand, 1943; Anthony et al., 1975). However, since reactions with the lowest activation energies generally participate in the reaction first, a form of the DAEM model was formulated to use reactions in series (Fletcher et al., 1992), which is much more

computationally efficient and physically more realistic. The series reaction formulation calculates the effective activation energy as a function of the extent of reaction based on a Gaussian distribution, as follows:

$$\frac{dV}{dt} = A \exp\left(-\frac{(E_a + \sigma_E Z)}{RT}\right) (V_\infty - V) \quad (8-2)$$

$$Z = \text{erfinv}(1 - 2 \times (V_\infty - V)) \quad (8-3)$$

where σ_E is the standard deviation for the activation energy distribution, E_a is the mean activation energy, Z is an inverse cumulative Gaussian distribution of activation energies based on fuel conversion, R is the gas constant, V is the normalized mass of volatiles, V_∞ is the final value of V , and erfinv is the inverse of the error function.

The series reaction form of the DAEM model was used in this analysis. Using the DAEM model with one set of coefficients, the cumulative mass data and the derivative of the mass from the heating rates of 10, 20, and 30 °C min⁻¹ were fitted simultaneously in a manner similar to Hillier et al. (2010). Representative curve-fits of the TGA and DTGA single peak and multiple peak pyrolysis data for live little bluestem grass and live water oak using the single-reaction DAEM model are presented in Figure 8-4. The curves for other plant species are presented in Appendix G (Figure G-1). The model matched the DTG peaks fairly well for the single peak curves (top left panel in Figure 8-4), but did not agree as well with the multi-peak data (bottom left panel). The values of E_a , σ_E , and A for the pyrolysis zones (after drying zone) of each plant species were determined using the combined data from the experiments at three constant heating rates of 10, 20, and 30 °C min⁻¹. The resulting coefficients determined for each plant species are presented in Table 8-2. For live samples, activation energies obtained from the single-reaction DAEM model were in the range of 124.1 – 269.4 kJ mol⁻¹. Yaupon had the lowest activation energy with a value of 124.1 kJ mol⁻¹. The highest activation energy with a value of 269.4 kJ

mol^{-1} were obtained from pyrolysis of saw palmetto. For dead samples, activation energies were in the range of $129.1 - 266.7 \text{ kJ mol}^{-1}$. The lowest activation energy with a value of $129.1 \pm 1.3 \text{ kJ mol}^{-1}$ was obtained from pyrolysis of yaupon. Saw palmetto had the highest activation energy with a value of $266.7 \pm 2.4 \text{ kJ mol}^{-1}$. Among all plant species, pine straw exhibited the largest difference in activation energy value (15.6 kJ mol^{-1}) between the live and dead samples. The next largest difference in activation energies were observed between live and dead samples of sparkleberry (5.5 kJ mol^{-1}) and wax myrtle (5.3 kJ mol^{-1}). Water oak had the lowest difference (0.1 kJ mol^{-1}) in activation energy values based on the single-reaction DAEM model between live and dead samples.

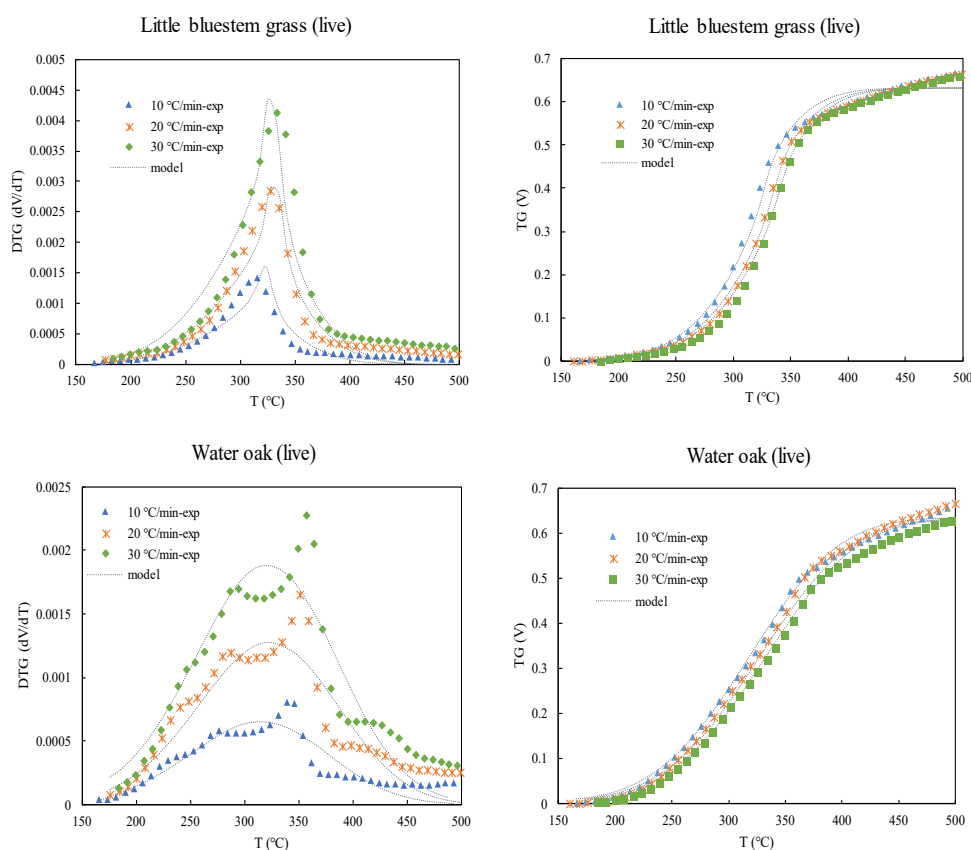


Figure 8-4: Comparison of best-fit single-reaction DAEM model (lines) with TGA and DTG data (points) for live little bluestem grass and water oak at three heating rates of 10, 20 and 30 °C min^{-1} .

Table 8-2: Kinetic parameters (mean values of three replicates) obtained from the single-reaction DAEM model for each plant species (the 95% confidence intervals are reported in the parentheses)

Species	E _a (kJ mol ⁻¹)		Log ₁₀ A (s ⁻¹)		σ _E (kJ mol ⁻¹)		V _∞ (normalized)	
	Live	Dead	Live	Dead	Live	Dead	Live	Dead
Darrow's blueberry	163.4(5.5)	163.8(3.6)	21.80(1.21)	21.60(1.28)	24.4(1.7)	15.5(1.4)	0.68(0.06)	0.66(0.07)
Dwarf palmetto	198.6(4.8)	201.9(3.6)	23.46(1.30)	23.59(1.22)	20.7(0.8)	18.9(0.5)	0.63(0.06)	0.66(0.02)
Fetterbush	212.4(5.1)	217.7(3.8)	17.46(1.49)	18.72(1.50)	14.8(0.6)	19.0(0.4)	0.65(0.03)	0.65(0.03)
Inkberry	175.5(3.8)	178.5(2.7)	18.56(1.26)	18.28(1.15)	17.3(1.2)	4.5(0.7)	0.66(0.03)	0.66(0.03)
Live oak	183.3(5.5)	182.9(4.3)	20.17(1.30)	20.63(2.00)	15.8(1.4)	19.4(0.8)	0.58(0.04)	0.59(0.02)
Little bluestem grass	213.1(4.5)	215.3(4.1)	19.52(2.14)	19.91(1.03)	11.5(2.2)	15.2(1.4)	0.61(0.05)	0.61(0.02)
Longleaf pine foliage	223.5(5.9)	220.5(6.1)	21.17(2.20)	21.85(1.02)	11.7(2.1)	12.5(2.5)	0.67(0.03)	0.64(0.03)
Longleaf pine litter	-	239.6(5.7)	-	14.63(1.06)	-	13.9(0.6)	-	0.66(0.02)
Saw palmetto	270.1(4.8)	266.7(3.9)	18.04(1.13)	18.23(2.25)	28.9(2.4)	15.3(1.4)	0.57(0.04)	0.58(0.05)
Sparkleberry	185.6(3.3)	180.1(5.3)	19.18(1.09)	19.72(1.13)	13.4(2.7)	14.8(1.4)	0.60(0.02)	0.59(0.07)
Swamp bay	201.7(6.1)	200.2(2.8)	18.81(1.27)	19.18(1.06)	7.6(2.2)	19.0(1.8)	0.64(0.09)	0.65(0.07)
Water oak	169.9(2.8)	169.8(2.2)	16.93(1.03)	17.61(2.01)	14.2(2.9)	26.4(5.0)	0.64(0.03)	0.64(0.05)
Wax myrtle	212.4(5.3)	217.7(1.8)	22.19(2.16)	22.54(2.10)	22.3(3.5)	15.6(2.6)	0.55(0.02)	0.52(0.08)
Wire Grass	219.0(5.9)	216.0(2.1)	17.83(1.15)	17.74(1.43)	11.8(2.5)	8.0(1.0)	0.67(0.05)	0.65(0.02)
Yaupon	123.7(5.8)	129.1(2.1)	19.51(1.49)	19.93(1.44)	8.7(0.9)	8.2(2.6)	0.59(0.02)	0.59(0.03)

8.3.2 Multiple-Reaction DAEM Model

According to this model, a plant sample consists of multiple pseudocomponents, where a pseudocomponent is a group of reactive species that show similar reactivity. Each pseudocomponent is comprised of a theoretically infinite number of fractions with different activation energies that usually follows a Gaussian distribution. A series formulation of the first-order DAEM is assumed for each pseudocomponent, which defines the time and temperature dependence of the released volatiles, V_j :

$$\frac{dV_j}{dt} = A \exp\left(-\frac{(E_{aj} + \sigma_{Ej} Z_j)}{RT}\right) (V_{\infty j} - V_j) \quad (8-4)$$

$$Z_j = \text{erfinv}(1 - 2 \times (V_{\infty j} - V_j)) \quad (8-5)$$

where σ_{Ej} , E_{aj} , Z_j , V_j , and $V_{\infty j}$ are the standard deviation for the activation energy distribution, the mean activation energy, the distribution based on fuel conversion, normalized mass of volatiles, and the final value of V_j for the pseudocomponent j , respectively. The resulting final reaction rate curve is the weighted sum of the individual dV_j/dt rates:

$$\frac{dV}{dt} = \sum \frac{dV_j}{dt} \quad (8-6)$$

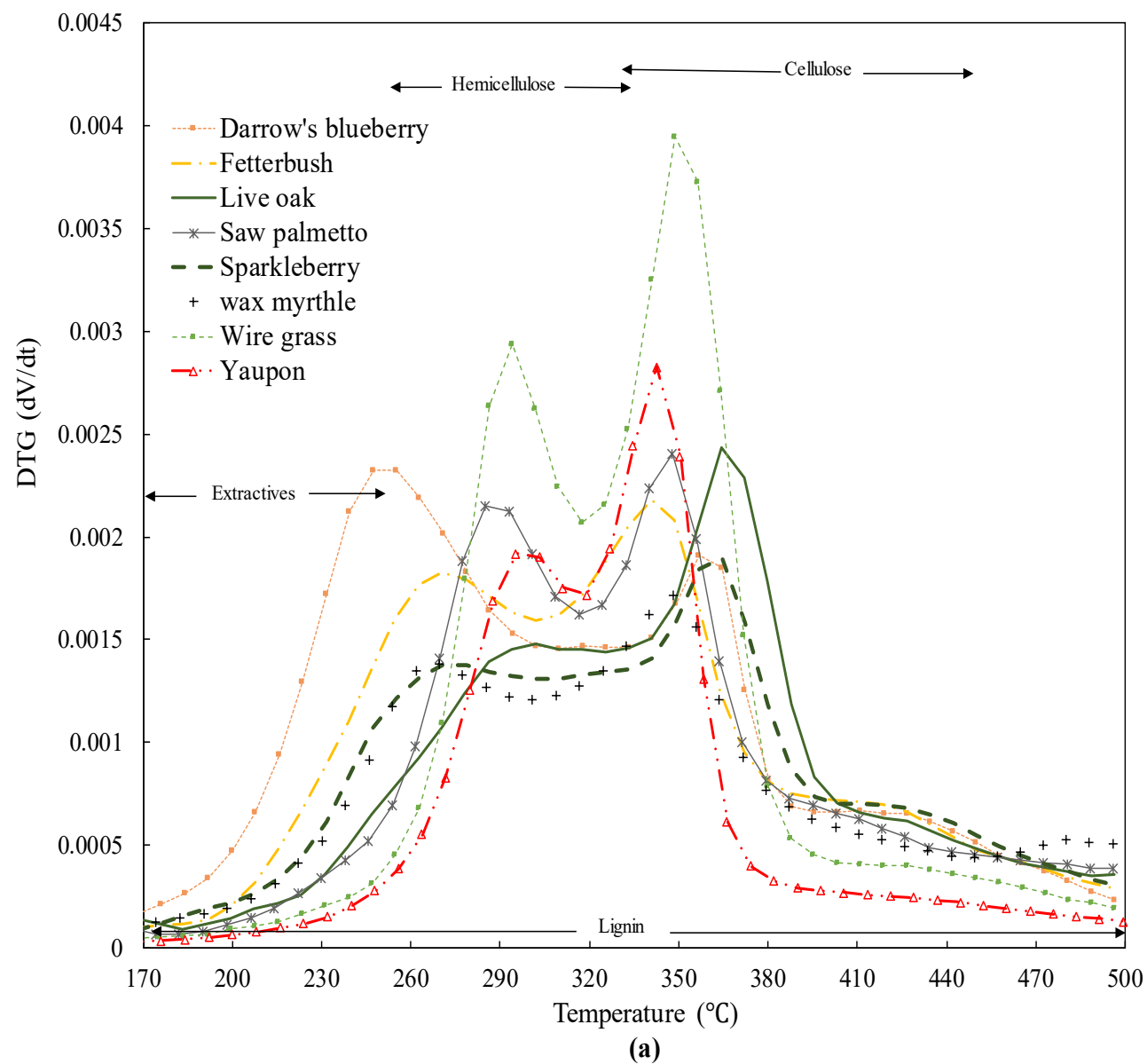
$$V_{\infty} = \sum V_{\infty j} \quad (8-7)$$

A different number of reactions corresponding to the number of DTG peaks and shoulders were considered for each plant species. Note that the DTG peaks occurred at different temperatures for each plant type (Figure 8-5). The DTG curves for all plant species are presented in separate graphs in Appendix D (Figure D-1).

For Darrow's blueberry, fetterbush, live oak, saw palmetto, sparkleberry, water oak, wax myrtle, wire grass, and yaupon, the DTG curves at a heating rate of $30 \text{ }^{\circ}\text{C min}^{-1}$ have two main peaks at $250 - 320 \text{ }^{\circ}\text{C}$ and $320 - 355 \text{ }^{\circ}\text{C}$ followed by a side peak or shoulder around $420 \text{ }^{\circ}\text{C}$.

Based on the biomass pyrolysis literature, the first peak can be attributed mainly to hemicellulose decomposition. Cellulose decomposition is thought to form two groups of reactions (second and third peaks) due to the more complex structures of these plant species than pure cellulose. Water oak also has a shoulder around 240 °C, which may be attributed to the decomposition of extractives. The decomposition of components obviously depends on the structure of the plant species. The plant species with more complex structures are more difficult to decompose.

For all plant species, lignin is thought to decompose during a wide range of temperatures (100 – 600 °C), overlapping the other peaks, so that each reaction modeled likely describes some portion of lignin degradation. Dwarf palmetto exhibits a main pyrolysis peak around 330 °C and a side peak around 410 °C, both of which are likely attributed to cellulose decomposition. The two side shoulders around 220 °C and 290 °C are likely attributed to the extractives and hemicellulose decomposition, respectively. Inkberry exhibits a main peak around 290 °C. The two peaks around 360 and 430 °C and a shoulder around 450 °C are attributed to the cellulose decomposition. A side shoulder around 230 °C is related to the decomposition of extractives. For little bluestem grass, the two cellulose peaks and the hemicellulose peak observed for most of the plant species are highly merged around 320 °C, which may be due to the catalytic activity of the mineral content for this species. Swamp bay has a main peak and a shoulder that occurred around 355 °C and 410 °C, respectively. Two observed shoulders around 240 °C and 325 °C are mainly attributed to the extractives and hemicellulose decomposition, respectively. For longleaf pine foliage and pine straw, the main pyrolysis peak occurred around 370 and 355 °C, respectively, which is attributed to the cellulose decomposition. Both of these samples also showed a side peak between 410 – 430 °C. Two observed shoulders between 230 and 350 – 350 °C are attributed to the extractives and hemicellulose decomposition.



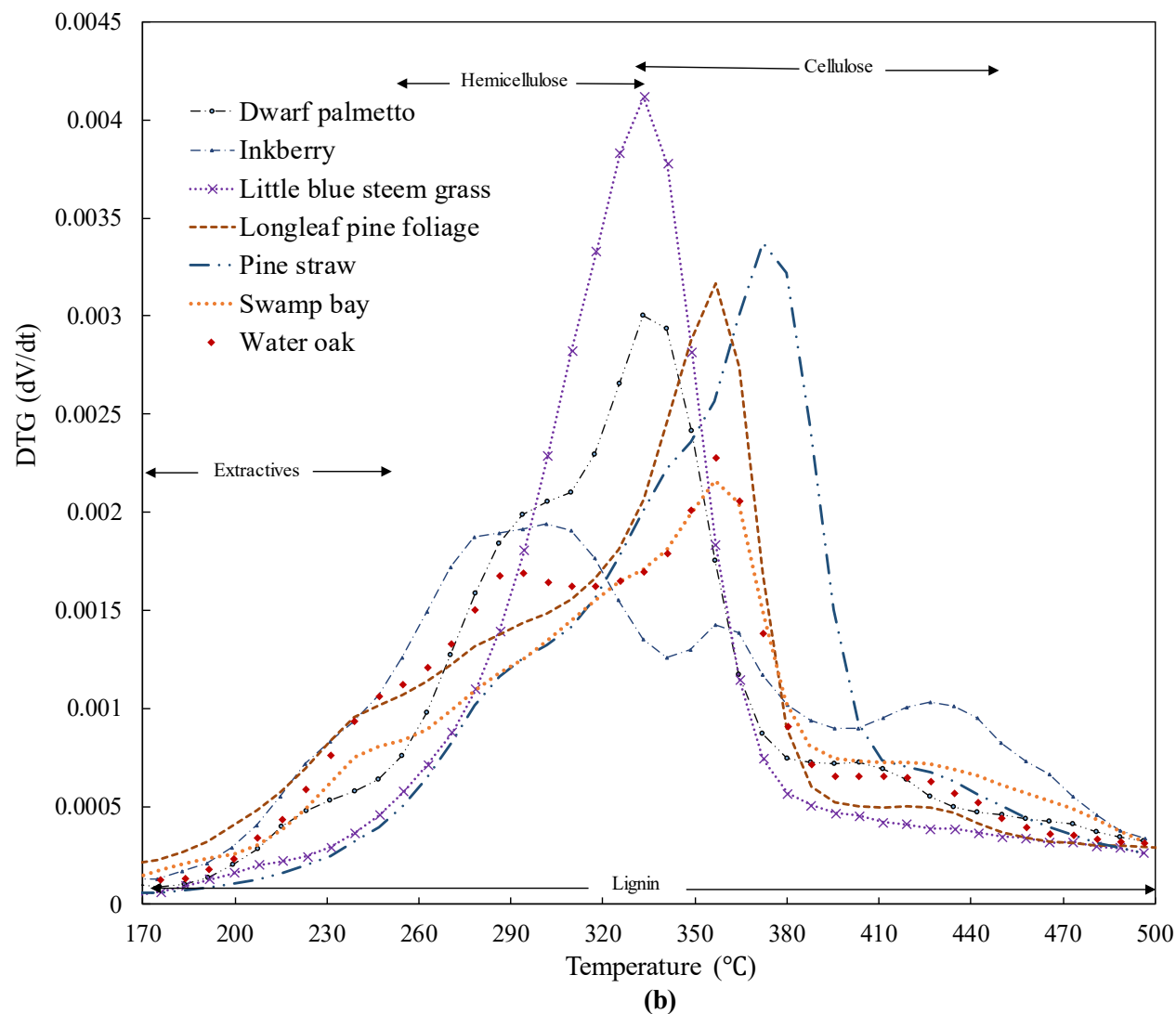


Figure 8-5: DTG pyrolysis curves at a heating rate of 30 °C min⁻¹ for (a) Darrow's blueberry, fetterbush, live oak, saw palmetto, sparkleberry, wax myrtle, wire grass and yaupon (b) dwarf palmetto, inkberry, little bluestem grass, longleaf pine, pine straw, swamp bay and water oak.

Similar DTG curves and the same number of reactions were observed for both longleaf pine foliage and pine straw. However, a shift in the temperatures of the peaks in the DTG curve of pine straw was observed, which could be attributed to the lower amount of extractives in pine straw (which have been shown to have catalytic effects during pyrolysis). Swamp bay exhibited a similar pyrolysis behavior to longleaf pine foliage.

Even though the peaks and shoulders for all plant species are mainly attributed to the decomposition of main components (e.g. cellulose, hemicellulose, lignin), there are significant amounts of other components such as proteins, sugars, lipids, starch, etc. (Matt et al., 2020), which decompose during each reaction. However, it is beyond the scope of this current work to assign reaction kinetics specifically to each component.

Using one set of coefficients for each DAEM reaction (i.e., corresponding to each major peak in the DTG curve), the cumulative mass and the derivative of the mass from all heating rates of 10, 20, and 30 °C min⁻¹ were fitted simultaneously for each plant species. Representative curve-fits of the TGA and DTGA data for live little bluestem grass (single peak) and live water oak (multiple peak) using the multiple-reaction DAEM model are presented in Figure 8-6. The curves for other plant species are presented in Appendix H (Figure H-1). The resulting coefficients determined for each plant species are presented in Table 8-3.

According to the fits for the both single and multiple pyrolysis peaks curves, this model worked well for both single and multiple pyrolysis peaks. The model matches the DTG peaks as well as the cumulative TGA data for both single and multiple peak pyrolysis curves. The pyrolysis of both live and dead samples of Darrow's blueberry, fetterbush, live oak, saw palmetto, sparkleberry, wax myrtle, wire grass, and yaupon consisted of four reactions (R_{Jio}). R_1 and R_4 are mainly attributed to the hemicellulose and lignin decomposition, respectively. Cellulose decomposition is mainly attributed to two reactions (R_2 and R_3). The pyrolysis of little bluestem

grass consisted of three reactions of R₁, R₂, and R₃ which were attributed to the decomposition of hemicellulose, cellulose and lignin, respectively.

The pyrolysis of both live and dead samples of dwarf palmetto, longleaf pine, swamp bay and water oak consisted of five reactions. R₁, R₂, and R₅ were mainly attributed to the decomposition of extractives, hemicellulose, and lignin, respectively. Cellulose decomposition occurred during two reactions (R₃ and R₄).

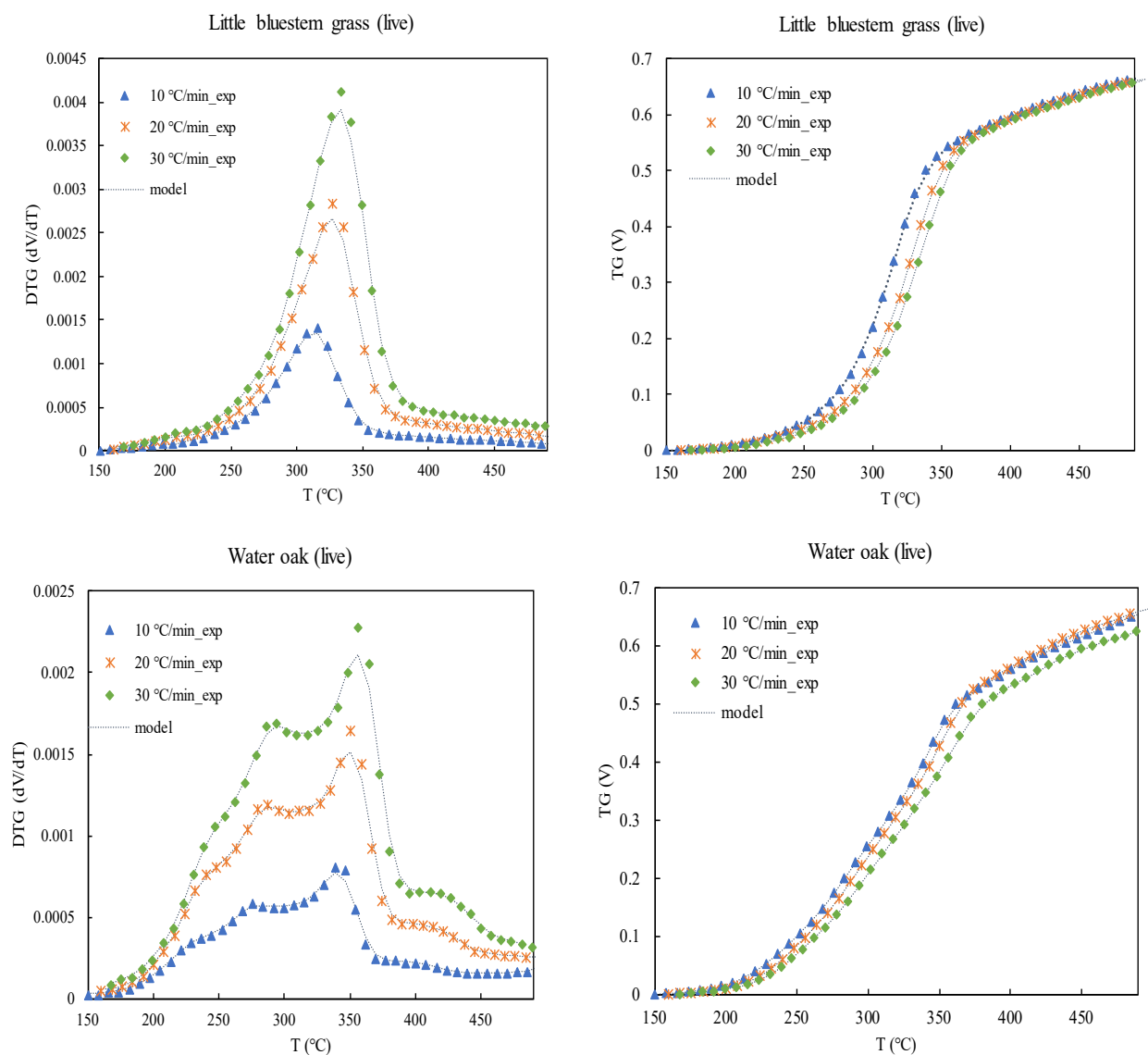


Figure 8-6: TG and DTG curves for live little bluestem grass and water oak resulted from experimental data and multiple-reaction DAEM model in heating rates of 10, 20, and 30 °C min⁻¹.

Table 8-3: The kinetic parameters (mean values of three replicates) obtained from the multiple-DAEM-reaction model for each plant species (the 95% confidence intervals are reported in the parentheses)

Plant	Darrow's blueberry		Dwarf palmetto		Fetterbush		Inkberry	
Parameter	Live	Dead	Live	Dead	Live	Dead	Live	Dead
$\text{Log}_{10} A_1^a$	11.82(1.03)	10.81(1.05)	8.41(1.04)	8.94(1.21)	9.58(1.41)	9.95(1.46)	10.51(1.05)	10.77(1.11)
E_1^b	112.83(2.63)	110.90(1.72)	123.13(9.4)	125.33(7.6)	130.40(6.9)	134.67(2.74)	98.03(4.05)	99.43(1.04)
σ_1^c	5.4(0.51)	6.4(1.35)	5.17(0.25)	4.40(0.17)	5.40(0.29)	7.43(1.20)	8.10(0.67)	7.47(0.47)
$V_{\infty 1}^d$	0.03(0.01)	0.02(0.01)	0.01(0.00)	0.02(0.00)	0.05(0.01)	0.03(0.01)	0.04(0.00)	0.03(0.01)
$\text{Log}_{10} A_2^a$	14.38(2.11)	14.48(1.03)	12.45(2.14)	12.83(1.82)	13.57(1.52)	13.81(2.03)	14.41(1.84)	14.26(1.12)
E_2^b	150.13(6.49)	145.53(8.17)	157.17(5.74)	160.07(7.51)	178.73(1.44)	179.97(3.26)	120.33(7.84)	121.37(1.05)
σ_2^c	1.93(0.72)	2.30(0.17)	5.20(0.09)	5.40(0.64)	3.97(0.18)	4.57(0.34)	5.27(0.51)	5.13(0.31)
$V_{\infty 2}^d$	0.21(0.01)	0.16(0.02)	0.20(0.01)	0.18(0.02)	0.23(0.01)	0.23(0.02)	0.21(0.01)	0.21(0.02)
$\text{Log}_{10} A_3^a$	16.30(2.02)	16.47(2.74)	14.86(1.82)	14.68(1.52)	15.88(1.49)	15.65(2.03)	16.80(2.62)	16.87(1.91)
E_3^b	183.60(1.54)	185.40(1.69)	200.03(2.49)	197.75(2.16)	223.73(1.72)	223.90(3.61)	159.33(5.17)	156.83(4.10)
σ_3^c	2.40(0.09)	2.20(0.17)	1.97(0.68)	2.30(0.10)	2.47(0.44)	3.77(0.34)	2.23(0.18)	2.53(0.31)
$V_{\infty 3}^d$	0.26(0.02)	0.29(0.01)	0.19(0.03)	0.21(0.01)	0.22(0.03)	0.26(0.01)	0.20(0.02)	0.22(0.01)
$\text{Log}_{10} A_4^a$	17.57(2.17)	17.44(1.95)	15.80(1.21)	15.47(1.91)	16.85(2.71)	16.99(2.63)	17.94(2.10)	17.59(1.99)
E_4^b	207.87(1.41)	204.60(7.42)	222.33(1.88)	228.73(3.63)	268.10(2.09)	269.33(3.26)	185.83(4.02)	185.15(8.51)

Table 8-3 Continued

Plant	Darrow's blueberry		Dwarf palmetto		Fetterbush		Inkberry	
Parameter	Live	Dead	Live	Dead	Live	Dead	Live	Dead
σ_4^c	27.70(3.80)	21.03(1.26)	3.30(0.51)	4.30(0.26)	33.40(2.30)	34.10(4.64)	3.93(0.34)	4.13(0.12)
$V_{\infty 4}^d$	0.18(0.01)	0.22(0.02)	0.19(0.01)	0.18(0.01)	0.16(0.01)	0.13(0.02)	0.12(0.02)	0.12(0.02)
$\text{Log}_{10} A_5^a$	-	-	17.75(1.24)	17.82(1.11)	-	-	19.67(1.00)	18.92(1.21)
E_5^b	-	-	257.03(1.97)	264.90(7.60)	-	-	224.63(2.44)	225.23(8.51)
σ_5^c	-	-	27.77(4.05)	29.37(1.42)	-	-	3.03(0.12)	3.13(0.14)
$V_{\infty 5}^d$	-	-	0.10(0.01)	0.10(0.01)	-	-	0.03(0.00)	0.03(0.01)
$\text{Log}_{10} A_6^a$	-	-	-	-	-	-	20.69(2.51)	20.69(2.01)
E_6^b	-	-	-	-	-	-	251.80(7.60)	255.67(8.44)
σ_6^c	-	-	-	-	-	-	19.73(1.10)	24.63(3.67)
$V_{\infty 6}^d$	-	-	-	-	-	-	0.10(0.01)	0.09(0.01)
Plant	Little bluestem grass		Live oak		Longleaf pine			
Parameter	Live	Dead	Live	Dead	Live	Dead	Pine straw	
$\text{Log}_{10} A_1^a$	11.94(1.00)	11.81(1.30)	8.66(1.01)	9.00(1.05)	10.32(1.11)	9.99(2.02)	9.87(1.81)	
E_1^b	112.10(1.82)	113.83(2.51)	122.03(1.79)	123.47(5.23)	135.67(6.34)	134.33(5.59)	132.93(4.98)	
σ_1^c	4.97(0.28)	3.93(0.94)	6.20(0.84)	7.63(1.31)	4.43(0.34)	3.80(0.76)	3.17(0.31)	

Table 8-3 Continued

Plant	Little Bluestem grass		Live oak		Longleaf pine		
Parameter	Live	Dead	Live	Dead	Live	Dead	Pine straw
$V_{\infty 1}^d$	0.03(0.01)	0.02(0.00)	0.03(0.01)	0.02(0.00)	0.03(0.00)	0.03(0.00)	0.02(0.00)
$\text{Log}_{10} A_2^a$	13.51(1.01)	13.62(1.00)	12.93(1.33)	12.88(1.55)	13.53(2.05)	13.75(2.44)	14.14(2.06)
E_2^b	167.87(2.98)	176.43(5.57)	171.90(1.63)	171.00(1.36)	180.63(7.42)	185.07(1.40)	189.93(7.50)
σ_2^c	2.90(0.59)	2.50(0.67)	4.77(0.68)	3.73(0.45)	5.43(0.28)	5.17(0.16)	5.43(0.36)
$V_{\infty 2}^d$	0.52(0.01)	0.51(0.01)	0.19(0.02)	0.21(0.02)	0.19(0.01)	0.19(0.02)	0.20(0.01)
$\text{Log}_{10} A_3^a$	16.62(2.66)	16.83(2.30)	14.89(1.90)	14.91(1.00)	15.89(2.07)	15.62(2.02)	15.15(2.39)
E_3^b	240.33(8.01)	248.20(3.20)	224.17(2.81)	224.93(8.43)	214.37(1.76)	215.27(1.36)	220.63(5.59)
σ_3^c	41.07(8.01)	38.00(3.04)	5.07(0.47)	3.87(0.59)	3.47(0.78)	2.77(0.67)	2.70(0.76)
$V_{\infty 3}^d$	0.14(0.01)	0.13(0.02)	0.25(0.02)	0.22(0.02)	0.29(0.02)	0.28(0.02)	0.30(0.01)
$\text{Log}_{10} A_4^a$	-	-	15.83(1.11)	15.76(1.81)	16.81(1.33)	16.40(1.51)	16.51(2.00)
E_4^b	-	-	258.07(4.91)	262.97(5.94)	257.20(2.54)	256.83(1.12)	267.00(4.47)
σ_4^c	-	-	28.07(1.91)	36.90(1.94)	3.10(0.67)	2.87(0.34)	1.93(0.36)
$V_{\infty 4}^d$	-	-	0.13(0.01)	0.14(0.01)	0.09(0.01)	0.08(0.01)	0.09(0.02)
$\text{Log}_{10} A_5^a$	-	-	-	-	18.76(1.05)	18.85(1.12)	18.68(1.75)
E_5^b	-	-	-	-	253.30(1.32)	284.53(2.03)	254.13(5.97)

Table 8-3 Continued

Plant	Little bluestem grass		Live oak		Longleaf pine			
Parameter	Live	Dead	Live	Dead	Live	Dead	Pine straw	
σ_5^c	-	-	-	-	37.27(4.64)	34.57(3.68)	36.83(1.31)	
$V_{\infty 5}^d$	-	-	-	-	0.09(0.01)	0.09(0.01)	0.09(0.01)	
Plant	Saw palmetto		Sparkleberry		Swamp bay		Water oak	
Parameter	Live	Dead	Live	Dead	Live	Dead	Live	Dead
$\text{Log}_{10} A_1^a$	10.65(1.31)	11.00(0.90)	11.83(1.03)	11.05(1.87)	12.28(1.03)	12.37(1.44)	9.69(1.05)	9.80(1.49)
E_1^b	143.10(3.2)	139.93(3.87)	121.00(7.83)	117.03(2.44)	123.97(1.53)	121.07(3.48)	99.36(6.57)	98.17(4.37)
σ_1^c	7.27(0.40)	5.93(0.98)	5.77(1.04)	5.27(0.42)	5.60(0.76)	5.20(0.35)	2.7(0.76)	3.5(0.35)
$V_{\infty 1}^d$	0.02(0.01)	0.02(0.01)	0.02(0.01)	0.02(0.01)	0.01(0.00)	0.01(0.00)	0.03(0.01)	0.02(0.01)
$\text{Log}_{10} A_2^a$	12.95(2.20)	12.69(1.34)	12.97(2.08)	12.63(1.22)	14.72(1.45)	14.63(1.99)	11.93(1.24)	11.79(1.31)
E_2^b	195.87(2.1)	192.23(1.88)	156.50(9.29)	158.80(5.43)	158.83(1.48)	159.03(5.56)	141.6(6.17)	145.73(1.67)
σ_2^c	6.03(0.06)	4.70(1.51)	3.07(0.92)	2.67(0.56)	4.93(0.19)	5.40(0.35)	4.97(0.86)	5.87(0.23)
$V_{\infty 2}^d$	0.19(0.01)	0.19(0.02)	0.20(0.02)	0.19(0.04)	0.20(0.03)	0.20(0.01)	0.22(0.02)	0.23(0.02)
$\text{Log}_{10} A_3^a$	14.08(1.44)	13.25(2.11)	13.29(2.35)	13.45(1.22)	15.23(0.78)	15.26(1.09)	13.90(1.42)	13.65(1.08)
E_3^b	241.20(6.78)	239.37(4.23)	204.10(1.54)	199.07(1.30)	196.87(1.92)	201.83(4.41)	165.57(8.69)	171.47(5.83)
σ_3^c	4.30(0.01)	4.13(0.02)	2.77(1.23)	3.30(1.10)	2.07(0.06)	2.47(0.23)	2.50(0.33)	5.13(0.29)

Table 8-3 Continued

Plant	Saw palmetto		Sparkleberry		Swamp bay		Water oak	
Parameter	Live	Dead	Live	Dead	Live	Dead	Live	Dead
$V_{\infty 3}^d$	0.25(0.01)	0.26(0.02)	0.25(0.03)	0.24(0.02)	0.22(0.00)	0.21(0.01)	0.22(0.01)	0.24(0.02)
$\text{Log}_{10} A_4^a$	15.74(2.34)	15.58(2.22)	15.88(1.45)	15.59(1.48)	16.91(2.01)	16.80(2.34)	15.22(2.12)	16.00(2.09)
E_4^b	302.00(9.95)	301.80(4.25)	241.53(6.27)	244.33(1.68)	218.03(4.56)	222.67(5.43)	191.97(10.12)	191.37(5.83)
σ_4^c	35.60(4.30)	41.33(1.85)	26.47(1.68)	26.43(1.21)	1.87(0.51)	1.30(0.19)	2.20(0.34)	6.73(0.29)
$V_{\infty 4}^d$	0.14(0.01)	0.14(0.01)	0.13(0.01)	0.14(0.01)	0.13(0.02)	0.12(0.01)	0.10(0.01)	0.09(0.02)
$\text{Log}_{10} A_5^a$	-	-	-	-	18.58(2.24)	18.76(2.12)	16.75(2.07)	16.94(2.22)
E_5^b	-	-	-	-	281.70(5.45)	278.47(1.38)	256.53(2.57)	250.57(3.10)
σ_5^c	-	-	-	-	31.23(2.92)	30.77(4.30)	31.43(8.21)	33.93(5.57)
$V_{\infty 5}^d$	-	-	-	-	0.09(0.02)	0.10(0.01)	0.08(0.01)	0.09(0.01)
Plant	Wax myrtle		Wire grass		Yaupon			
Parameter	Live	Dead	Live	Dead	Live		Dead	
$\text{Log}_{10} A_1^a$	10.82(0.99)	10.12(0.87)	8.75(0.87)	8.11(1.05)	9.53(1.11)		9.96(1.06)	
E_1^b	119.87(2.24)	120.83(5.46)	131.97(7.58)	126.03(8.53)	95.93(8.36)		93.67(3.78)	
σ_1^c	3.03(0.14)	4.33(0.97)	5.23(0.21)	5.00(0.19)	7.20(0.80)		4.77(1.01)	
$V_{\infty 1}^d$	0.02(0.01)	0.02(0.01)	0.02(0.01)	0.02(0.01)	0.02(0.01)		0.02(0.01)	

Table 8-3 Continued

Plant	Wax myrtle		Wire grass		Yaupon	
Parameter	Live	Dead	Live	Dead	Live	Dead
$\text{Log}_{10} A_2^a$	12.96(1.24)	12.61(1.98)	10.93(1.44)	10.50(1.32)	12.81(1.47)	12.88(1.99)
E_2^b	183.57(2.40)	182.90(7.56)	169.23(8.51)	159.50(4.14)	133.70(9.27)	130.83(7.08)
σ_2^c	6.10(0.97)	6.13(1.02)	2.13(0.51)	2.40(0.17)	2.00(0.19)	3.40(0.33)
$V_{\infty 2}^d$	0.15(0.07)	0.14(0.09)	0.20(0.03)	0.20(0.01)	0.21(0.03)	0.22(0.02)
$\text{Log}_{10} A_3^a$	13.24(1.08)	13.38(2.03)	11.89(1.99)	11.52(1.65)	15.16(2.23)	13.91(2.14)
E_3^b	228.73(3.46)	220.73(6.54)	201.70(6.74)	200.13(8.36)	165.40(2.26)	169.03(1.19)
σ_3^c	2.97(0.60)	1.70(0.58)	3.30(0.33)	2.97(0.42)	3.03(0.41)	1.93(0.76)
$V_{\infty 3}^d$	0.22(0.02)	0.23(0.02)	0.33(0.03)	0.30(0.03)	0.22(0.03)	0.23(0.02)
$\text{Log}_{10} A_4^a$	15.88(2.21)	15.45(2.07)	13.87(2.11)	13.46(2.09)	17.12(2.75)	16.77(2.41)
E_4^b	262.73(8.32)	266.83(5.14)	259.23(8.14)	265.17(4.76)	195.60(3.11)	189.93(7.41)
σ_4^c	27.70(2.95)	24.67(1.47)	21.97(0.62)	25.50(0.99)	32.60(4.30)	28.90(1.66)
$V_{\infty 4}^d$	0.22(0.01)	0.23(0.02)	0.13(0.03)	0.15(0.03)	0.14(0.03)	0.15(0.02)

^a s⁻¹

^b kJ mol⁻¹

^c kJ mol⁻¹

^d Normalized volatiles

The pyrolysis of live and dead inkberry consisted of six reactions. R_1 and R_2 were attributed to the decomposition of extractives and hemicellulose, respectively. Cellulose decomposition occurred during three reactions (R_3 , R_4 , and R_5). The last reaction (R_6) was mainly attributed to the lignin decomposition. The order of mean activation energies for all plant species indicated that hemicellulose and extractives are easier to decompose than cellulose, and cellulose is easier to decompose than lignin, which is consistent with other biomass pyrolysis studies (Varhegyi et al., 2011; Cai et al., 2013; Chen et al., 2015b).

Comparing the DTG curves for different types of plant species revealed that the pyrolysis behavior was not consistent between species of the same groups. For example, for grass type species, wire grass had four reactions and little bluestem grass showed three reactions. A similar result was observed for broadleaf species such as inkberry, fetterbush, live oak, water oak, etc. which showed different pyrolysis behaviors. However, palmetto type species of dwarf palmetto and saw palmetto showed similar pyrolysis behavior, each with two main peaks.

8.4 Comparison between Three Models

The three models used above to find the kinetic parameters of slow pyrolysis reaction of all plant species were the simple one-step model, the single-reaction DAEM model, and the multiple-reaction DAEM model. The goal was to fit the TGA and DTG data at multiple heating rates in order to provide a model that possibly may be extrapolated to the heating conditions in fires (approximately $100\text{ }^{\circ}\text{C s}^{-1}$). Figure 8-7 shows the comparison of these three models vs. the DTG data for live little bluestem grass (one peak) and live water oak (multiple peaks). The lack of fit exhibited in Figure 8-7a by the simple one-step model is because the model was fit to the data from all three heating rates. As expected, this model did not agree well with the data where multiple peaks were observed (Figure 8-7b).

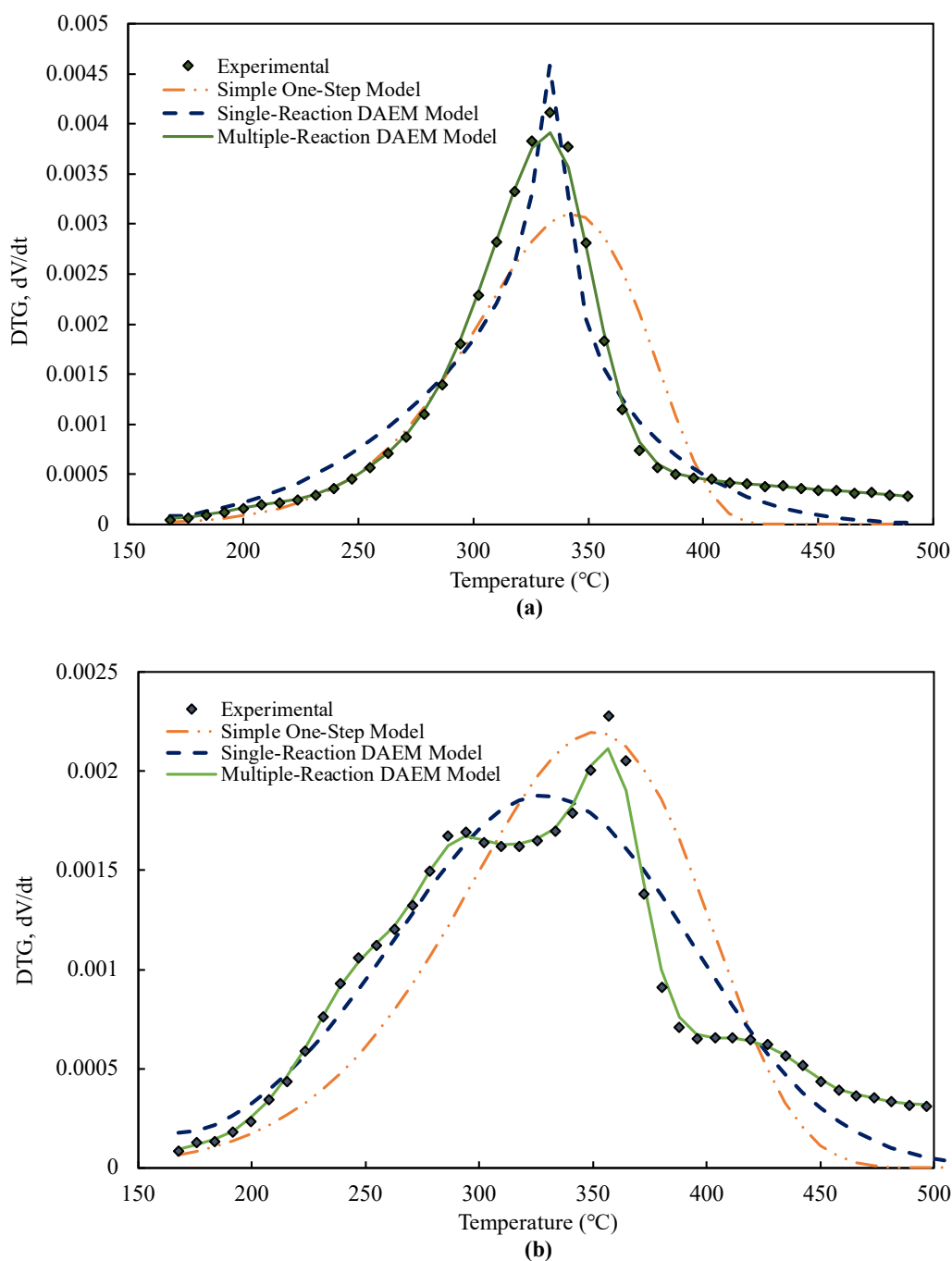


Figure 8-7: Comparison of best-fit simple one-step model, single-reaction DAEM model, and multiple-reaction DAEM model with DTG data for (a) live little bluestem grass and (b) live water oak at heating rate of 30 °C min⁻¹.

The single-reaction DAEM model matched the DTG peaks fairly well for the plant species with single peak pyrolysis curves, but not the data with multiple peaks. However, the multiple-reaction DAEM model shows the best fit to the experimental data. In particular, the multiple-

reaction DAEM model is able to describe the slow decay in the reaction rate at temperatures above 375 °C. The multiple-reaction DAEM model using the series reaction formulation is not much more complex and almost as fast as the simple first-order model and should be useful over a broader range of heating rates.

To evaluate the quality of the fit between experimental and predicted data and have a quantified comparison between the models, both root mean square error (RMSE) and mean average error (MAE) values corresponding to the simulated datasets in Figure 8-7 were calculated, and the results are presented in Table 8-4. The RMSE and MAE values corresponding to the DTG curves at heating rate of 30 °C min⁻¹ for all live and dead plant species are presented in Table I-1, and Table I-2, respectively (Appendix I).

Table 8-4. RMSE and MAE values corresponding to the simulated datasets in Figure 8-7

plant	Simple One-Step Model		Single-Reaction DAEM Model		Multiple-Reaction DAEM Model	
	RMSE	MAE	RMSE	MAE	RMSE	MAE
Little bluestem grass	5.2×10^{-4}	4.6×10^{-4}	2.5×10^{-4}	2.1×10^{-4}	5.9×10^{-5}	5.5×10^{-5}
Water oak	3.9×10^{-4}	3.2×10^{-4}	2.3×10^{-4}	1.8×10^{-4}	4.6×10^{-5}	4.9×10^{-5}

The RMSE and MAE are commonly used together to evaluate the quality of the fit and the variation in the errors of a set of predicted data. The lower values of RMSE and MAE show better fit. The RMSE values are normally equal or greater than the MAE values. The larger the difference between RMSE and MAE values, the larger the variance of errors in the set of predictions. The equal values of RMSE and MAE show that all individual errors are of the same order of magnitude for a given model (Torres-Garcia and Brachi, 2019). According to Table 8-4, the multiple-reaction DAEM model had the lowest values of RMSE for both little bluestem grass and water oak, which indicates that this model had the best fit to the experimental data, compared

to simple one-step and single-reaction DAEM models. The multiple-reaction DAEM had the lowest values of RMSE and MAE for all species (see Tables I-1 and I-2) by approximately an order of magnitude. For all models, the small difference between RMSE and MAE values indicated that the variance in the errors of individual predicted data was relatively small.

8.5 Correlation between Activation Energies and the Main Components Content

This section describes the attempts to describe the statistical correlation of the activation energies determined from the reaction rate analysis and the component analysis of each plant species. The correlation coefficient measures the direction and strength of a linear relationship between two variables on a scatterplot. Activation energies from the multiple-reaction DAEM model which corresponded to cellulose, hemicellulose and lignin decomposition were compared with the fraction of each main component (e.g. cellulose, hemicellulose and lignin). Table 8-5 shows the normalized values of these components (neglecting the other components). The actual values were presented earlier in Table 4-2.

Table 8-5: The normalized values of cellulose, hemicellulose and lignin contents in each plant species

Common name	Hemicellulose ^a (%)	Cellulose ^a (%)	Lignin ^a (%)
Dwarf palmetto	39.1	23.9	36.9
Fetterbush	12.8	30.8	56.3
Inkberry	13.0	26.7	60.2
Little bluestem	29.0	42.3	28.6
Live oak	20.2	35.6	44.0
Longleaf pine foliage	26.0	33.0	40.8
Saw palmetto	31.3	18.5	50.1
Swamp bay	17.0	29.6	53.3
Water oak	12.3	33.5	54.0
Wax myrtle	18.6	31.3	50.0
Wire grass	29.8	45.6	24.5
Yaupon	17.6	21.3	61.0

^a Dry basis

For the sake of comparison, when multiple activation energies were attributed to a particular component, an average value was considered. The scatter plots of corresponding activation energies vs. the respective cellulose, hemicellulose and lignin contents based on multi-DAEM-reaction model are presented in Figure 8-8.

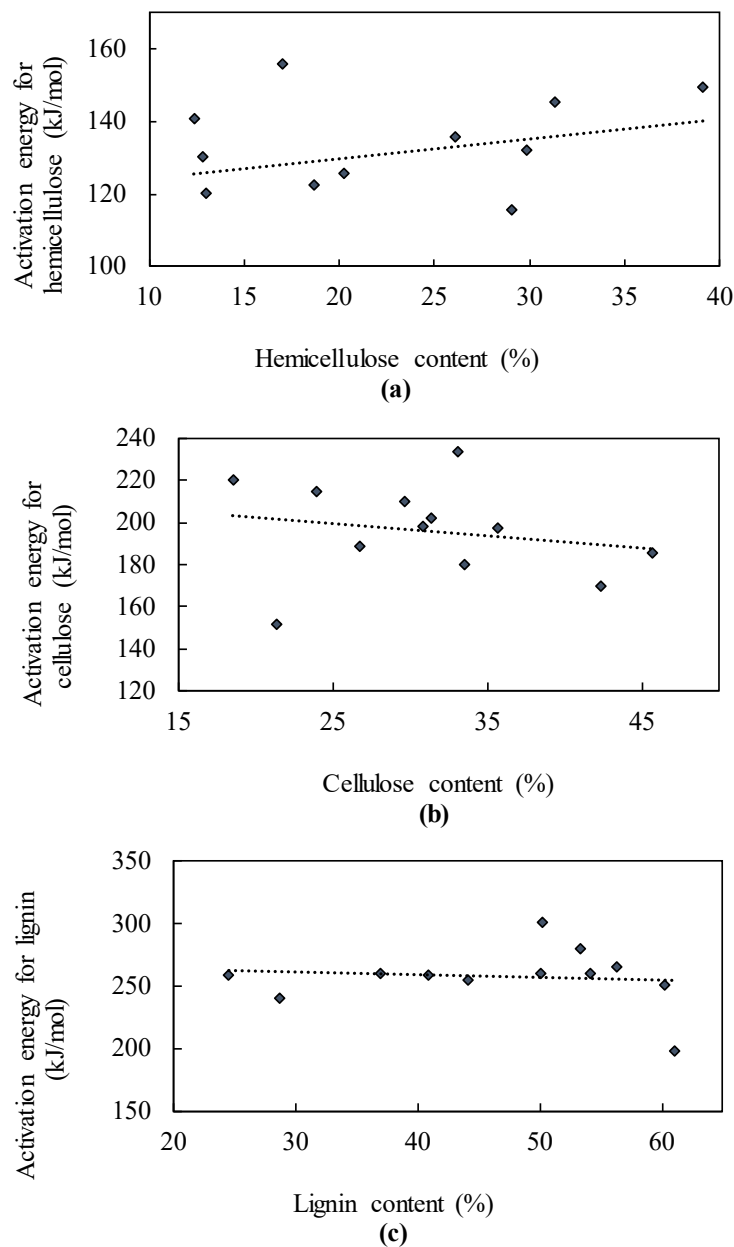


Figure 8-8: Scatterplots of activation energy vs. the corresponding component. (a) hemicellulose (b) cellulose and (c) lignin.

The correlation coefficients between cellulose, hemicellulose, and lignin content and corresponding activation energies were calculated and presented in Table 8-6. According to the correlation coefficient values, no significant correlation between cellulose, hemicellulose and lignin content and corresponding activation energies were found. This could be due to the fact that different plant species have different structures and the matrices of amorphous hemicellulose, cellulose and lignin vary in different plant species (Chen et al., 2015b), or could be attributed to the fact that the plants are composed of many more components than cellulose, hemicellulose, and lignin. The lack of correlation of activation energies with these three components is consistent with the work of Pasangulapati et al. (2012), who observed that no significant relationship was observed between the pyrolysis kinetic parameters of different biomass samples with cellulose, hemicellulose and lignin contents.

Table 8-6: The correlation coefficients between cellulose, hemicellulose and lignin content and corresponding activation energies

Correlation Coefficient		
Hemicellulose	Cellulose	Lignin
0.29	- 0.19	- 0.09

8.6 Summary and Conclusion

In this chapter, first the pyrolysis completion temperatures were found for all plant species, and it was observed that different plant species had different completion temperatures. Increasing heating rate increased the completion temperature. Next, three models (the simple one-step model and the single and multiple reaction DAEM models) were used to fit the TGA pyrolysis data. The mass loss and derivative mass loss data were fitted simultaneously at three heating rates of 10, 20, and 30 °C min⁻¹ to find kinetic parameters for these model forms. The simple one-step model was not able to give as good of fits to the one-peak pyrolysis data as the DAEM model over the

range of heating rates. However, the multiple-reaction DAEM model showed very good fits to the experimental data where multiple peaks were observed, even at different heating rates. Finally, activation energies determined from the multi-reaction DAEM model fits to the data were compared with the corresponding contents of cellulose, hemicellulose and lignin. Results indicated that there was no significant statistical correlation between cellulose, hemicellulose and lignin content and corresponding activation energies.

9 SUMMARY AND CONCLUSION

The pyrolysis product and species yields of 14 plant species native to forests in the southern United States was investigated under slow heating conditions. These plant species were selected since they were commonly-burned fuels in wildland and prescribed fires. The slow pyrolysis experiments were performed in a pyrolyzer apparatus using different heating rates ranging from 10 to 30 °C min⁻¹. Yields of pyrolysis products (tar, light gas, and char) were measured for all live and dead plant species. Tar species were analyzed using a GC-MS instrument, and light gas species were analyzed using a GC-TCD. In addition, slow pyrolysis experiments were conducted in a TGA to find the kinetic parameters for slow pyrolysis of all live and dead plant species. Kinetic coefficients were determined from the data using a model-free method (i.e., KAS) and model-fitting methods (i.e., the simple one-step and a series form of the distributed activation energy model).

9.1 Yields of Pyrolysis Products

Slow pyrolysis experiments of longleaf pine litter were conducted in the pyrolyzer at different temperatures, heating rates, and sweep gas flow rates to find an optimum operating condition which results the highest tar yield. The change in heating rate had only a small effect on tar yield at slow heating rates, but a greater impact on char yield. Among the pyrolysis operating parameters, temperature had the most important effect on product yields. A temperature of 500 °C, heating rate of 30 °C min⁻¹, and sweep gas flowrate of 100 ml min⁻¹ was found to be

the optimum condition to produce the highest amount of tar from slow pyrolysis of dead longleaf pine litter. This optimum condition was used to operate the pyrolyzer for all subsequent experiments. Pyrolysis heating rate, temperature and plant species had significant effects on the yields and compositions of the pyrolysis products (tar, light gas, and char). However, the yields of slow pyrolysis products (on a dry basis) did not significantly differ between live and dead samples of a specific plant species. Significant variation in pyrolysis products yields between different plant species were observed at the same operating condition, which was likely caused by the different composition of the plant species (i.e. cellulose, hemicellulose, and lignin).

9.2 Light Gas Species Analysis

CO was the dominant light gas species for all plant samples on a dry, wt% basis, followed by CO₂, CH₄ and H₂. Live plant species had slightly higher weight fractions of CO and H₂ (average differences of 3.8 and 0.3 wt% absolute, respectively) than corresponding dead samples, but slightly lower weight fractions of CO₂ and CH₄ (average differences of 2.5 and 1.6 wt% absolute, respectively). For most plant species, light gas yields were not significantly different between live and dead samples for a specific plant species. However, the light gas species yields varied more between different plant species than between live and dead samples of the same species.

9.3 Tar Species Analysis

The main constituents identified in the tar obtained from the slow pyrolysis of live and dead plant samples were oxygenated aromatics (ArO), which were mainly phenolic compounds (-OH). Single-ring aromatics with OH attachments were the most prevalent compounds observed in the tar obtained from both live and dead samples at these conditions. Very few multi-ring compounds were observed.

No significant differences between the distribution of functional groups in tar were

observed for live and dead plant samples for a given plant species. In contrast, there were significant differences in the functional groups distribution in tars obtained from pyrolysis of different plant species.

9.4 TGA Results

The results of TGA experiments showed that the condition of the plant (live vs. dead) did not affect the number of pyrolysis peaks or zones of a particular plant species. The DTG peaks of live and dead samples were similar in position and height except for the first peak representing the mass loss due to evaporation. Studying the effect of heating rate on pyrolysis behavior of the plant species revealed that the heating rate did not affect the number of the peaks of the DTG curve for a plant species. The mass loss pattern was same at all heating rates except for a shift in the temperature of the peak mass loss rates. In addition, the maximum pyrolysis rate increased slightly with increasing heating rate.

9.5 Kinetic Analysis Based on KAS Method

Kinetic analysis for the drying zone using model-free KAS method showed that the live samples with higher moisture contents had higher activation energies during the drying zone. The iso-conversion analysis of activation energies as a function of the extent of conversion showed similar trends for both live and dead samples of a given plant species.

For all live and dead plant species, the pyrolysis rate distribution as a function of conversion was studied. Results of this analysis showed that different plant species had different rates at different conversions. During the sample decomposition, the highest rates were observed at the beginning of the pyrolysis between $\alpha=10-20\%$, for all samples. Between $\alpha=80-90\%$, the rate of pyrolysis became very low and approached zero.

The effect of aging on activation energy was studied using long leaf pine needles. Results showed that aging made the pyrolysis process slower and led to higher activation energy values. However, aging did not influence the trend of activation energy distribution increasing with degree of conversion.

9.6 Kinetic Analysis Based on Model-Fitting Methods

Three models were used to find the kinetic parameters of slow pyrolysis reaction of each plant species: a simple one-step model; a single-reaction distributed activation energy model (DAEM); and a multiple-reaction DAEM model. The multiple-DAEM-reaction model gave the best fit to the pyrolysis data at multiple heating rates when multiple peaks were observed. The multiple pyrolysis peaks were attributed to decomposition of hemicellulose, cellulose, and lignin, based on literature observations for biomass. The order of activation energies for pyrolysis of all plant species indicated that hemicellulose and extractives are easier to decompose than cellulose, and cellulose is easier to decompose than lignin.

9.7 Correlation Between Activation Energies and the Main Components Content

The activation energies obtained from multiple-reaction DAEM model for each plant species were compared with the corresponding contents of cellulose, hemicellulose and lignin. No significant statistical correlation was observed between cellulose, hemicellulose and lignin content and the corresponding activation energies.

9.8 Recommendations for Future Work

A list of recommended future research on the pyrolysis of live and dead vegetation is summarized below:

- Study the effect of single-leaf vs. multi-leaf pyrolysis on the products characteristics using the pyrolyzer. It may also be interesting to study multiple leaves of different species to look for synergistic effects.
- Compare the tar and light gases characteristics obtained from laboratory experiments with results measured in outdoor field experiments. This comparison may be problematic because it is difficult to measure pure pyrolysis species or product yields in outdoor field environments.
- Compare the pyrolysis results of the southeastern United States vegetation with similar experiments on vegetation from other areas of the United States, such as Utah or the California chaparral.
- Develop a pyrolysis model that includes reaction mechanisms for each component in the summative analysis to see if such a model can be applied for all fuels.
- Determine if rates of pyrolysis from slow heating rate experiments can be applied to describe the pyrolysis behavior from previous fast heating rate experiments.
- Develop a model to describe the secondary reactions of pyrolysis products from live fuels including soot formation. This model may lead to predictions of smoke behavior.

REFERENCES

- Abnisa, F., W. M. A. W. Daud, W. N. W. Husin and J. N. Sahu, "Utilization possibilities of palm shell as a source of biomass energy in Malaysia by producing bio-oil in pyrolysis process," *Biomass and Bioenergy*, **35**(5), 1863-1872 (2011).
- Akhtar, J. and N. Saidina Amin, "A review on operating parameters for optimum liquid oil yield in biomass pyrolysis," *Renewable and Sustainable Energy Reviews*, **16**(7), 5101-5109 (2012).
- Amini, E., M.-S. Safdari, J. T. DeYoung, D. R. Weise and T. H. Fletcher, "Characterization of pyrolysis products from slow pyrolysis of live and dead vegetation native to the southern United States," *Fuel*, **235**, 1475-1491 (2019).
- Ansah, E., L. Wang and A. Shahbazi, "Thermogravimetric and calorimetric characteristics during co-pyrolysis of municipal solid waste components," *Waste Manag*, **56**, 196-206 (2016).
- Anthony, D. B., J. B. Howard, H. C. Hottel and H. P. Meissner, "Rapid devolatilization of pulverized coal," *Symposium (International) on Combustion*, **15**(1), 1303-1317 (1975).
- Antonakou, E., A. Lappas, M. H. Nilsen, A. Bouzga and M. Stöcker, "Evaluation of various types of Al-MCM-41 materials as catalysts in biomass pyrolysis for the production of bio-fuels and chemicals," *Fuel*, **85**(14-15), 2202-2212 (2006).
- AntonioVega-Gálvez, M. Miranda, L. P. Díaz, L. Lopez, K. Rodriguez and K. D. Scala, "Effective moisture diffusivity determination and mathematical modelling of the drying curves of the olive-waste cake," *Bioresource Technology*, **101**(19), 7265-7270 (2010).
- Aysu, T. and M. M. Küçük, "Biomass pyrolysis in a fixed-bed reactor: Effects of pyrolysis parameters on product yields and characterization of products," *Energy*, **64**, 1002-1025 (2014).
- Babu, B. V., "Biomass pyrolysis: a state-of-the-art review," *Biofuels, Bioproducts and Biorefining*, **2**(5), 393-414 (2008).
- Bai, F., Y. Sun, Y. Liu, Q. Li and M. Guo, "Thermal and kinetic characteristics of pyrolysis and combustion of three oil shales," *Energy Conversion and Management*, **97**, 374-381 (2015).

- Balogun, A. O., O. A. Lasode and A. G. McDonald, "Devolatilisation kinetics and pyrolytic analyses of *Tectona grandis* (teak)," *Bioresource Technology*, **156**, 57-62 (2014).
- Banon, E., A. Marcilla, A. N. Garcia, P. Martinez and M. Leon, "Kinetic model of the thermal pyrolysis of chrome tanned leather treated with NaOH under different conditions using thermogravimetric analysis," *Waste Management*, **48**, 285-299 (2016).
- Becidan, M., G. Várhegyi, J. E. Hustad and Ø. Skreiberg, "Thermal decomposition of biomass wastes. A kinetic study," *Industrial & Engineering Chemistry Research*, **46**(8), 2428-2437 (2007).
- Beringer, J., B. L. Hutley, N. Tapper, A. Coutts, A. Kerley and A. P. O'Grady, "Fire impacts on surface heat, moisture and carbon fluxes from a tropical savanna in northern Australia.," *International Journal of Wildland Fire*, **12**, 333-340 (2003).
- Boateng, A. A. and P. L. Mtui, "CFD modeling of space-time evolution of fast pyrolysis products in a bench-scale fluidized-bed reactor," *Applied Thermal Engineering*, **33-34**, 190-198 (2012).
- Bonelli, P. R., E. L. Buonomo and A. L. Cukierman, "Pyrolysis of sugarcane bagasse and co-pyrolysis with an argentinean subbituminous coal," *Energy Sources, Part A: Recovery, Utilization, and Environmental Effects*, **29**(8), 731-740 (2007).
- Bordoloi, N., R. Narzari, D. Sut, R. Saikia, R. S. Chutia and R. Kataki, "Characterization of bio-oil and its sub-fractions from pyrolysis of *Scenedesmus dimorphus*," *Renewable Energy*, **98**, 245-253 (2016).
- Bradbury, A. W., Y. Sakai and F. Shafizadeh, "A kinetic model for pyrolysis of cellulose," *Journal of applied polymer science*, **23**(11), 3271-3280 (1979).
- Bridgwater, A. V., D. Meier and D. Radlein, "An overview of fast pyrolysis of biomass," *Organic Geochemistry*, **30**(12), 1479-1493 (1999).
- Buessing, L. and L. J. Goldfarb, "Energy along Interstate I-95: Pyrolysis kinetics of Floridian cabbage palm (*Sabal palmetto*)," *Journal of Analytical and Applied Pyrolysis*, **96**, 78-85 (2012).
- Byram, G. M., "Forest fire: control and use," Combustion of forest fuels, Eds. K. P. Davis, New York, NY: McGraw-Hill: 61-89 (1959).
- Cai, J. and S. Chen, "Determination of drying kinetics for biomass by thermogravimetric analysis under nonisothermal condition," *Drying Technology*, **26**(12), 1464-1468 (2010).
- Ceylan, S. and Y. Topcu, "Pyrolysis kinetics of hazelnut husk using thermogravimetric analysis," *Bioresour Technol*, **156**, 182-8 (2014).

- Chan, W.-C. R., M. Kelbon and B. B. Krieger, "Modelling and experimental verification of physical and chemical processes during pyrolysis of a large biomass particle," *Fuel*, **64**(11), 1505-1513 (1985).
- Chaos, M., M. M. Khan, N. Krishnamoorthy, J. L. De Ris and S. B. Dorofeev, "Evaluation of optimization schemes and determination of solid fuel properties for CFD fire models using bench-scale pyrolysis tests," *Proceedings of the Combustion Institute*, **33**(2), 2599-2606 (2011).
- Chen, D.-Y., D. Zhang and X.-F. Zhu, "Heat/mass transfer characteristics and nonisothermal drying kinetics at the first stage of biomass pyrolysis," *Journal of Thermal Analysis and Calorimetry*, **109**(2), 847-854 (2012).
- Chen, D., Y. Zheng and X. Zhu, "In-depth investigation on the pyrolysis kinetics of raw biomass. Part I: Kinetic analysis for the drying and devolatilization stages," *Bioresource Technology*, **131**, 40-46 (2013).
- Chen, D., J. Zhou and Q. Zhang, "Effects of heating rate on slow pyrolysis behavior, kinetic parameters and products properties of moso bamboo," *Bioresource Technology*, **169**, 313-319 (2014).
- Chen, D., D. Liu, H. Zhang, Y. Chen and Q. Li, "Bamboo pyrolysis using TG–FTIR and a lab-scale reactor: Analysis of pyrolysis behavior, product properties, and carbon and energy yields," *Fuel*, **148**, 79-86 (2015a).
- Chen, D., Y. Li, K. Cen, M. Luo, H. Li and B. Lu, "Pyrolysis polygeneration of poplar wood: Effect of heating rate and pyrolysis temperature," *Bioresource Technology*, **218**, 780-8 (2016).
- Chen, H. X., N. A. Liu and W. C. Fan, "Two-step consecutive reaction model and kinetic parameters relevant to the decomposition of Chinese forest fuels," *Journal of Applied Polymer Science*, **102**(1), 571-576 (2006).
- Chen, Z., M. Hu, X. Zhu, D. Guo, S. Liu, Z. Hu, B. Xiao, J. Wang and M. Laghari, "Characteristics and kinetic study on pyrolysis of five lignocellulosic biomass via thermogravimetric analysis," *Bioresource Technology*, **192**, 441-450 (2015b).
- Chen, Z., Q. Zhu, X. Wang, B. Xiao and S. Liu, "Pyrolysis behaviors and kinetic studies on Eucalyptus residues using thermogravimetric analysis," *Energy Conversion and Management*, **105**, 251-259 (2015c).
- Collard, F.-X. and J. Blin, "A review on pyrolysis of biomass constituents: Mechanisms and composition of the products obtained from the conversion of cellulose, hemicelluloses and lignin," *Renewable and Sustainable Energy Reviews*, **38**, 594-608 (2014).

- Cortés, A. M. and A. V. Bridgwater, "Kinetic study of the pyrolysis of miscanthus and its acid hydrolysis residue by thermogravimetric analysis," *Fuel Processing Technology*, **138**, 184-193 (2015).
- Costa, V. J., R. M. Vieira, S. Girotto and F. J. Simioni, "Pyrolysis and thermogravimetry of blended and nonblended residues of pine and eucalyptus forestry woods," *Environmental Progress & Sustainable Energy*, **35**(5), 1521-1528 (2016).
- Countryman, C. M., "Physical characteristics of some Northern California brush fuels," General Technical Report PSW-61, Pacific Southwest Forest and Range Experiment Station, Berkeley, CA (1982).
- Damartzis, T., D. Vamvuka, S. Sfakiotakis and A. Zabaniotou, "Thermal degradation studies and kinetic modeling of cardoon (*Cynara cardunculus*) pyrolysis using thermogravimetric analysis (TGA)," *Bioresource Technology*, **102**(10), 6230-6238 (2011).
- Demiral, İ., A. Eryazıcı and S. Şensöz, "Bio-oil production from pyrolysis of corncob (*Zea mays* L.)," *Biomass and Bioenergy*, **36**, 43-49 (2012).
- Demirbaş, A., "Mechanisms of liquefaction and pyrolysis reactions of biomass," *Energy Conversion and Management*, **41**(6), 633-646 (2000).
- Dennison, P. E. and M. A. Moritz, "Critical live fuel moisture in chaparral ecosystems: a threshold for fire activity and its relationship to antecedent precipitation," *International Journal of Wildland Fire*, **18**, 1021-1027 (2009).
- Dhaundiyal, A., S. B. Singh, M. M. Hanon and R. Rawat, "Determination of kinetic parameters for the thermal decomposition of parthenium hysterophorus," *Environmental and Climate Technologies*, **22**(1), 5-21 (2018).
- Dhyani, V. and T. Bhaskar, "A comprehensive review on the pyrolysis of lignocellulosic biomass," *Renewable Energy*, **129**, 695-716 (2017).
- DiBlasi, C., "Numerical simulation of cellulose pyrolysis," *Biomass and Bioenergy*, **7**, 87-98 (1994).
- Diebold, J. P., "A unified, global-model for the pyrolysis of cellulose," *Biomass & Bioenergy*, **7**(1-6), 75-85 (1994).
- Dimitrakopoulos, A. P., I. D. Mitsopoulos and K. Gatoulas, "Assessing ignition probability and moisture of extinction in a Mediterranean grass fuel," *International Journal of Wildland Fire*, **19**(1), 29-34 (2010).
- Du, Y., X. Jiang, G. Lv, X. Ma, Y. Jin, F. Wang, Y. Chi and J. Yan, "Thermal behavior and kinetics of bio-ferment residue/coal blends during co-pyrolysis," *Energy Conversion and Management*, **88**, 459-463 (2014).

- Duvvuri, M. S., S. P. Muhlenkamp, K. Z. Iqbal and J. R. Welker, "The pyrolysis of natural fuels," *Journal of Fire and Flammability*, **6** (1975).
- El-Sayed, S. A. and M. E. Mostafa, "Pyrolysis characteristics and kinetic parameters determination of biomass fuel powders by differential thermal gravimetric analysis (TGA/DTG)," *Energy Conversion and Management*, **85**, 165-172 (2014).
- Encinar, J. M., J. F. Gonzalez and J. Gonzalez, "Fixed-bed pyrolysis of *Cynara cardunculus* L. product yields and compositions," *Fuel Processing Technology*, **68**, 209–222 (2000).
- Engstrom, J. D., J. K. Bulter, S. G. Smith, L. L. Baxter, T. H. Fletcher and D. R. Weise, "Ignition behavior of live California chaparral leaves," *Combustion Science and Technology*, **176**(9), 1577-1591 (2010).
- Farag, S., D. Fu, P. G. Jessop and J. Chaouki, "Detailed compositional analysis and structural investigation of a bio-oil from microwave pyrolysis of kraft lignin," *Journal of Analytical and Applied Pyrolysis*, **109**, 249-257 (2014).
- Fazlollahi, F., S. Saeidi, M. S. Safdari, M. Sarkari, J. J. Klemes and L. L. Baxter, "Effect of operating conditions on cryogenic carbon dioxide removal," *Energy Technology*, **5**(9), 1588-1598 (2017).
- Ferguson, S. C., A. Dahale, B. Shotorban, S. Mahalingam and D. R. Weise, "The Role of Moisture on Combustion of Pyrolysis Gases in Wildland Fires," *Combustion Science and Technology*, **185**(3), 435-453 (2013).
- Fernandes, P. M. and S. H. Botelho, "A review of prescribed burning effectiveness in fire hazard reduction," *International Journal of Wildland Fire*, **12**, 117-128 (2003).
- Fletcher, T. H., A. R. Kerstein, R. J. Pugmire, M. S. Solum and D. M. Grant, "Chemical Percolation Model for Devolatilization .3. Direct use of C-13 NMR Data to Predict Effects of Coal Type," *Energy & Fuels*, **6**(4), 414-431 (1992).
- Flynn, J. H. and L. A. Wall, "A quick, direct method for the determination of activation energy from thermogravimetric data," *Journal of Polymer Science*, **4**(5), 323-328 (1966).
- Fons, W. L., "Analysis of fire spread in light forest fuels.," *Journal of Agricultural Research*, **72**(3), 93-121 (1946).
- Fourty, T., F. Baret, S. Jacquemoud, G. Schmuck and J. Verdebout, "Leaf optical properties with explicit description of its biochemical composition: Direct and inverse problems," *Remote Sensing of Environment*, **56**(2), 104-117 (1996).
- Fu, P., W. Yi, X. Bai, Z. Li, S. Hu and J. Xiang, "Effect of temperature on gas composition and char structural features of pyrolyzed agricultural residues," *Bioresource Technology*, **102**(17), 8211-9 (2011).

- Gai, C., Y. Dong and T. Zhang, "The kinetic analysis of the pyrolysis of agricultural residue under non-isothermal conditions," *Bioresource Technology*, **127**, 298-305 (2013).
- Gao, Z., M. Nakada and I. Amasaki, "A consideration of errors and accuracy in the isoconversional methods," *Thermochimica Acta*, **369**(1–2), 137-142 (2001).
- Gomez-Barea, A. and B. Leckner, "Modeling of biomass gasification in fluidized bed," *Progress in Energy and Combustion Science*, **36**(4), 444-509 (2010).
- Goyal, H. B., D. Seal and R. C. Saxena, "Bio-fuels from thermochemical conversion of renewable resources: A review," *Renewable and Sustainable Energy Reviews*, **12**(2), 504-517 (2008).
- Haykiri-Acma, H., S. Yaman and S. Kucukbayrak, "Comparison of the thermal reactivities of isolated lignin and holocellulose during pyrolysis," *Fuel Processing Technology*, **91**, 759–764 (2010).
- Hillier, J., T. Bezzant and T. H. Fletcher, "Improved method for the determination of kinetic parameters from non-isothermal thermogravimetric analysis (TGA) data," *Energy & Fuels*, **24**(5), 2841-2847 (2010).
- Hillier, J. L. and T. H. Fletcher, "Pyrolysis kinetics of a Green River oil shale using a pressurized TGA," *Energy & Fuels*, **25**(1), 232-239 (2011).
- Hillier, J. L., T. H. Fletcher, M. S. Solum and R. J. Pugmire, "Characterization of macromolecular structure of pyrolysis products from a Colorado Green River oil shale," *Industrial & Engineering Chemistry Research*, **52**(44), 15522-15532 (2013).
- Horne, P. A. and P. T. Williams, "Influence of temperature on the products from the flash pyrolysis of biomass," *Fuel* **75**, 1051-1059 (1996).
- Hosoya, T., H. Kawamoto and S. Saka, "Pyrolysis behaviors of wood and its constituent polymers at gasification temperature," *Journal of Analytical and Applied Pyrolysis*, **78**(2), 328-336 (2007).
- Hu, M., X. Wang, J. Chen, P. Yang, C. Liu, B. Xiao and D. Guo, "Kinetic study and syngas production from pyrolysis of forestry waste," *Energy Conversion and Management*, **135**, 453-462 (2017).
- Hu, S., A. Jess and M. Xu, "Kinetic study of Chinese biomass slow pyrolysis: Comparison of different kinetic models," *Fuel*, **86**(17-18), 2778-2788 (2007).
- Hu, Z., Y. Zheng, F. Yan, B. Xiao and S. Liu, "Bio-oil production through pyrolysis of blue-green algae blooms (BGAB): Product distribution and bio-oil characterization," *Energy*, **52**, 119-125 (2013).

- Huang, Y., Z. Wei, Z. Qiu, X. Yin and C. Wu, "Study on structure and pyrolysis behavior of lignin derived from corn cob acid hydrolysis residue," *Journal of Analytical and Applied Pyrolysis*, **93**, 153-159 (2012).
- Imam, T. and S. Capareda, "Characterization of bio-oil, syn-gas and bio-char from switchgrass pyrolysis at various temperatures," *Journal of Analytical and Applied Pyrolysis*, **93**, 170-177 (2012).
- Isahak, W. N. R. W., M. W. M. Hisham, M. A. Yarmo and T.-y. Yun Hin, "A review on bio-oil production from biomass by using pyrolysis method," *Renewable and Sustainable Energy Reviews*, **16**(8), 5910-5923 (2012).
- Jahirul, M. I., M. G. Rasul, A. A. Chowdhury and N. Ashwath, "Biofuels production through biomass pyrolysis—A technological review," *Energies*, **5**, 4952-5001 (2012).
- Jolly, W. M., A. M. Hadlow and K. Huguet, "De-coupling seasonal changes in water content and dry matter to predict live conifer foliar moisture content," *International Journal of Wildland Fire*, **23**, 480–9 (2014).
- Jolly, W. M. and B. Butler, "Linking photosynthesis and combustion characteristics in live fuels: The role of soluble carbohydrates in fuel preheating," Joint Fire Science Program (2015).
- Jolly, W. M. and D. M. Johnson, "Pyro-ecophysiology: shifting the paradigm of live wildland fuel research," *Fire*, **1**, 8 (2018).
- Kar, Y., "Co-pyrolysis of walnut shell and tar sand in a fixed-bed reactor," *Bioresource Technology*, **102**(20), 9800-5 (2011).
- Kissinger, H. E., "Reaction kinetics in differential thermal analysis," *Analytical Chemistry* **29**, 1702-1706 (1957).
- Kök, M. V. and M. R. Pamir, "Non-isothermal pyrolysis and kinetics of oil shales," *Journal of Thermal Analysis and Calorimetry*, **56**, 953-958 (1999).
- Kongkaew, N., W. Pruksakit and S. Patumsawad, "Thermogravimetric kinetic analysis of the pyrolysis of rice straw," *Energy Procedia*, **79**, 663-670 (2015).
- Kovalov, K. M., O. M. Alekseev, M. M. Lazarenko, Y. F. Zabashta, Y. E. Grabovskii and S. Y. Tkachov, "Influence of water on the structure and dielectric properties of the microcrystalline and nano-cellulose," *Nanoscale Research Letters*, **12**(1), 468 (2017).
- Krishna, B. B., B. Biswas, P. Ohri, J. Kumar, R. Singh and T. Bhaskar, "Pyrolysis of Cedrus deodara saw mill shavings in hydrogen and nitrogen atmosphere for the production of bio-oil," *Renewable Energy*, **98**, 238-244 (2016).
- Lamorlette, A., M. El Houssami and D. Morvan, "An improved non-equilibrium model for the ignition of living fuel," *International Journal of Wildland Fire*, **27**(1), 29 (2018).

- Lapuerta, M., J. J. Hernandez and J. Rodriguez, "Kinetics of devolatilisation of forestry wastes from thermogravimetric analysis," *Biomass & Bioenergy*, **27**(4), 385-391 (2004).
- Lazzari, E., T. Schena, C. T. Primaz, G. P. d. S. Maciel, M. E. Machado, C. A. L. Cardoso, R. A. Jacques and E. B. Caramão, "Production and chromatographic characterization of bio-oil from the pyrolysis of mango seed waste," *Industrial Crops and Products*, **83**, 529-536 (2016).
- Lewis, A. D. and T. H. Fletcher, "Prediction of sawdust pyrolysis yields from a flat-flame burner using the CPD model," *Energy & Fuels*, **27**(2), 942-953 (2013).
- Li, Z. and N. Kobayashi, "Determination of moisture diffusivity by thermo-gravimetric analysis under non-isothermal condition," *Drying Technology*, **23**(6), 1331-1342 (2005).
- Lin, S., P. Sun and X. Huang, "Can peat soil support a flaming wildfire?," *International Journal of Wildland Fire*, **28**(8), 601-613 (2019).
- Lopez-Velazquez, M. A., V. Santes, J. Balmaseda and E. Torres-Garcia, "Pyrolysis of orange waste: A thermo-kinetic study," *Journal of Analytical and Applied Pyrolysis*, **99**, 170-177 (2013).
- Lu, H., W. Robert, G. Peirce, B. Ripa and L. L. Baxter, "Comprehensive study of biomass particle combustion," *Energy & Fuels*, **22**(4), 2826-2839 (2008).
- Lu, K.-M., W.-J. Lee, W.-H. Chen and T.-C. Lin, "Thermogravimetric analysis and kinetics of co-pyrolysis of raw/torrefied wood and coal blends," *Applied Energy*, **105**, 57-65 (2013).
- Luo, G., D. S. Chandler, L. C. A. Anjos, R. J. Eng, P. Jia and F. L. P. Resende, "Pyrolysis of whole wood chips and rods in a novel ablative reactor," *Fuel*, **194**, 229-238 (2017).
- M. Vleeskens, J. and B. N. Nandi, "Burnout of coals: Comparative bench-scale experiments on pulverized fuel and fluidized bed combustion," *Fuel*, **65**(6), 797-802 (1986).
- Ma, Z. Q., D. Y. Chen, J. Gu, B. F. Bao and Q. S. Zhang, "Determination of pyrolysis characteristics and kinetics of palm kernel shell using TGA-FTIR and model-free integral methods," *Energy Conversion and Management*, **89**, 251-259 (2015).
- Maia, A. A. D. and L. C. de Moraes, "Kinetic parameters of red pepper waste as biomass to solid biofuel," *Bioresource Technology*, **204**, 157-163 (2016).
- Majhi, A., Y. K. Sharma, D. V. Naik and R. Chauhan, "The production and evaluation of bio-oil obtained from the *Jatropha Curcas* cake," *Energy Sources, Part A: Recovery, Utilization, and Environmental Effects*, **37**(16), 1782-1789 (2015).
- Matt, F. J., M. A. Dietenberger and D. R. Weise, "Summative and ultimate analysis of live leaves from southern U.S. forest plants for use in fire modeling," *Energy & Fuels*, (2020).

- McAllister, S., I. Grenfell, A. Hadlow, W. M. Jolly, M. Finney and J. Cohen, "Piloted ignition of live forest fuels," *Fire Safety Journal*, **51**, 133-142 (2012).
- McKendry, P., "Energy production from biomass (part 2): conversion technologies," *Bioresource Technology*, **83**, 47-54 (2002).
- Mehmood, M. A., G. Ye, H. Luo, C. Liu, S. Malik, I. Afzal, J. Xu and M. S. Ahmad, "Pyrolysis and kinetic analyses of Camel grass (*Cymbopogon schoenanthus*) for bioenergy," *Bioresource Technology*, **228**, 18-24 (2017).
- Meng, A., Y. Zhang, J. Zhuo, Q. Li and L. Qin, "Investigation on pyrolysis and carbonization of *Eupatorium adenophorum* Spreng and tobacco stem," *Journal of the Energy Institute*, **88**(4), 480-489 (2015).
- Mishra, R. K. and K. Mohanty, "Pyrolysis kinetics and thermal behavior of waste sawdust biomass using thermogravimetric analysis," *Bioresource Technology*, **251**, 63-74 (2018).
- Morali, U., N. Yavuzel and S. Sensoz, "Pyrolysis of hornbeam (*Carpinus betulus* L.) sawdust: Characterization of bio-oil and bio-char," *Bioresource Technology*, **221**, 682-685 (2016).
- Munir, S., S. S. Daood, W. Nimmo, A. M. Cunliffe and B. M. Gibbs, "Thermal analysis and devolatilization kinetics of cotton stalk, sugar cane bagasse and shea meal under nitrogen and air atmospheres," *Bioresource Technology*, **100**(3), 1413-1418 (2009).
- Nassar, M. M., "Kinetic studies on thermal degradation of nonwood plants," *Wood and Fiber Science*, **17**, 266-273 (1985).
- Nomanbhay, S., B. Salman, R. Hussain and M. Y. Ong, "Microwave pyrolysis of lignocellulosic biomass—a contribution to power Africa," *Energy, Sustainability and Society*, **7**(1), 23 (2017).
- Onay, O. and O. M. Kockar, "Slow, fast and flash pyrolysis of rapeseed," *Renewable Energy*, **28**(15), 2417-2433 (2003).
- Özbay, N., E. Apaydın-Varol, B. Burcu Uzun and A. Eren Pütün, "Characterization of bio-oil obtained from fruit pulp pyrolysis," *Energy*, **33**(8), 1233-1240 (2008).
- Ozsin, G. and A. E. Putun, "Kinetics and evolved gas analysis for pyrolysis of food processing wastes using TGA/MS/FT-IR," *Waste Management*, **64**, 315-326 (2017).
- Papari, S. and K. Hawboldt, "A review on the pyrolysis of woody biomass to bio-oil: Focus on kinetic models," *Renewable and Sustainable Energy Reviews*, **52**, 1580-1595 (2015).
- Pasangulapati, V., K. D. Ramachandriya, A. Kumar, M. R. Wilkins, C. L. Jones and R. L. Huhnke, "Effects of cellulose, hemicellulose and lignin on thermochemical conversion characteristics of the selected biomass," *Bioresource Technology*, **114**, 663-669 (2012).

- Perez, J., J. Munoz-Dorado, T. d. l. Rubia and J. Martinez, "Biodegradation and biological treatments of cellulose, hemicellulose and lignin: an overview," *International Microbiology*, **5**, 53-63 (2002).
- Philpot, C. W., "Influence of mineral content on the pyrolysis of plant materials," *Forest Science*, **16**(4), 461-471 (1970).
- Pickett, B., C. Isackson, R. Wunder, T. H. Fletcher, B. W. Butler and D. R. Weise, "Experimental measurements during combustion of moist individual foliage samples," *International Journal of Wildland Fire*, **19**, 153–162 (2010).
- Prince, D. R., "Measurement and modeling of fire behavior in leaves and sparse shrubs," PhD, Chemical Engineering, Brigham Young University (2014).
- Prince, D. R. and T. H. Fletcher, "Differences in burning behavior of live and dead leaves, Part 1: Measurements," *Combustion Science and Technology*, **186**(12), 1844-1857 (2014).
- Pütün, A. E., N. Özbay, E. P. Önal and E. Pütün, "Fixed-bed pyrolysis of cotton stalk for liquid and solid products," *Fuel Processing Technology*, **86**(11), 1207-1219 (2005).
- Radhakumari, M., D. J. Prakash and B. Satyavathi, "Pyrolysis characteristics and kinetics of algal biomass using tga analysis based on ICTAC recommendations," *Biomass Conversion and Biorefinery*, **6**(2), 189-195 (2016).
- Rahmati, M., B. Huang, M. K. Mortensen, K. Keyvanloo, T. H. Fletcher, B. F. Woodfield, W. C. Hecker and M. D. Argyle, "Effect of different alumina supports on performance of cobalt Fischer-Tropsch catalysts," *Journal of Catalysis*, **359**, 92-100 (2018).
- Ramajo-Escalera, B., A. Espina, J. R. García, J. H. Sosa-Arno and S. A. Nebra, "Model-free kinetics applied to sugarcane bagasse combustion," *Thermochimica Acta*, **448**(2), 111-116 (2006).
- Rao, T. R. and A. Sharma, "Pyrolysis rates of biomass materials," *Energy*, **23**(11), 973-978 (1998).
- Raveendran, K., A. Ganesh and K. C. Khilar, "Pyrolysis characteristics of biomass and biomass components," *Fuel*, **75**(8), 987-998 (1996).
- Richards, A. P. and T. H. Fletcher, "A comparison of simple global kinetic models for coal devolatilization with the CPD model," *Fuel*, **185**, 171-180 (2016).
- Safdari, M.-S., H.-R. Kariminia, Z. Ghobadi Nejad and T. H. Fletcher, "Study potential of Indigenous *Pseudomonas aeruginosa* and *Bacillus subtilis* in bioremediation of diesel-contaminated water," *Water, Air, & Soil Pollution*, **228**(1) (2016).
- Safdari, M.-S., "Characterization of pyrolysis products from fast pyrolysis of live and dead vegetation," PhD dissertation, Chemical Engineering, Brigham Young University (2018).

- Safdari, M.-S., M. Rahmati, E. Amini, J. E. Howarth, J. P. Berryhill, M. Dietenberger, D. R. Weise and T. H. Fletcher, "Characterization of pyrolysis products from fast pyrolysis of live and dead vegetation native to the Southern United States," *Fuel*, **229**, 151-166 (2018a).
- Safdari, M.-S., E. Amini, D. R. Weise and T. H. Fletcher, "Heating rate and temperature effects on pyrolysis products from live wildland fuels," *Fuel*, **242**, 295-304 (2019).
- Safdari, M.-S., E. Amini, D. R. Weise and T. H. Fletcher, "Comparison of pyrolysis of live wildland fuels heated by radiation vs. convection (under review)," *Fuel*, (2020).
- Safdari, M. S., H. R. Kariminia, M. Rahmati, F. Fazlollahi, A. Polasko, S. Mahendra, W. V. Wilding and T. H. Fletcher, "Development of bioreactors for comparative study of natural attenuation, biostimulation, and bioaugmentation of petroleum-hydrocarbon contaminated soil," *Journal of Hazardous Materials*, **342**, 270-278 (2018b).
- Shadangi, K. P. and K. Mohanty, "Thermal and catalytic pyrolysis of Karanja seed to produce liquid fuel," *Fuel*, **115**, 434-442 (2014).
- Sharma, A., V. Pareek and D. Zhang, "Biomass pyrolysis—A review of modelling, process parameters and catalytic studies," *Renewable and Sustainable Energy Reviews*, **50**, 1081-1096 (2015).
- Shen, D. K., S. Gu, B. Jin and M. X. Fang, "Thermal degradation mechanisms of wood under inert and oxidative environments using DAEM methods," *Bioresource Technology*, **102**(2), 2047-52 (2011).
- Soria-Verdugo, A., N. Garcia-Hernando, L. M. Garcia-Gutierrez and U. Ruiz-Rivas, "Analysis of biomass and sewage sludge devolatilization using the distributed activation energy model," *Energy Conversion and Management*, **65**, 239-244 (2013).
- Starink, M. J., "Thermogravimetric analysis—fourier transform infrared analysis of Palm Oil waste pyrolysis," *Thermochimica Acta*, **288**, 97-104 (1996).
- Susott, R. A., "Effect of heating rate on char yield from forest fuels," N. A. L. U.S. Department of Agriculture, Ogden, Utah, Forest Service, Intermountain Forest and Range Experiment Station, **295** (1980).
- Tihay, V. and P. Gillard, "Comparison of several kinetic approaches to evaluate the pyrolysis of three Mediterranean forest fuels," *International Journal of Wildland Fire*, **20**, 407-417 (2011).
- Torres-Garcia, E. and P. Brachi, "Non-isothermal pyrolysis of grape marc," *Journal of Thermal Analysis and Calorimetry*, **139**, 1463-1478 (2019).

- Uçar, S. and S. Karagöz, "The slow pyrolysis of pomegranate seeds: The effect of temperature on the product yields and bio-oil properties," *Journal of Analytical and Applied Pyrolysis*, **84**(2), 151-156 (2009).
- Uzun, B. B., E. Apaydin-Varol, F. Ateş, N. Özbay and A. E. Pütün, "Synthetic fuel production from tea waste: Characterisation of bio-oil and bio-char," *Fuel*, **89**(1), 176-184 (2010).
- Vamvuka, D., E. Kakaras, E. Kastanaki and P. Grammelis, "Pyrolysis characteristics and kinetics of biomass residuals mixtures with lignite," *Fuel*, **82**(15), 1949-1960 (2003).
- Van de Velden, M., J. Baeyens, A. Brems, B. Janssens and R. Dewil, "Fundamentals, kinetics and endothermicity of the biomass pyrolysis reaction," *Renewable Energy*, **35**(1), 232-242 (2010).
- Vand, V., "A theory of the irreversible electrical resistance changes of metallic films evaporated in vacuum," *Proceedings of the Physical Society*, **55**, 222-246 (1943).
- Varma, A. K. and P. Mondal, "Pyrolysis of pine needles: effects of process parameters on products yield and analysis of products," *Journal of Thermal Analysis and Calorimetry*, (2017).
- Viney, N. R., "A review of fine fuel moisture modelling," *International Journal of Wildland Fire*, **1**(4), 215-235 (1991).
- Vyazovkin, S. and A. C. Wight, "Model-free and model-fitting approaches to kinetic analysis of isothermal and nonisothermal data," *Thermochimica Acta*, **340-341**, 53-68 (1999).
- Wade, D. D. and J. D. Lunsford, "A guide for prescribed fire in southern forests," R8-T5 11, Atlanta, GA (1989).
- Weise, D. R. and C. S. Wright, "Wildland fire emissions, carbon and climate: Characterizing wildland fuels," *Forest Ecology and Management*, **317**, 26-40 (2014).
- Weise, D. R., T. H. Fletcher and T. J. Johnson, "A project to measure and model pyrolysis to improve prediction of prescribed fire behavior," Coimbra University Press, Portugal (2018).
- White, J. E., W. J. Catallo and B. L. Legendre, "Biomass pyrolysis kinetics: A comparative critical review with relevant agricultural residue case studies," *Journal of Analytical and Applied Pyrolysis*, **91**(1), 1-33 (2011).
- Xiong, Q., J. Zhang, F. Xu, G. Wiggins and C. Stuart Daw, "Coupling DAEM and CFD for simulating biomass fast pyrolysis in fluidized beds," *Journal of Analytical and Applied Pyrolysis*, **117**, 176-181 (2016).
- Xue, Q., D. Dalluge, T. J. Heindel, R. O. Fox and R. C. Brown, "Experimental validation and CFD modeling study of biomass fast pyrolysis in fluidized-bed reactors," *Fuel*, **97**, 757-769 (2012).

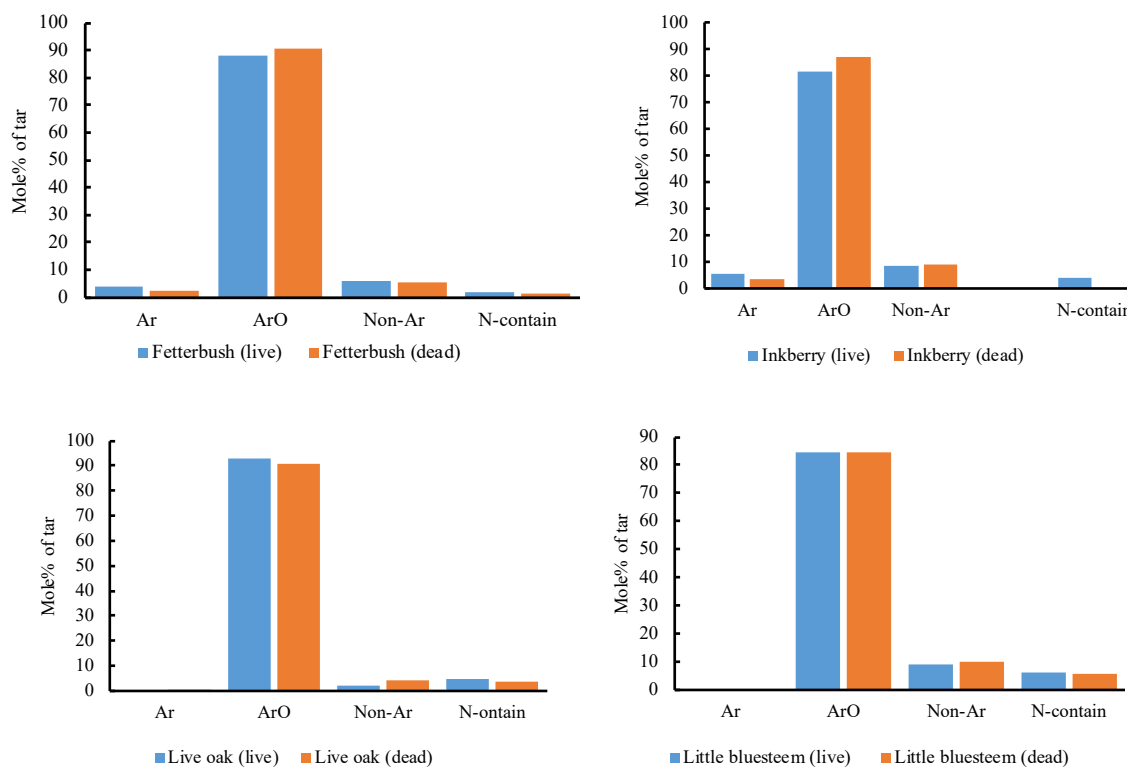
- Yang, H., R. Yan, T. Chin, D. T. Liang, H. Chen and C. Zheng, "Thermogravimetric analysis–fourier transform infrared analysis of palm oil waste pyrolysis," *Energy Fuels*, **18**, 1814-21 (2004).
- Yang, H., R. Yan, H. Chen, D. H. Lee and C. Zheng, "Characteristics of hemicellulose, cellulose and lignin pyrolysis," *Fuel*, **86**(12-13), 1781-1788 (2007).
- Yang, H. P., R. Yan, H. P. Chen, C. G. Zheng, D. H. Lee and D. T. Liang, "In-depth investigation of biomass pyrolysis based on three major components: Hemicellulose, cellulose and lignin," *Energy & Fuels*, **20**(1), 388-393 (2006).
- Yu, J., N. Paterson, J. Blamey and M. Millan, "Cellulose, xylan and lignin interactions during pyrolysis of lignocellulosic biomass," *Fuel*, **191**, 140-149 (2017).
- Yuan, T., A. Tahmasebi and J. Yu, "Comparative study on pyrolysis of lignocellulosic and algal biomass using a thermogravimetric and a fixed-bed reactor," *Bioresource Technology*, **175**, 333-41 (2015).
- Yuan, X., T. He, H. Cao and Q. Yuan, "Cattle manure pyrolysis process: Kinetic and thermodynamic analysis with isoconversional methods," *Renewable Energy*, **107**, 489-496 (2017).
- Yurdakul, S., "Determination of co-combustion properties and thermal kinetics of poultry litter/coal blends using thermogravimetry," *Renewable Energy*, **89**, 215-223 (2016).
- Zabaniotou, A. A., "Pyrolysis of forestry biomass by-products in Greece," *Energy Sources*, **21**(5), 395-403 (1999).

APPENDIX

- A. The Yields of Tar Components Categorized as Ar, ArO, Non-Ar, and N-Containing Compounds
- B. All Identified Tar Components
- C. The Distribution of the Most Prevalent Components in Tar
- D. TG and DTG Curves for All Plant Species
- E. Regression Lines Used to Obtain Apparent Activation Energies for Drying and Major Pyrolysis Zones Using the KAS Method
- F. TG and DTG Curves Resulted from Experimental Data and Simple One-Step Model
- G. TG and DTG Curves Resulted from Experimental Data and Single-Reaction DAEM Model
- H. TG and DTG Curves Resulted from Experimental Data and Multiple-Reaction-DAEM Model
- I. RMSE and MAE Values for All Model Fitting Methods

APPENDIX A. THE YIELDS OF TAR COMPONENTS CATEGORIZED AS AR, ARO, NON-AR, AND N-CONTAIN COMPOUNDS

The yields of tar components were categorized as Ar, ArO, Non-Ar, and N-contain components for all live and dead plant species and are presented in Figure A-1.



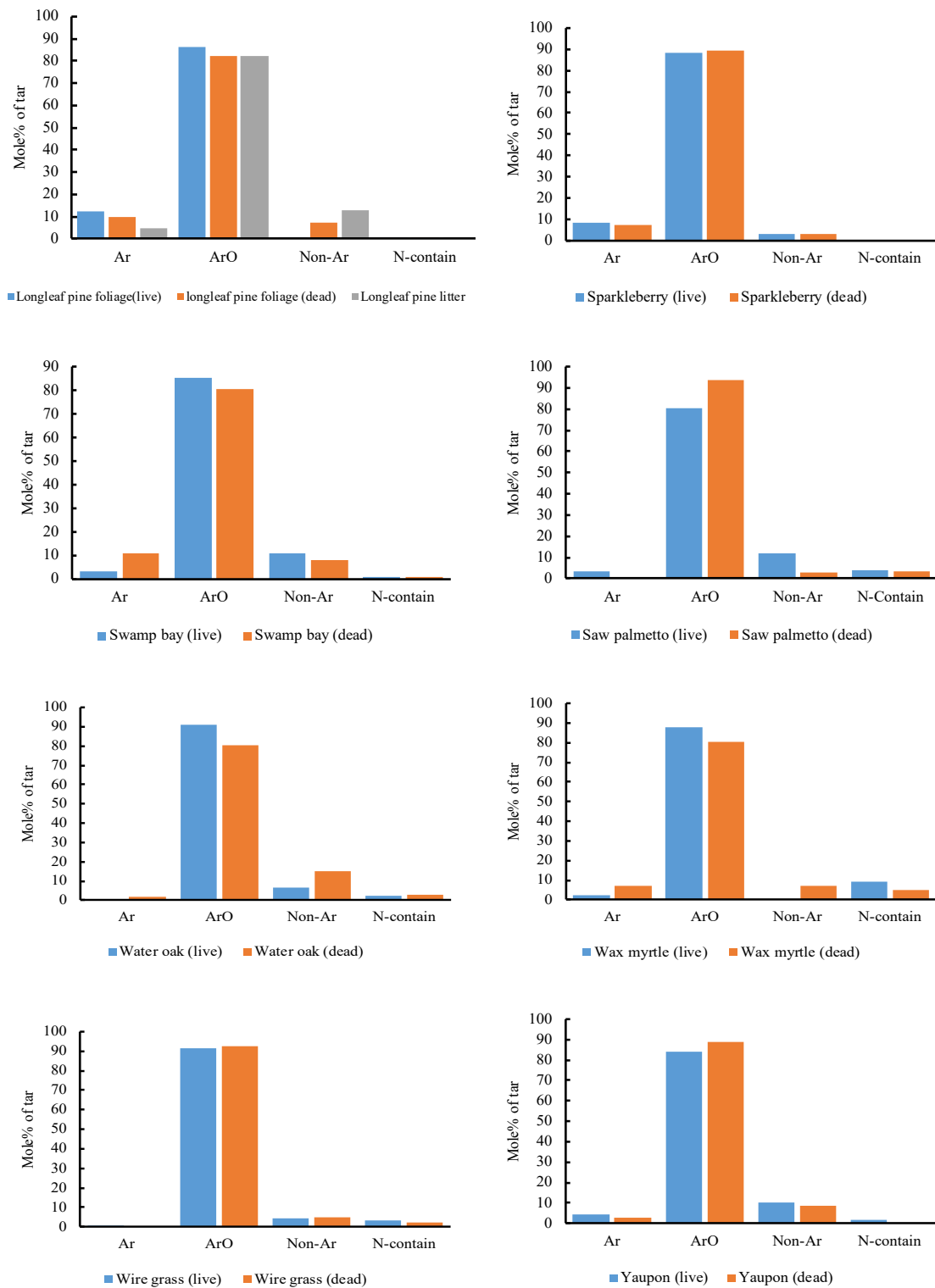


Figure A-1: The yields of tar components categorized as Ar, ArO, Non-Ar, and N-contain components for all live and dead plant species.

APPENDIX B. ALL IDENTIFIED TAR COMPONENTS

Table B-1 contains all identified tar components from slow pyrolysis of all plant species.

Table B-1: All identified tar components from pyrolysis of all plant species

#	R.T. min	Component	M.F.	Group
1	8.163	N-Nitrosodimethylamine	C ₂ H ₆ N ₂ O	N-contain
2	10.238	Pyridine	C ₅ H ₅ N	N-contain
3	10.969	1-Hydroxy-2-butanone	C ₄ H ₈ O ₂	NAr
4	9.077	Propanoic acid	C ₃ H ₆ O ₂	NAr
5	9.178	Methyl propyl ether	C ₄ H ₁₀ O	Non-Ar
6	9.202	3-Pentanone	C ₅ H ₁₀ O	NAr
7	9.34	Pentanoic acid, 2-methyl-	C ₆ H ₁₂ O ₂	NAr
8	11.171	Benzene, [3-(2-cyclohexylethyl)-6-cyclopentylhexyl]-	C ₂₅ H ₄₀	Ar
9	11.607	Pyrrolidine, 2-butyl-1-methyl-	C ₉ H ₁₉ N	Ar
10	11.616	Carbonocyanidic acid, ethyl ester	C ₄ H ₅ NO ₂	N-contain
11	12.538	2-Butenedioic acid (Z)-	C ₄ H ₄ O ₄	NAr
12	12.548	Maleic anhydride	C ₄ H ₂ O ₃	ArO
13	12.618	2-Cyclopenten-1-one	C ₅ H ₆ O	ArO
14	12.659	3-Furaldehyde	C ₅ H ₄ O ₂	ArO
15	12.778	1,3-Cyclopentanedione	C ₅ H ₆ O ₂	ArO
16	13.656	Pentanol, 5-amino-	C ₅ H ₁₃ NO	N-contain
17	13.671	1,3-Cyclopentadiene, 5-(1-methylethylidene	C ₈ H ₁₀	Ar
18	12.673	Furfural	C ₅ H ₄ O ₂	ArO
19	12.848	s-Triazolo[4,3-b]pyridazine, 6,7-dimethyl-	C ₇ H ₈ N ₄	N-contain
20	12.881	3(2H)-Pyridazinone, 6-methyl-	C ₅ H ₆ N ₂ O	N-contain
21	12.986	2-Pentanone, 4-hydroxy-4-methyl-	C ₆ H ₁₂ O ₂	NAr
22	13.243	3-Furanmethanol	C ₅ H ₆ O ₂	ArO
23	13.254	2-Furanmethanol	C ₅ H ₆ O ₂	ArO
24	13.481	2(3H)-Furanone, 5-methyl-	C ₅ H ₆ O ₂	ArO
25	14.054	2(3H)-Furanone	C ₄ H ₄ O ₂	ArO
26	14.528	Ethanone, 1-(2-furanyl)-	C ₆ H ₆ O ₂	ArO
27	14.734	2-Cyclopenten-1-one, 2-hydroxy-	C ₅ H ₆ O ₂	ArO
28	15.173	4H-Pyran-4-one	C ₅ H ₄ O ₂	ArO
29	15.311	2,3-Pentanedione	C ₅ H ₈ O ₂	NAr

Table B-1 Continued

#	R.T. min	Component	M.F.	Group
30	15.312	Propanoic acid, ethenyl ester	C ₅ H ₈ O ₂	NAr
31	15.367	2-Butanone, 1-(acetyloxy)-	C ₆ H ₁₀ O ₃	NAr
32	15.589	2-Furancarboxaldehyde, 5-methyl-	C ₆ H ₆ O ₂	ArO
33	15.611	2-Cyclopenten-1-one, 3-methyl-	C ₆ H ₈ O	ArO
34	15.619	2-Cyclohexen-1-one, 4-ethyl-4-methyl-	C ₉ H ₁₄ O	ArO
35	15.798	3-Pyrazolidinone, 1,4-dimethyl	C ₅ H ₁₀ N ₂ O	N-contain
36	15.817	2-Methyliminoperhydro-1,3-oxazine	C ₅ H ₁₀ N ₂ O	N-contain
37	15.907	Phenol	C ₆ H ₆ O	ArO
38	16.039	1-Hydroxy-2-pentanone	C ₅ H ₁₀ O ₂	NAr
39	16.199	2-Pentenoic acid, 2-methyl-, (E)-	C ₆ H ₁₀ O ₂	NAr
40	16.203	3-Cyclobutene-1,2-dione, 3,4-dihydroxy-	C ₄ H ₂ O ₄	Ar
41	16.211	3-Cyclobutene-1,2-dione, 3,4-dihydroxy-	C ₄ H ₂ O ₄	ArO
42	16.44	1,2-Cyclohexanedione	C ₆ H ₈ O ₂	ArO
43	16.451	1,4-Cyclohexanedione	C ₆ H ₈ O ₂	ArO
44	16.467	Cyclohexane, 1,4-dimethyl-2-octadecyl-	C ₂₆ H ₅₂	Ar
45	16.496	3,4-Dihydro-6-methyl-2H-pyran-2-one	C ₆ H ₈ O ₂	ArO
46	16.868	Benzene, 1-methyl-2-(1-methylethyl)-	C ₁₀ H ₁₄	ArO
47	16.872	2-Cyclopenten-1-one, 2-hydroxy-3-methyl-	C ₆ H ₈ O ₂	ArO
48	16.894	1,2-Cyclopentanedione, 3-methyl-	C ₆ H ₈ O ₂	ArO
49	16.971	Phenol, 3-methyl-	C ₇ H ₈ O	ArO
50	17.025	Benzene, 1-methoxy-4-methyl-	C ₈ H ₁₀ O	ArO
51	17.091	Benzyl Alcohol	C ₇ H ₈ O	ArO
52	17.146	2-Octanone	C ₈ H ₁₆ O	NAr
53	17.198	2-Cyclopenten-1-one, 3,4-dimethyl-	C ₇ H ₁₀ O	ArO
54	17.289	Benzene, 1,3-diethyl-	C ₁₀ H ₁₄	Ar
55	17.291	Benzene, 1,2,3-trimethyl-	C ₉ H ₁₂	Ar
56	17.299	Benzene, 1,4-diethyl-	C ₁₀ H ₁₄	Ar
57	17.372	Propanoic acid, anhydride	C ₆ H ₁₀ O ₃	NAr
58	17.387	Phenol, 2-methyl-	C ₇ H ₈ O	ArO
59	17.494	Cyclohexene, 1-methyl-4-(1-methylethenyl)-, (R)-	C ₁₀ H ₁₆	Ar
60	17.497	Cyclohexene, 1-methyl-4-(1-methylethenyl)-, (S)-	C ₁₀ H ₁₆	Ar
61	17.716	Phenol, 4-methyl-	C ₇ H ₈ O	ArO
62	17.746	Phenol, 4-methoxy-	C ₇ H ₈ O ₂	ArO
63	17.795	Propanoic acid, 2-propenyl ester	C ₆ H ₁₀ O ₂	Non-Ar
64	17.799	1-Hepten-3-ol	C ₇ H ₁₄ O	Non-Ar
65	17.801	1-Penten-3-ol	C ₅ H ₁₀ O	Non-Ar
66	17.804	2-Buten-1-ol	C ₄ H ₈ O	Non-Ar
67	17.812	5-Hepten-3-one, 5-methyl-	C ₈ H ₁₄ O	NAr
68	17.825	3-Butene-1,2-diol	C ₄ H ₈ O ₂	Non-Ar
69	17.903	3-Pyridinol	C ₅ H ₅ NO	N-contain
70	17.938	4-Aminopyrimidine	C ₄ H ₅ N ₃	N-contain
71	17.942	2,5-Dimethyl-4-hydroxy-3(2H)-furanone	C ₆ H ₈ O ₃	ArO
72	17.943	2,5-Dimethyl-4-hydroxy-3(2H)-furanone	C ₆ H ₈ O ₃	ArO
73	17.957	2,4(1H,3H)-Pyrimidinedione, dihydro-3-methyl-	C ₅ H ₈ N ₂ O ₂	N-contain
74	18.041	Pyrrolidine, 1-[1-(phenylmethyl)butyl]-	C ₁₅ H ₂₃ N	N-contain
75	18.108	2(3H)-Furanone, 5-acetyldihydro-	C ₆ H ₈ O ₃	ArO

Table B-1 Continued

#	R.T. min	Component	M.F.	Group
76	18.176	Phenol, 2-methoxy-	C ₇ H ₈ O ₂	ArO
77	18.404	Benzene, 4-ethenyl-1,2-dimethyl-	C ₁₀ H ₁₂	Ar
78	18.406	Benzene, 1-methyl-4-(1-methylethenyl)-	C ₁₀ H ₁₂	Ar
79	18.461	Maltol (Larixic acid)	C ₆ H ₆ O ₃	ArO
80	18.634	2-Cyclopenten-1-one, 3-ethyl-2-hydroxy-	C ₇ H ₁₀ O ₂	ArO
81	18.637	Nonane, 5-(1-methylpropyl)-	C ₁₃ H ₂₈	Non-Ar
82	18.648	Undecane	C ₁₁ H ₂₄	Non-Ar
83	18.655	Phenol, 2,3-dimethyl-	C ₈ H ₁₀ O	ArO
84	18.765	Benzofuran, 2-methyl-	C ₉ H ₈ O	ArO(2r)
85	19.067	Phenol, 2,5-dimethyl-	C ₈ H ₁₀ O	ArO
86	19.072	Phenol, 2,4-dimethyl-	C ₈ H ₁₀ O	ArO
87	19.075	Phenol, 3,4-dimethyl-	C ₈ H ₁₀ O	ArO
88	19.185	Benzoic Acid	C ₇ H ₆ O ₂	ArO
89	19.316	Phenol, 4-ethyl-	C ₈ H ₁₀ O	ArO
90	19.489	2-Pentanol, 5-(2-propynyloxy)-	C ₈ H ₁₄ O ₂	NAr
91	19.515	1,3-Benzenediol, 4-ethyl-	C ₈ H ₁₀ O ₂	ArO
92	19.532	2-Methoxy-6-methylphenol	C ₈ H ₁₀ O ₂	ArO
93	19.555	5-Hexyl-4-methyldihydro-2(3H)-furanone	C ₁₁ H ₂₀ O ₂	ArO
94	19.58	Benzene, 1-methyl-4-(1-propynyl)-	C ₁₀ H ₁₀	Ar
95	19.657	Benzaldehyde, 3-methyl-	C ₈ H ₈ O	ArO
96	19.636	Phenol, 4-ethenyl-, acetate	C ₁₀ H ₁₀ O ₂	ArO
97	19.678	1,2-Benzenediol	C ₆ H ₆ O ₂	ArO
98	19.785	4H-Pyran-4-one, 5-hydroxy-2-(hydroxymethyl)-	C ₆ H ₆ O ₄	ArO
99	19.948	Crotonic acid, menthyl ester	C ₁₄ H ₂₄ O ₂	ArO
100	19.949	2-Methoxy-5-methylphenol	C ₈ H ₁₀ O ₂	ArO
101	19.952	Phenol, 2-methoxy-4-methyl-	C ₈ H ₁₀ O ₂	ArO
102	20.018	2-Butenoic acid, ethyl ester, (E)-	C ₆ H ₁₀ O ₂	NAr
103	20.026	5-Decanone, 6-hydroxy-	C ₁₀ H ₂₀ O ₂	NAr
104	20.058	Benzaldehyde, 4-methyl-	C ₈ H ₈ O	ArO
105	20.073	Benzofuran, 2,3-dihydro-	C ₈ H ₈ O	Ar(2r)
106	20.125	Benzofuran, 4,7-dimethyl-	C ₁₀ H ₁₀ O	Ar(2r)
107	20.18	Cyclohexanone, 4-hydroxy-4-methyl-	C ₇ H ₁₂ O ₂	ArO
108	20.282	Dodecane, 2,6,10-trimethyl-	C ₁₅ H ₃₂	NAr
109	20.281	Dodecane	C ₁₂ H ₂₆	NAr
110	20.311	2,4,4-Trimethyl-1-hexene	C ₉ H ₁₈	NAr
111	20.476	6-Octen-1-ol, 3,7-dimethyl-, (R)-	C ₁₀ H ₂₀ O	NAr
112	20.599	1,3-Benzenediol	C ₆ H ₆ O ₂	ArO
113	20.632	1,4-Benzenediol	C ₆ H ₆ O ₂	ArO
114	20.753	1,2-Benzenediol, 3-methyl-	C ₇ H ₈ O ₂	ArO
115	21.027	1,2-Benzenediol, 3-methoxy-	C ₇ H ₈ O ₃	ArO
116	21.169	1,2-Benzenediol, 4-methyl-	C ₇ H ₈ O ₂	ArO
117	21.265	5-Acetoxymethyl-2-furaldehyde	C ₈ H ₈ O ₄	ArO
118	21.323	Phenol, 4-ethyl-2-methoxy-	C ₉ H ₁₂ O ₂	ArO
119	21.375	Ethanone, 1-(2-hydroxy-5-methylphenyl)-	C ₉ H ₁₀ O ₂	ArO
120	21.433	Ketole (Indole)	C ₈ H ₇ N	Ar(2r)
121	21.506	Naphthalene, 2-methyl-	C ₁₁ H ₁₀	Ar(2r)
122	21.641	1-Octene, 3,7-dimethyl-	C ₁₀ H ₂₀	NAr

Table B-1 Continued

#	R.T. min	Component	M.F.	Group
123	21.805	2-Methoxy-4-vinylphenol	C ₉ H ₁₀ O ₂	ArO
124	22.121	2,3-Dimethylhydroquinone	C ₈ H ₁₀ O ₂	ArO
125	22.152	Phenol, 3,4-dimethoxy-	C ₈ H ₁₀ O ₃	ArO
126	22.167	Phenol, 2,6-dimethoxy-	C ₈ H ₁₀ O ₃	ArO
127	22.191	Benzenemethanol, à-ethyl-4-methoxy-	C ₁₀ H ₁₄ O ₂	ArO
128	22.208	Benzaldehyde, 4-ethoxy-3-hydroxy-	C ₉ H ₁₀ O ₃	ArO
129	22.397	1,2,3-Benzenetriol	C ₆ H ₆ O ₃	ArO
130	22.432	1H-Indole, 3-methyl-	C ₉ H ₉ N	ArO
131	22.452	Phenol, 2-methoxy-6-(2-propenyl)-	C ₁₀ H ₁₂ O ₂	ArO
132	22.542	4-Ethylcatechol	C ₈ H ₁₀ O ₂	ArO
133	22.551	1,2-Benzenediol, 4-ethyl-	C ₈ H ₁₀ O ₂	ArO
134	22.56	Benzoic acid, 3-hydroxy-, methyl ester	C ₈ H ₈ O ₃	ArO
135	22.564	Benzoic acid, 4-hydroxy-, methyl ester	C ₈ H ₈ O ₃	ArO
136	22.639	Phenol, 2-methoxy-4-propyl-	C ₁₀ H ₁₄ O ₂	ArO
137	22.66	1,4-Benzenediol, 2-methoxy-	C ₇ H ₈ O ₃	ArO
138	22.866	4-Quinololinol, 2-methyl-	C ₁₀ H ₉ NO	N-contain
139	23	Benzoic acid, 4-hydroxy-, methyl ester	C ₈ H ₈ O ₃	ArO
140	23.055	1-Octanol, 3,7-dimethyl-	C ₁₀ H ₂₂ O	NAr
141	23.066	Benzeneethanol, 4-hydroxy-	C ₈ H ₁₀ O ₂	ArO
142	23.079	Phenol, 4-methoxy-3-(methoxymethyl)-	C ₉ H ₁₂ O ₃	ArO
143	23.176	1,2-Benzenediol, 3-methoxy-	C ₇ H ₈ O ₃	ArO
144	23.198	Decane, 2-methyl-	C ₁₁ H ₂₄	NAr
145	23.248	Benzenepropanoic acid, á-amino-4-methoxy-	C ₁₀ H ₁₃ NO ₃	N-contain
146	23.287	Phenol, 2-methoxy-4-(1-propenyl)-, (E)-	C ₁₀ H ₁₂ O ₂	ArO
147	23.359	Naphthalene, 1,5-dimethyl-	C ₁₂ H ₁₂	Ar(2r)
148	23.505	1,2,4-Trimethoxybenzene	C ₉ H ₁₂ O ₃	ArO
149	23.512	Ethanone, 1-(2,3,4-trihydroxyphenyl)-	C ₈ H ₈ O ₄	ArO
150	23.515	Ethanone, 1-(2,3,4-trihydroxyphenyl)-	C ₈ H ₈ O ₄	ArO
151	23.566	Naphthalene, 1,4-dimethyl-	C ₁₂ H ₁₂	Ar(2r)
152	23.638	Phenol, 3-methoxy-2,4,6-trimethyl-	C ₁₀ H ₁₄ O ₂	ArO
153	23.677	Undecanoic acid	C ₁₁ H ₂₂ O ₂	NAr
154	23.715	Phenol, 2-methoxy-4-(1-propenyl)-	C ₁₀ H ₁₂ O ₂	ArO
155	23.724	Phenol, 2-methoxy-4-(1-propenyl)-	C ₁₀ H ₁₂ O ₂	ArO
156	23.752	Benzoic acid, 3,4-dimethyl-	C ₉ H ₁₀ O ₂	ArO
157	23.801	Naphthalene, 1,8-dimethyl-	C ₁₂ H ₁₂	Ar(2r)
158	23.921	Naphthalene, 1,2,3,4,4a,5,6,8a-octahydro-7-methyl-4	C ₁₅ H ₂₄	Ar(2r)
159	23.921	1,6,10-Dodecatriene, 7,11-dimethyl-3-methylene-, (E)-	C ₁₅ H ₂₄	NAr
160	24.042	1,6,10-Dodecatriene, 7,11-dimethyl-3-methylene-	C ₁₅ H ₂₄	NAr
161	24.084	1-(3,6-Dimethyl-2-pyrazinyl)propanone	C ₉ H ₁₂ N ₂ O	N-contain
162	24.088	9-Octadecen-12-ynoic acid, methyl ester	C ₁₉ H ₃₂ O ₂	NArO
163	24.094	2H-1-Benzopyran-2-one, 3,4-dihydro-6-hydroxy-	C ₉ H ₈ O ₃	Ar(2r)
164	24.095	Ethanone, 1-(4-hydroxy-3-methoxyphenyl)-	C ₉ H ₁₀ O ₃	ArO
165	24.139	5-tert-Butyl-1,2,3-benzenetriol	C ₁₀ H ₁₄ O ₃	ArO
166	24.143	Trimethoxyamphetamine, 2,3,5-	C ₁₂ H ₁₉ NO ₃	N-contain
167	24.193	Propan-2-one, 1-(4-isopropoxy-3-methoxyphenyl)-	C ₁₃ H ₁₈ O ₃	ArO
168	24.392	Benzene, 1-(1,5-dimethyl-4-hexenyl)-4-methyl-	C ₁₅ H ₂₂	ArO
169	24.4	2-Decyn-1-ol	C ₁₀ H ₁₈ O	NAr

Table B-1 Continued

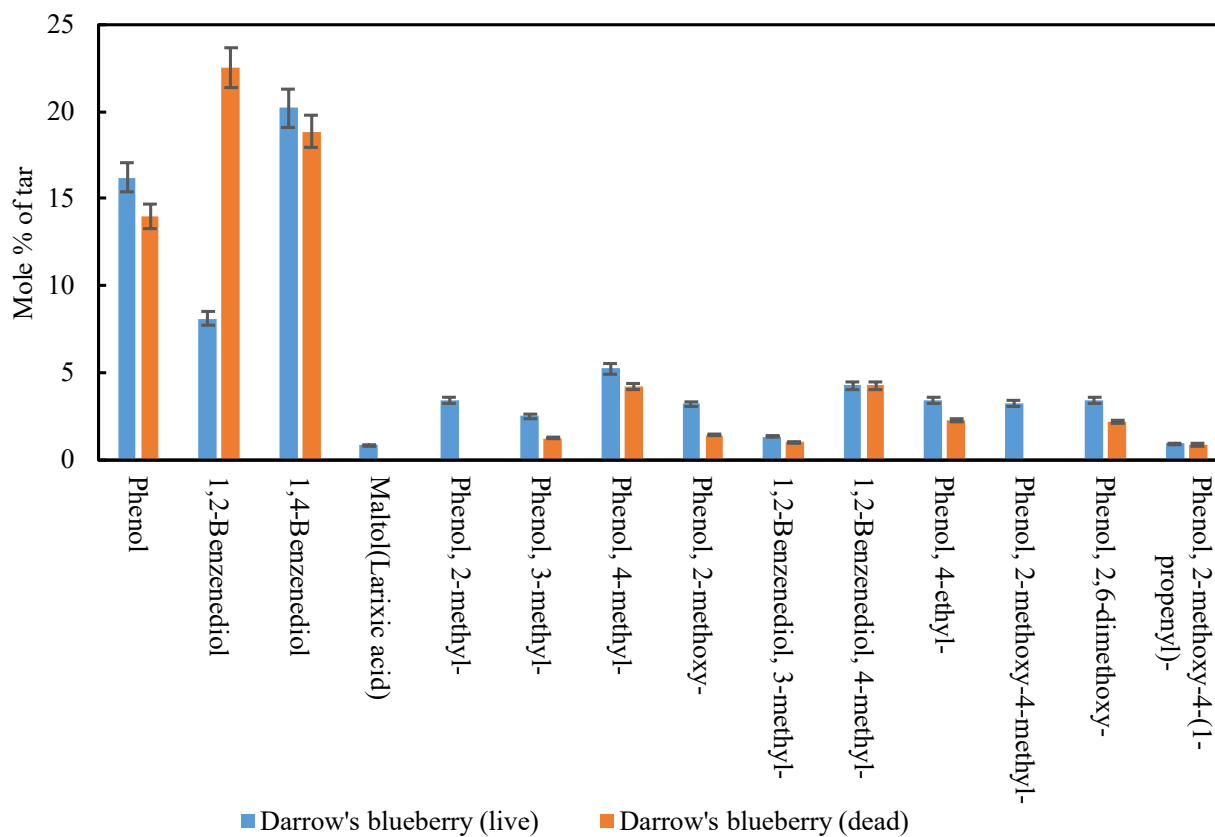
#	R.T. min	Component	M.F.	Group
170	24.531	Geranyl isovalerate	C ₁₅ H ₂₆ O ₂	NAr
171	24.524	Pentadecane	C ₁₅ H ₃₂	NAr
172	24.532	1-Dodecanol, 3,7,11-trimethyl-	C ₁₅ H ₃₂ O	NAr
173	24.568	5-tert-Butyl-1,2,3-benzenetriol	C ₁₀ H ₁₄ O ₃	ArO
174	24.57	5-tert-Butylpyrogallol	C ₁₀ H ₁₄ O ₃	ArO
175	24.579	Benzene, 1,2,3-trimethoxy-5-methyl-	C ₁₀ H ₁₄ O ₃	ArO
176	24.623	Ethanone, 1-(3,4-dimethoxyphenyl)-	C ₁₀ H ₁₂ O ₃	ArO
177	24.625	Furan, 2,5-dibutyl-	C ₁₂ H ₂₀ O	ArO
178	24.631	2-Propanone, 1-(4-hydroxy-3-methoxyphenyl)-	C ₁₀ H ₁₂ O ₃	ArO
179	24.634	2-Propanone, 1-(4-hydroxy-3-methoxyphenyl)-	C ₁₀ H ₁₂ O ₃	ArO
180	24.653	1-Penten-3-one, 1-(4-methoxyphenyl)-4-methyl-	C ₁₃ H ₁₆ O ₂	ArO
181	24.674	Benzyl alcohol, à-isobutyl-2,4,6-trimethyl-	C ₁₄ H ₂₂ O	ArO
182	24.677	3-(1-Ethoxy-ethoxy)-2-ethyl-butyric acid, ethyl ester	C ₁₂ H ₂₄ O ₄	NAr
183	24.952	Dodecanoic acid	C ₁₂ H ₂₄ O ₂	NAr
184	25.05	3',5'-Dimethoxyacetophenone	C ₁₀ H ₁₂ O ₃	ArO
185	25.105	Naphthalene, 1,2,3,4-tetrahydro-1,6-dimethyl-4-(1-methylethyl)-	C ₁₅ H ₂₂	Ar(2r)
186	25.146	6,9-Octadecadiynoic acid, methyl ester	C ₁₉ H ₃₀ O ₂	NAr
187	25.16	2H-1-Benzopyran-4-ol, 3,4-dihydro-	C ₉ H ₁₀ O ₂	Ar(2r)
188	25.237	3-(2-Methyl-propenyl)-1H-indene	C ₁₃ H ₁₄	Ar(2r)
189	25.39	à-Calacorene	C ₁₅ H ₂₀	Ar(2r)
190	25.552	Naphthalene, 1,6,7-trimethyl-	C ₁₃ H ₁₄	Ar(2r)
191	25.643	Naphthalene, 2,3,6-trimethyl-	C ₁₃ H ₁₄	Ar(2r)
192	25.653	Benzene, 1,1'-propylidenebis-	C ₁₅ H ₁₆	Ar(2r)
193	25.66	Naphthalene, 1,6,7-trimethyl-	C ₁₃ H ₁₄	Ar(2r)
194	26.011	Naphthalene, 2,3,6-trimethyl-	C ₁₃ H ₁₄	Ar(2r)
195	26.122	Methyl-(2-hydroxy-3-ethoxy-benzyl)ether	C ₁₀ H ₁₄ O ₃	ArO
196	26.125	Benzeneacetic acid, 4-hydroxy-3-methoxy-	C ₉ H ₁₀ O ₄	ArO
197	26.248	Phenol, 2,6-dimethoxy-4-(2-propenyl)-	C ₁₁ H ₁₄ O ₃	ArO
198	26.475	1,3-Cyclopentadiene, 1,2,3,4,5-pentamethyl-	C ₁₀ H ₁₆	Ar
199	26.65	2-Butenedioic acid, 2-[2-(1,3-diethenyl-2-pyrrolyl)](methyl)amino-, dimethyl ester	C ₁₈ H ₂₄ N ₂ O ₄	N-contain
200	26.654	Propanoic acid, 2-methyl-, (decahydro-6a-hydroxy-9a-methyl-3-methylene-2,9-dioxoazulenol[4,5-b]furan-6-yl)methyl ester, [3aS-(3aà,6a,6aà,9aà,9bà)]-	C ₁₉ H ₂₆ O ₆	ArO
201	26.706	Phenol, 2,6-dimethoxy-4-(2-propenyl)-	C ₁₁ H ₁₄ O ₃	ArO
202	26.906	Acetylcur-16-en-20-ol	C ₂₁ H ₂₆ N ₂ O ₂	N-contain
203	27.331	1-Undecene, 5-methyl-	C ₁₂ H ₂₄	NAr
204	27.447	2(3H)-Naphthalenone, 4,4a,5,6,7,8-hexahydro-4a-phenyl-, (R)-	C ₁₆ H ₁₈ O	Ar(3r)
205	27.863	Naphthalene, 1,2,3,4-tetramethyl-	C ₁₄ H ₁₆	Ar(2r)
206	28.057	3-Eicosyne	C ₂₀ H ₃₈	ArO
207	28.06	cis,cis-2,7-Nonadiene	C ₉ H ₁₆	Non-Ar
208	28.069	12-Methyl-E,E-2,13-octadecadien-1-ol	C ₁₉ H ₃₆ O	NArO
209	28.495	3,7,11,15-Tetramethyl-2-hexadecen-1-ol	C ₂₀ H ₄₀ O	NAr
210	28.501	3-Hexadecyne	C ₁₆ H ₃₀	ArO
211	28.504	Cyclopentane, 1,2-dimethyl-3-(1-methylethenyl)-	C ₁₀ H ₁₈	Non-Ar
212	28.507	2H-Pyran-2-one, 6-pentyl-	C ₁₀ H ₁₄ O ₂	Non-Ar

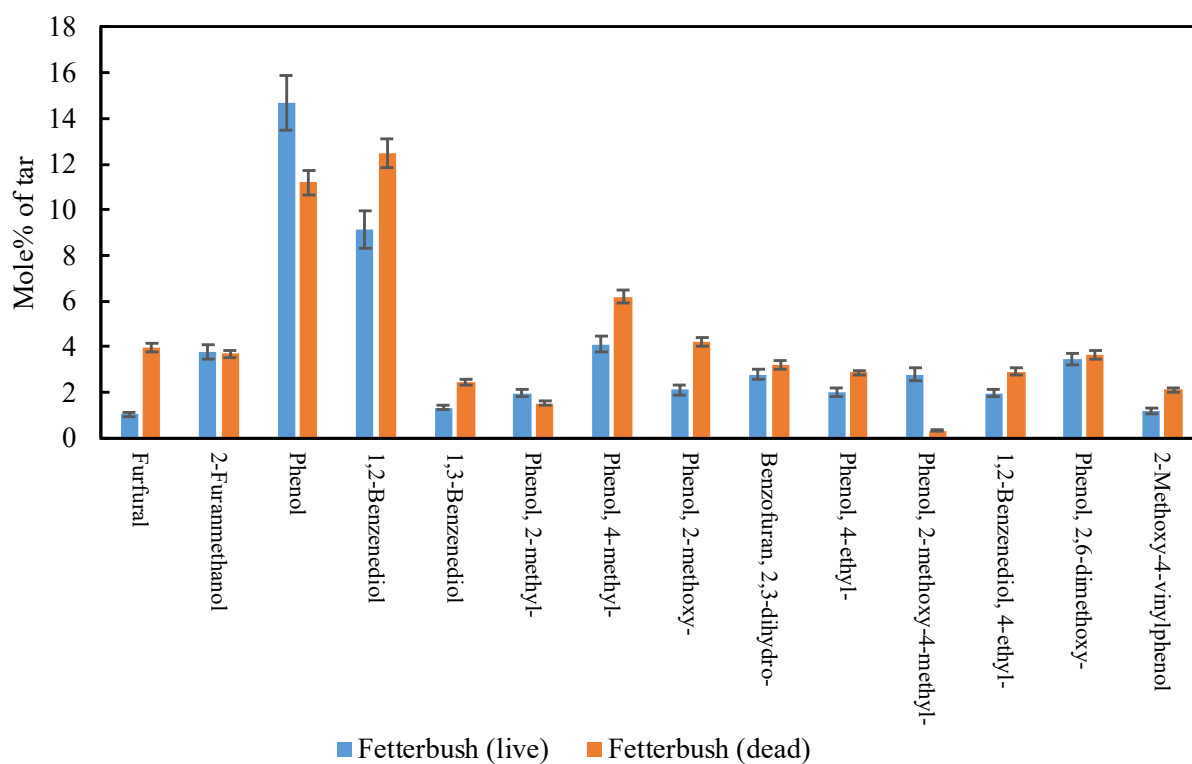
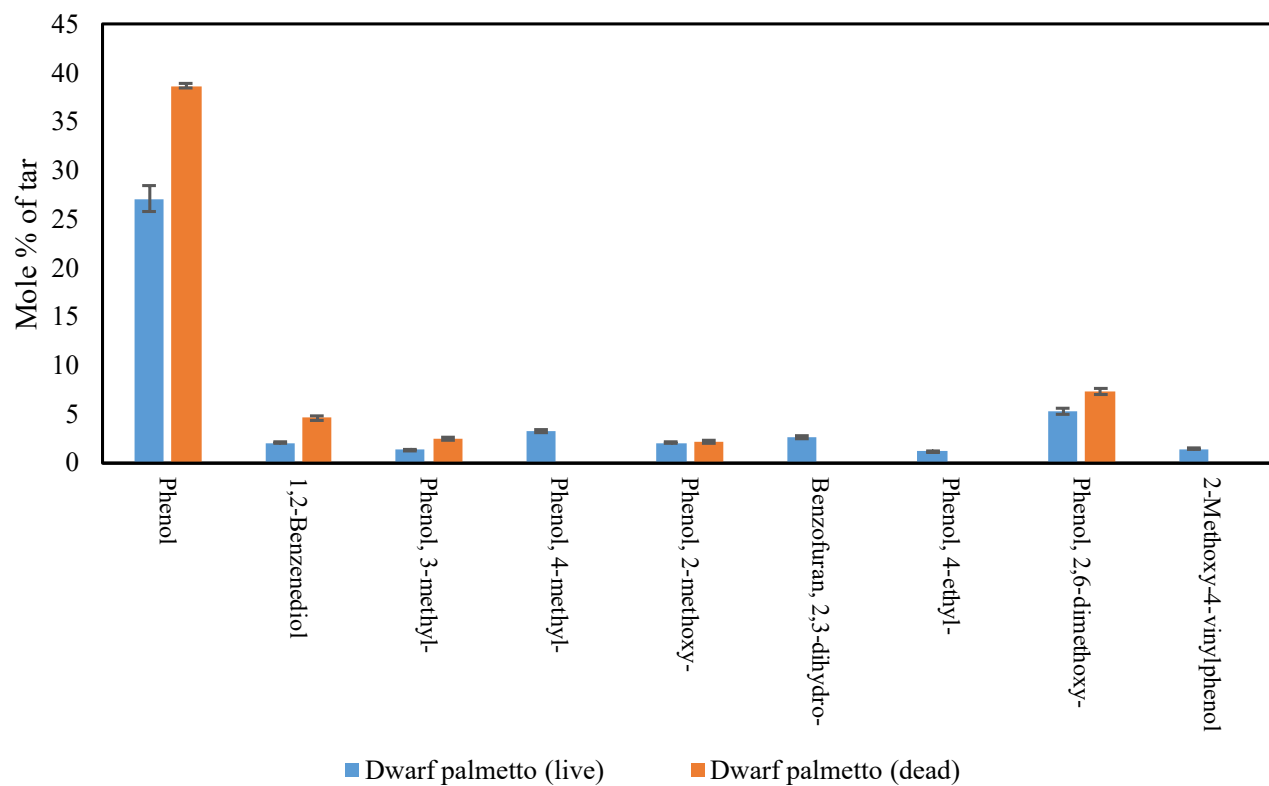
Table B-1 Continued

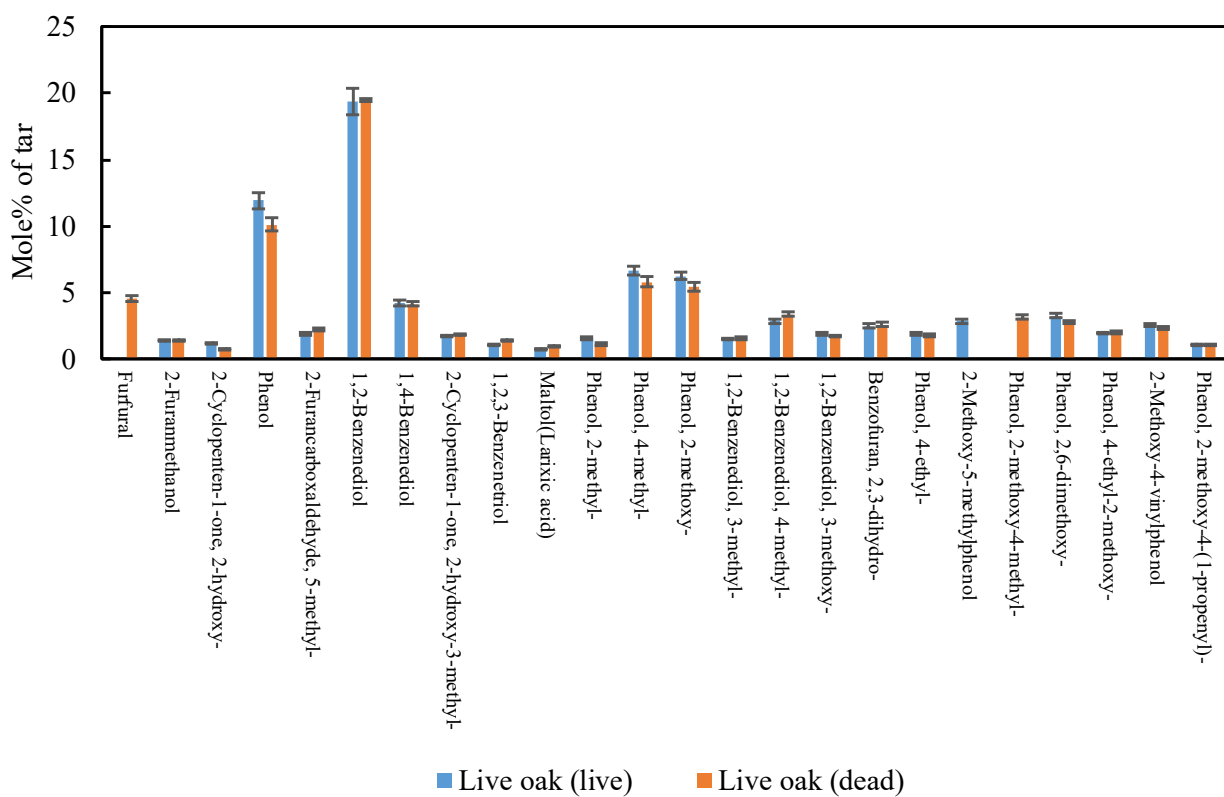
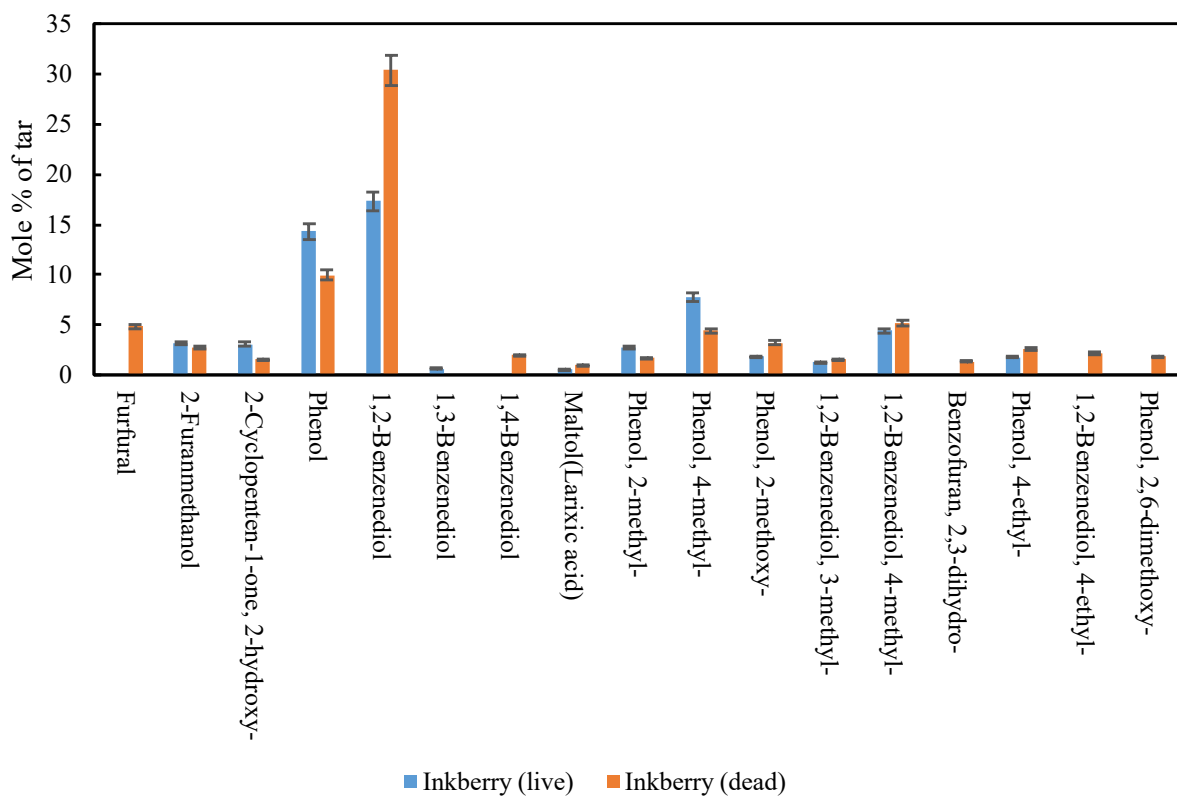
#	R.T. min	Component	M.F.	Group
213	28.508	Ethanol, 2-(9-octadecenyl)-, (Z)-	C ₂₀ H ₄₀ O ₂	NArO
214	28.759	Hexadecanoic acid, methyl ester	C ₁₇ H ₃₄ O ₂	Non-Ar
215	28.77	Pentadecanoic acid, 14-methyl-, methyl ester	C ₁₇ H ₃₄ O ₂	NArO
216	29.406	Z,Z-3,15-Octadecadien-1-ol acetate	C ₂₀ H ₃₆ O ₂	NArO
217	29.511	Undecanoic acid, hydroxy-, lactone	C ₁₁ H ₂₀ O ₂	ArO
218	29.796	6-Methyl-1,2,3,5,8,8a-hexahydronaphthalene	C ₁₁ H ₁₆	Ar
219	30.947	1-Propene, 1,2-bis(4-methoxyphenyl)-	C ₁₇ H ₁₈ O ₂	ArO
220	31.243	1,6,10,14-Hexadecatetraen-3-ol, 3,7,11,15-tetramethyl-, (E,E)-	C ₂₀ H ₃₄ O	Non-Ar
221	31.49	1,11-Dodecadiene	C ₁₂ H ₂₂	Non-Ar
222	32.12	1-Propene, 1,2-bis(4-methoxyphenyl)-	C ₁₇ H ₁₈ O ₂	ArO(2r)
223	32.318	Phenanthrene, 1-methyl-7-(1-methylethyl)-	C ₁₈ H ₁₈	Ar(3r)
224	32.34	2-Isopropyl-10-methylphenanthrene	C ₁₈ H ₁₈	Ar(3r)
225	32.515	Heptadecane, 9-hexyl-	C ₂₃ H ₄₈	Non-Ar
226	33.316	1-Phenanthrenecarboxylic acid, 1,2,3,4,4a,9,10,10a-octahydro-1,4a-dimethyl-7-(1-methylethyl)-, methyl ester, [1R-(1à,4aà,10aà)]-	C ₂₁ H ₃₀ O ₂	ArO(3r)
227	33.502	1-Decanol, 2-hexyl-	C ₁₆ H ₃₄ O	Non-Ar

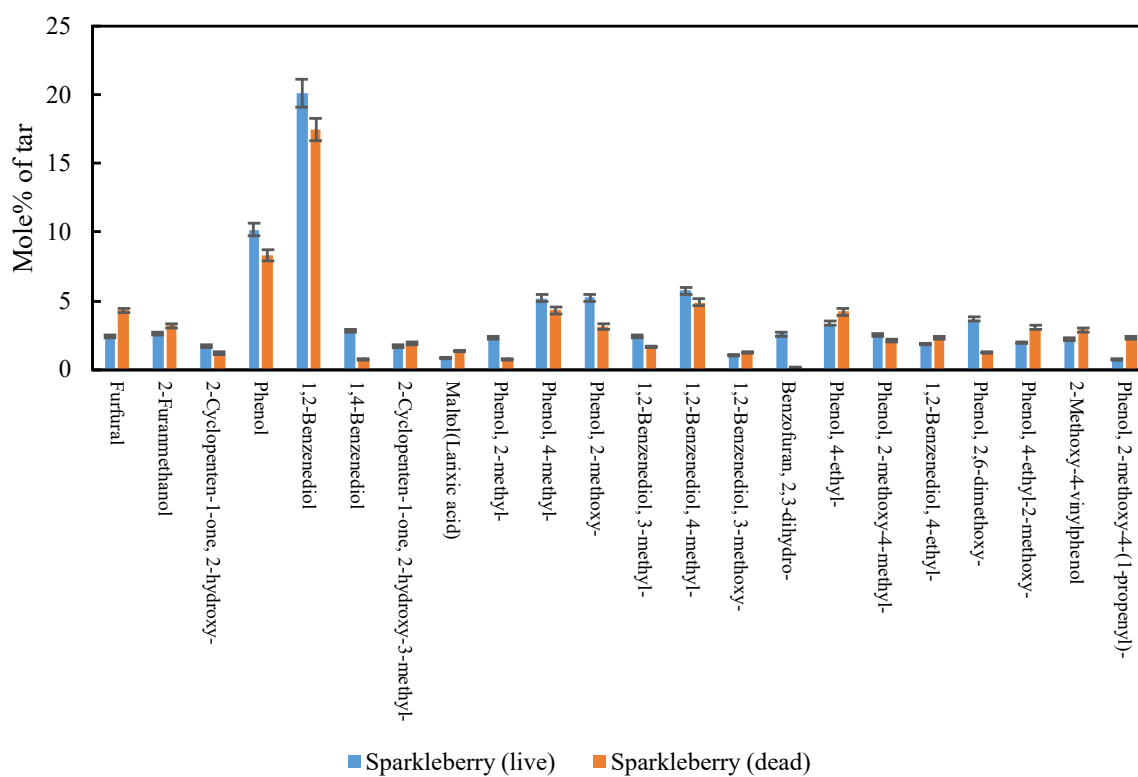
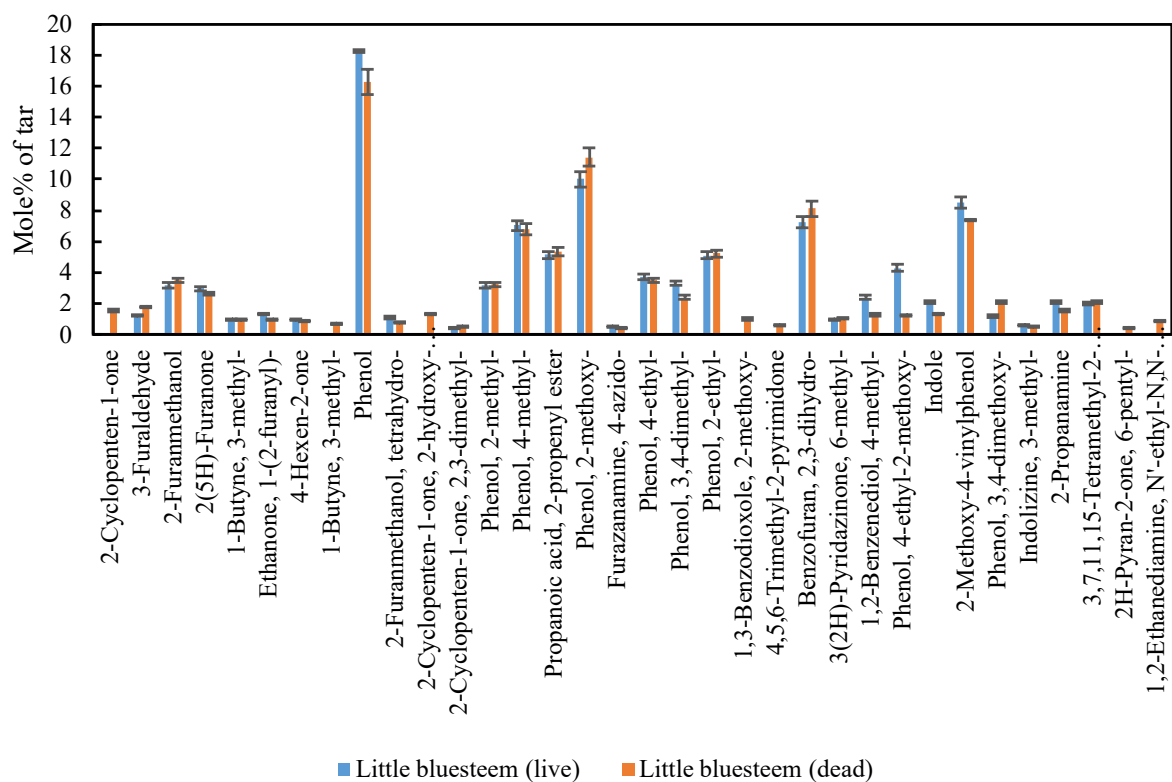
APPENDIX C. THE DISTRIBUTION OF THE MOST PREVALENT COMPONENTS IN TAR

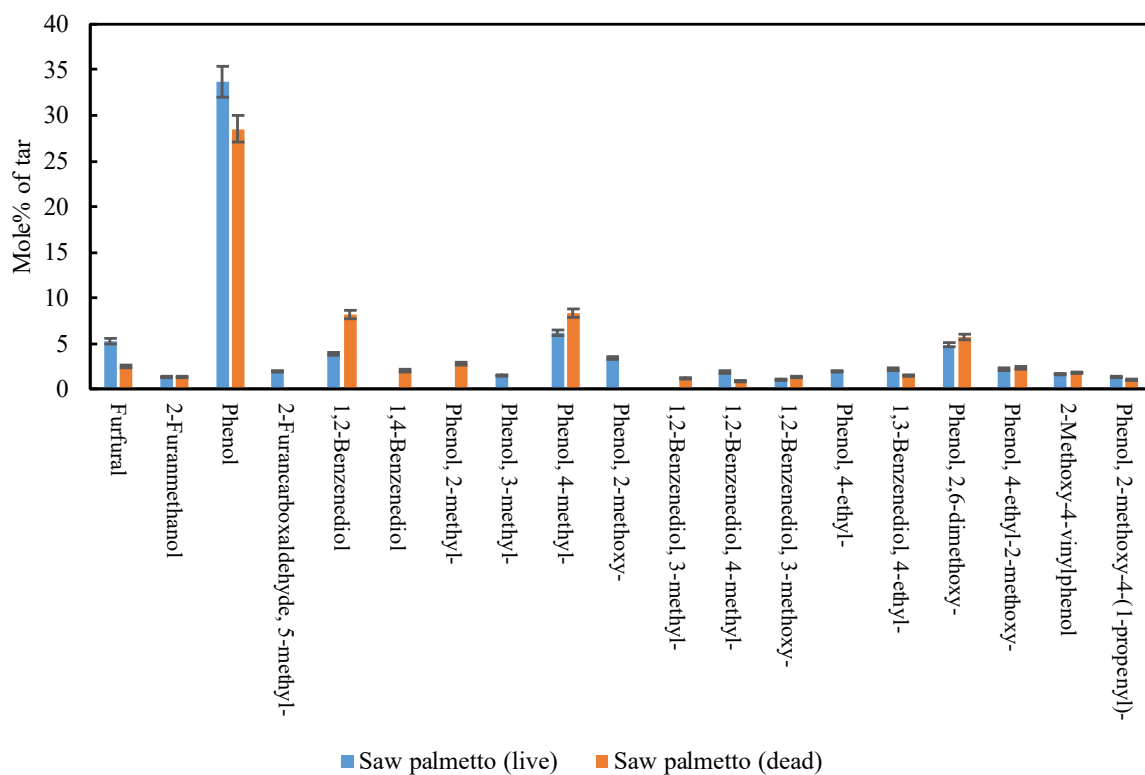
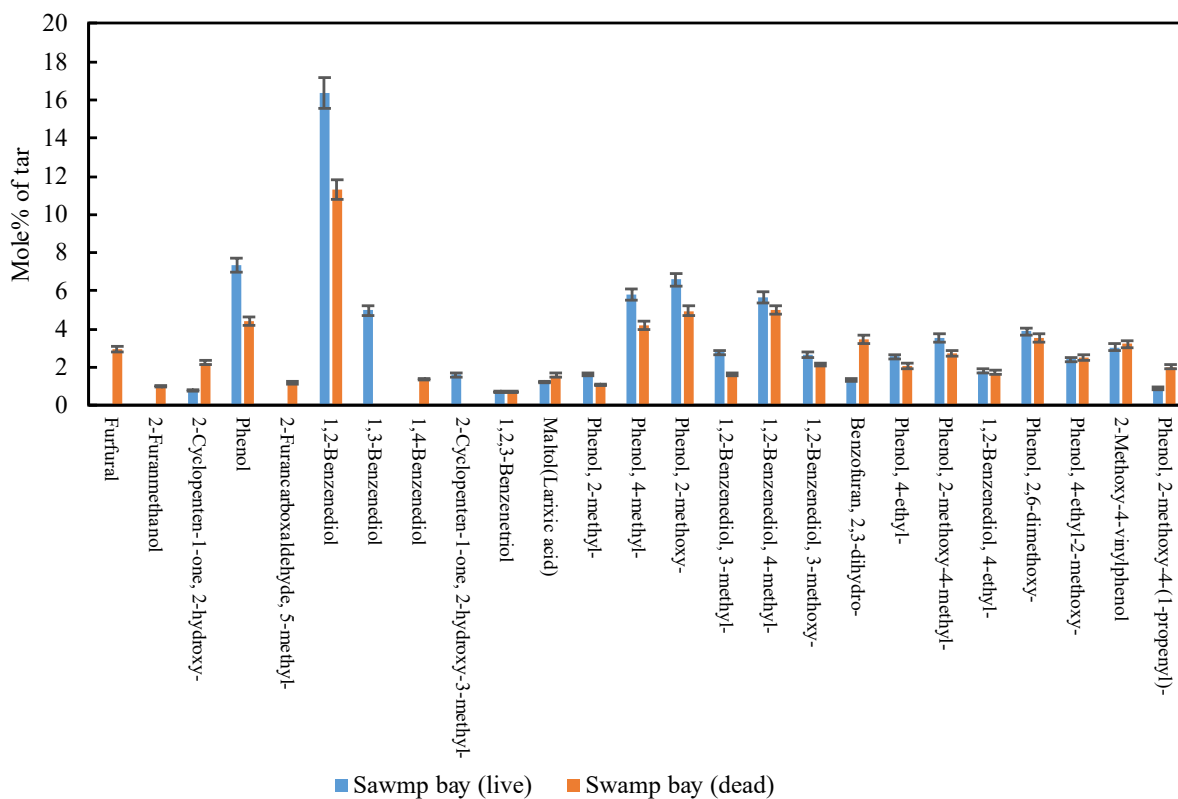
In this section, the distribution of most prevalent components in tar obtained from all live and dead plant species are presented in Figure C-1.

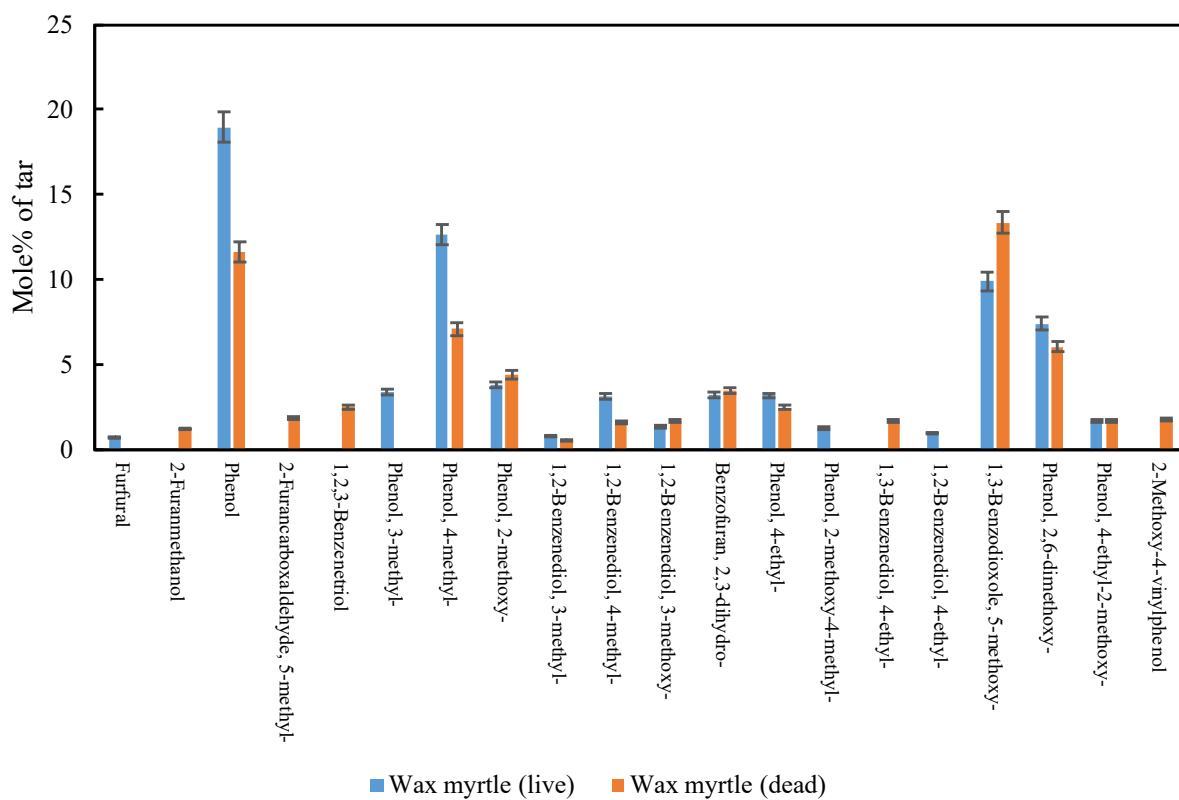
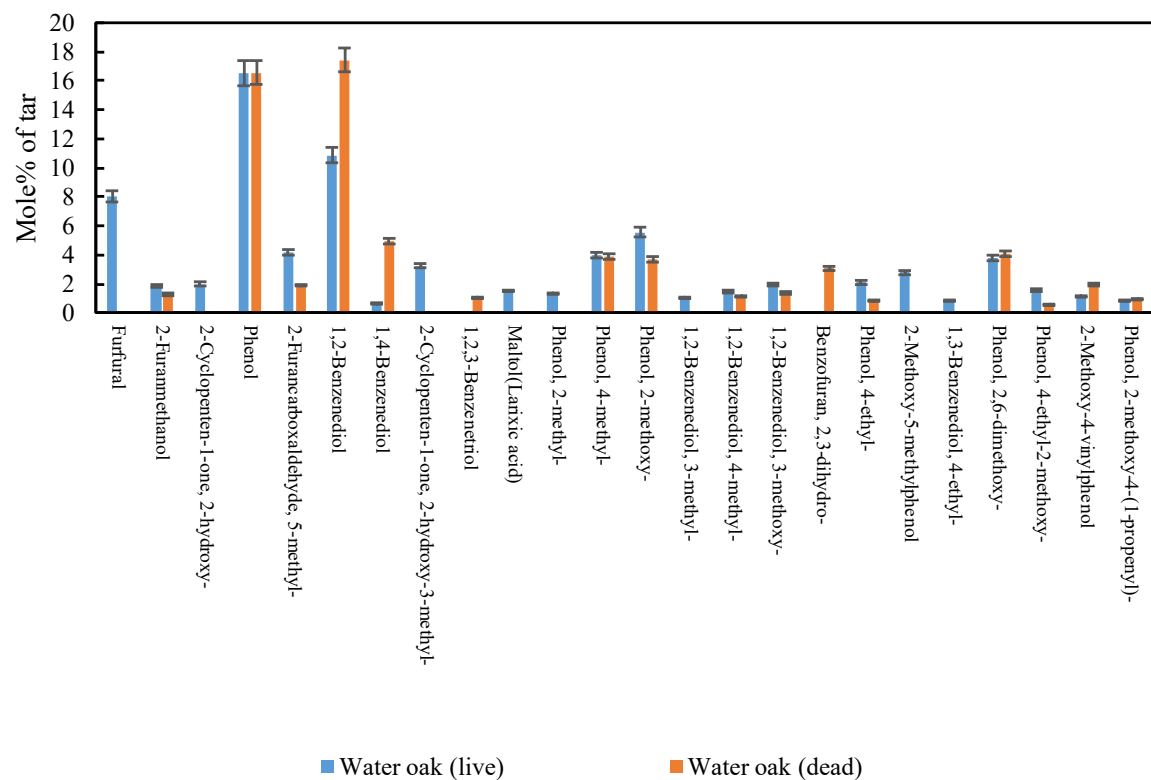












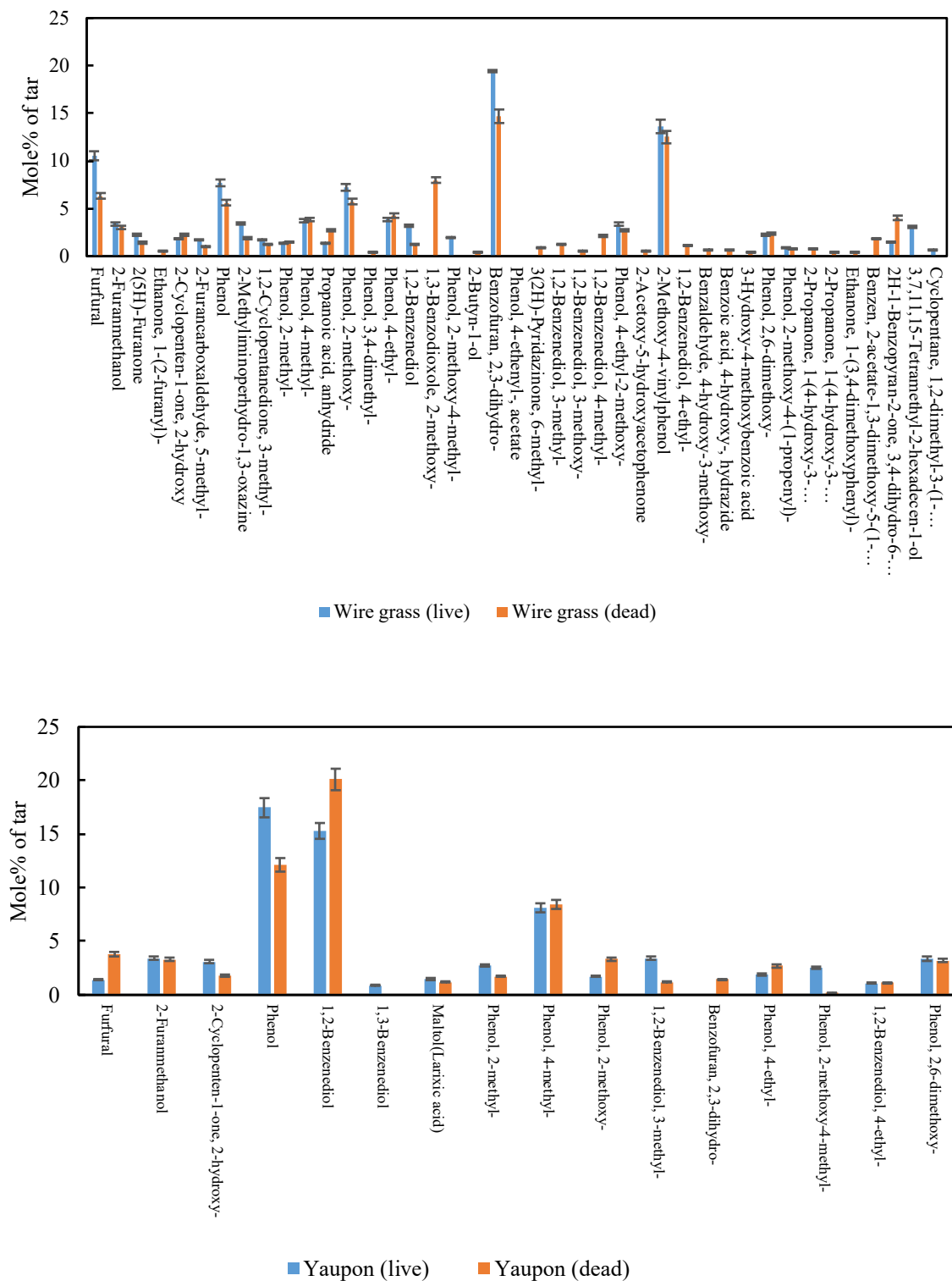
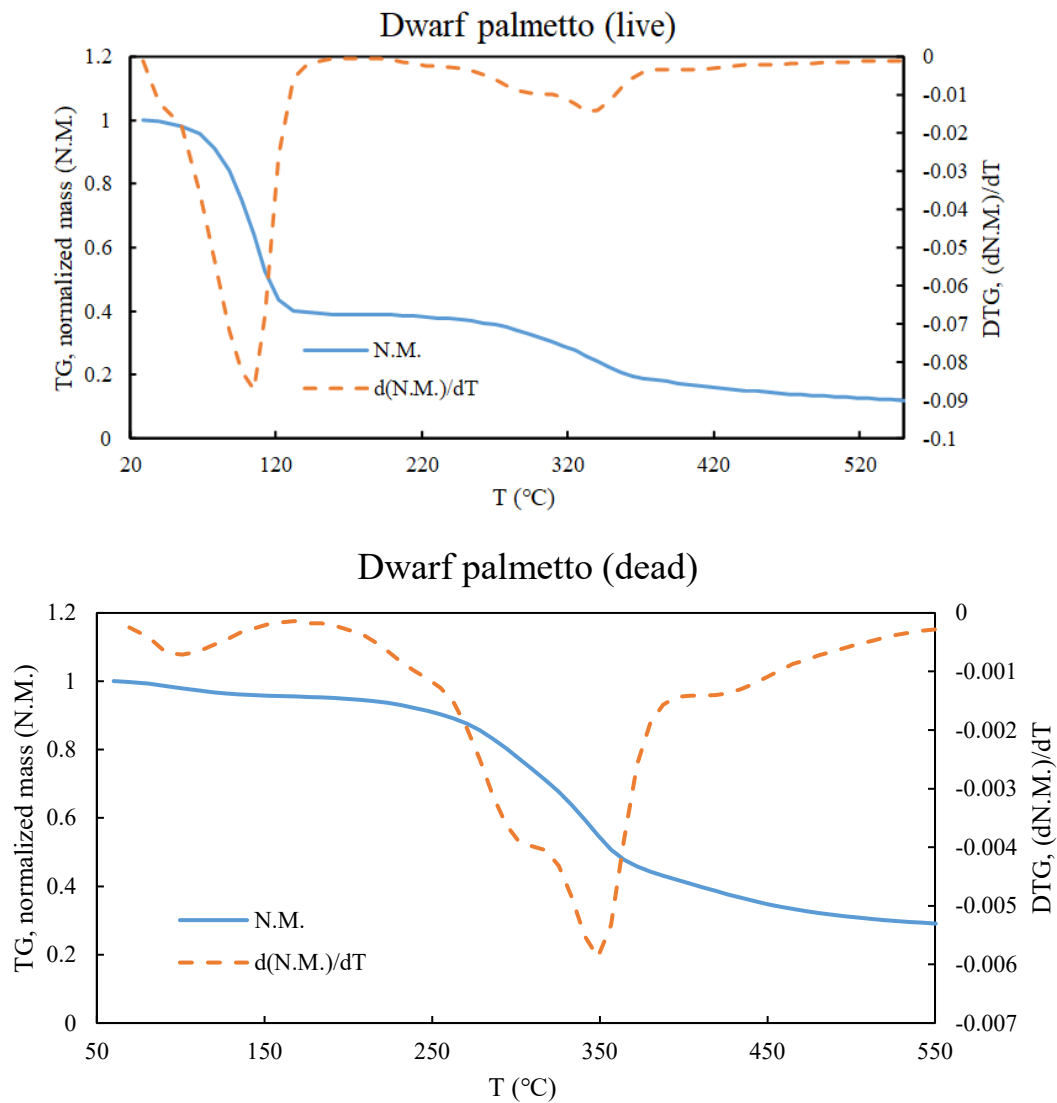
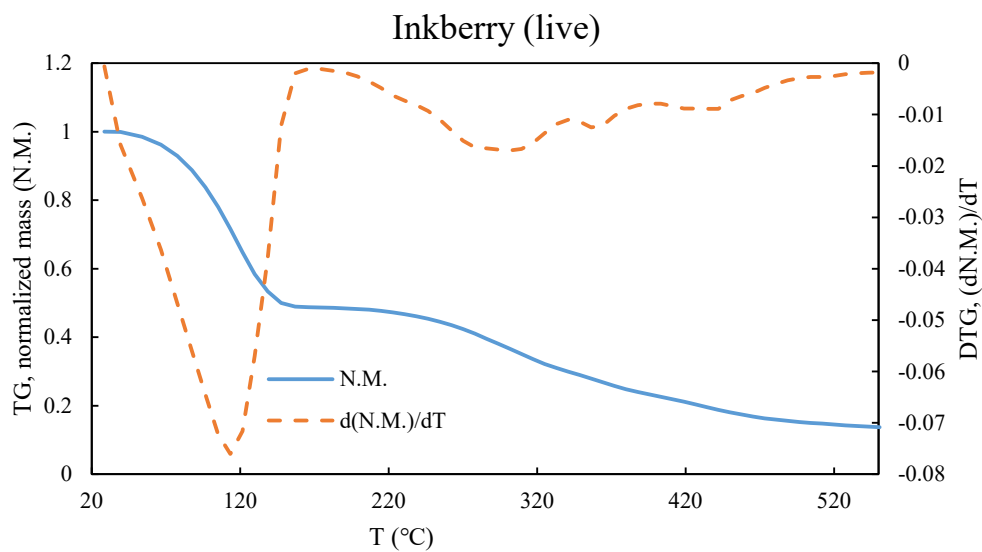
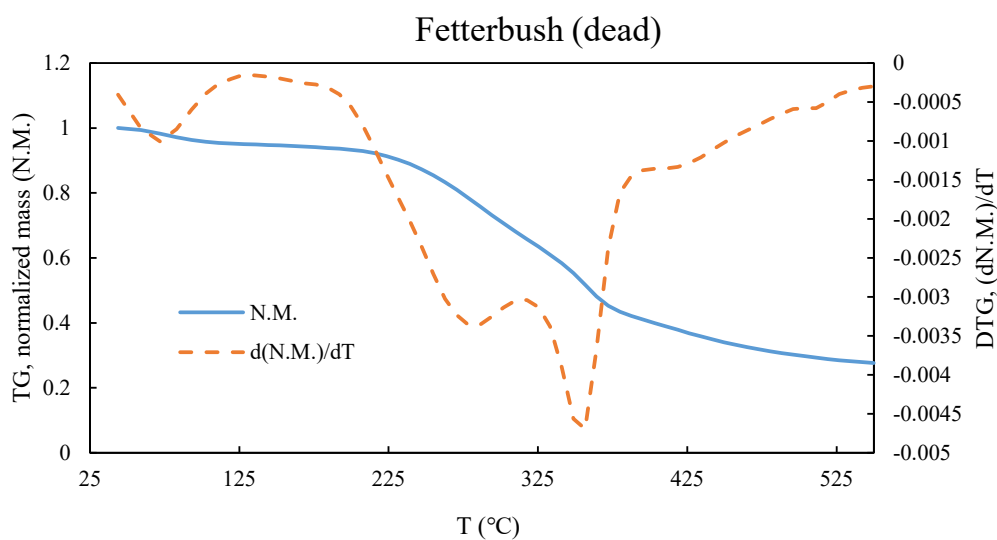
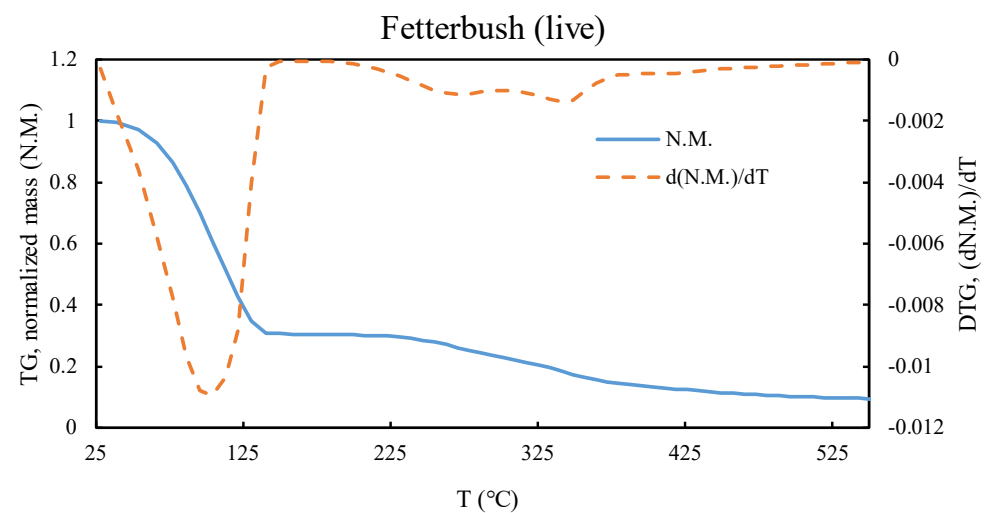


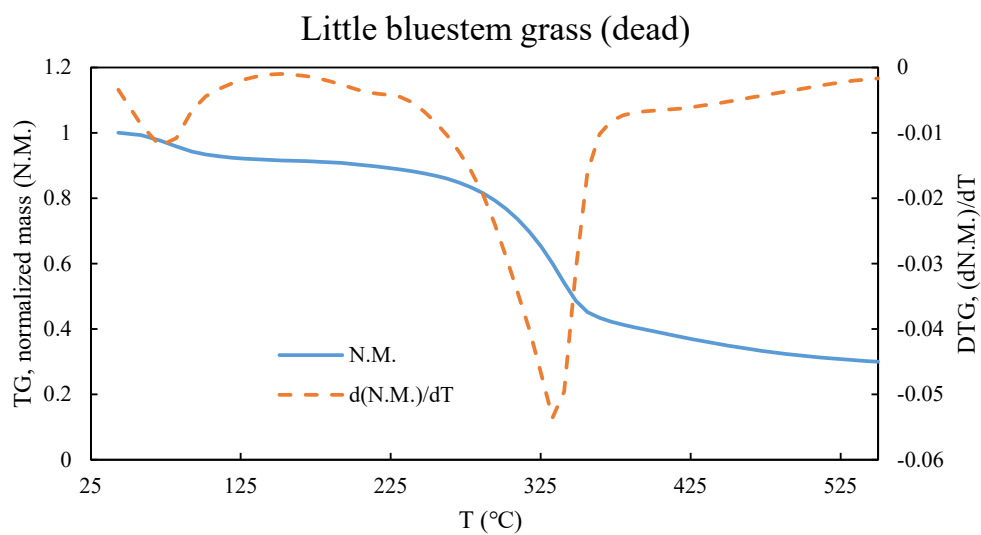
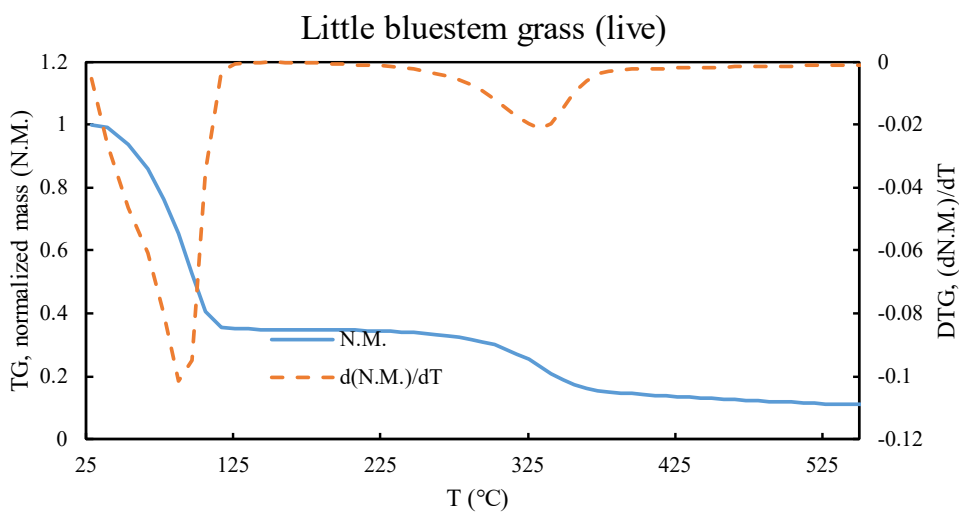
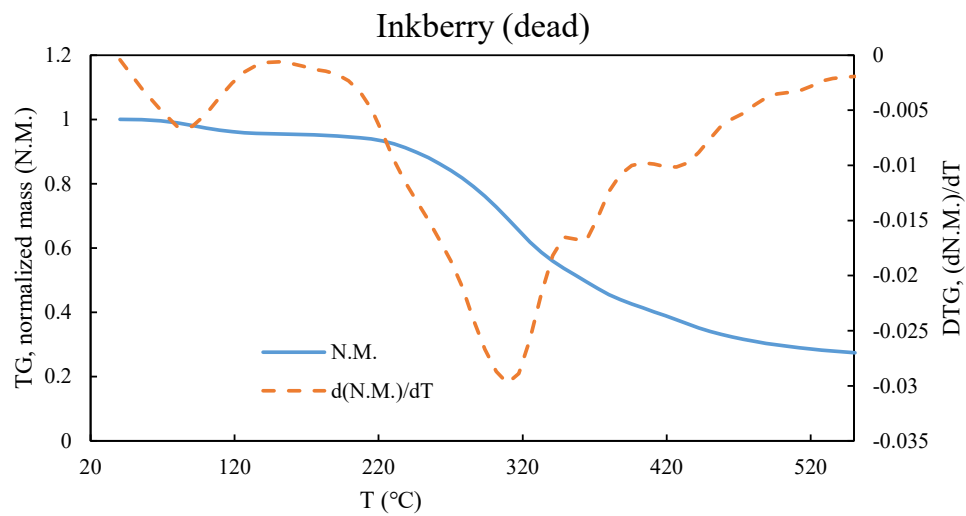
Figure C-1: The distribution of most prevalent components in tar obtained from pyrolysis of plant species. Error bars represent the 95% confidence intervals based on three samples.

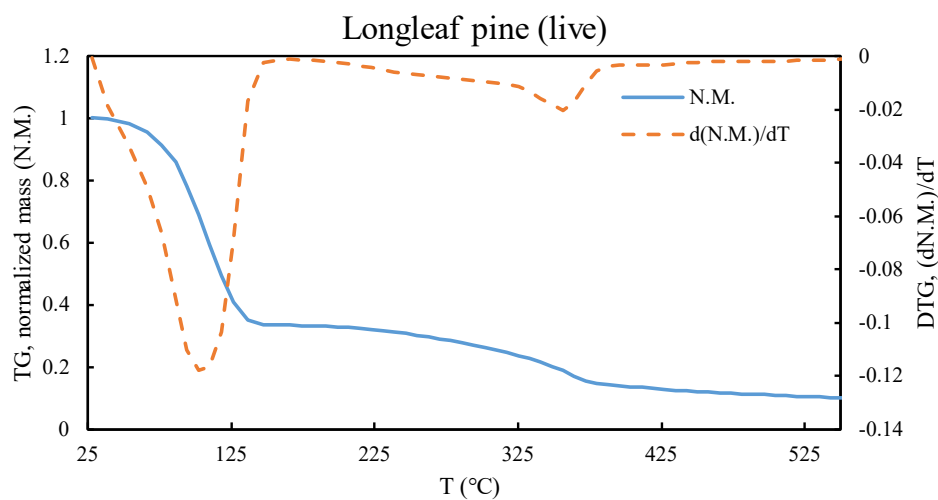
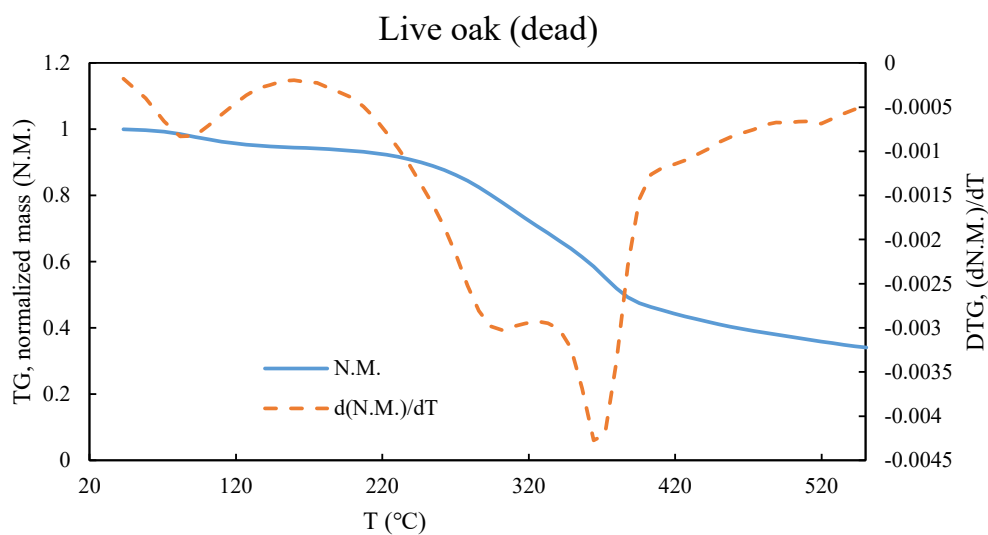
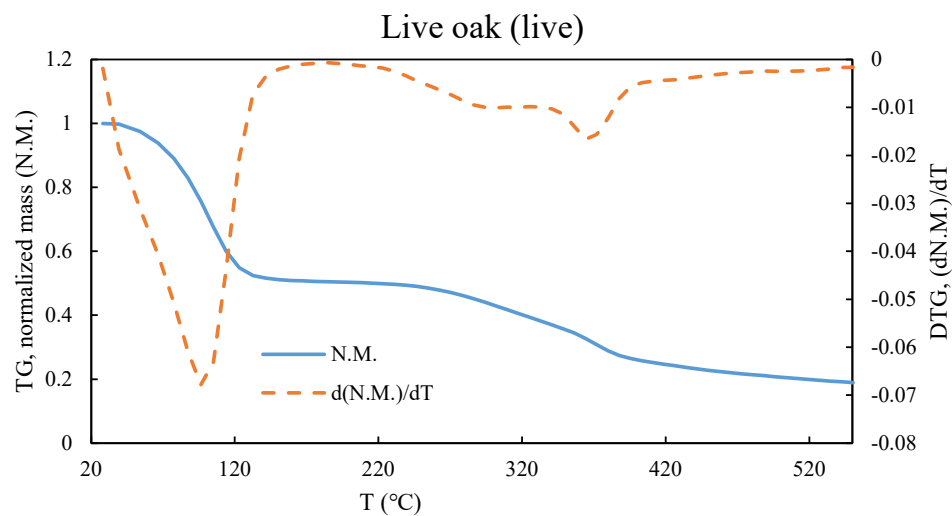
APPENDIX D. TG AND DTG CURVES

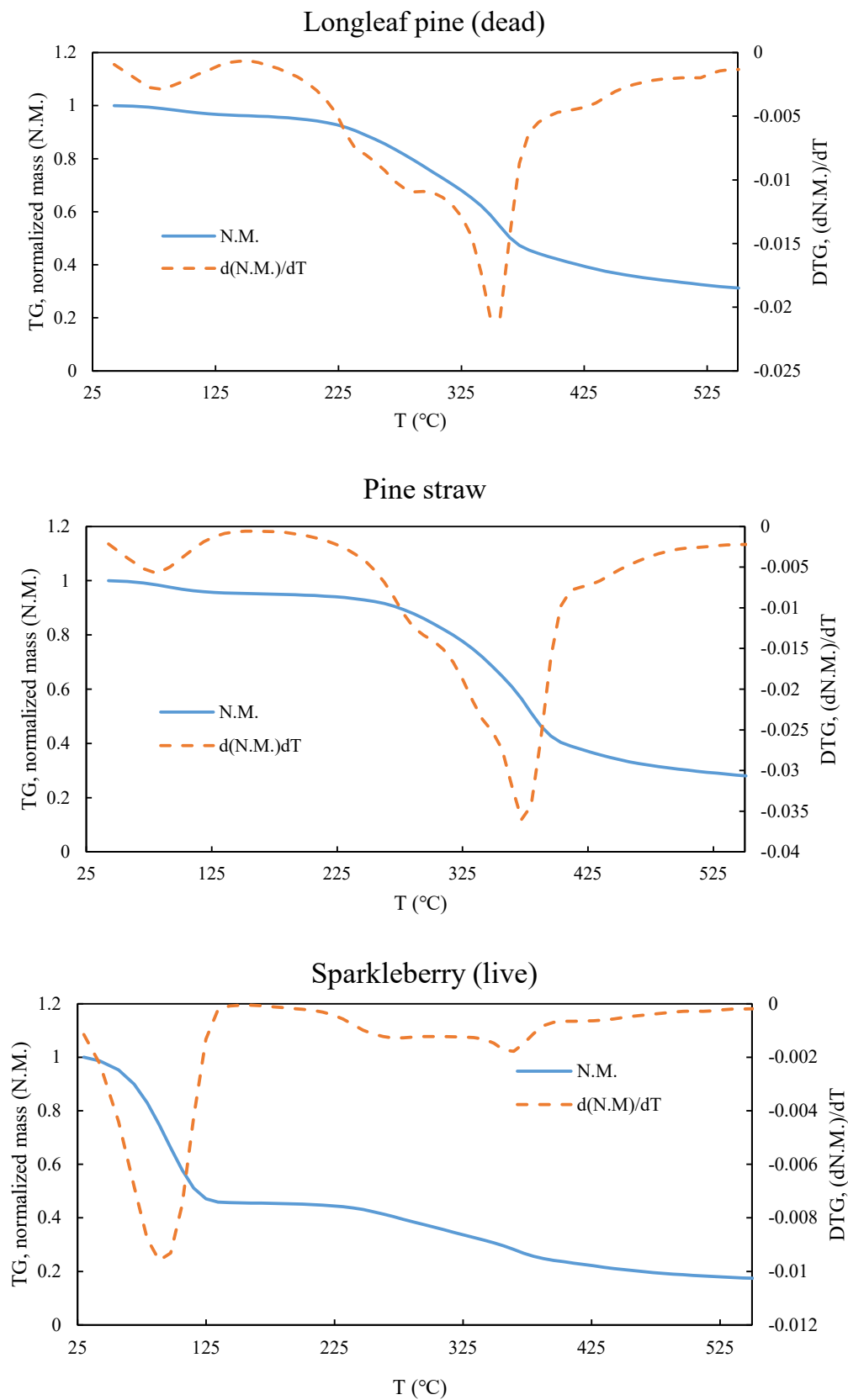
In this section, TG and DTG curves for all plant species resulted from TGA are presented in Figure D-1.

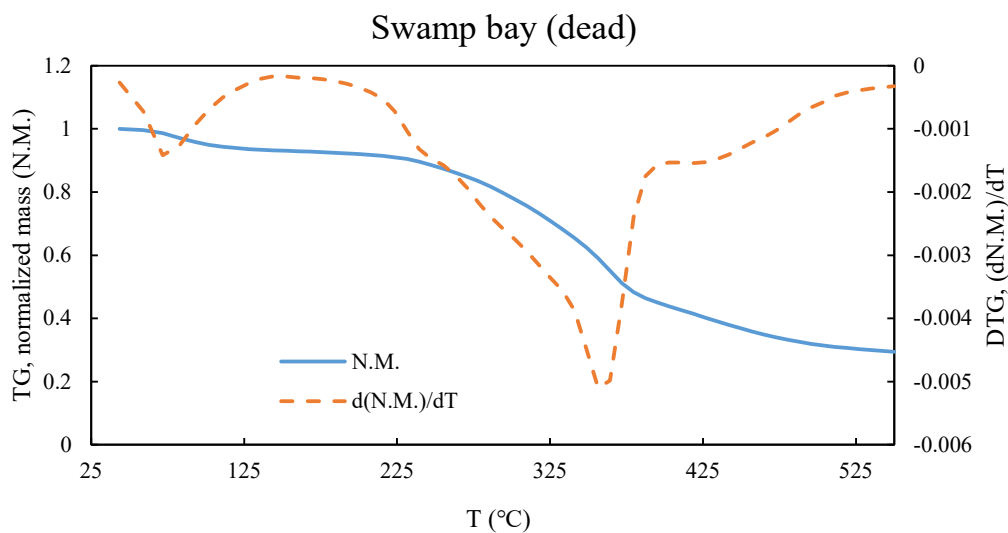
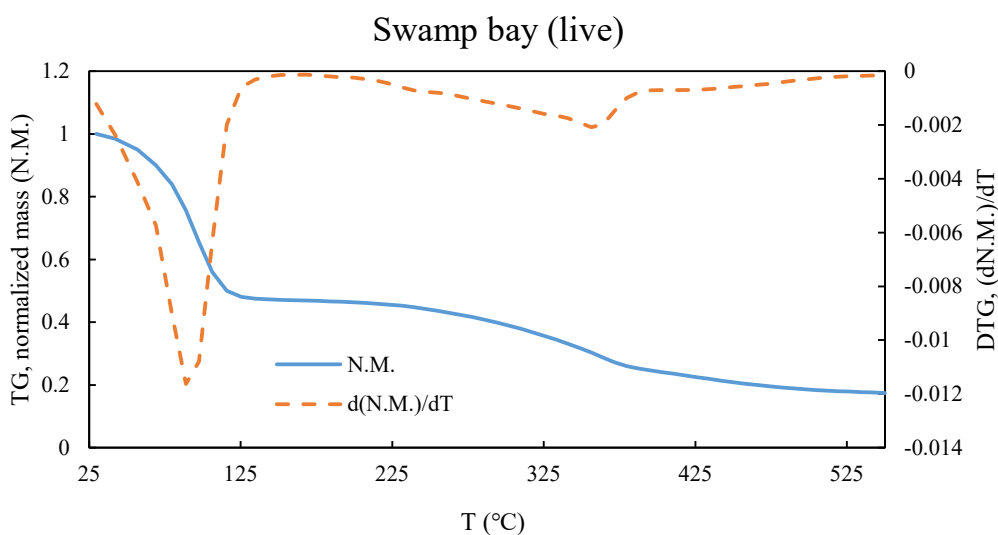
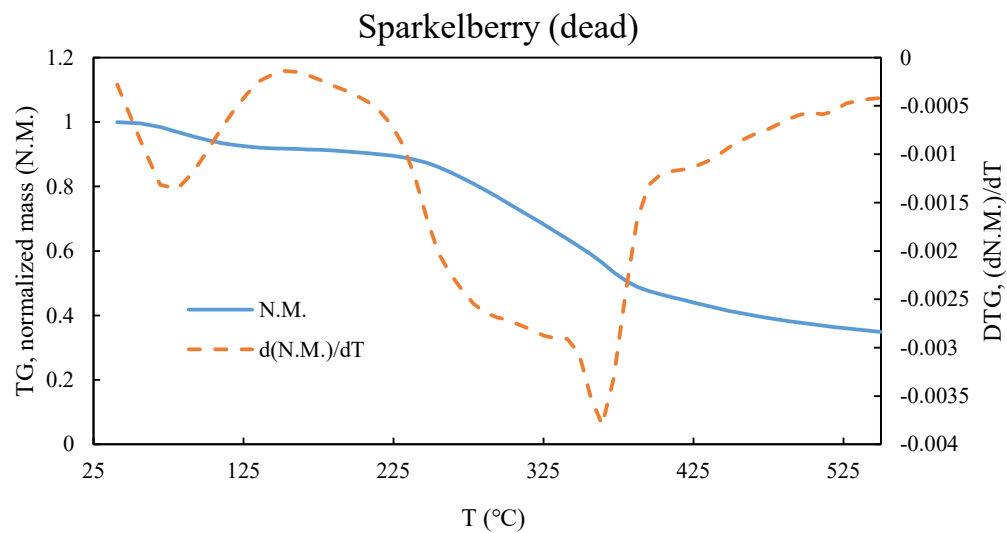


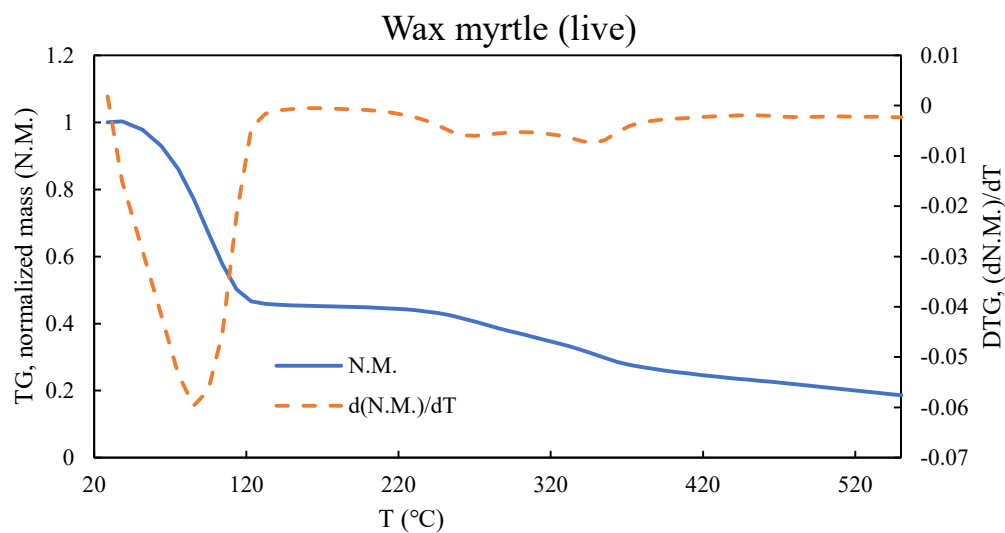
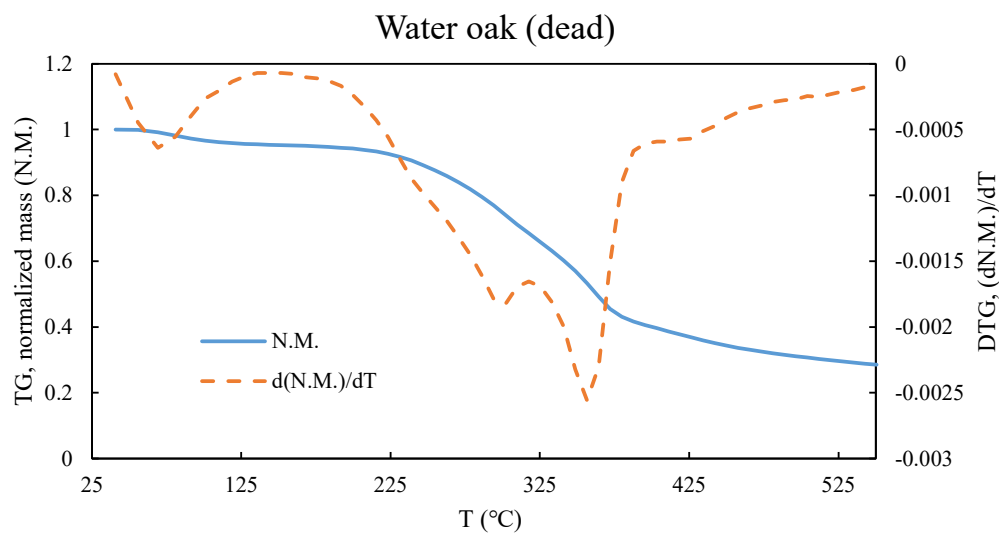
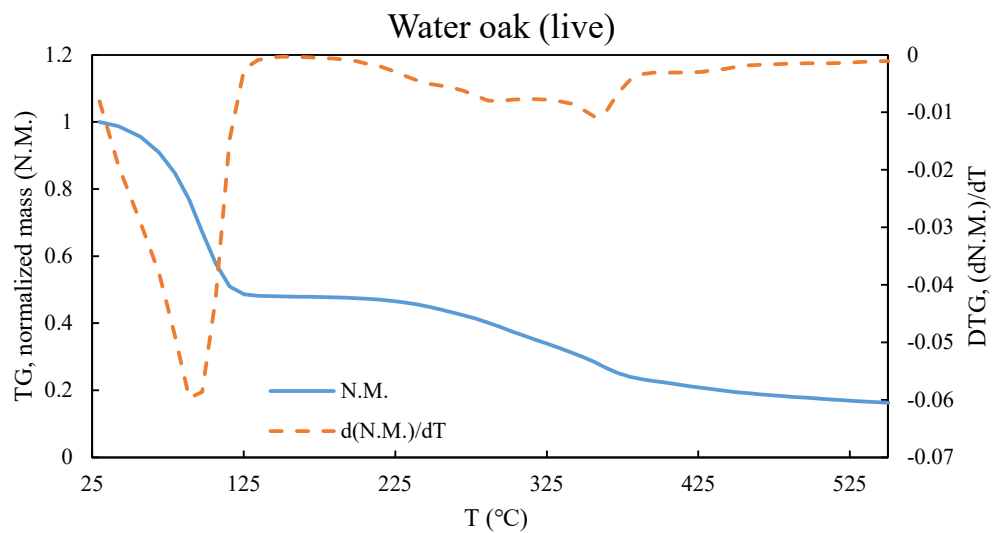












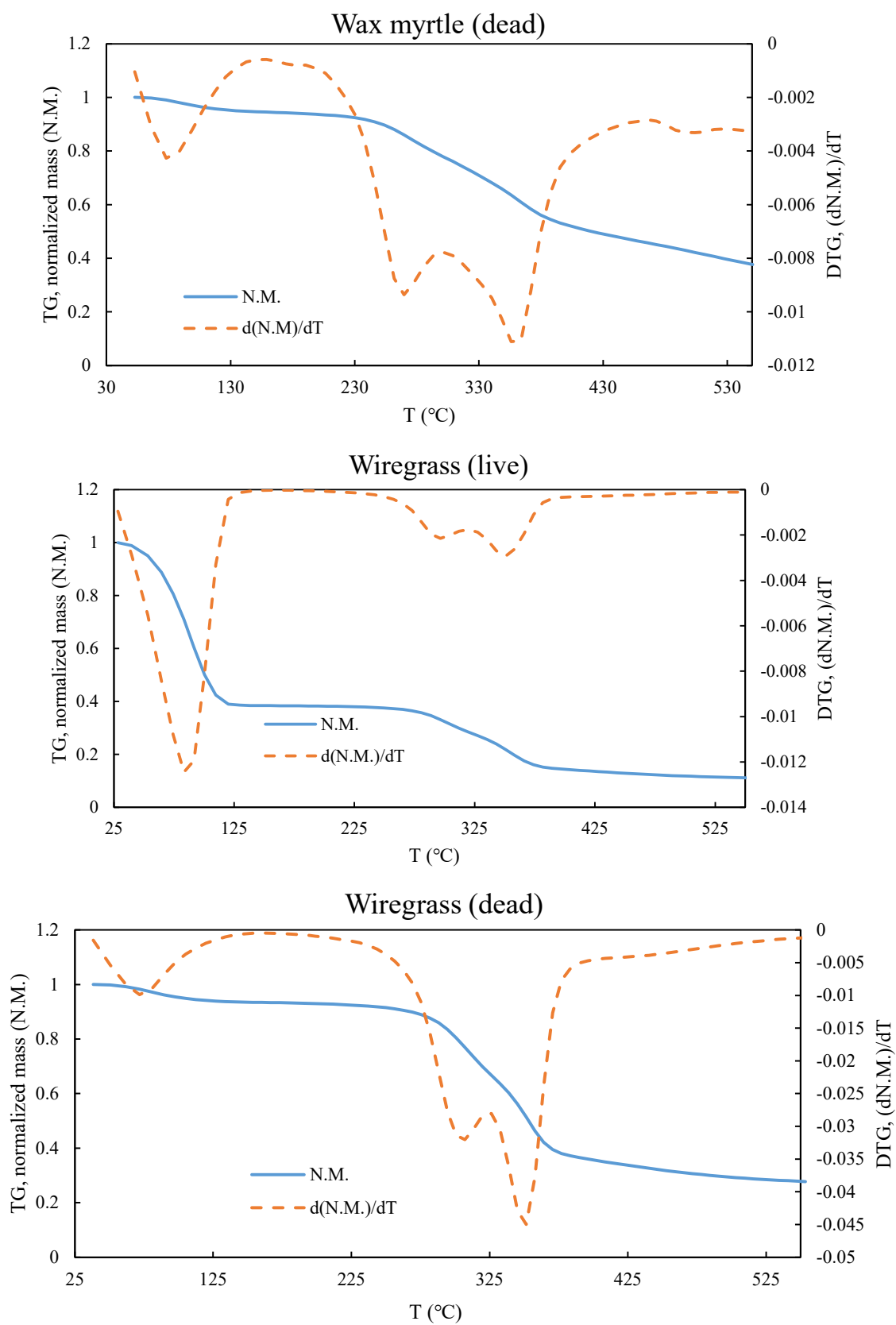
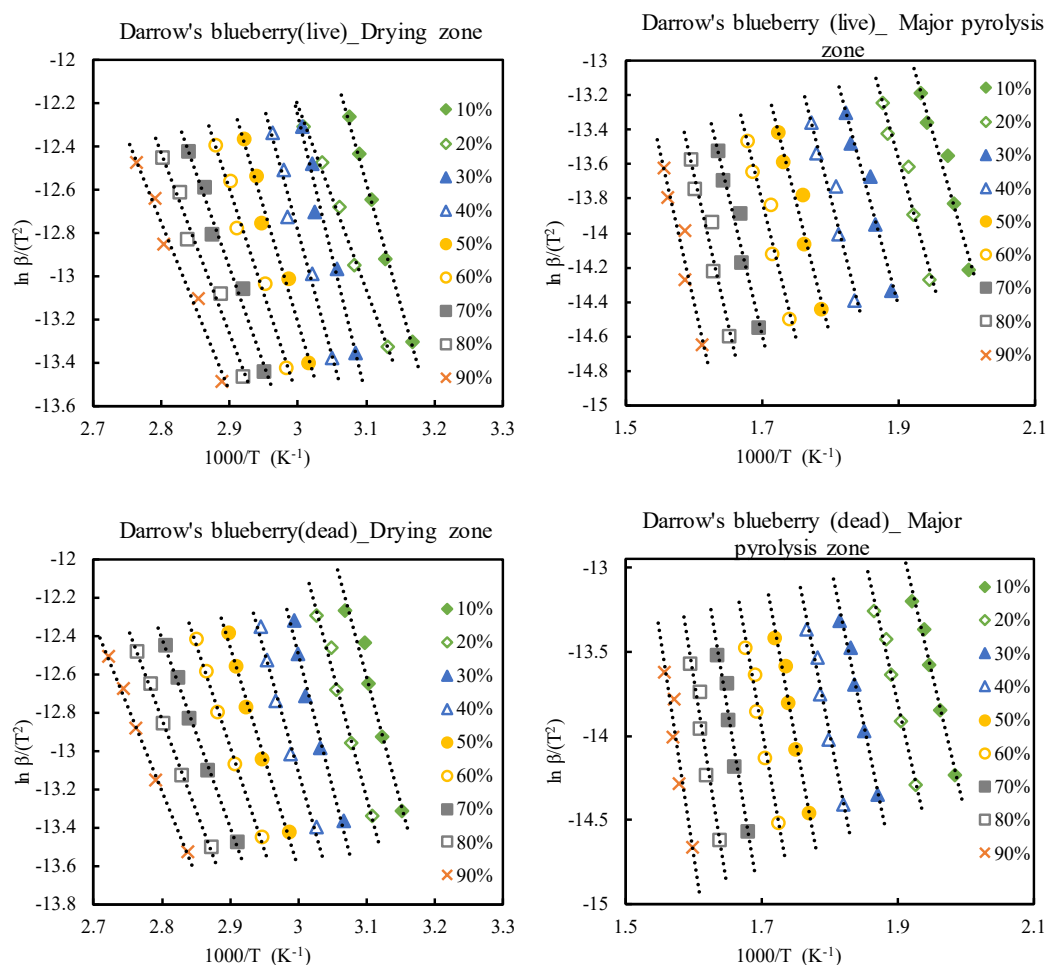
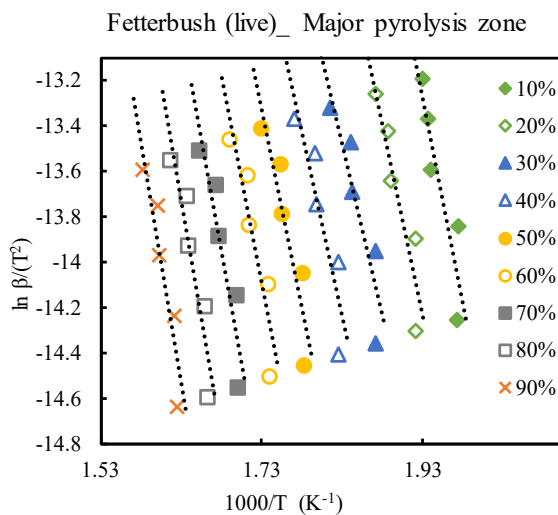
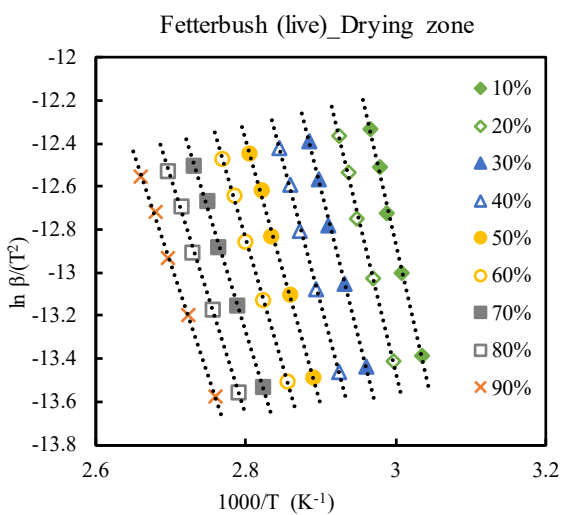
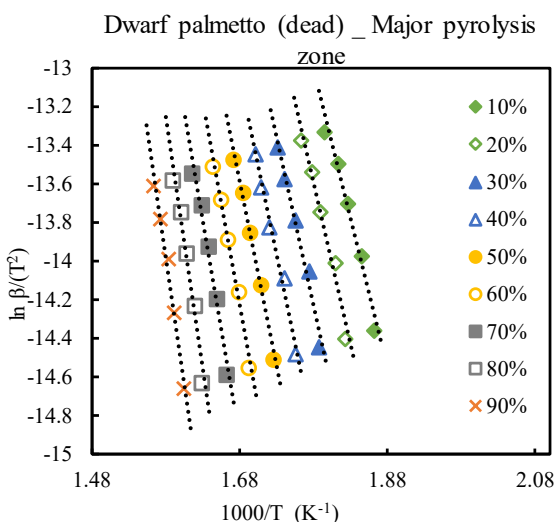
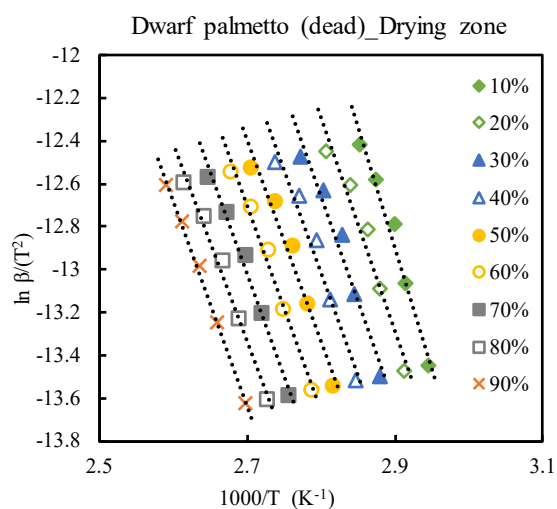
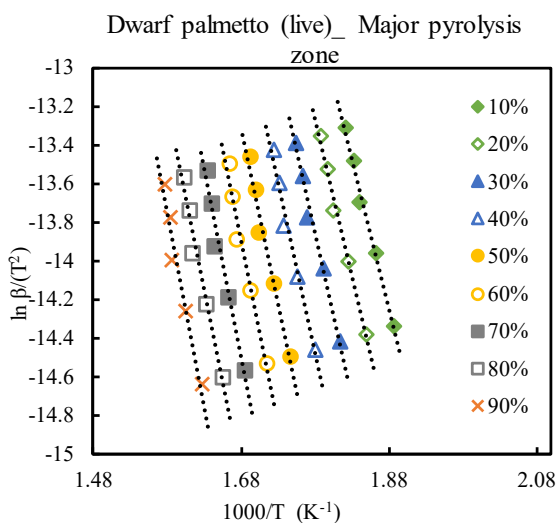
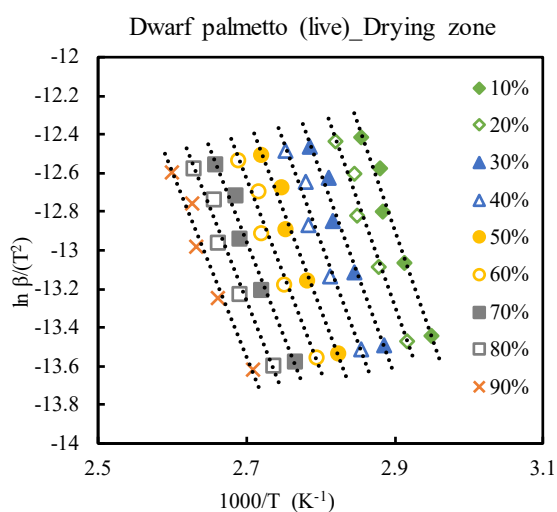


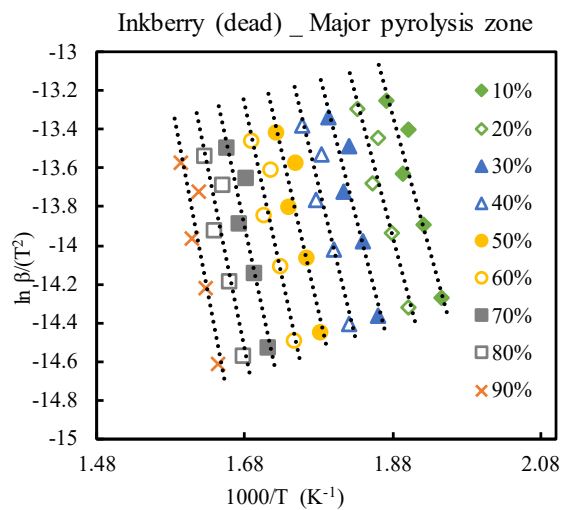
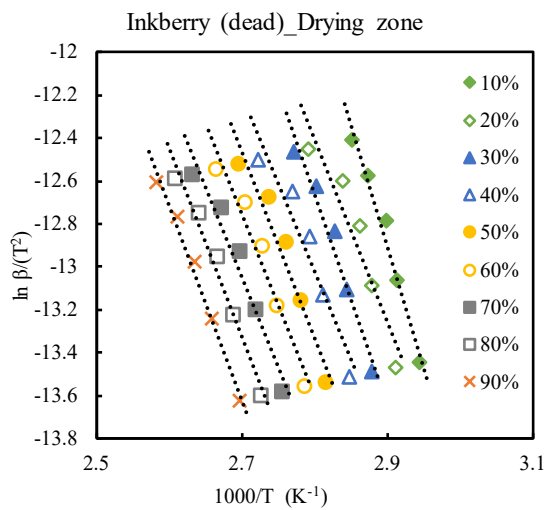
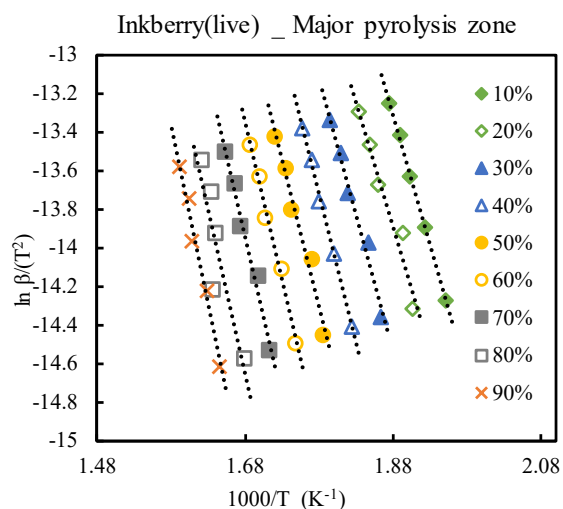
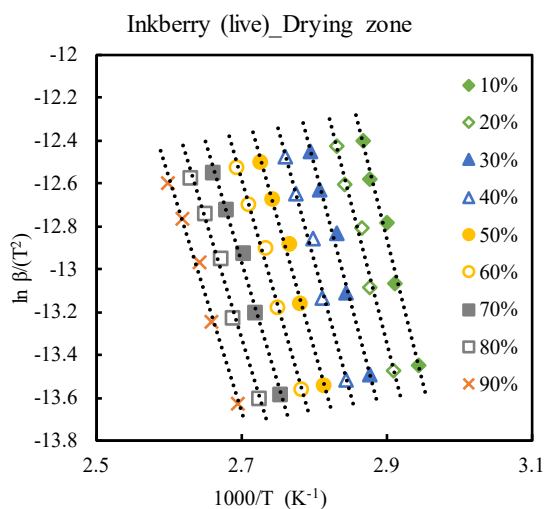
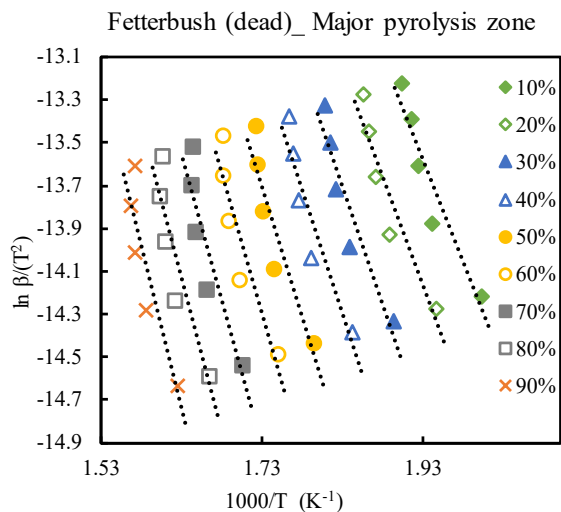
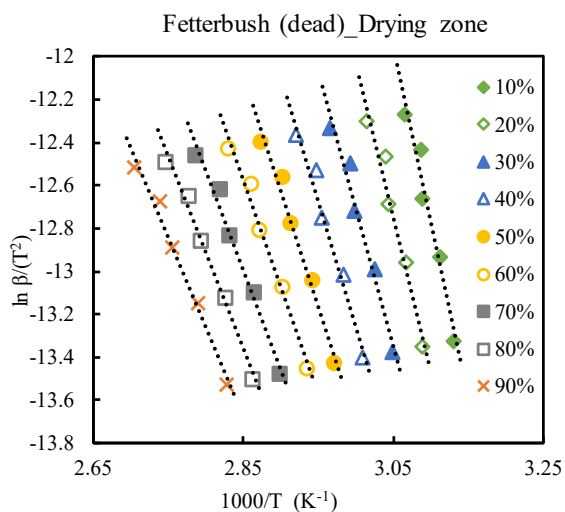
Figure D-1: TG and DTG curves for all live and dead plant species.

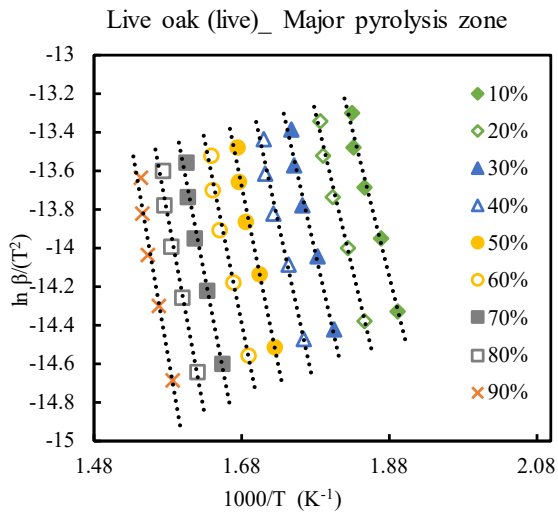
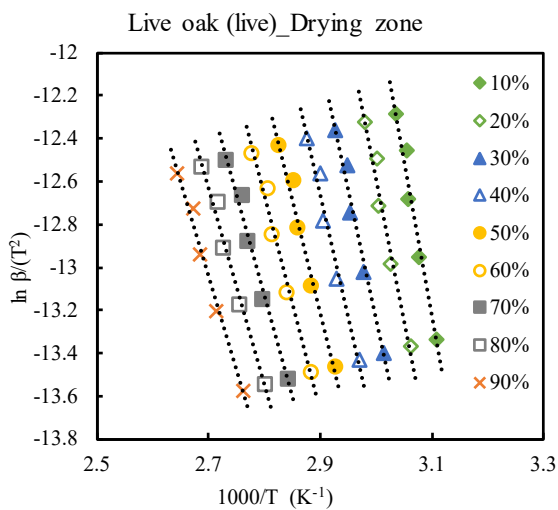
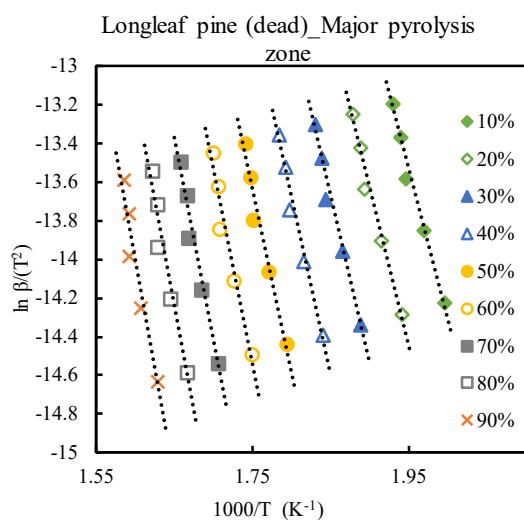
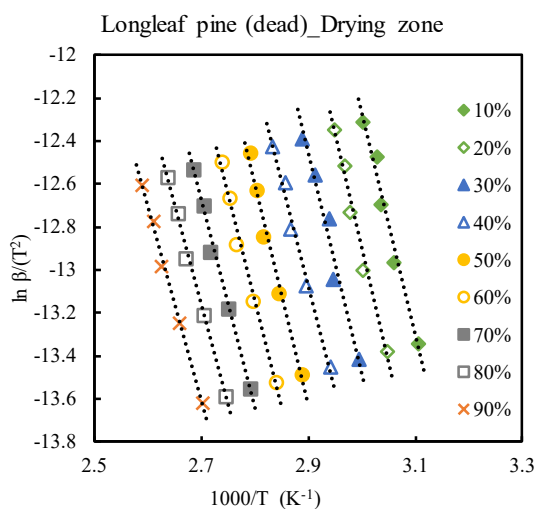
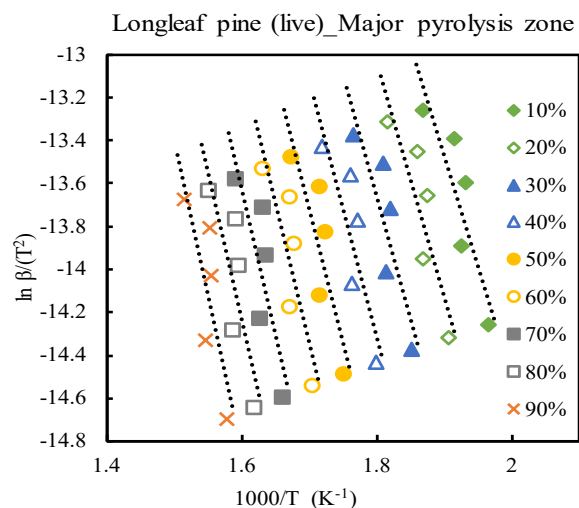
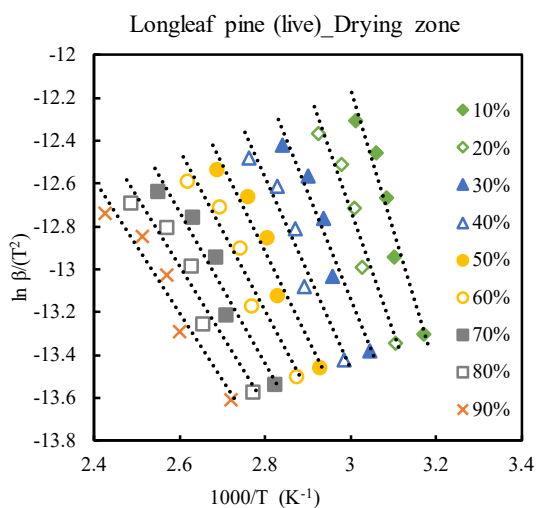
APPENDIX E. REGRESSION LINES USED IN THE KAS METHOD

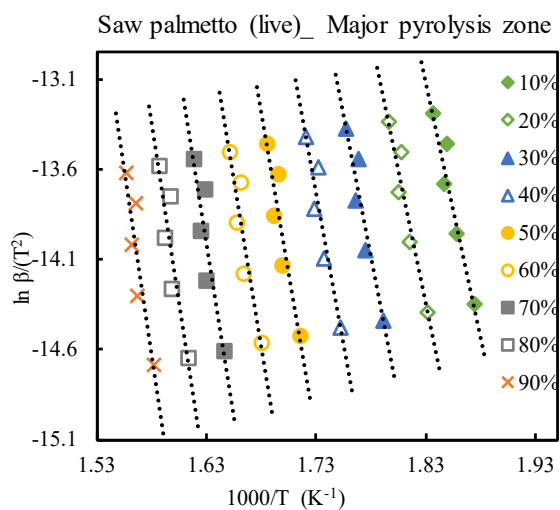
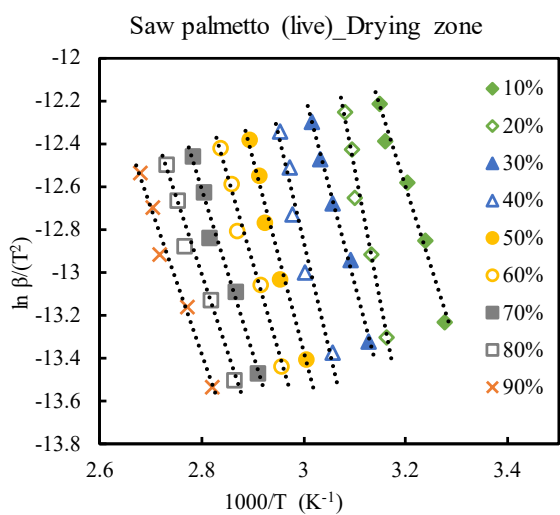
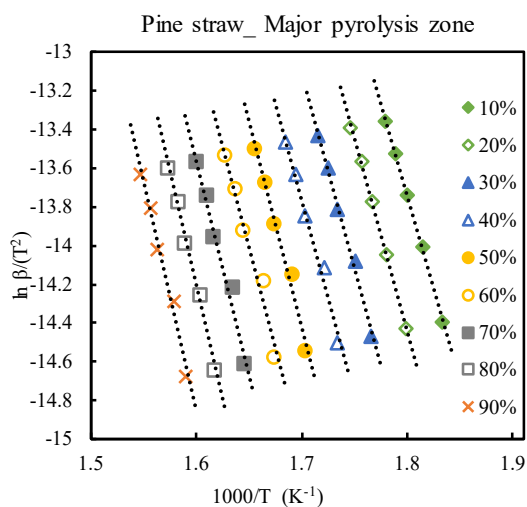
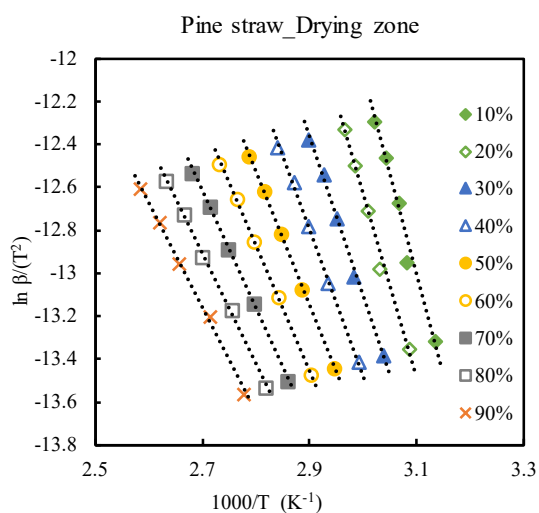
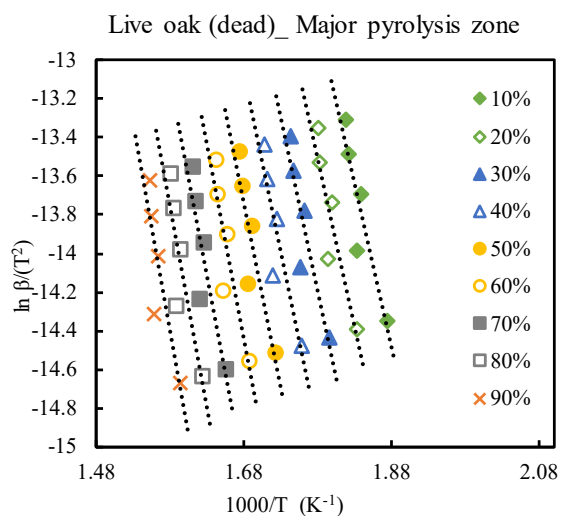
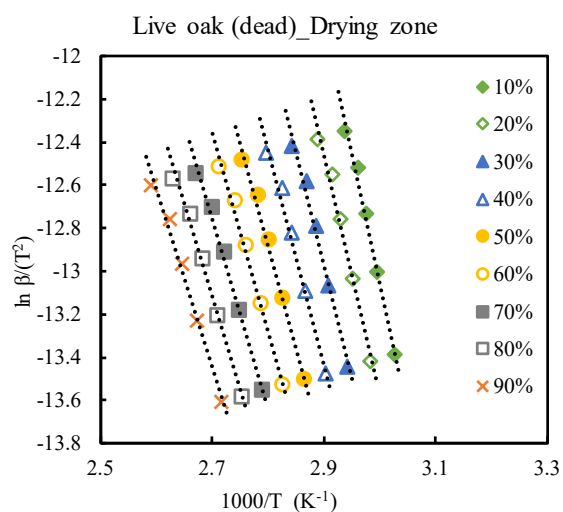
Figure E-1 shows the regression lines used to obtain apparent activation energies for drying and major pyrolysis zones using the KAS method.

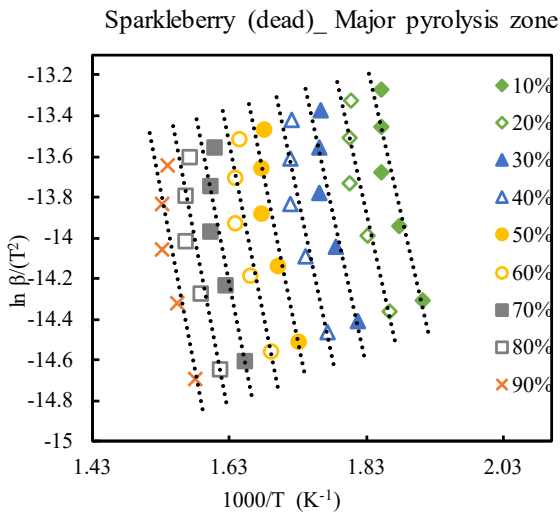
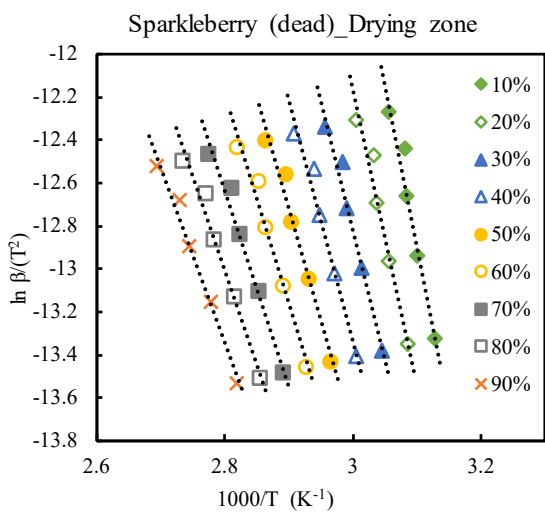
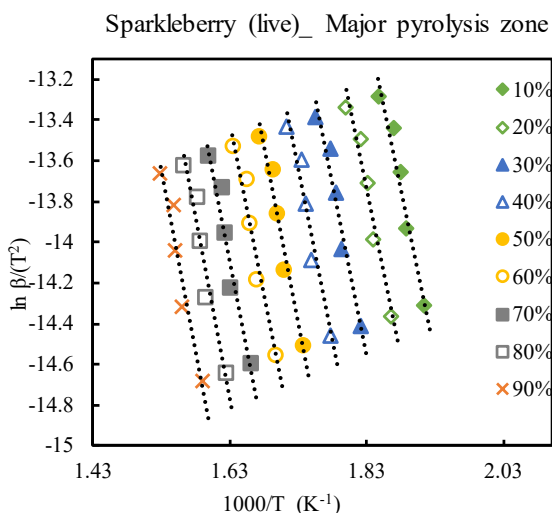
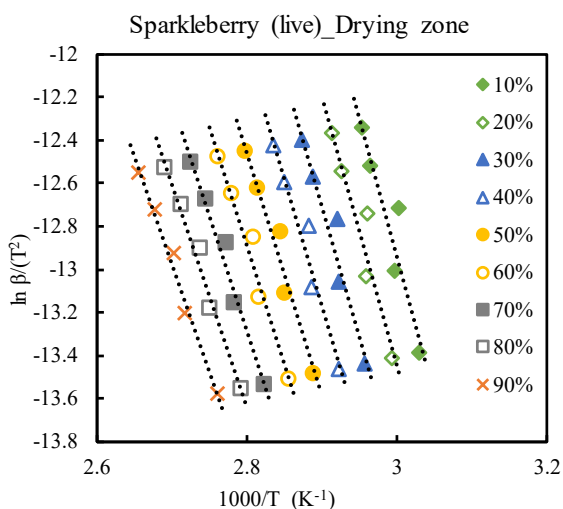
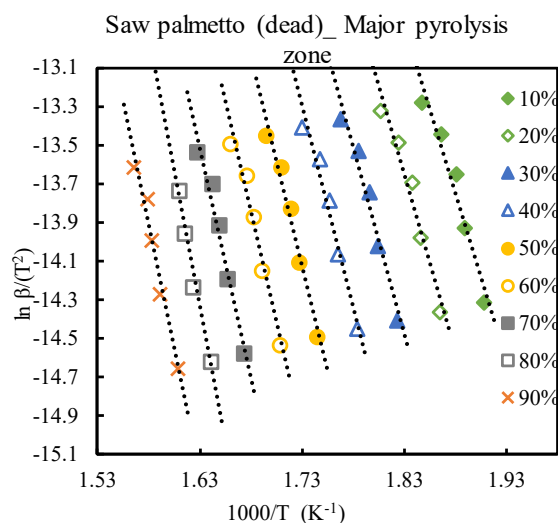
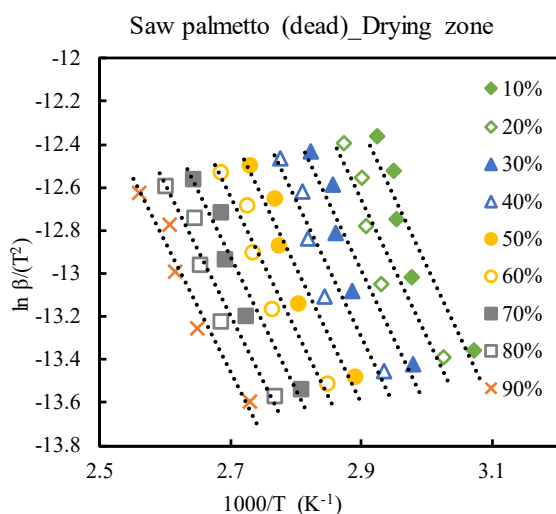


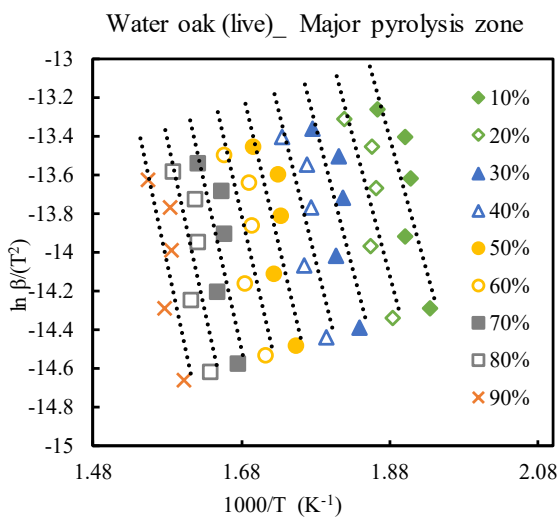
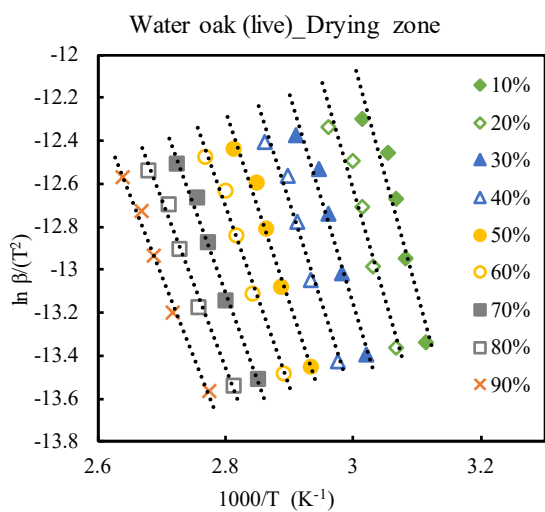
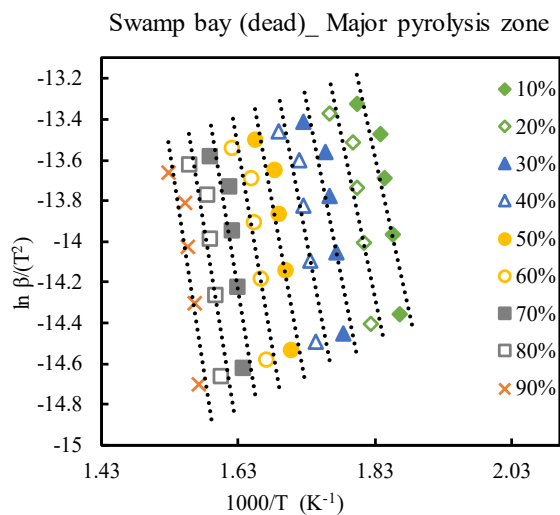
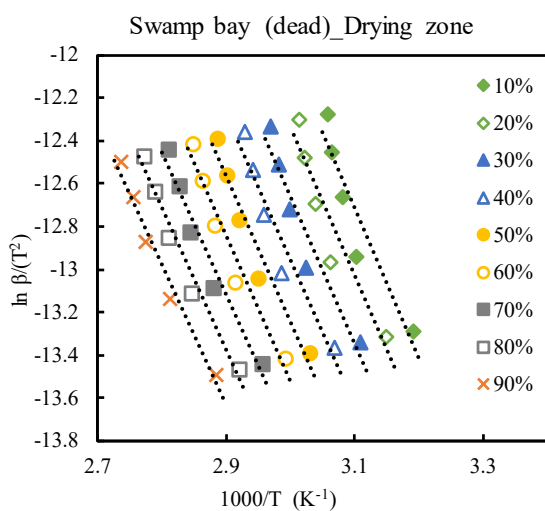
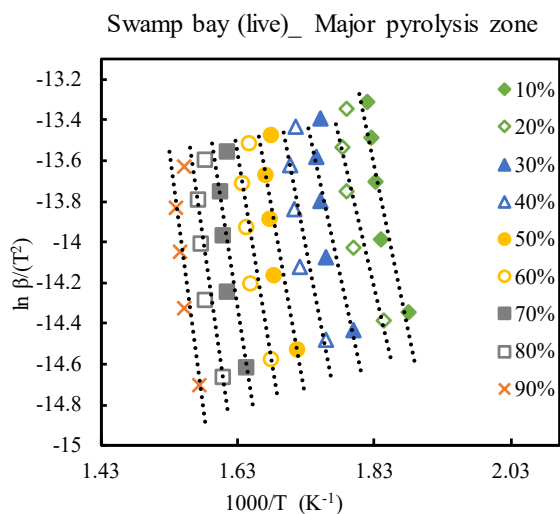
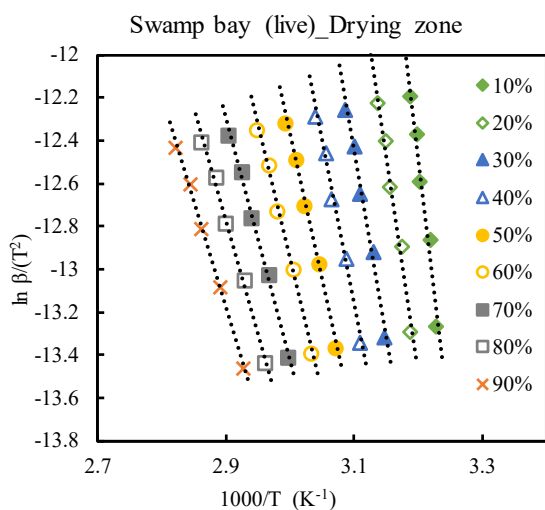


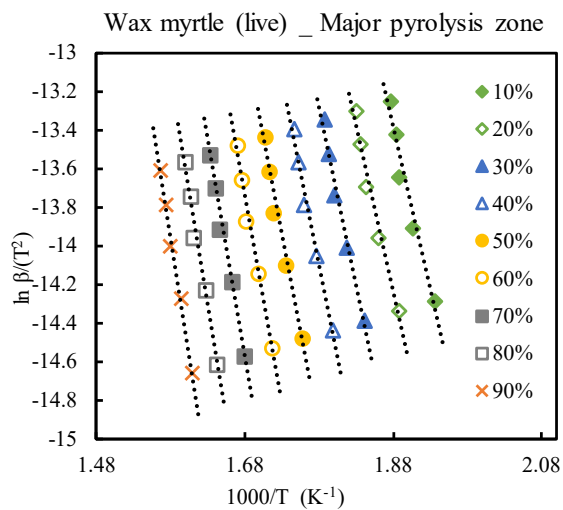
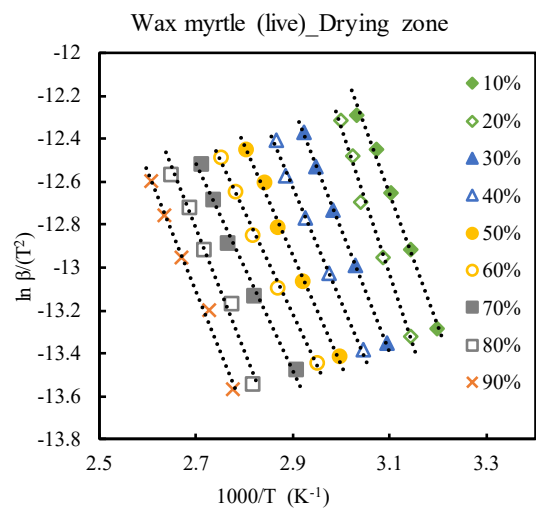
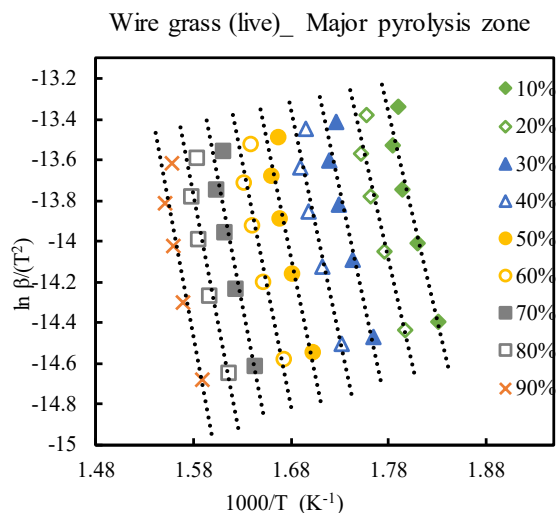
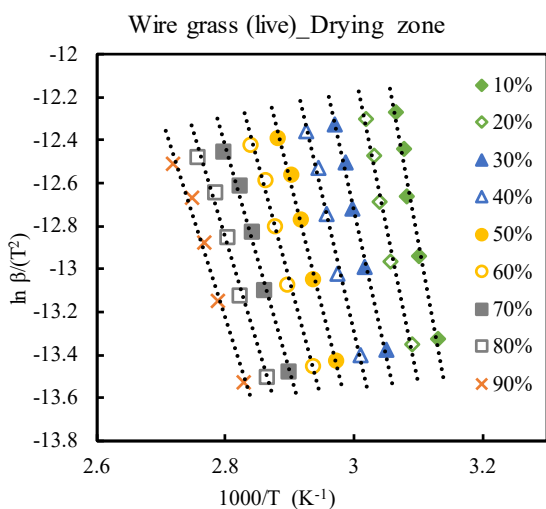
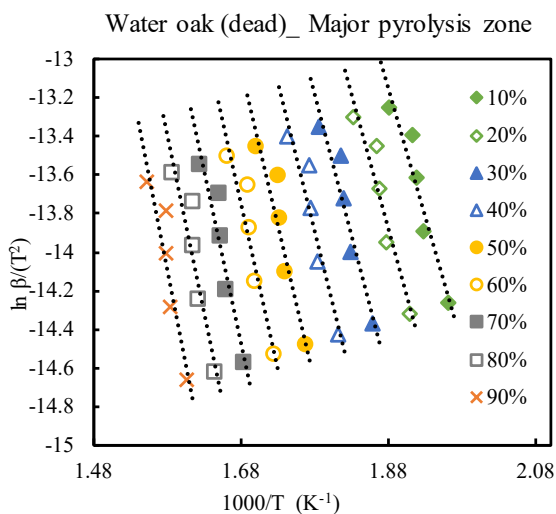
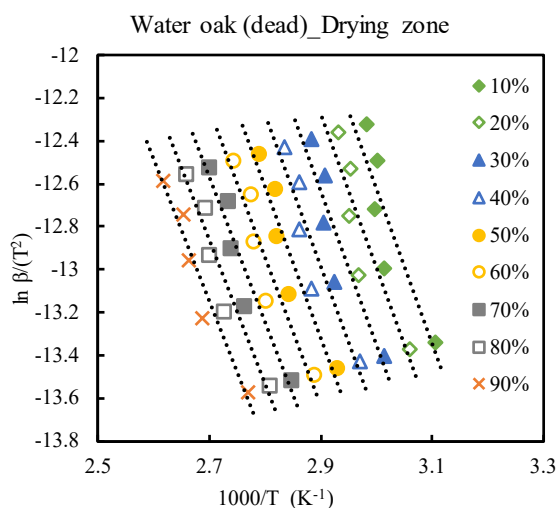


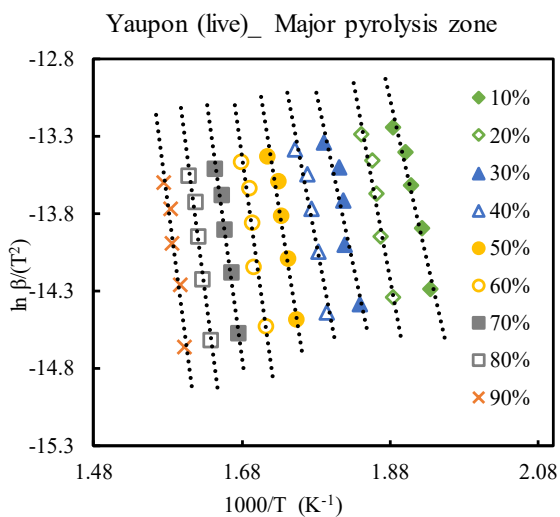
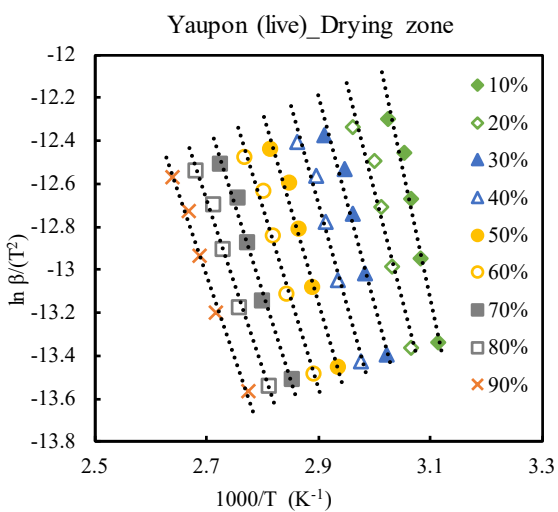
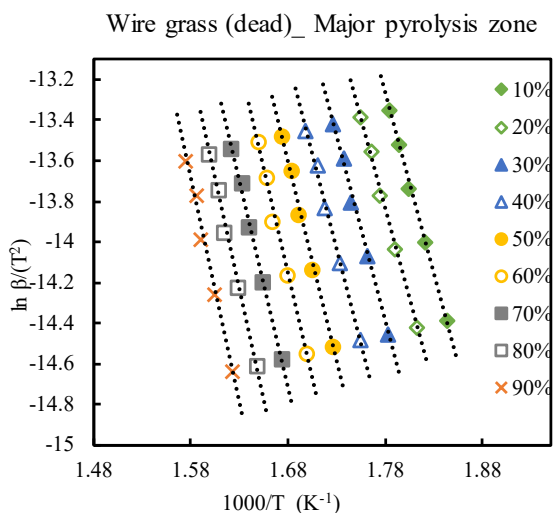
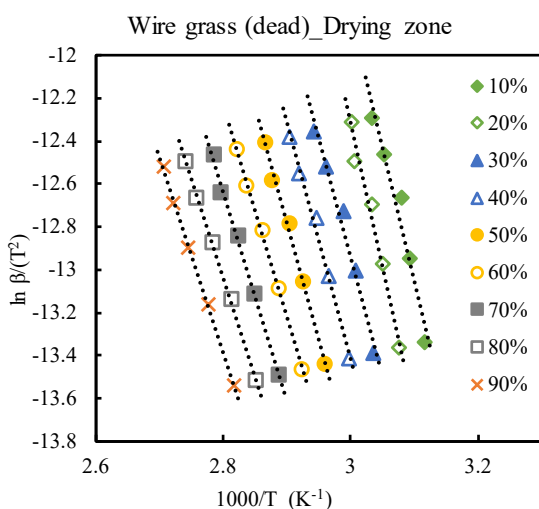
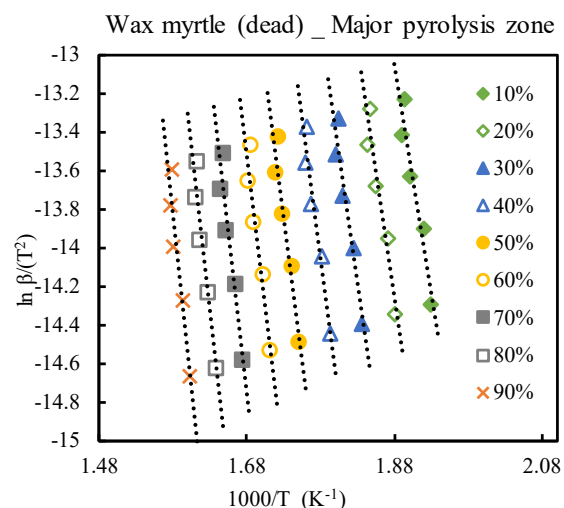
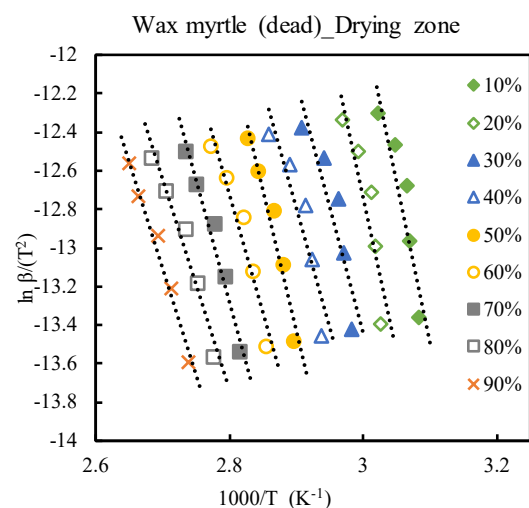












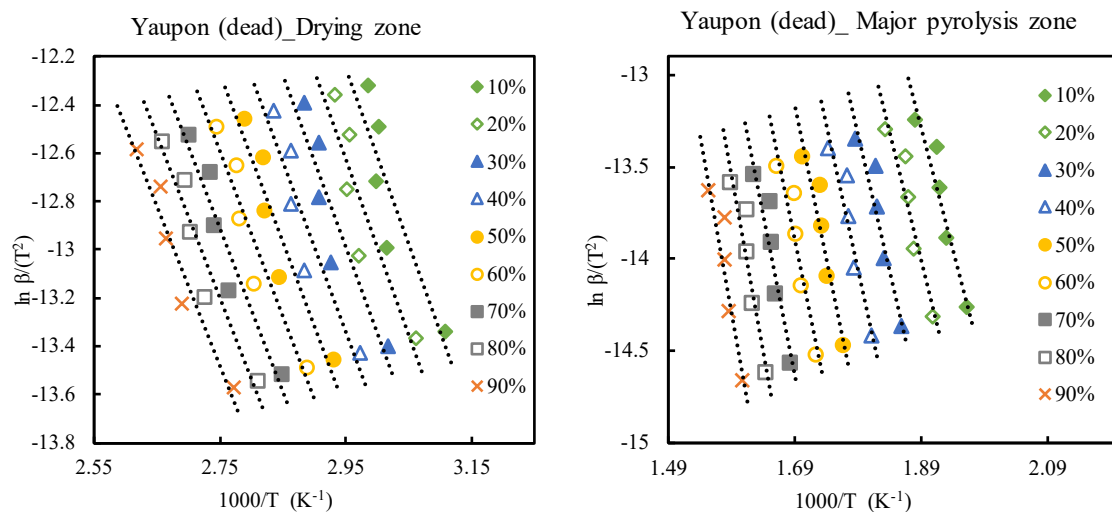
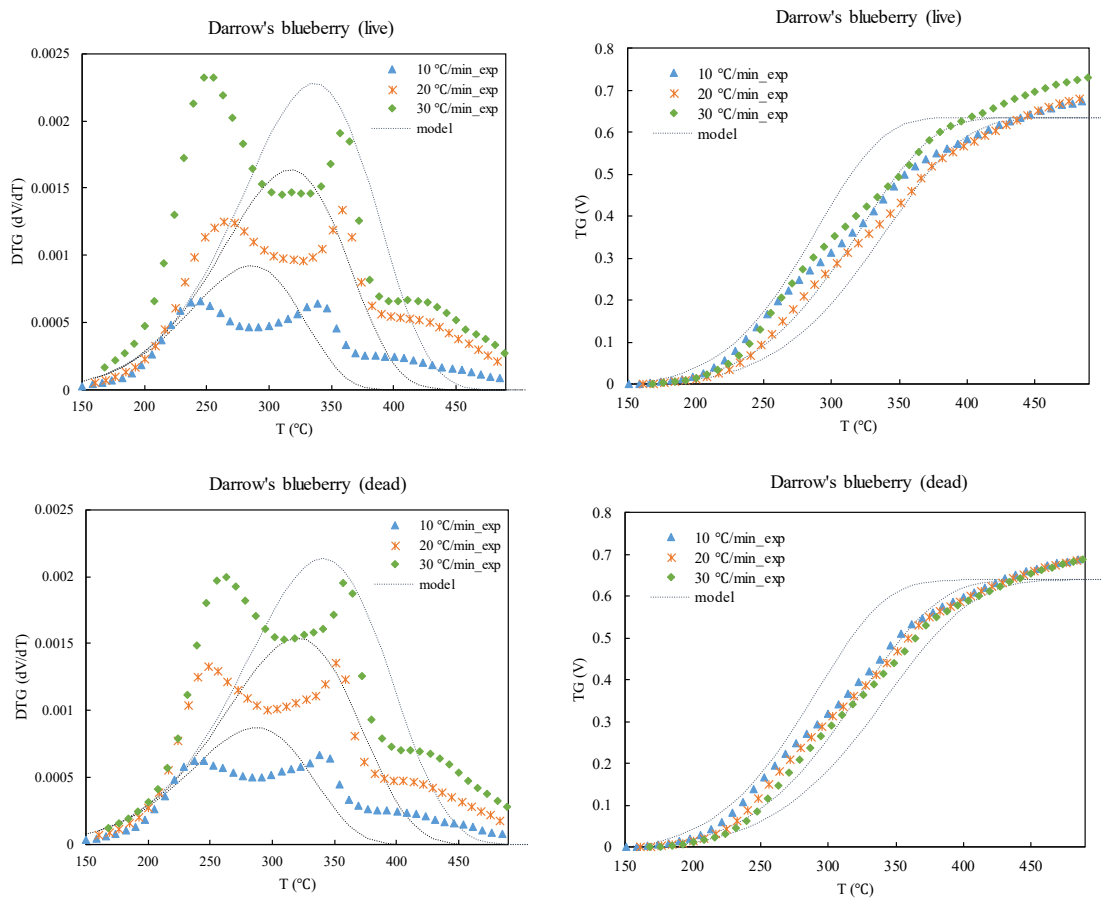
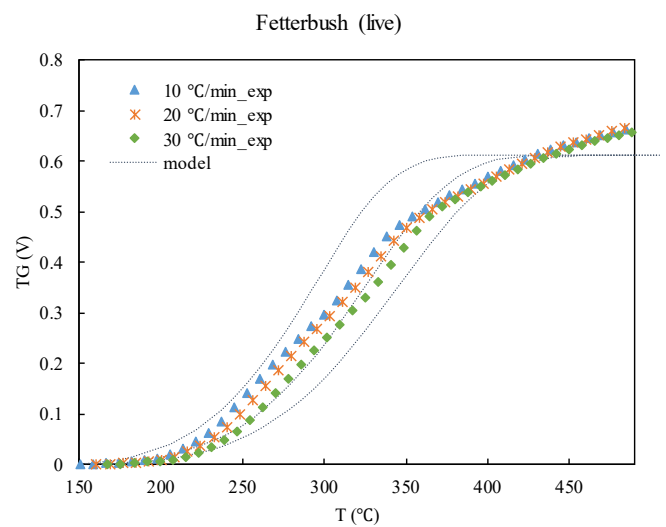
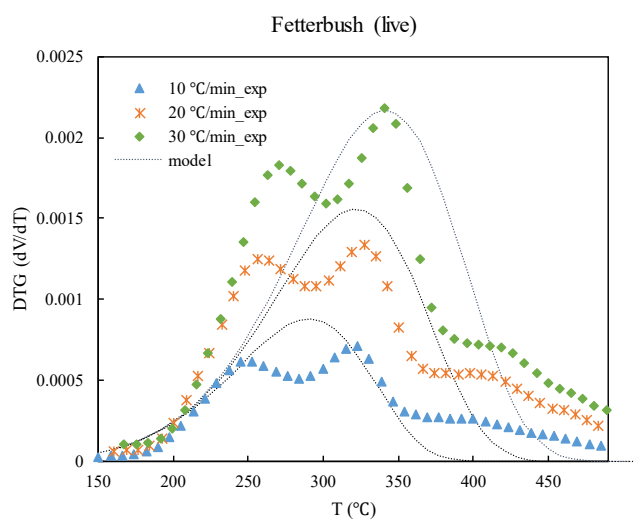
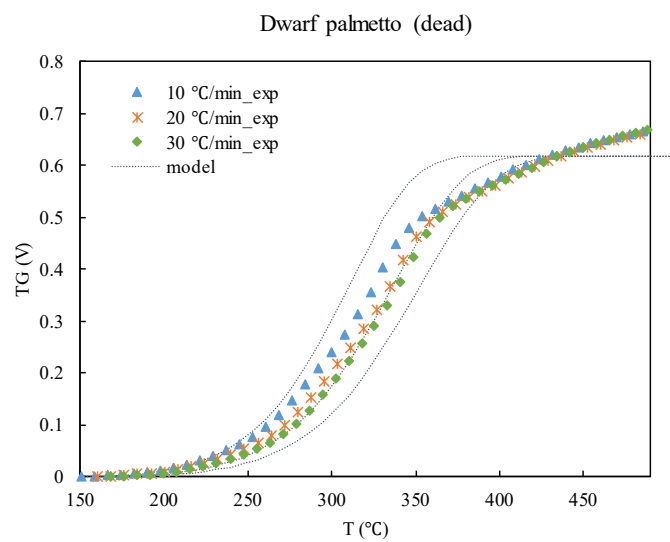
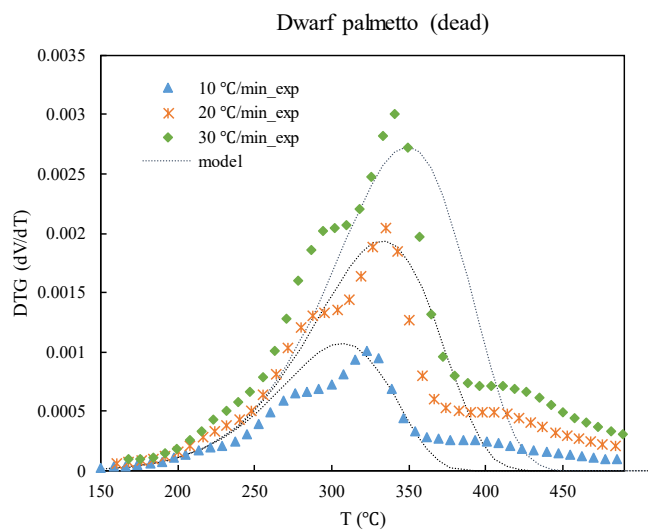
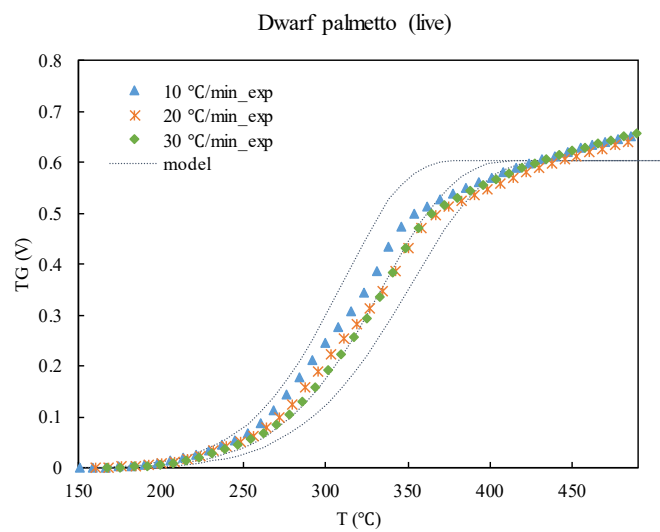
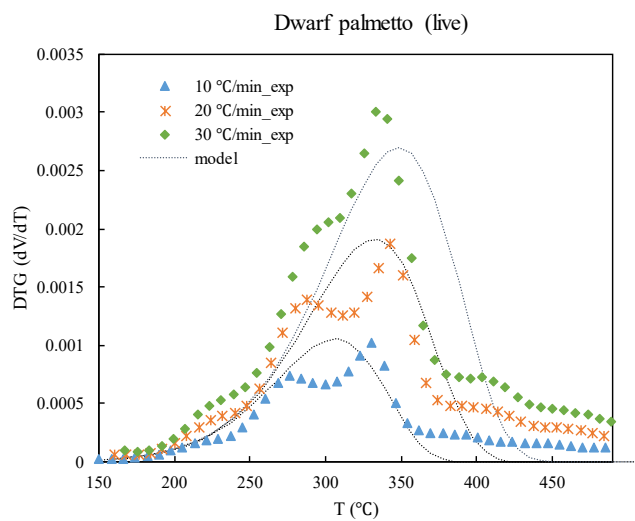


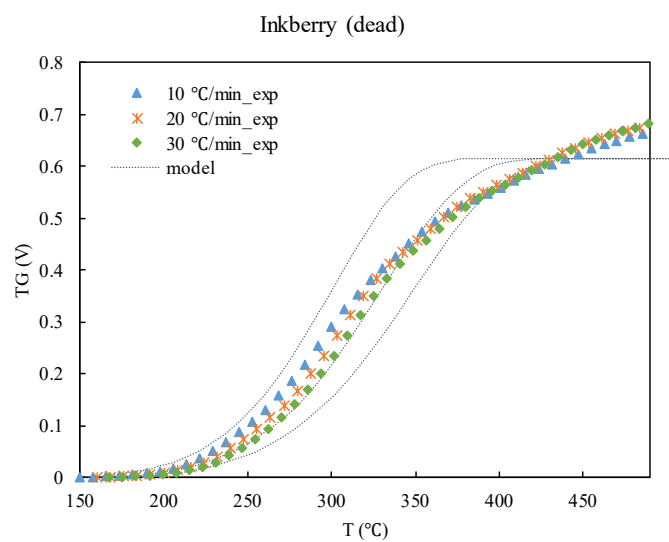
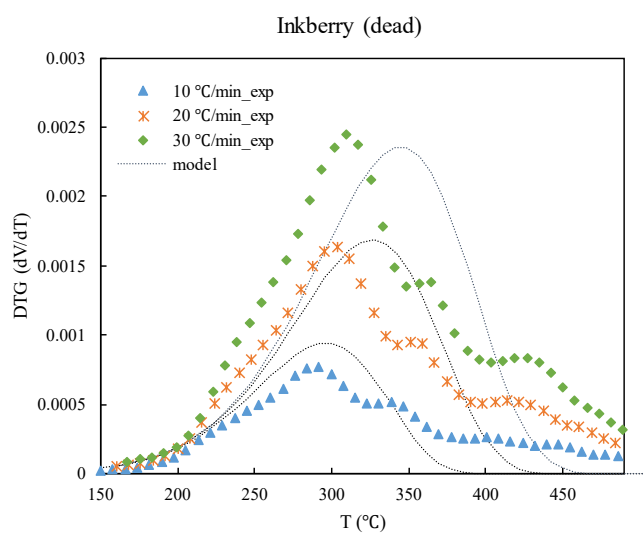
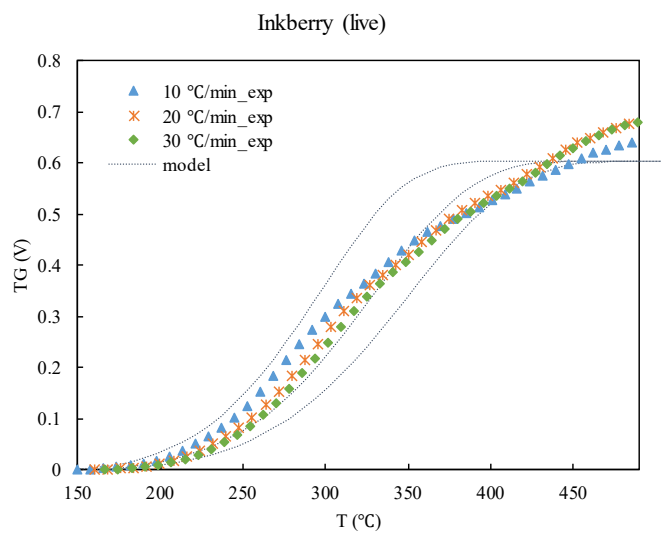
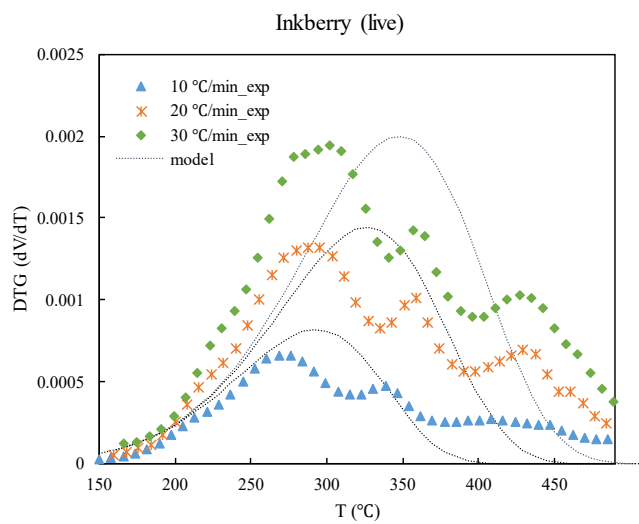
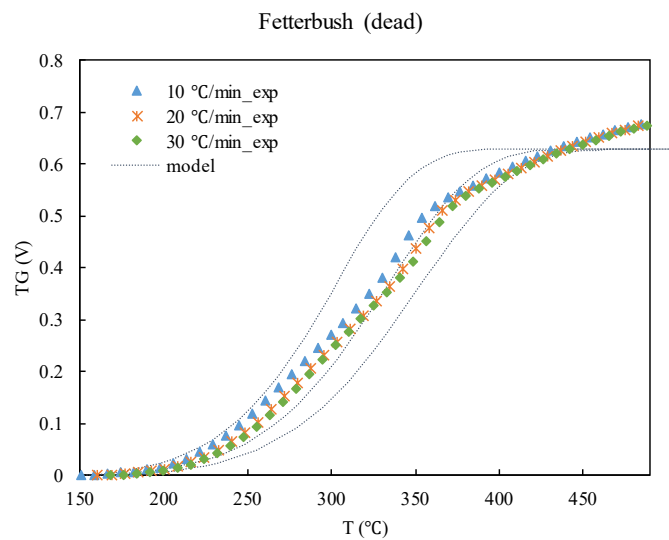
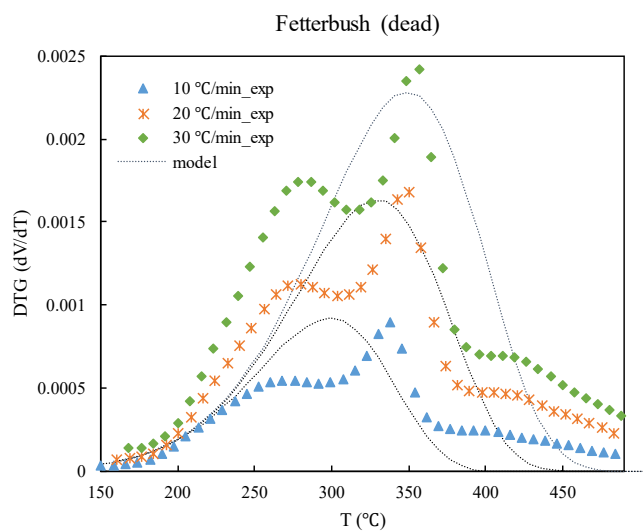
Figure E-1: Regression lines used to obtain apparent activation energies using the KAS method for pyrolysis of all plant species for drying and major pyrolysis zones.

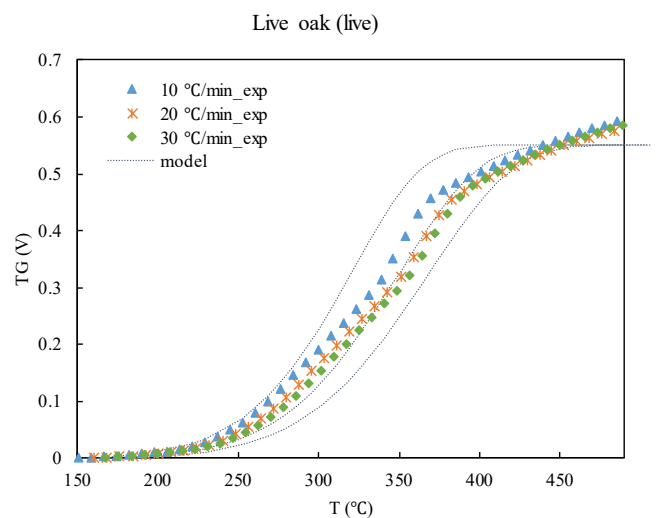
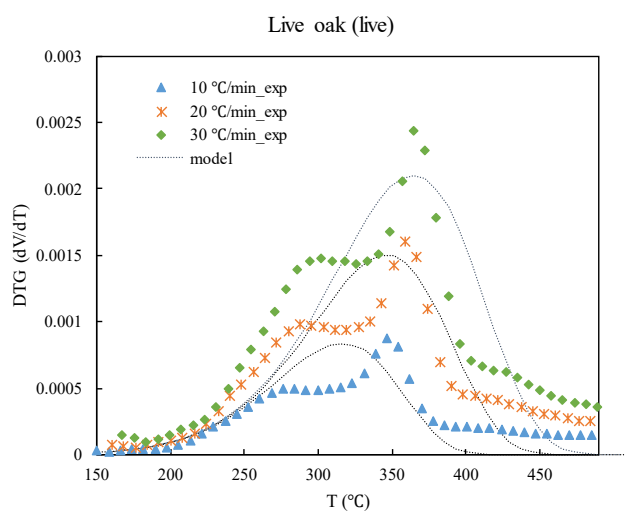
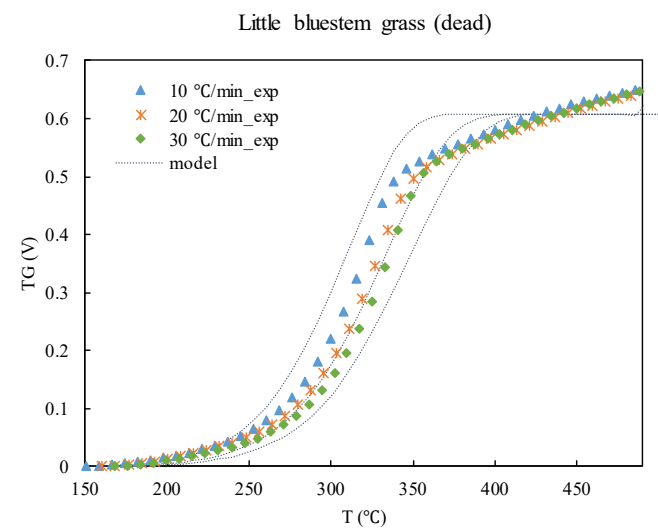
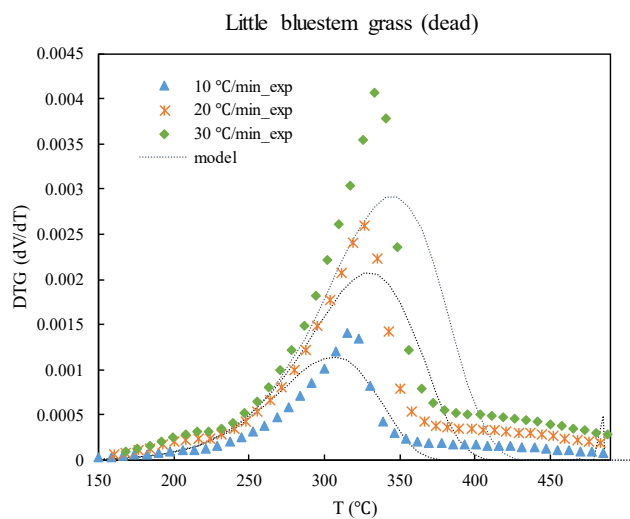
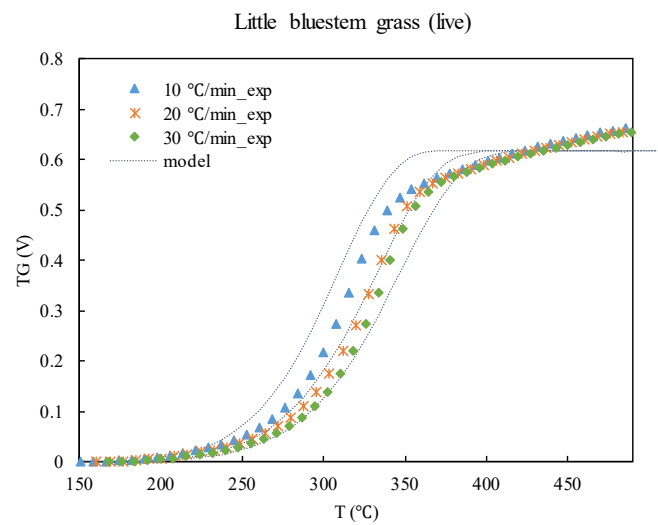
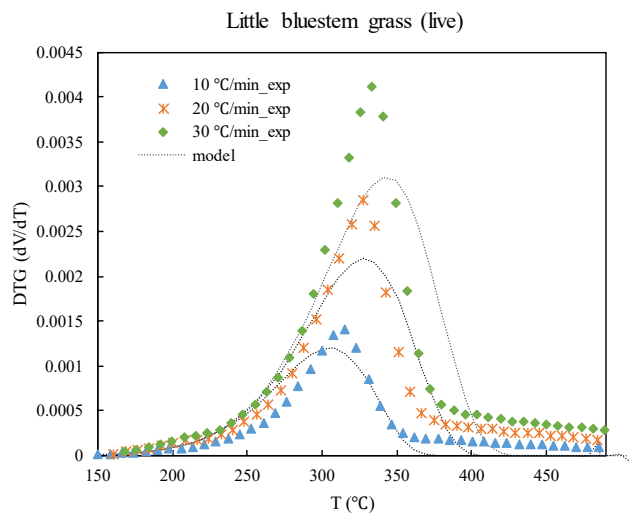
APPENDIX F. TG AND DTG CURVES RESULTED FROM THE SIMPLE ONE-STEP MODEL

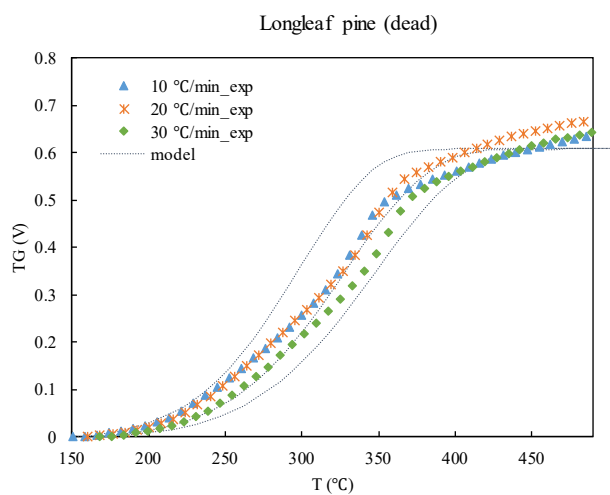
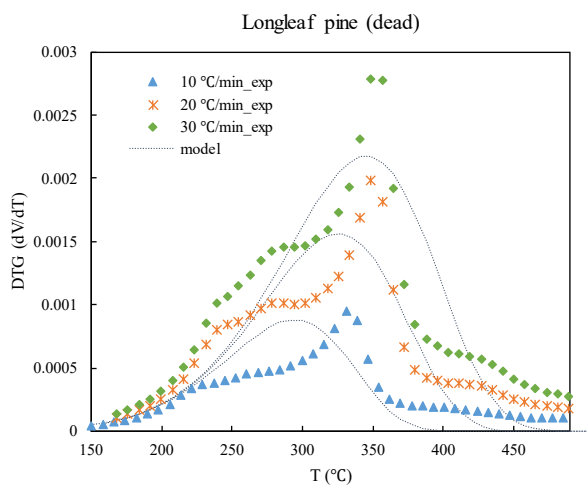
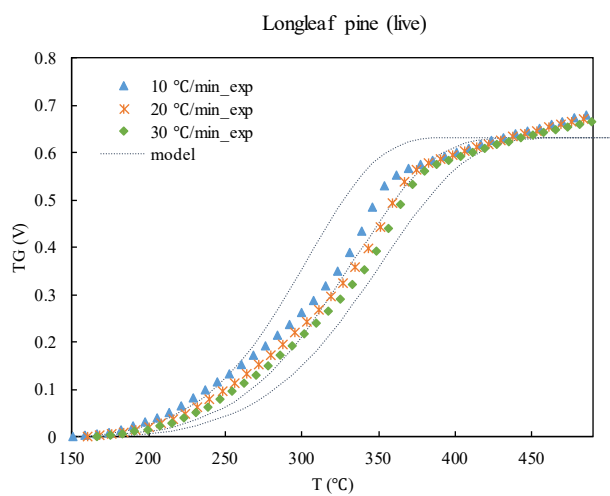
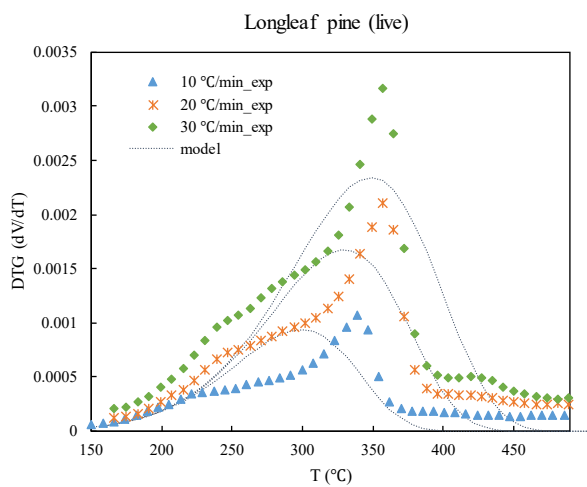
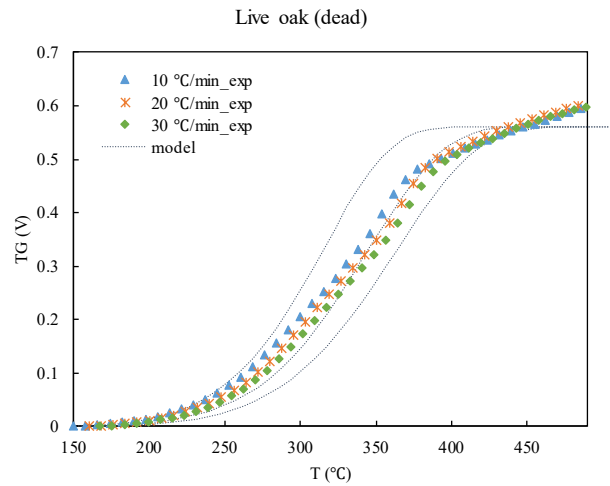
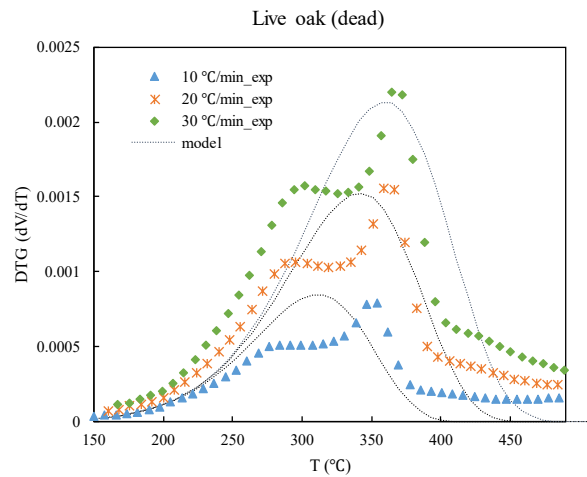
TG and DTG curves resulted from experimental data and the simple one-step model are presented in Figure F-1.

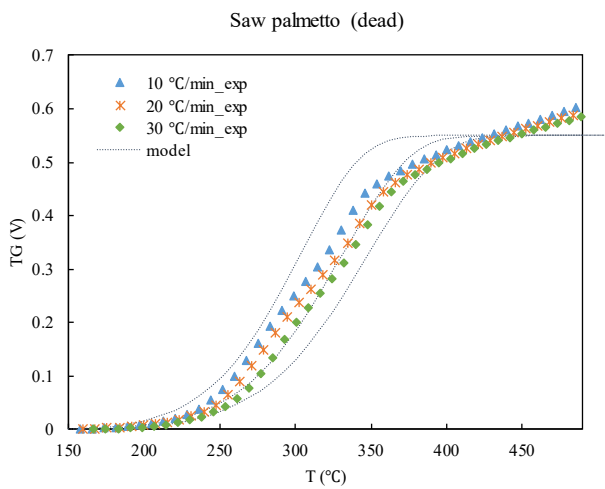
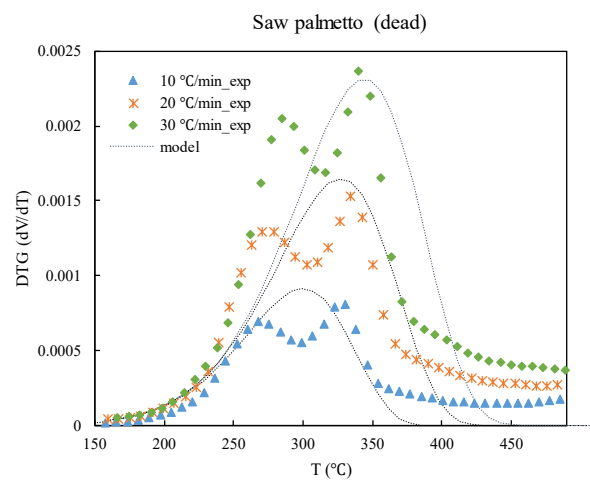
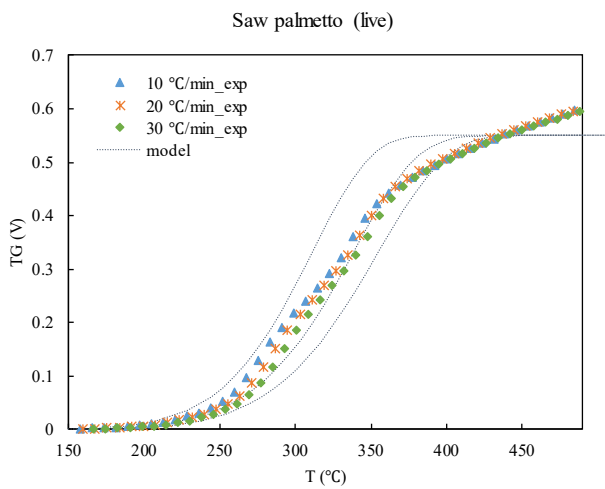
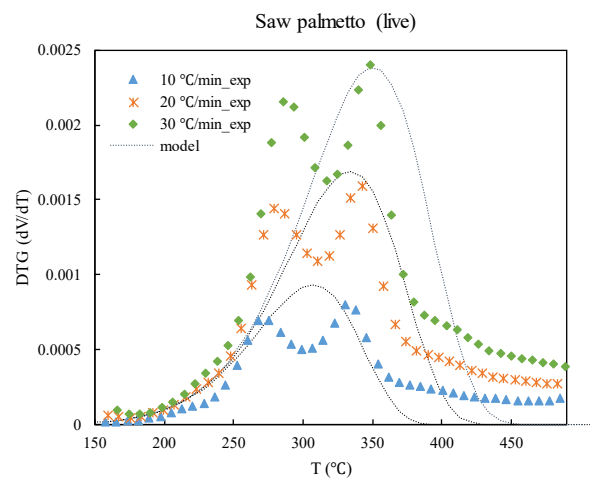
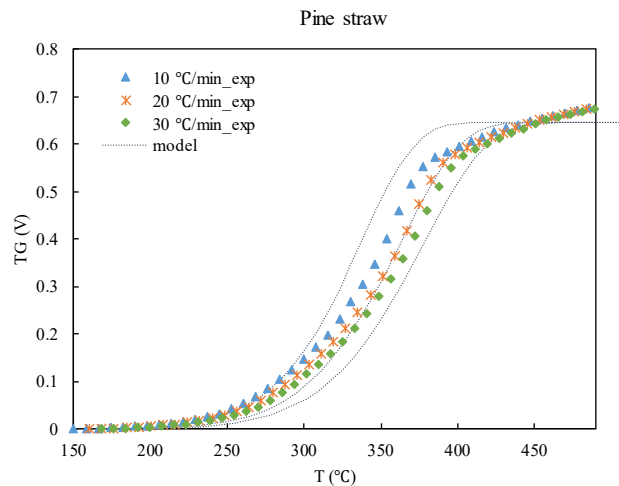
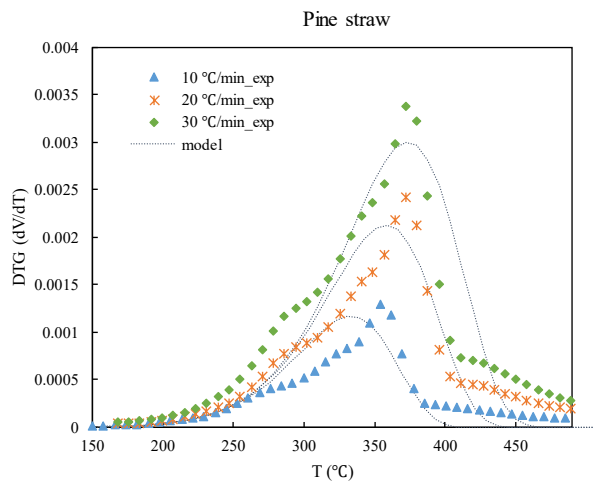


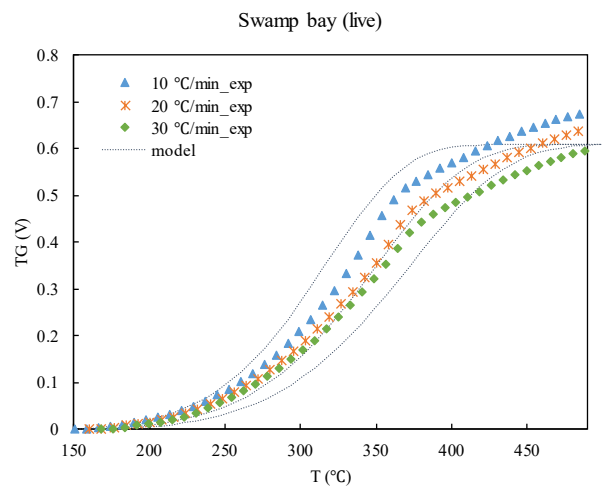
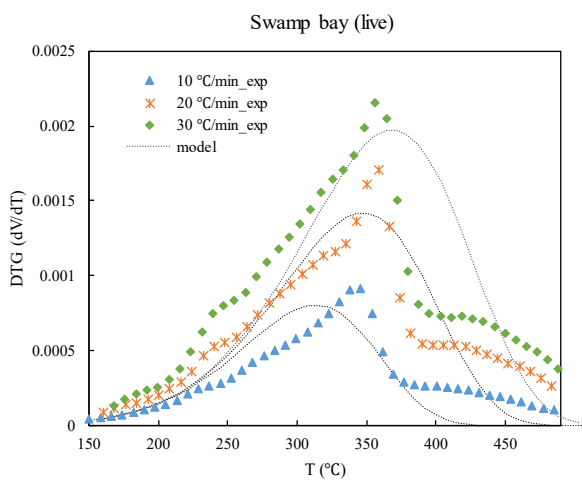
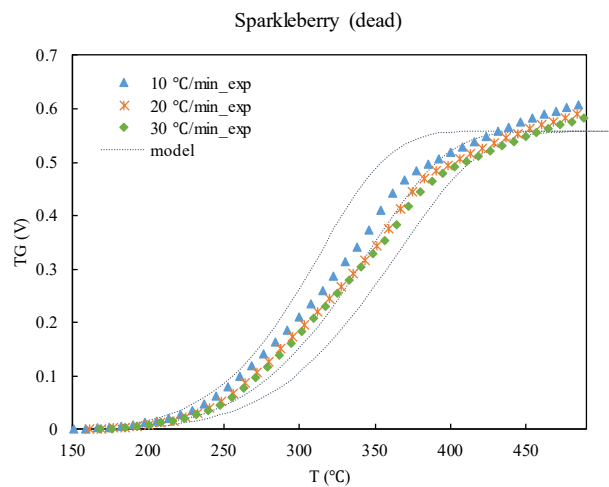
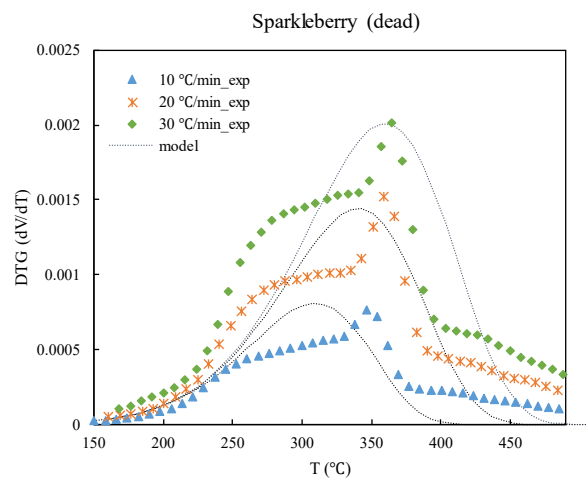
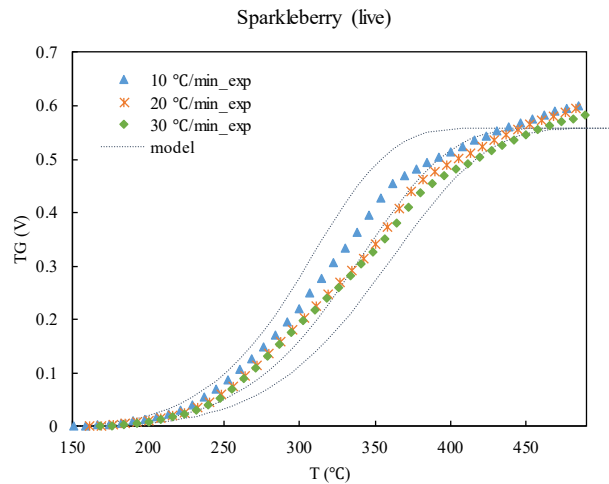
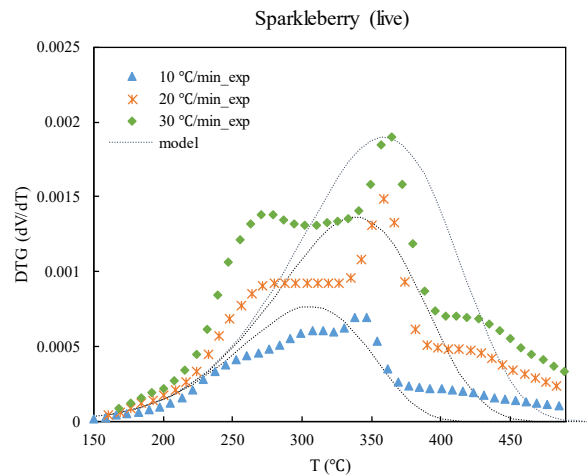


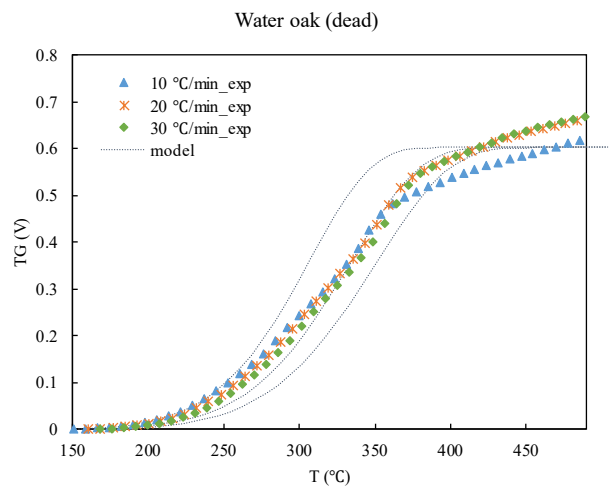
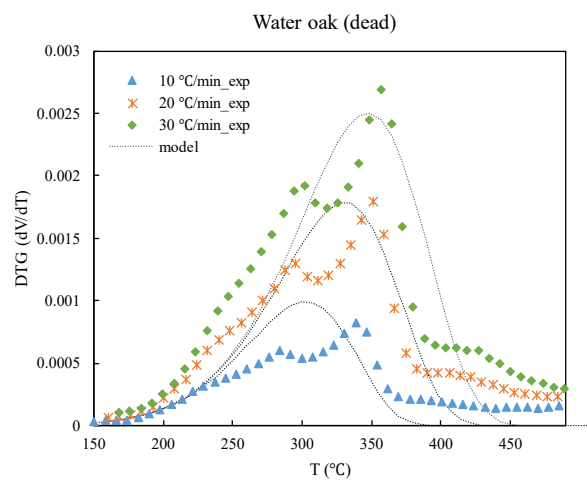
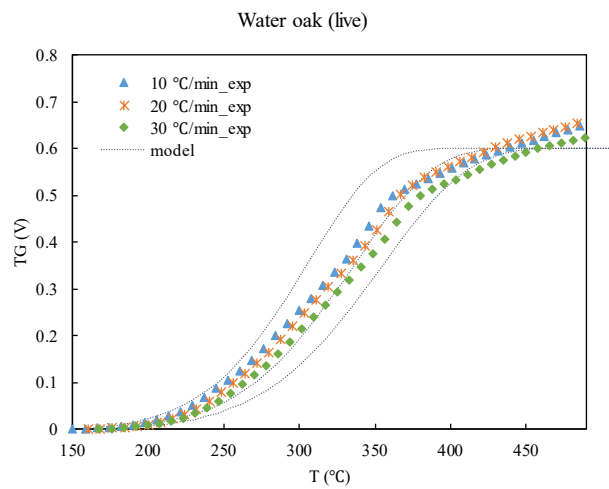
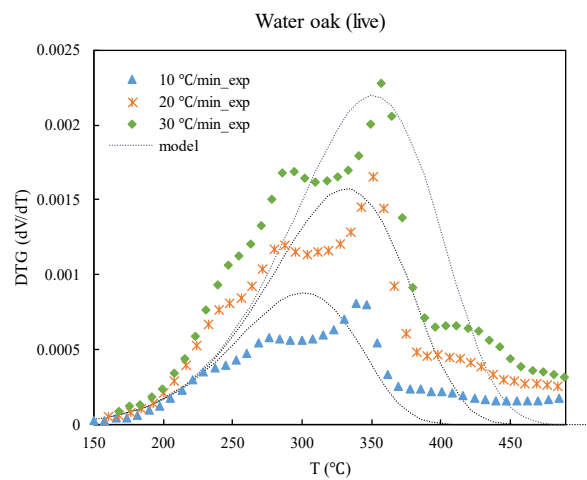
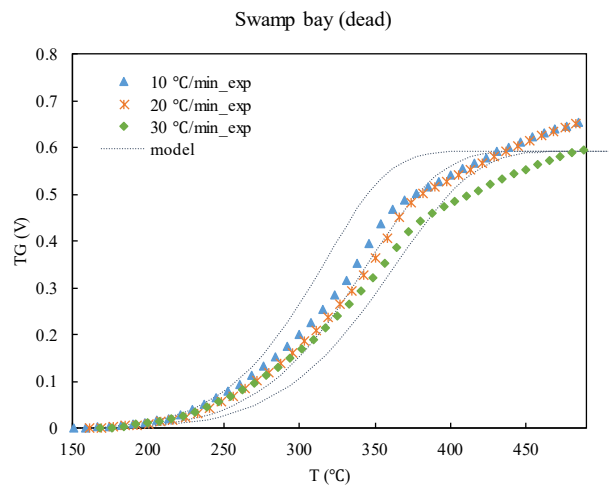
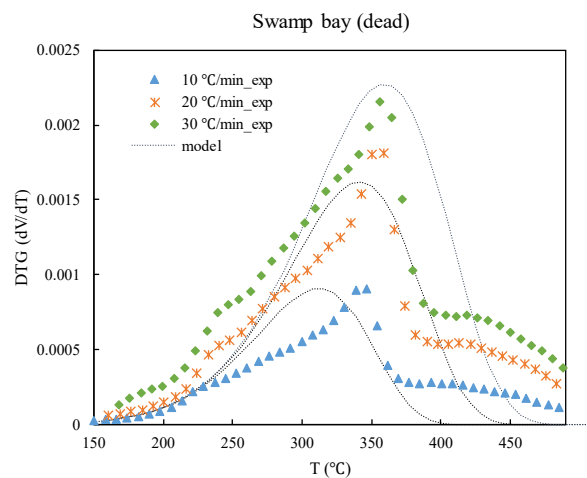


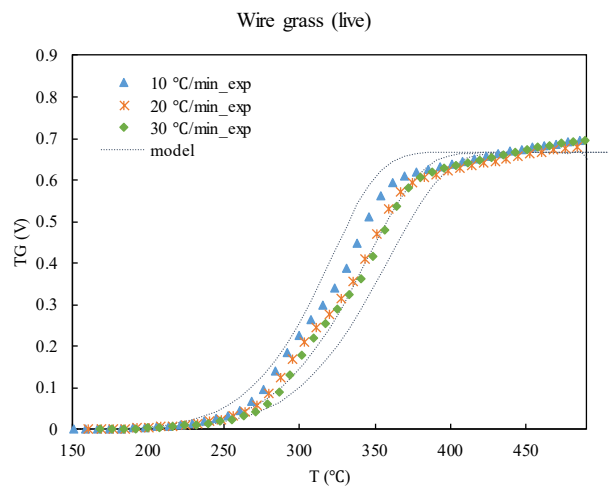
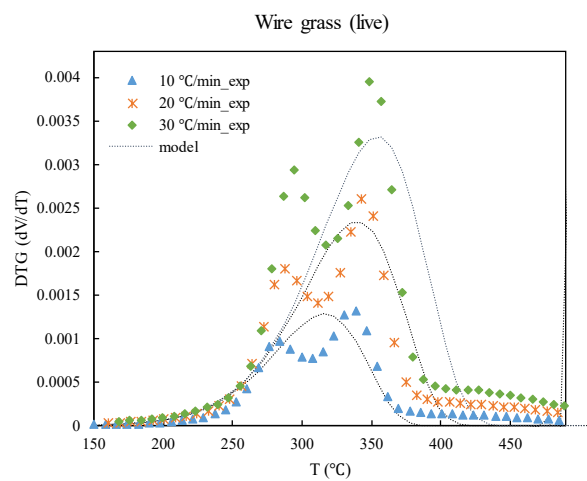
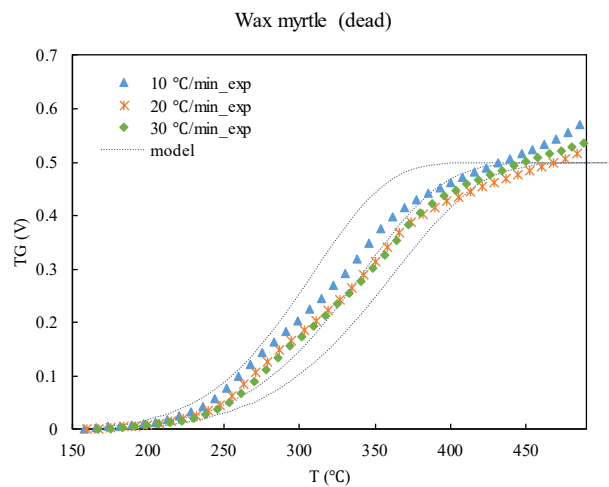
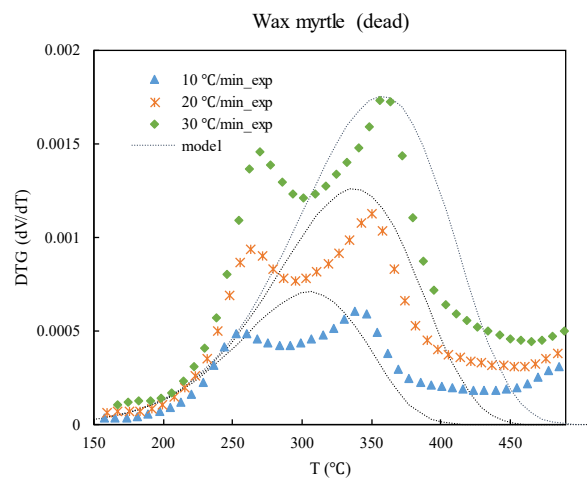
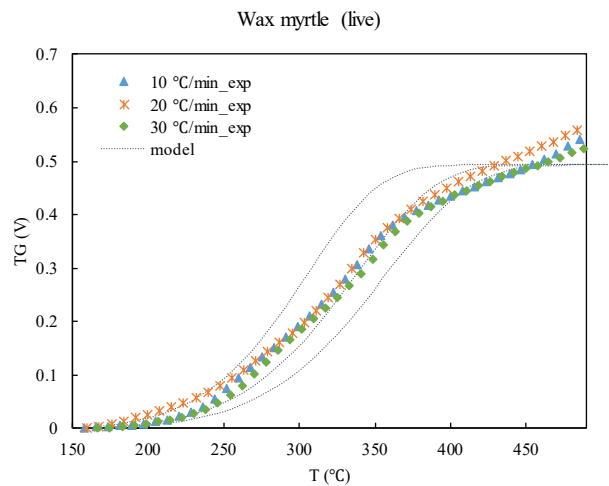
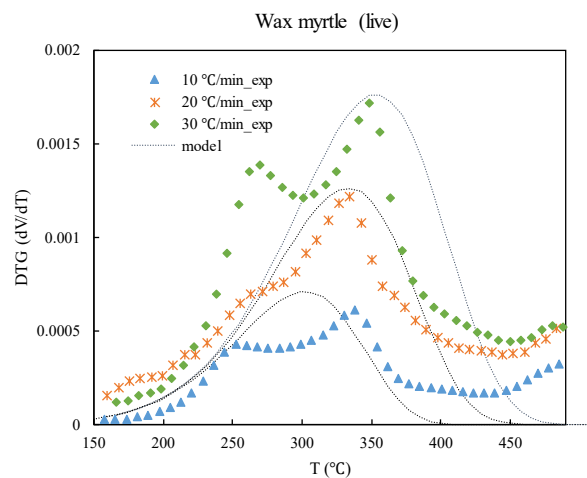












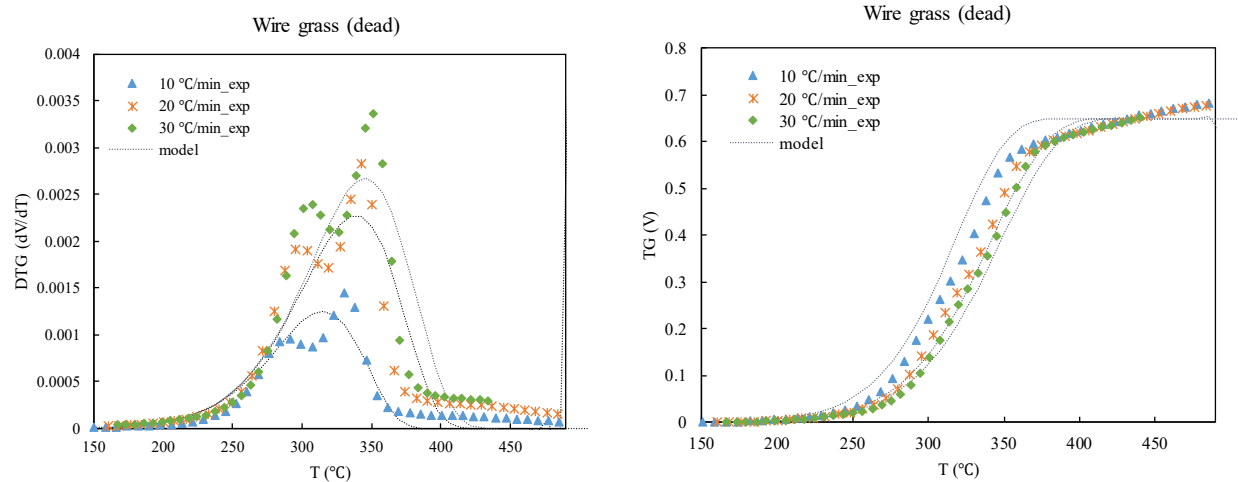
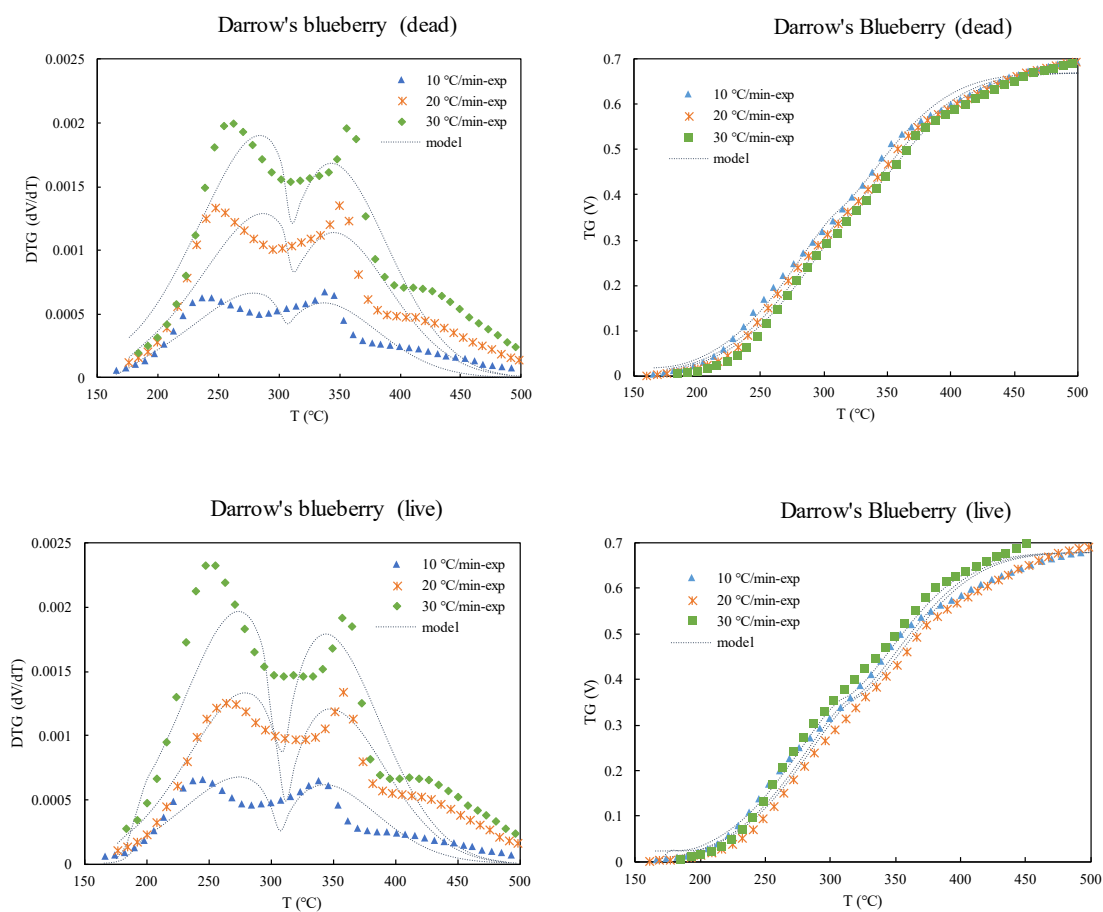
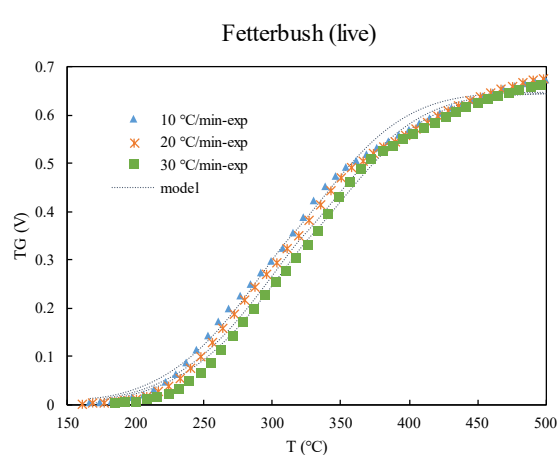
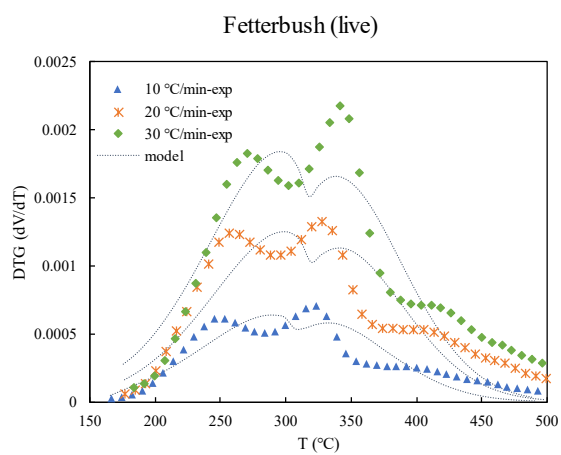
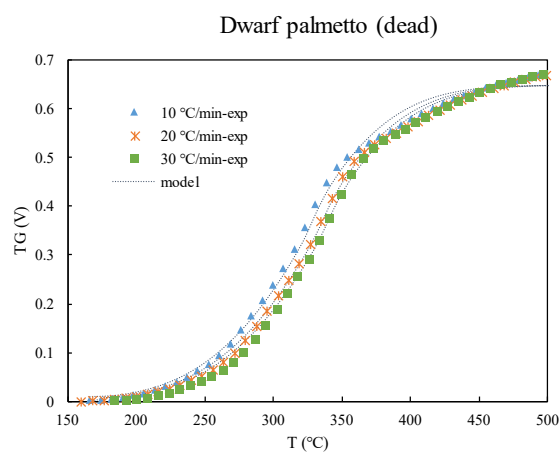
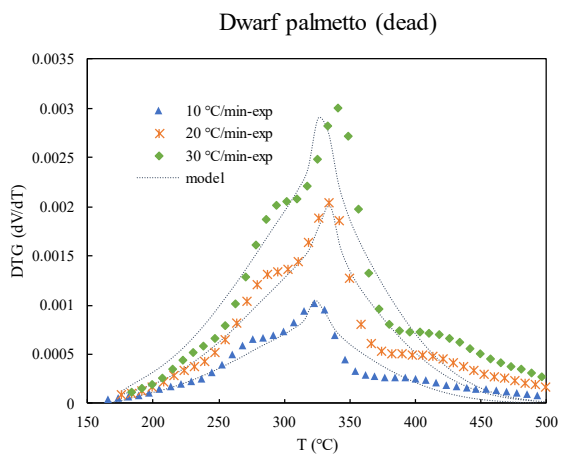
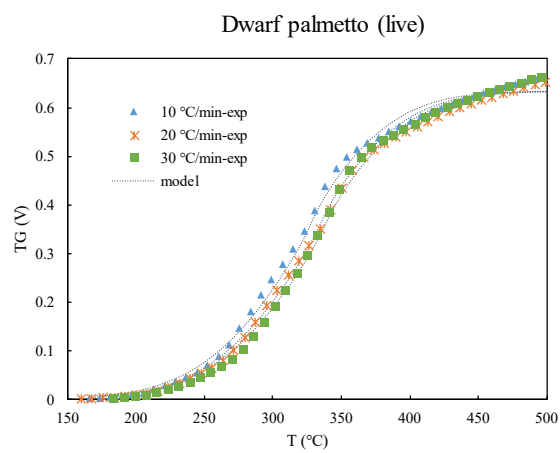
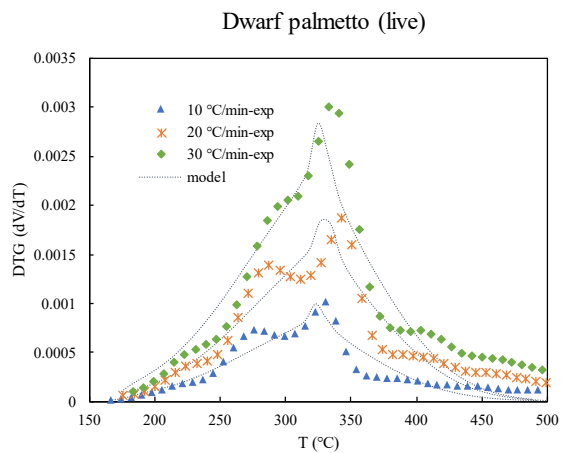


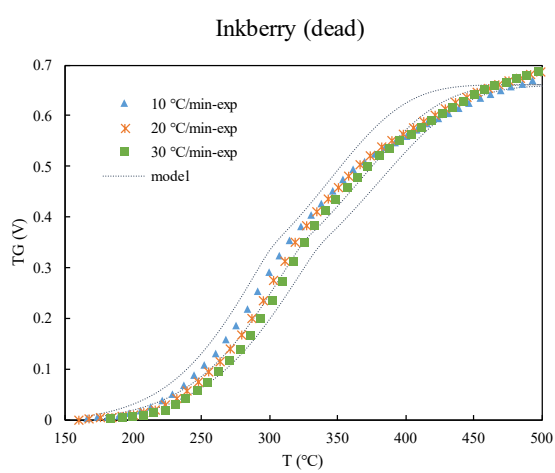
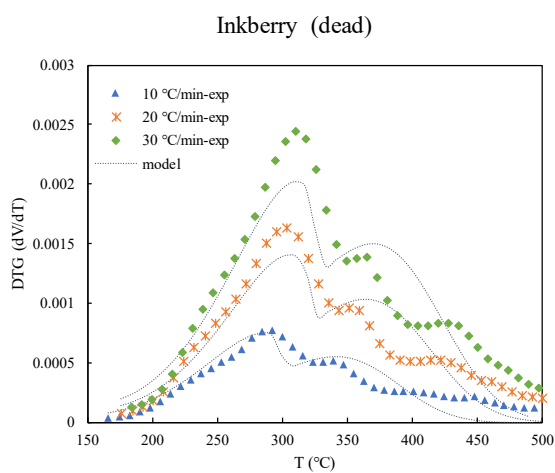
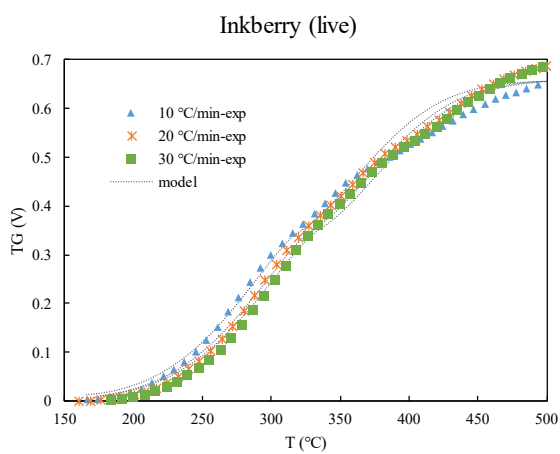
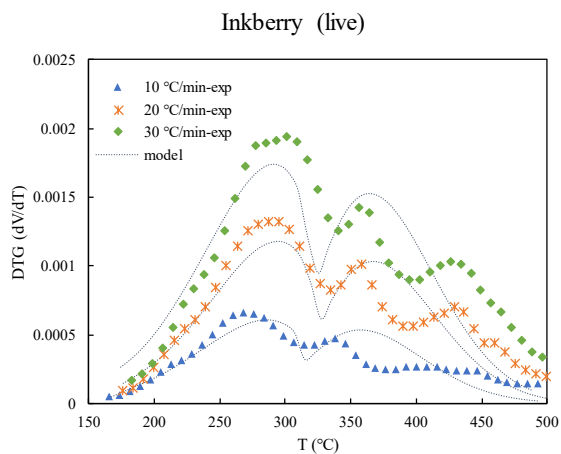
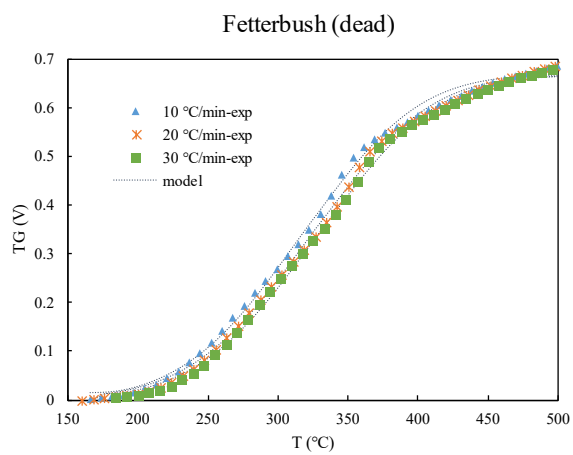
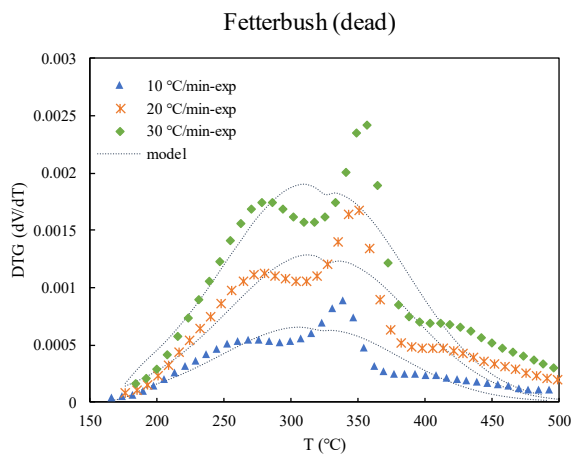
Figure F-1: Comparison of best-fit simple one-step model (dash lines) with TGA and DTG data (points) for all plant species at three heating rates of 10, 20 and 30 °C min⁻¹.

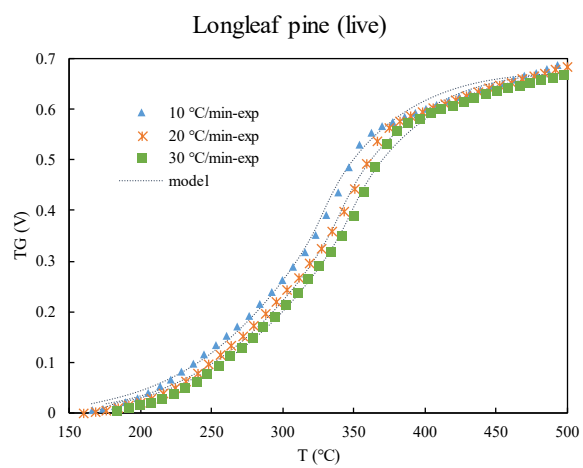
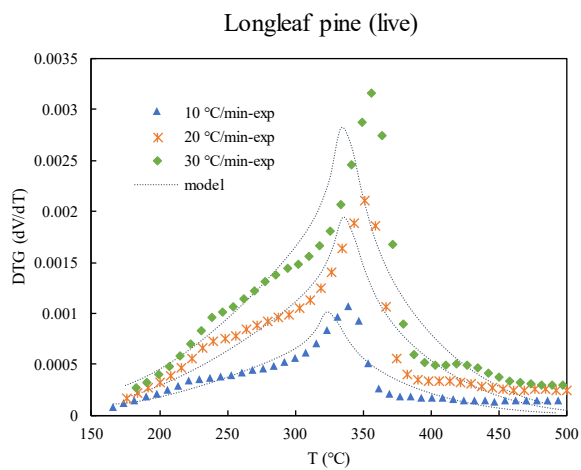
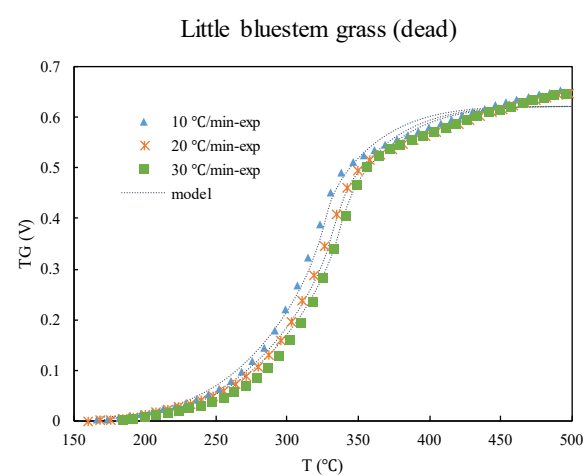
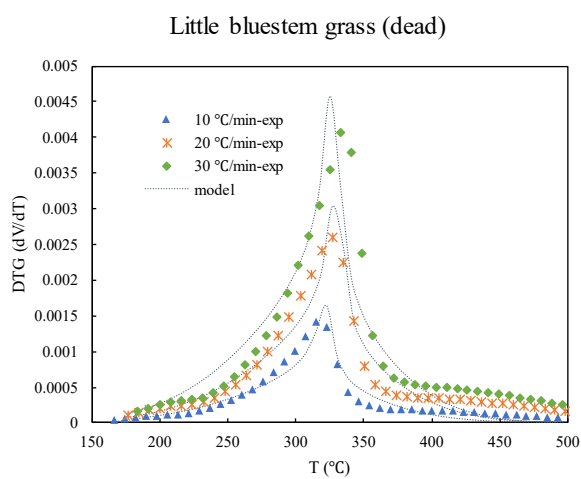
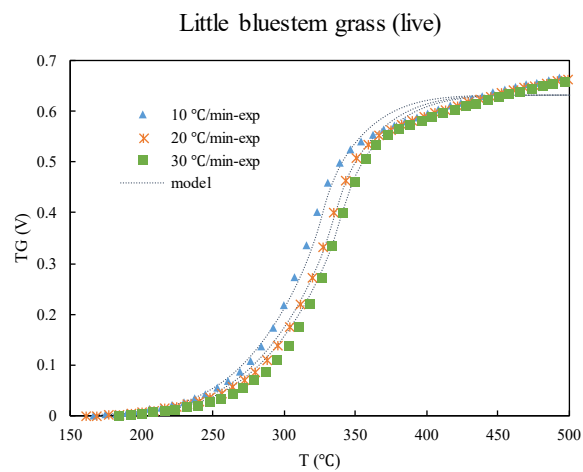
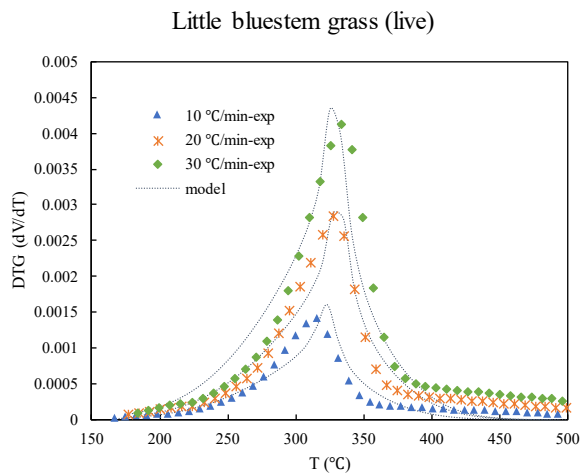
APPENDIX G. TG AND DTG CURVES RESULTED FROM THE SINGLE-REACTION DAEM MODEL

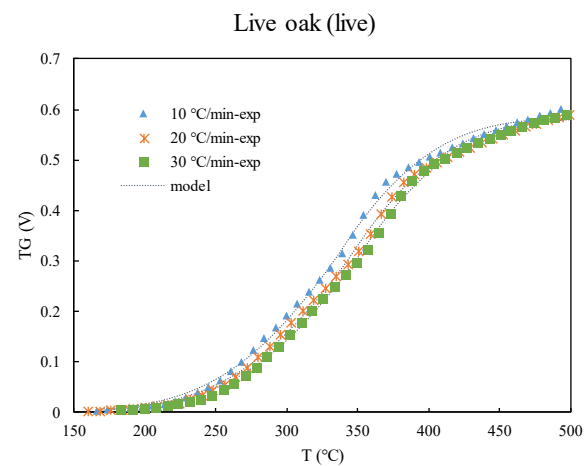
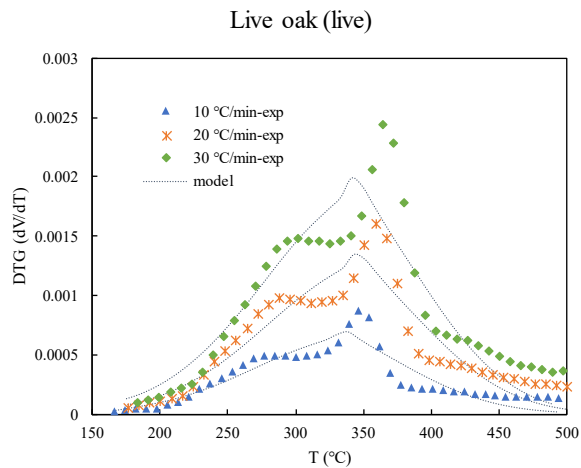
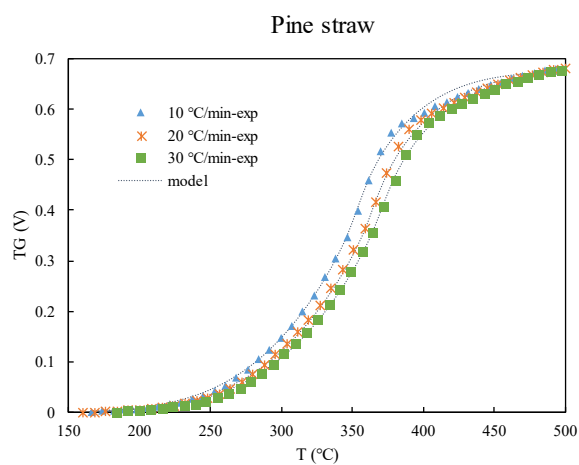
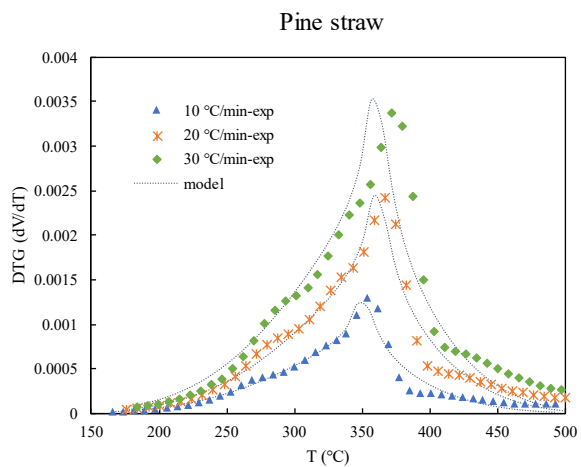
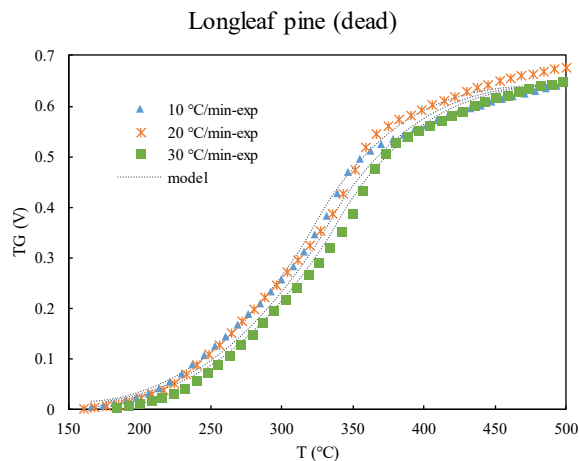
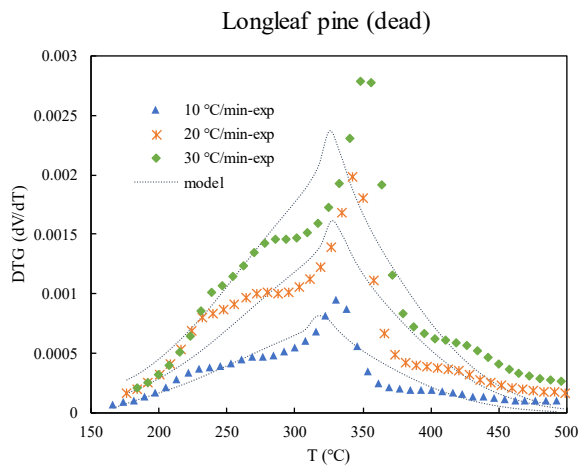
Figure G-1 shows the TG and DTG curves resulted from experimental data and the single-reaction DAEM model.

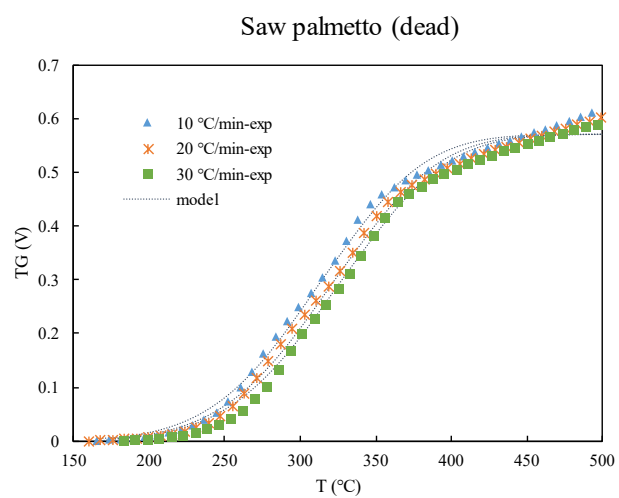
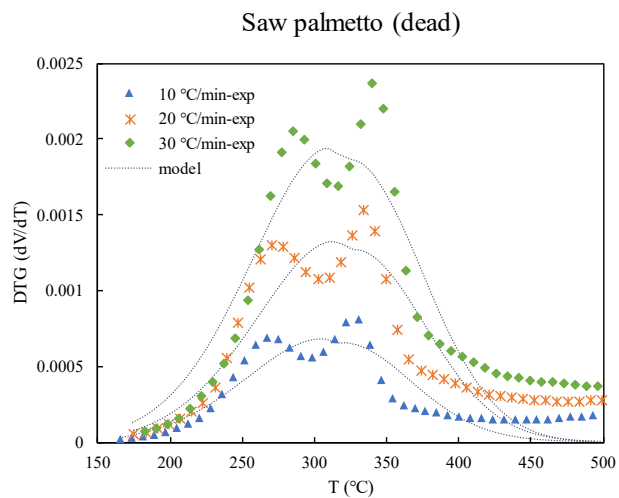
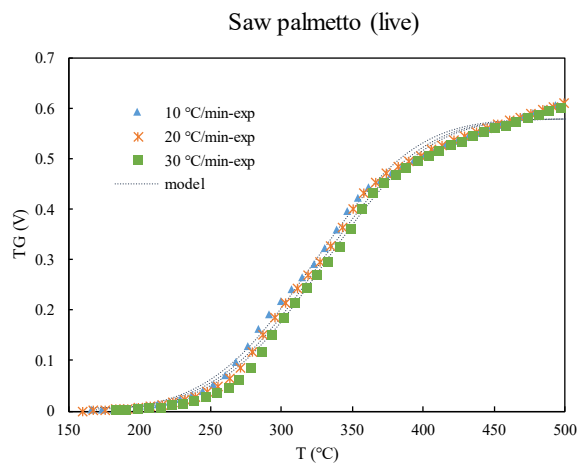
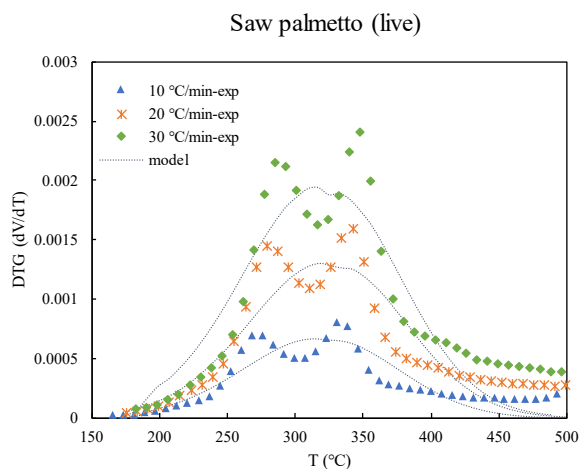
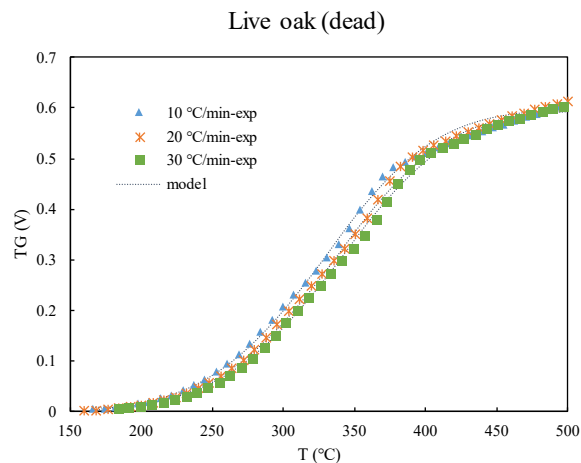
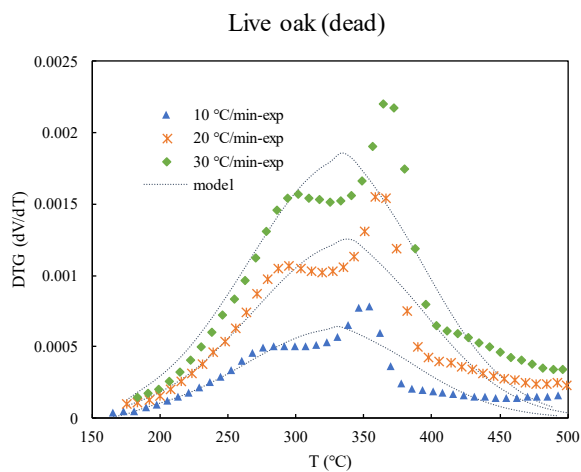


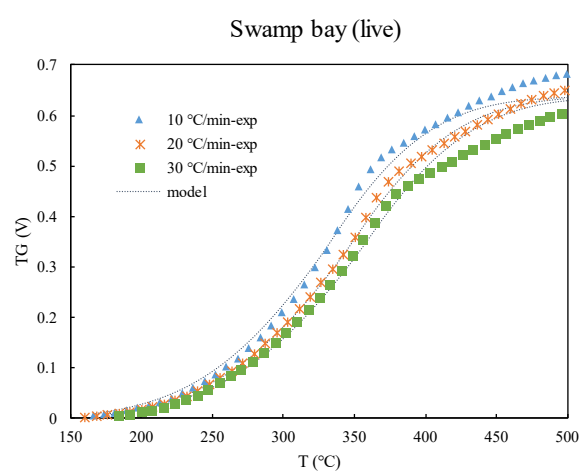
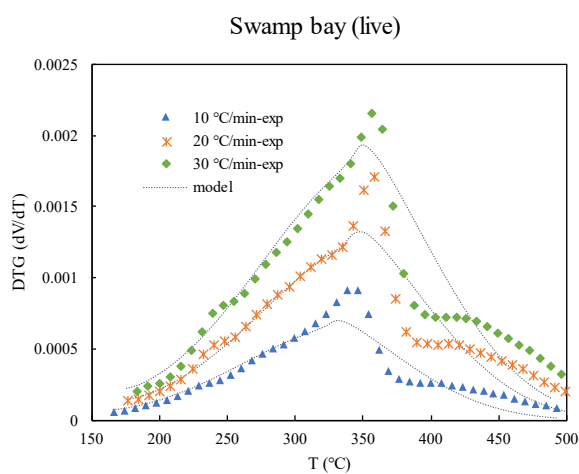
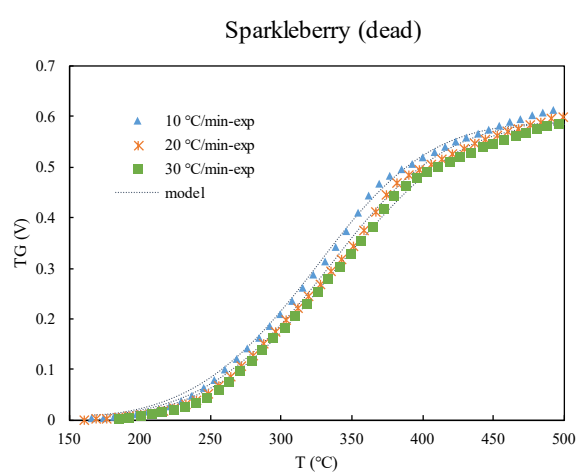
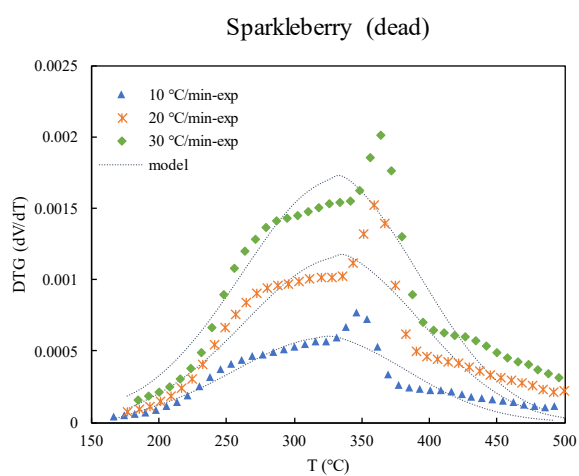
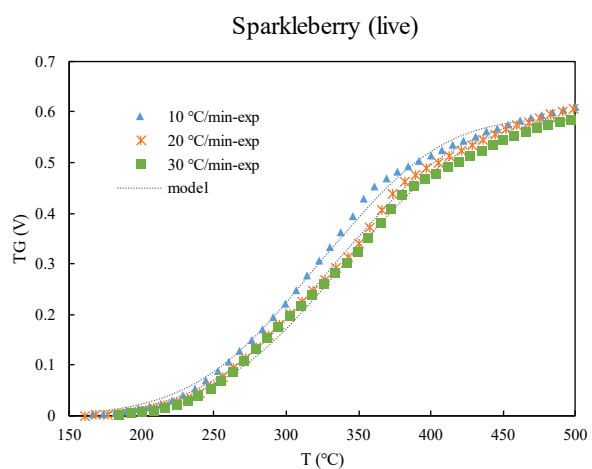
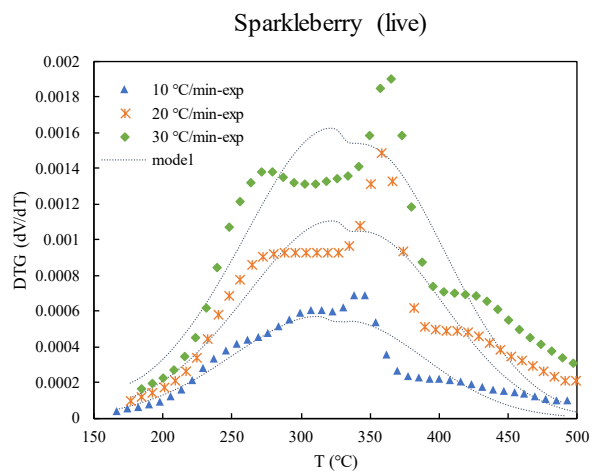


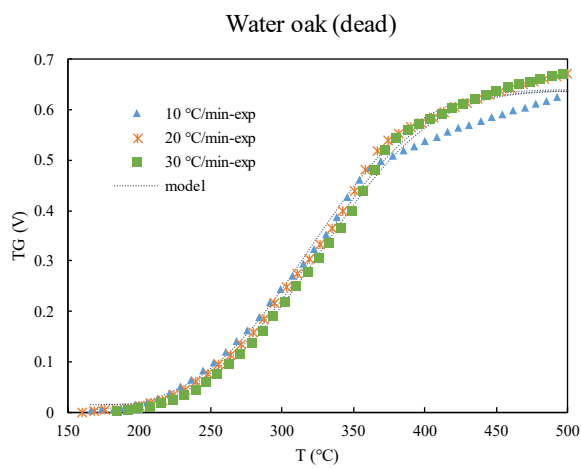
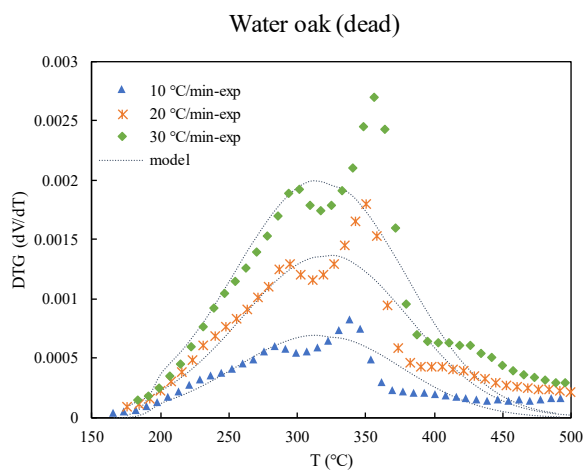
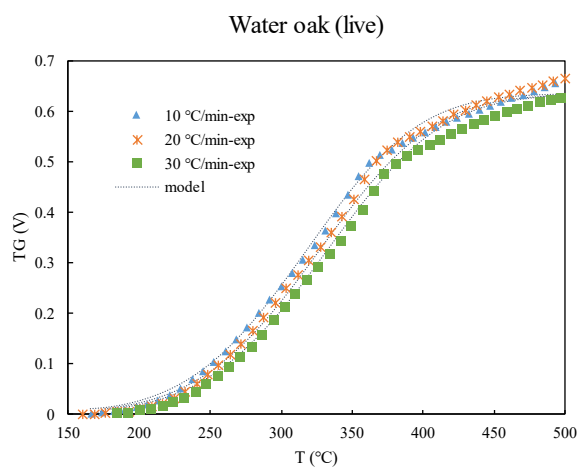
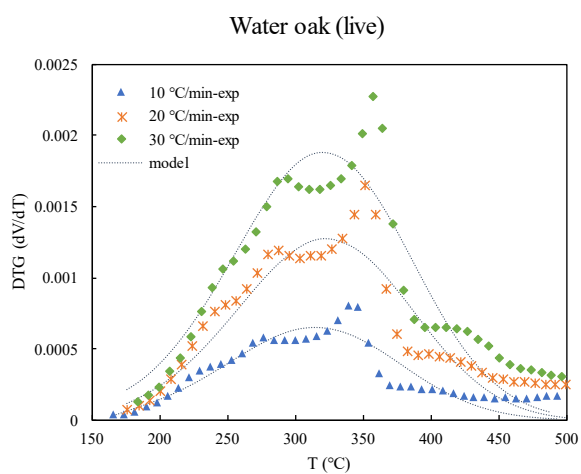
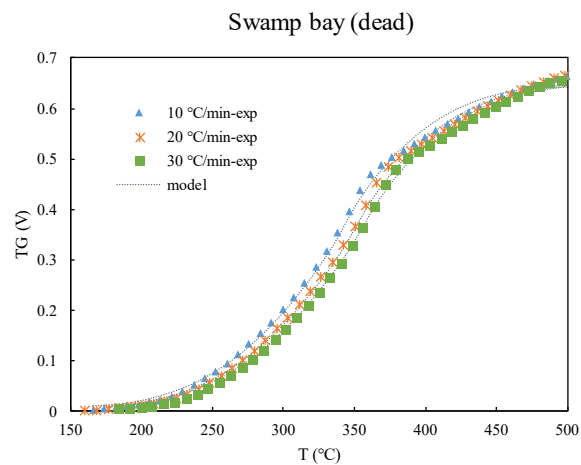
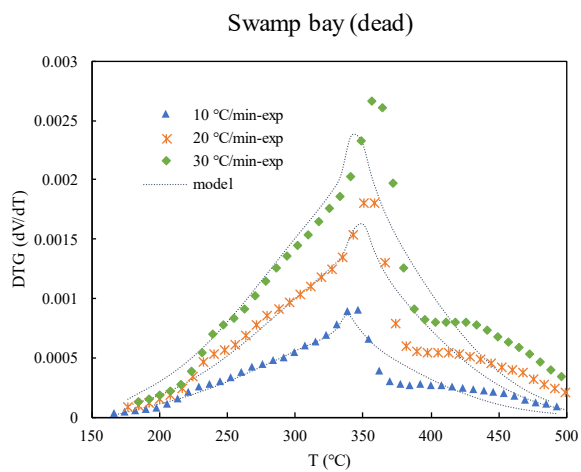


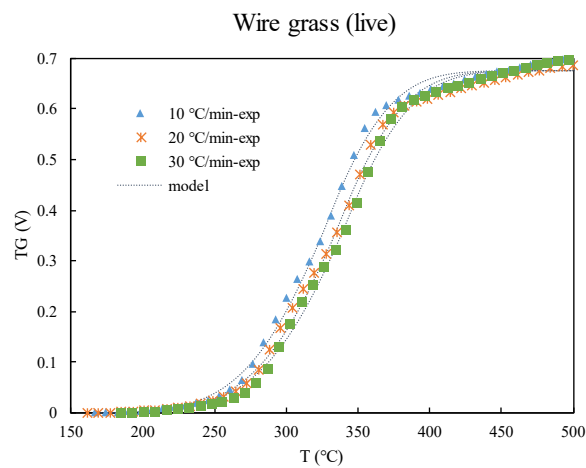
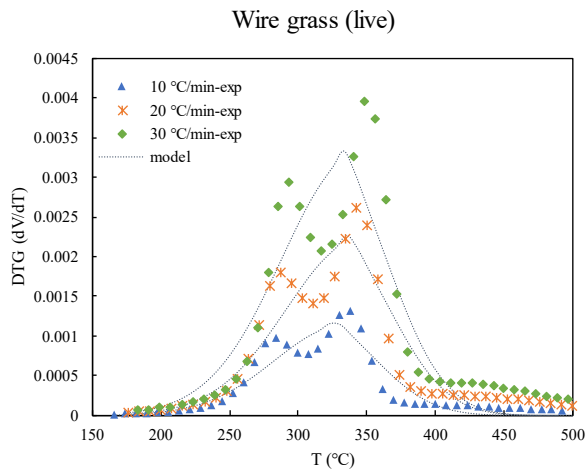
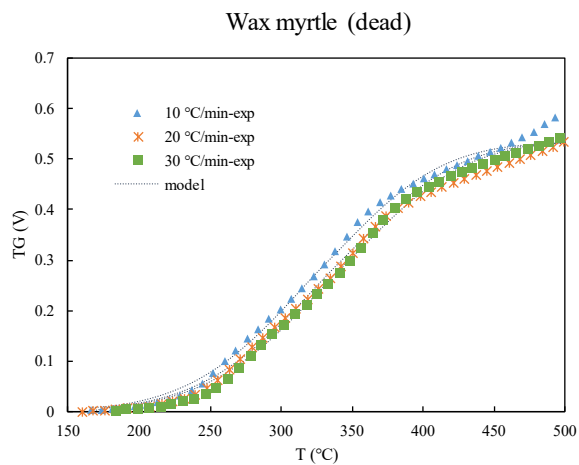
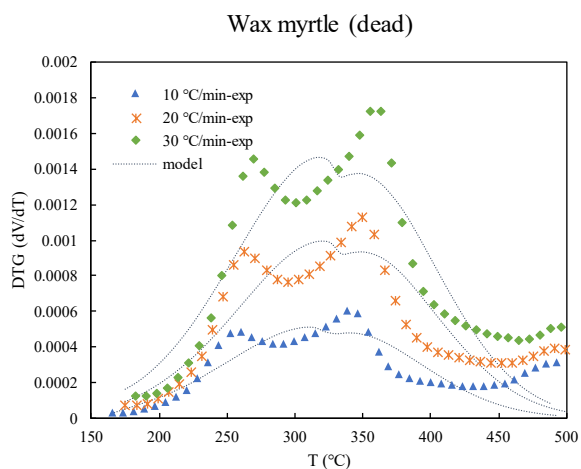
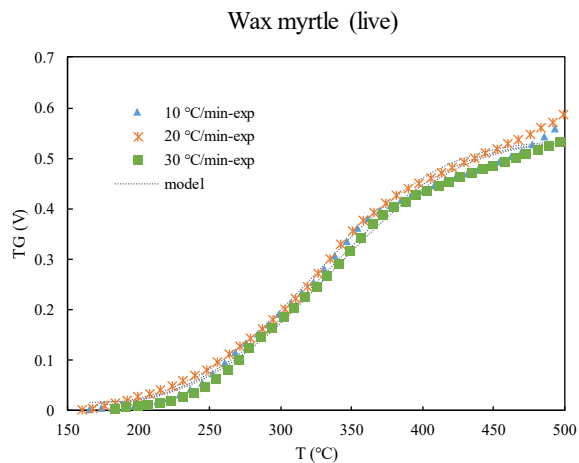
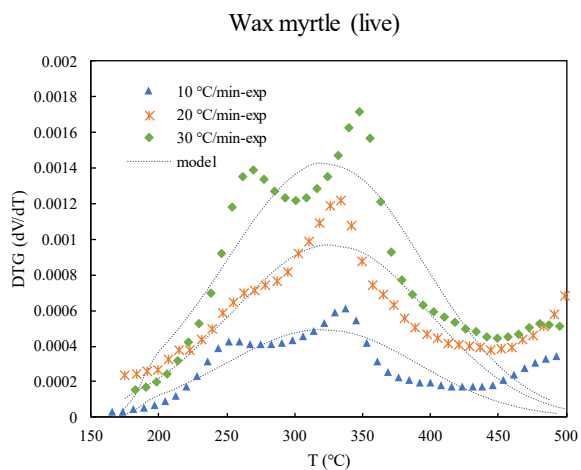












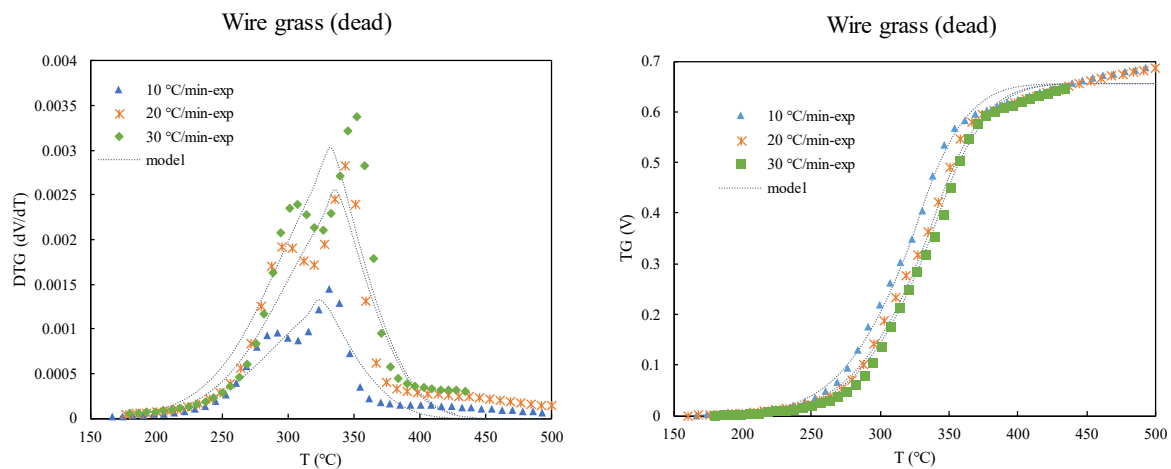
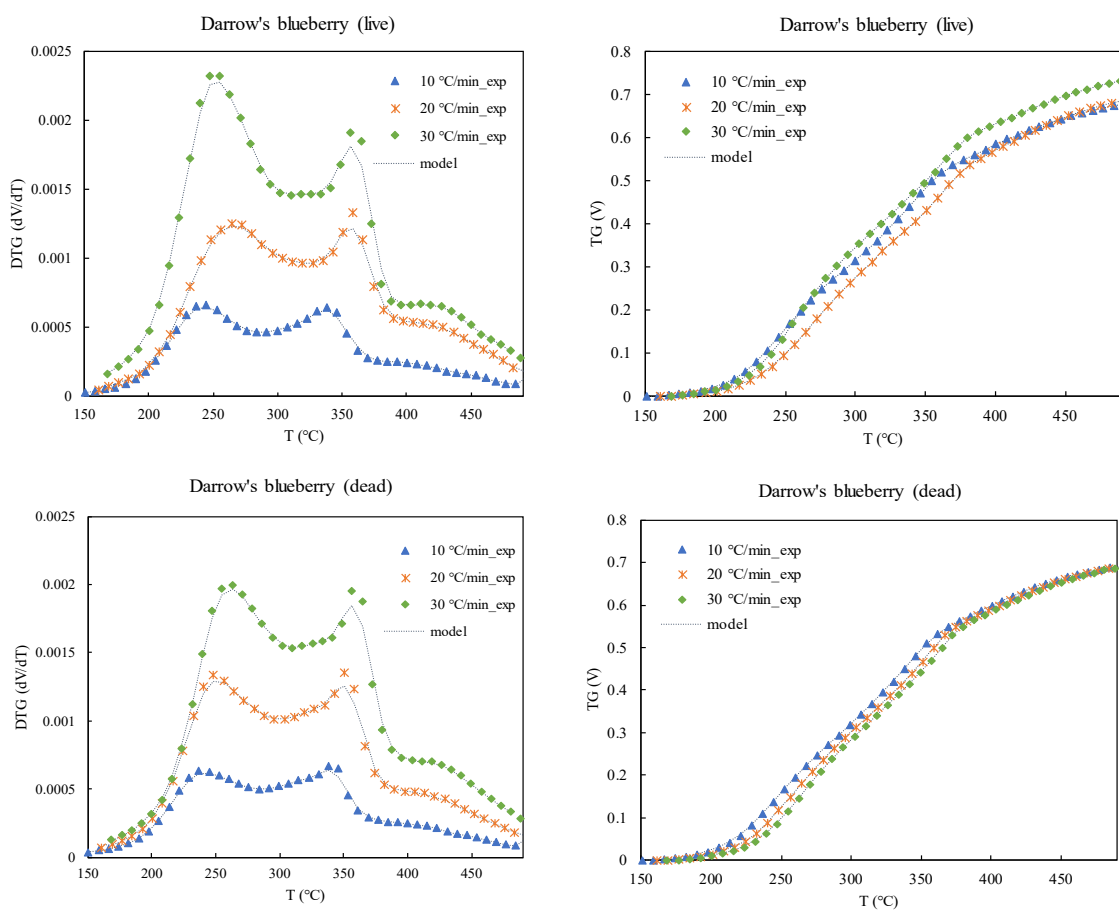
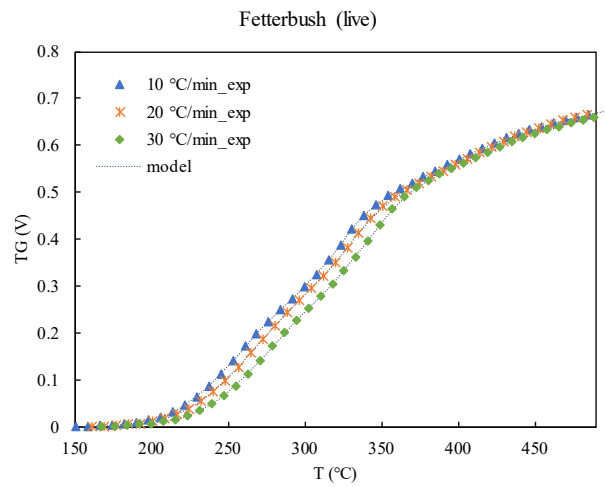
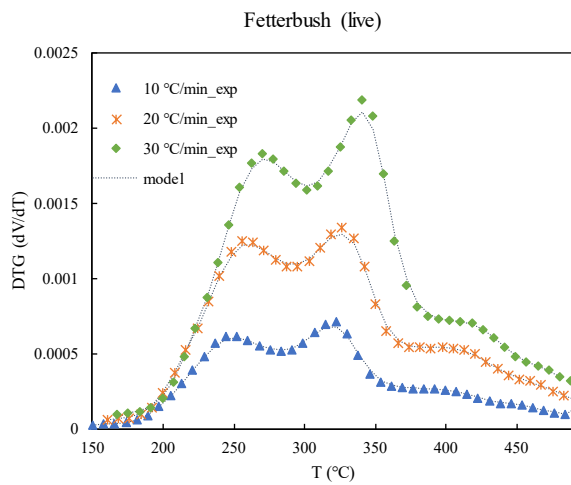
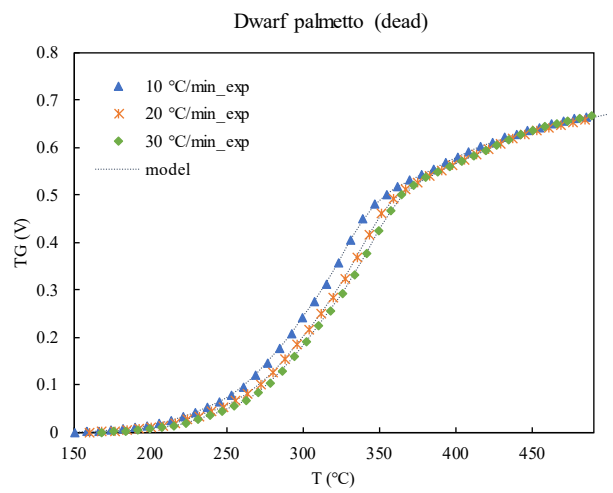
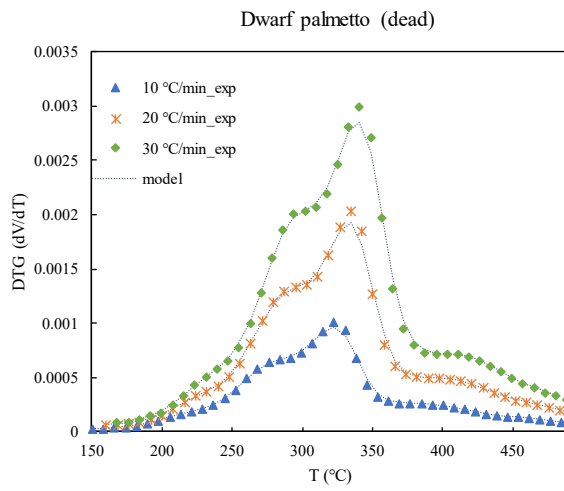
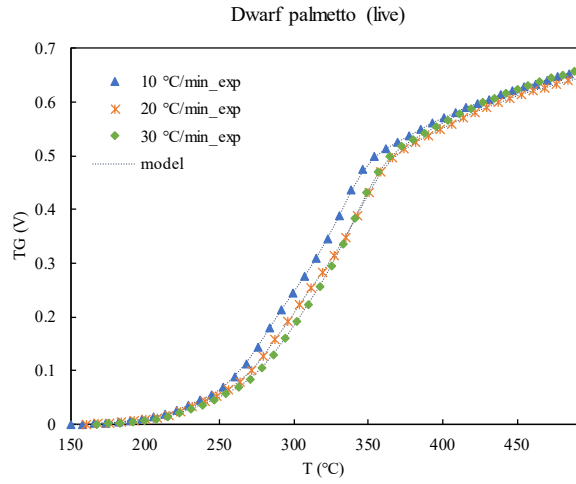
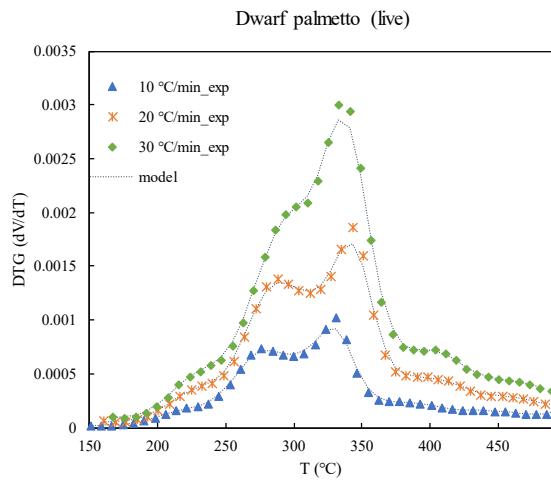


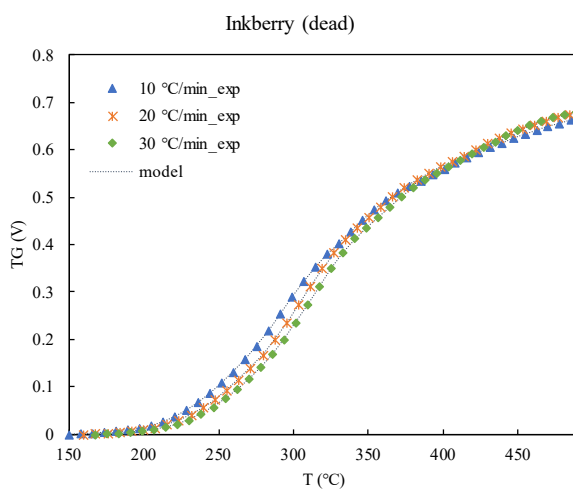
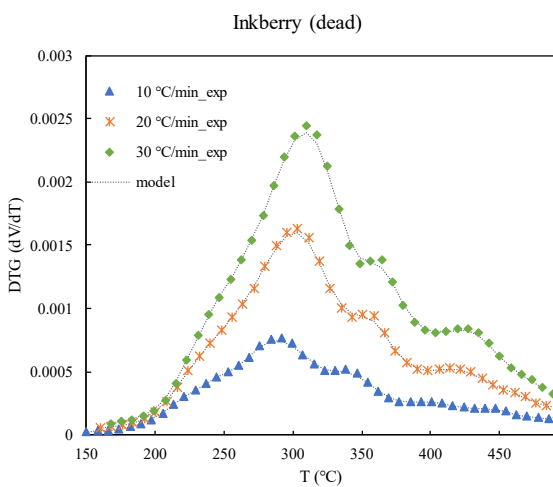
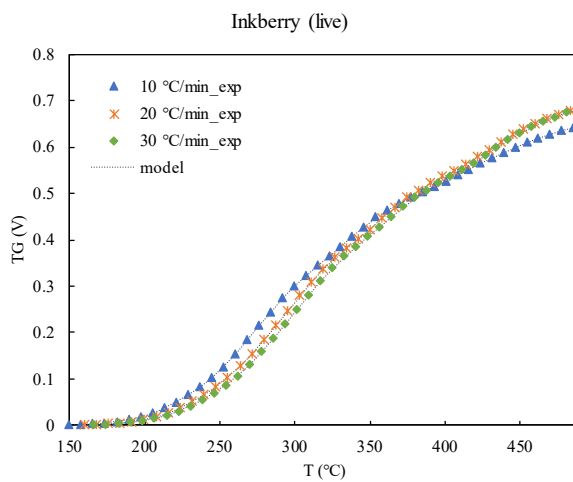
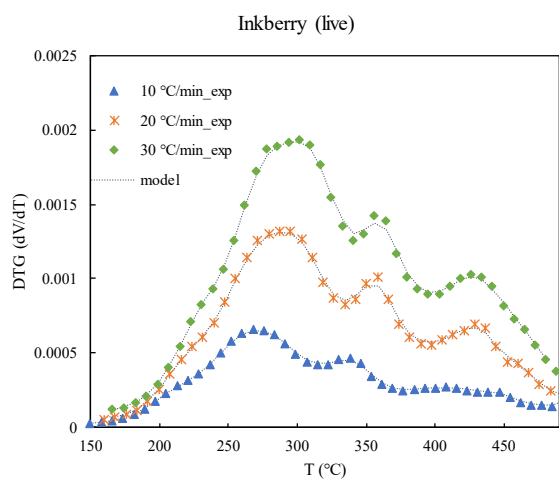
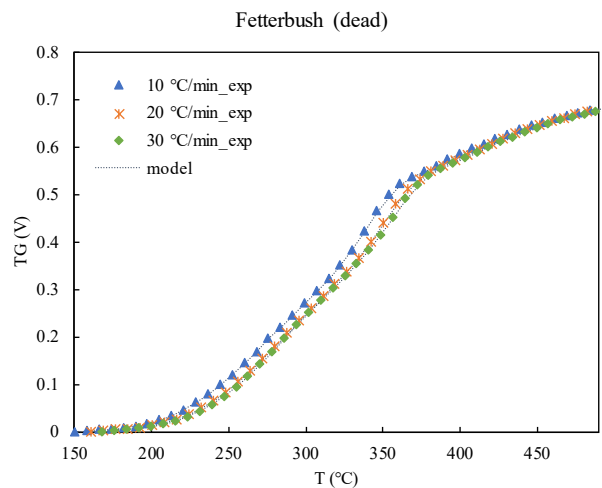
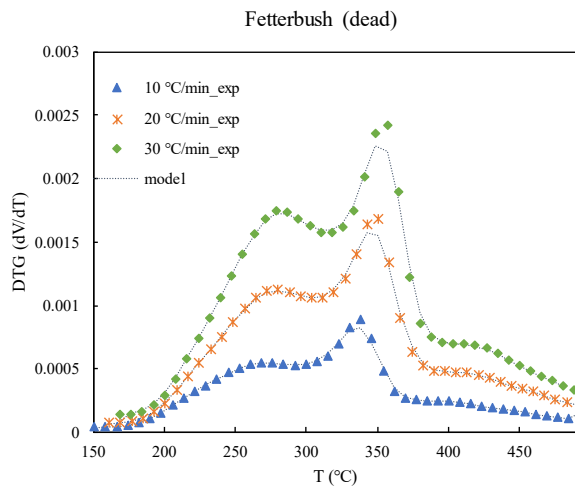
Figure G-1: Comparison of best-fit single-reaction DAEM model (dash lines) with TGA and DTG data (points) for all plant species at three heating rates of 10, 20 and 30 $^{\circ}\text{C min}^{-1}$.

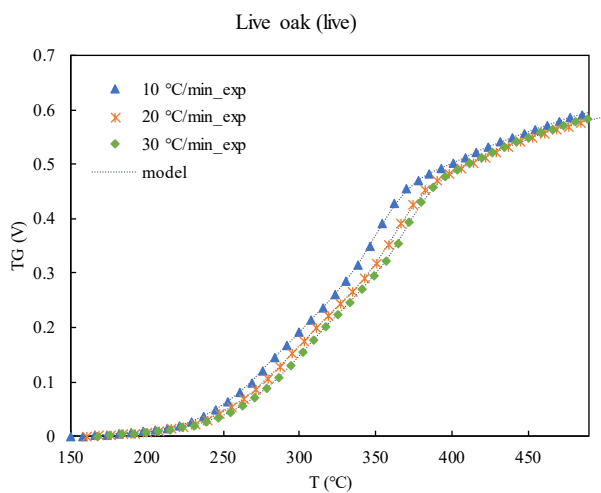
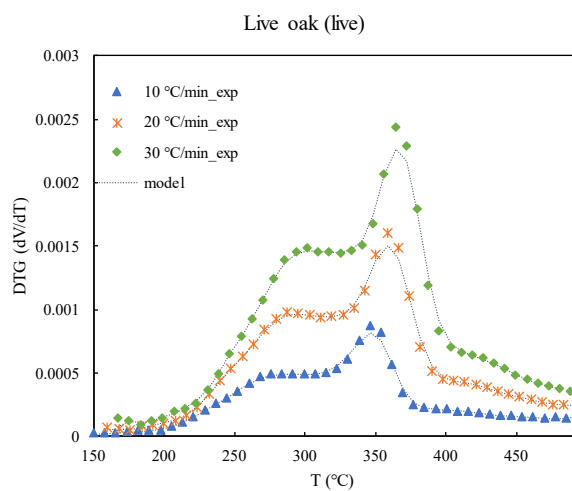
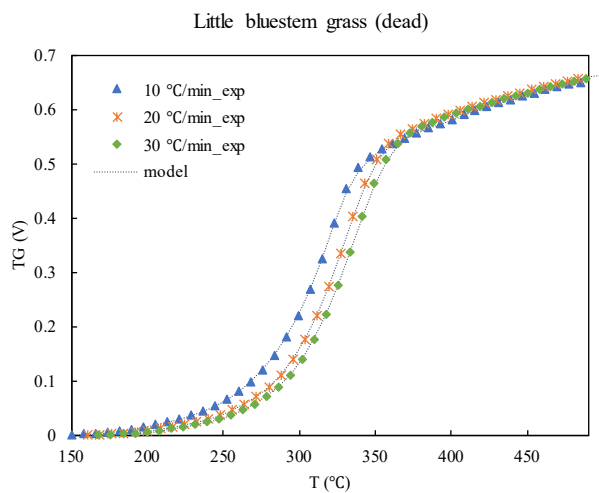
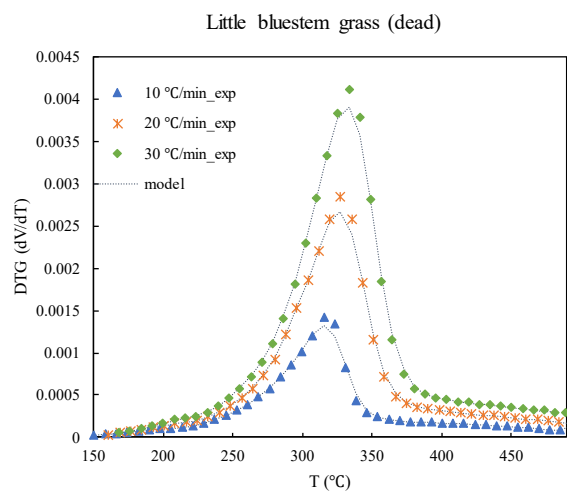
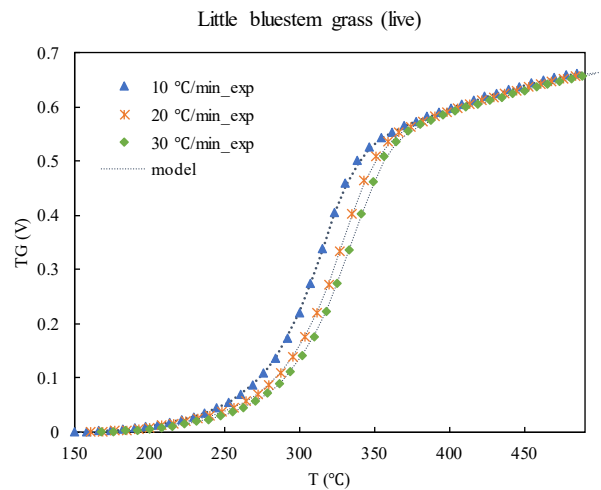
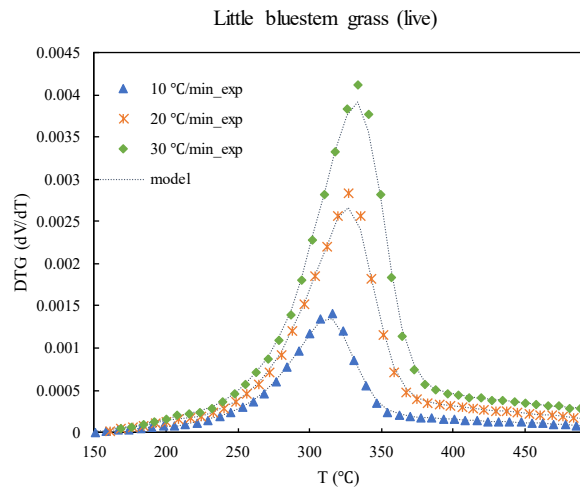
APPENDIX H. TG AND DTG CURVES RESULTED FROM THE MULTIPLE-REACTION DAEM MODEL

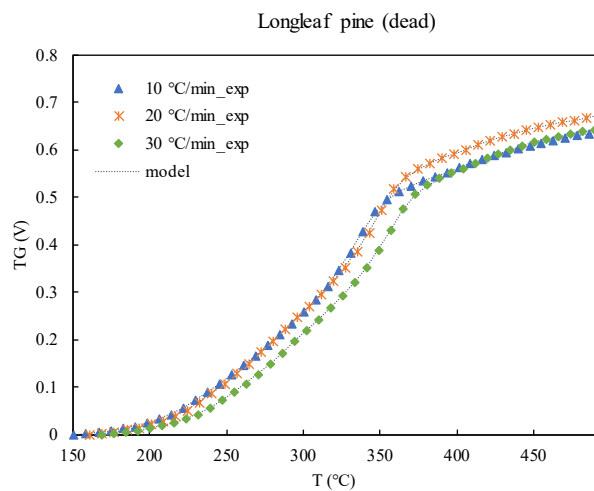
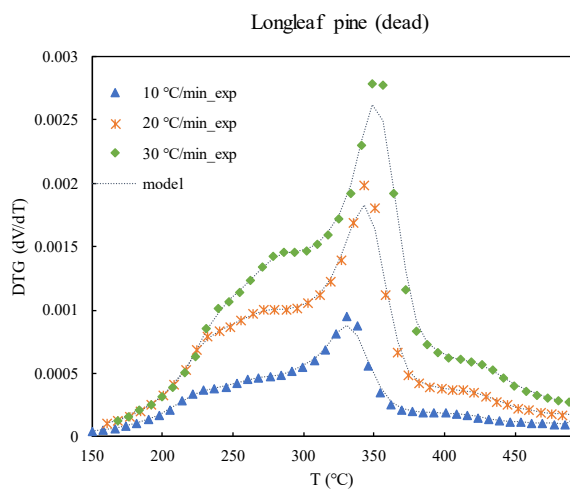
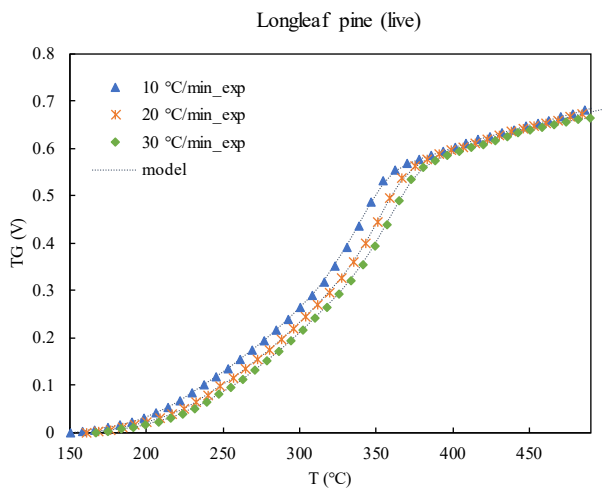
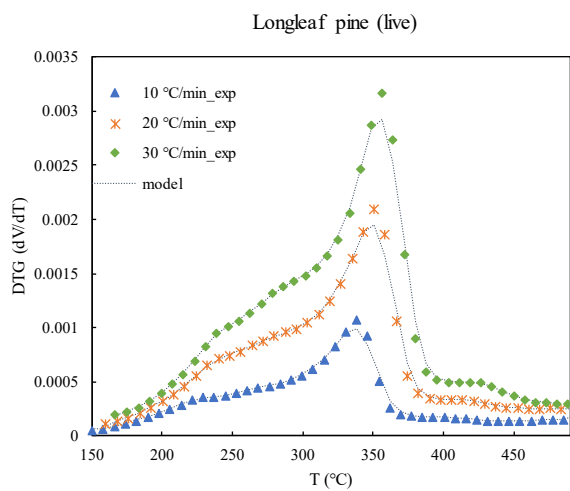
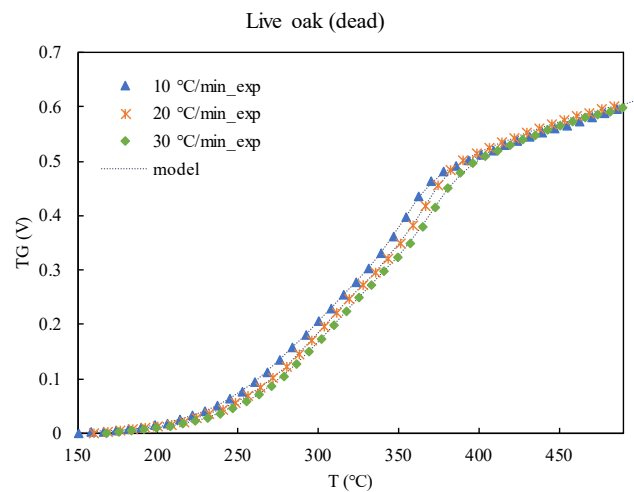
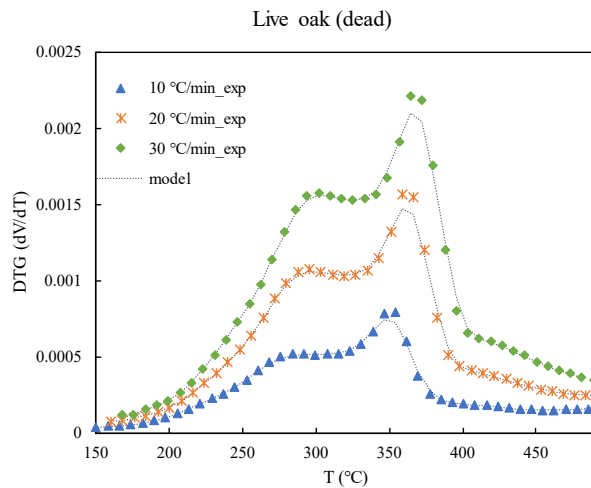
TG and DTG curves resulted from experimental data and the multiple-reaction DAEM model are presented in Figure H-1.

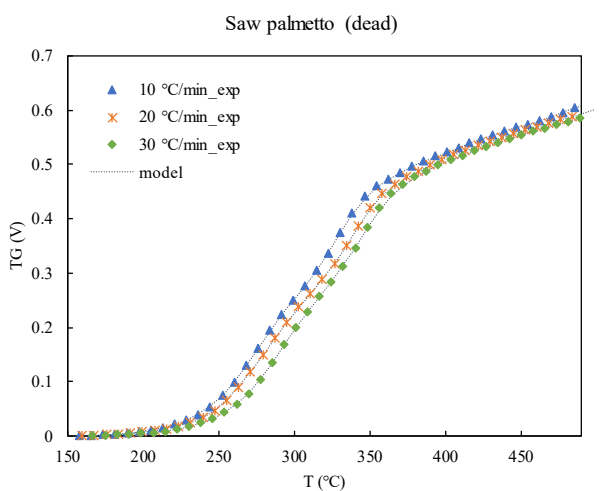
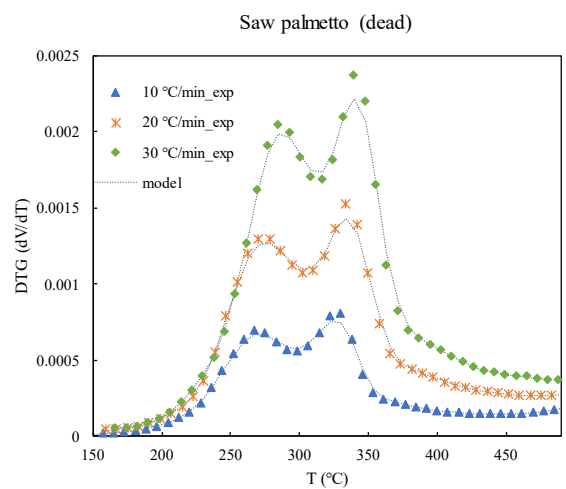
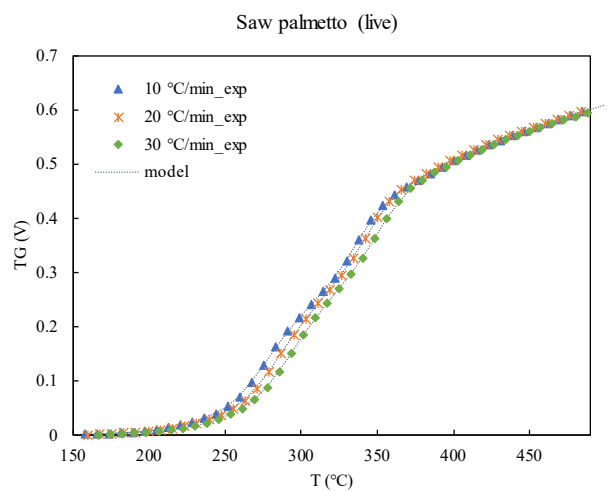
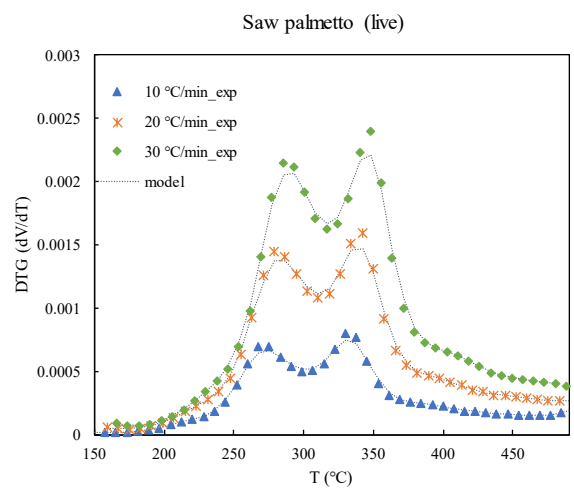
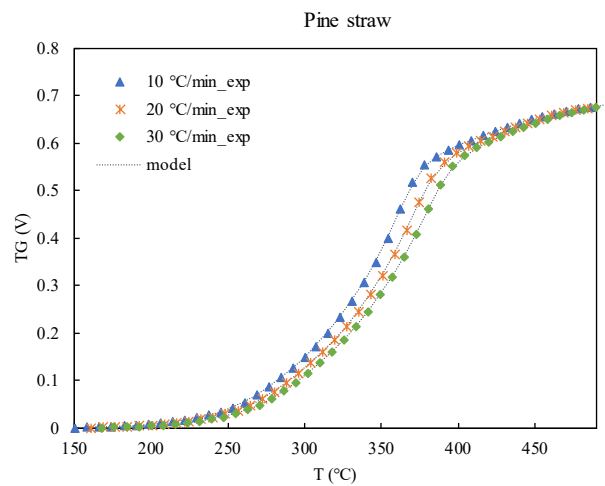
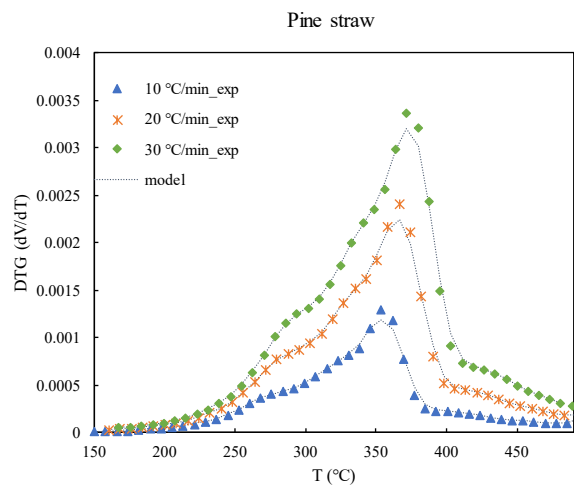


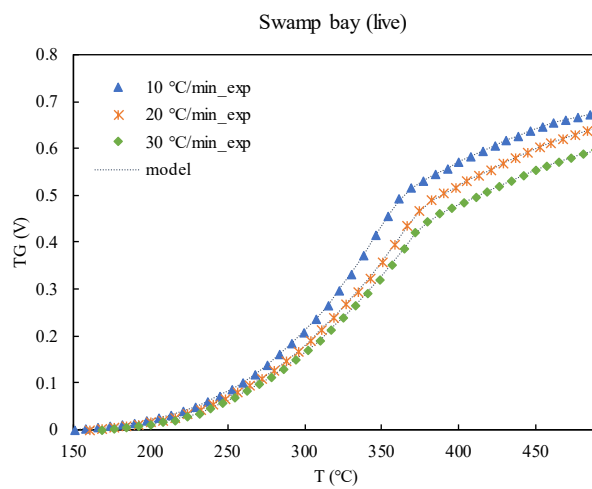
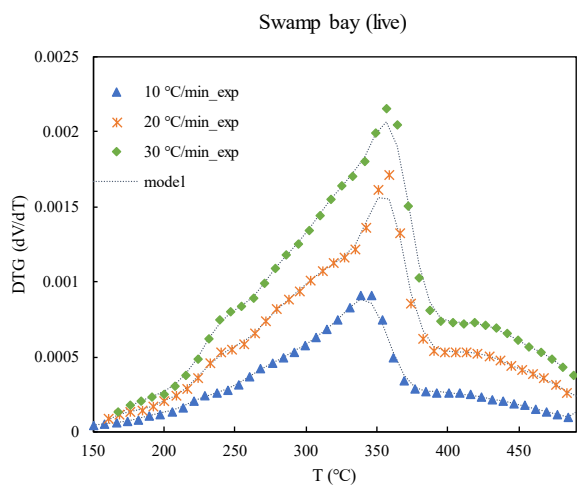
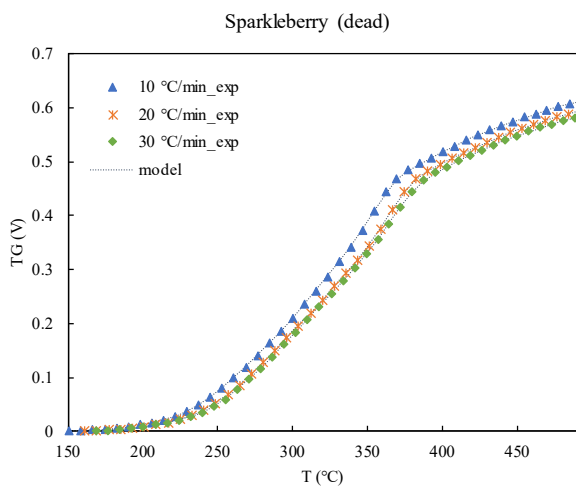
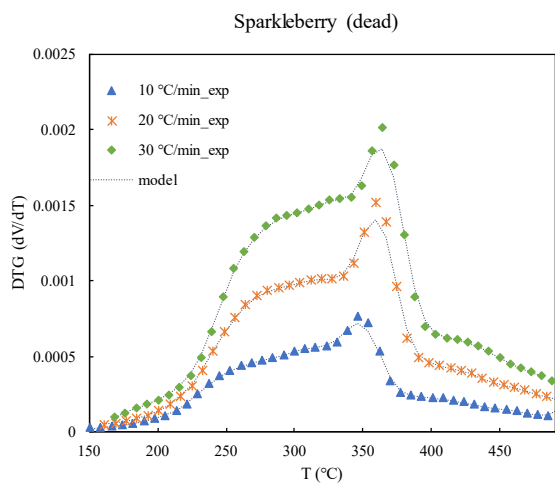
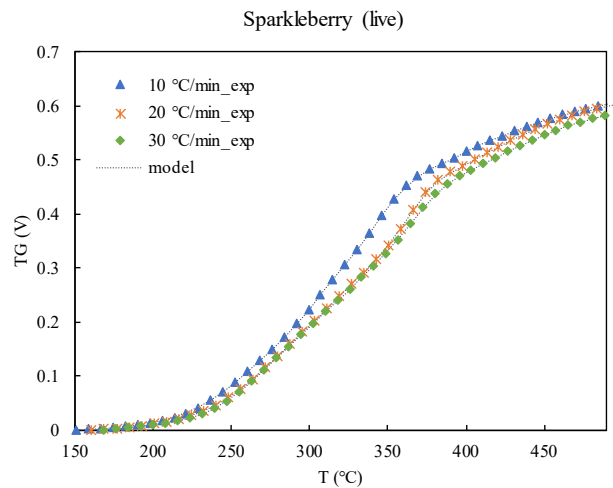
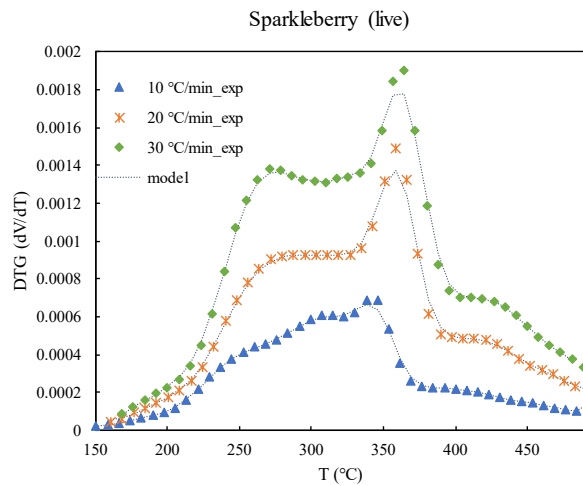


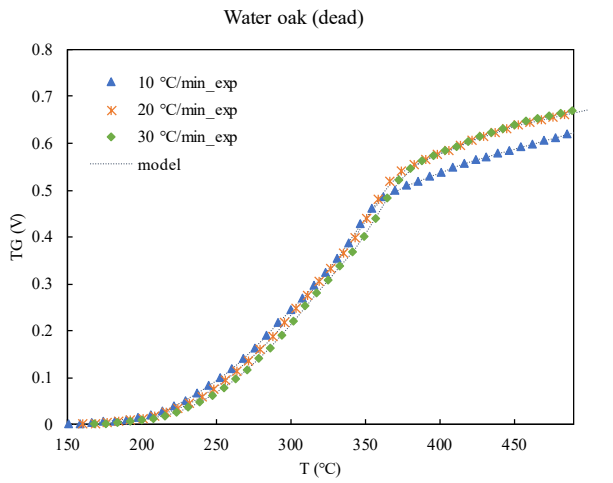
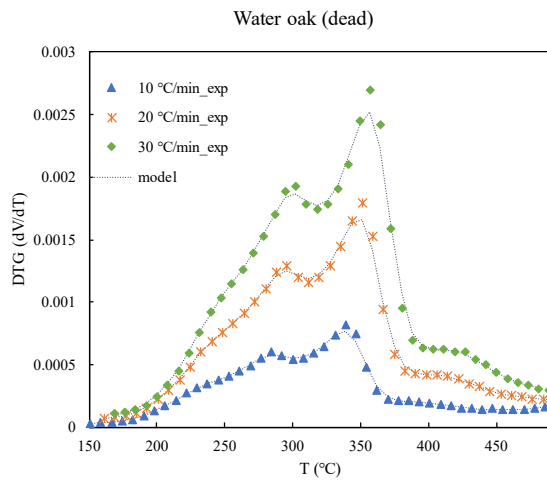
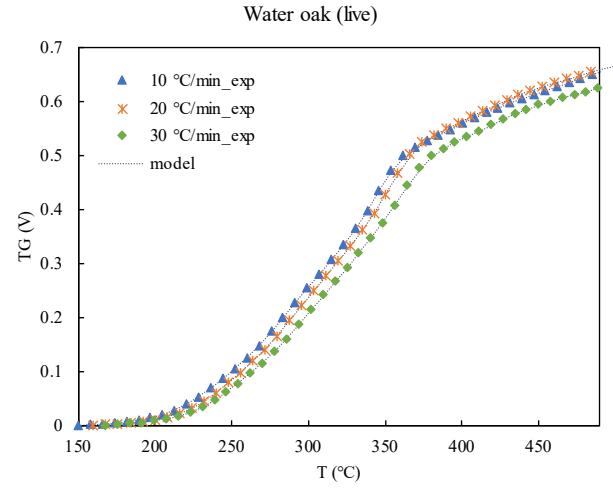
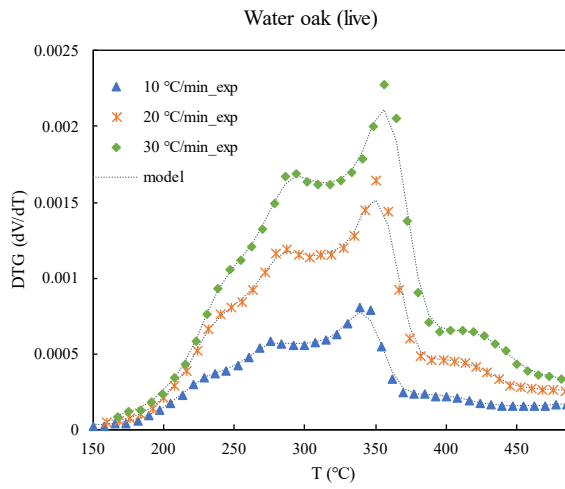
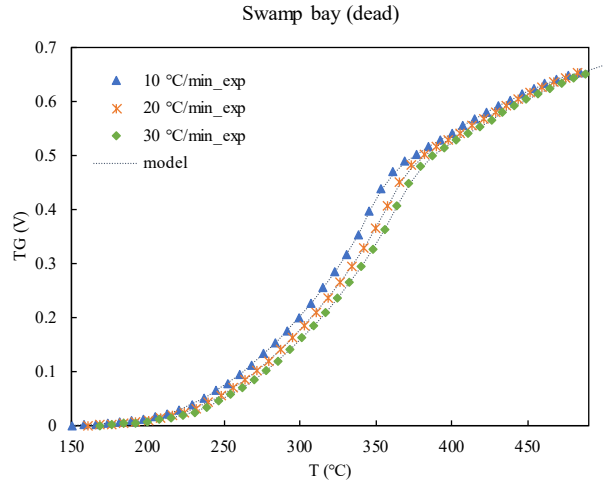
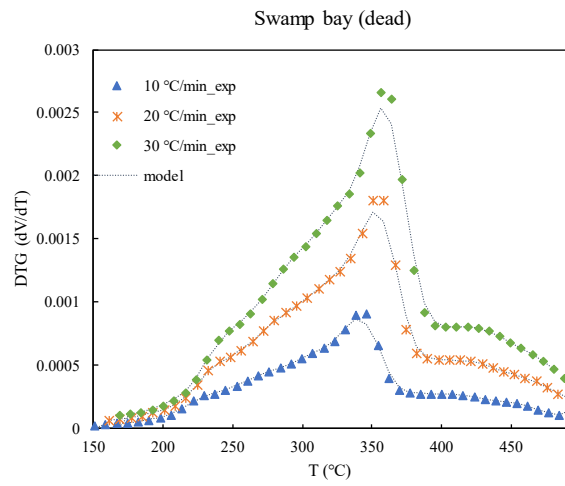


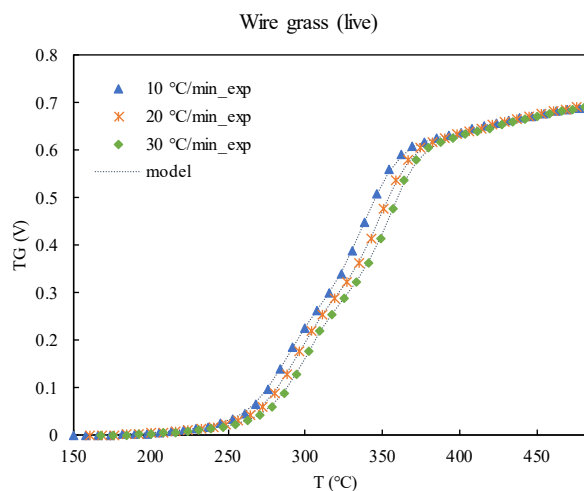
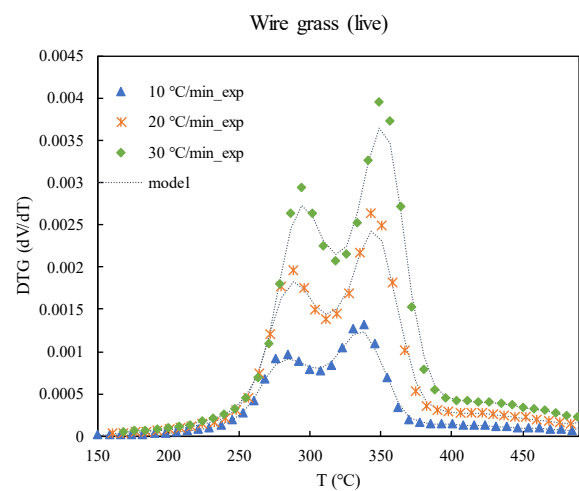
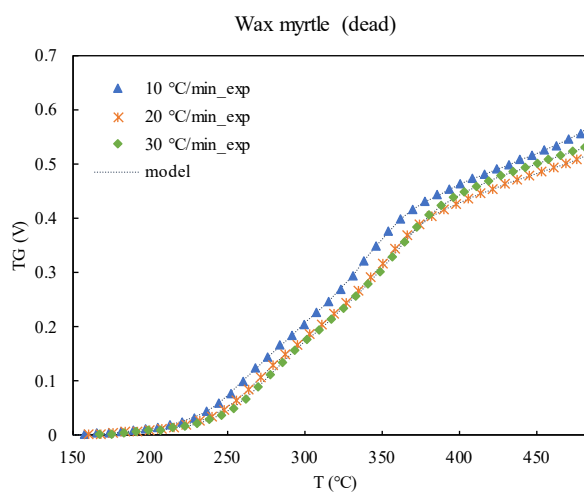
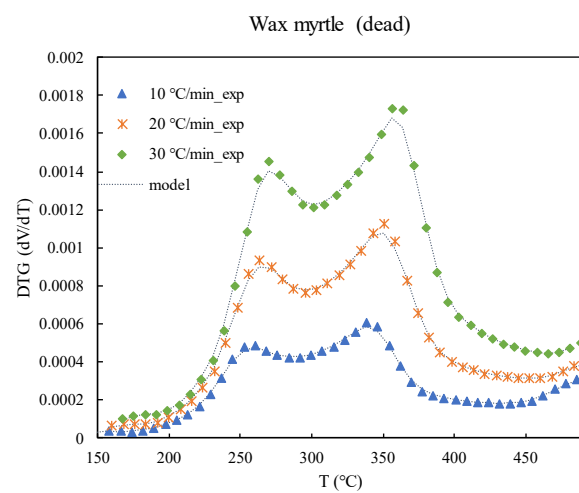
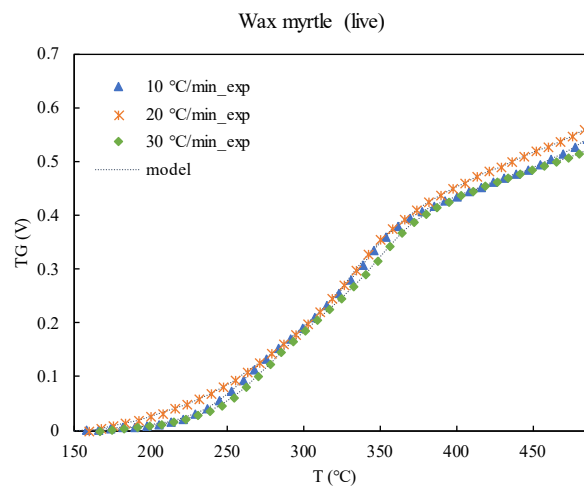
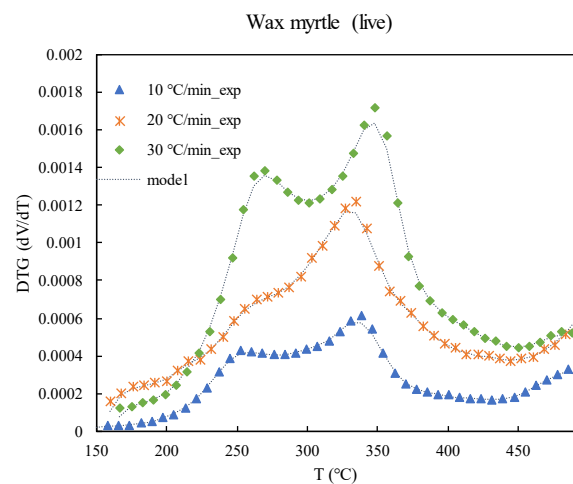












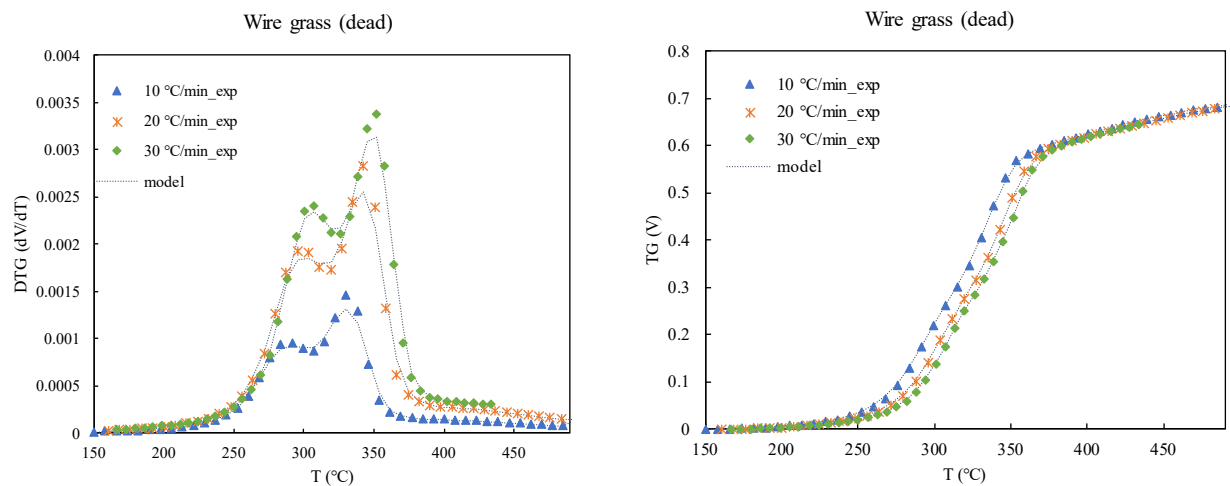


Figure H-1: Comparison of best-fit multiple-reaction DAEM model (dash lines) with TGA and DTG data (points) for all plant species at three heating rates of 10, 20 and 30 °C min⁻¹.

APPENDIX I. RMSE AND MAE VALUES FOR ALL MODEL FITTING METHODS

In this section, the RMSE and MAE values corresponding to the DTG curves at heating rate of 30 °C min⁻¹ for all live and dead plant species are presented in Table I-1, and Table I-2, respectively.

Table I-1: The RMSE and MAE values corresponding to the DTG curves for live plant species at heating rate of 30 °C min⁻¹

plant	Simple One-Step Model		Single-Reaction DAEM Model		Multiple-Reaction DAEM Model	
	RMSE	MAE	RMSE	MAE	RMSE	MAE
Darrow's blueberry	6.2×10^{-4}	5.1×10^{-4}	4.1×10^{-4}	3.3×10^{-4}	5.3×10^{-5}	4.9×10^{-5}
Dwarf palmetto	5.0×10^{-4}	4.0×10^{-4}	2.5×10^{-4}	2.1×10^{-4}	4.7×10^{-5}	4.4×10^{-5}
Fetterbush	4.2×10^{-4}	3.3×10^{-4}	2.8×10^{-4}	2.5×10^{-4}	3.6×10^{-5}	3.4×10^{-5}
Inkberry	4.7×10^{-4}	4.2×10^{-4}	2.6×10^{-4}	2.2×10^{-4}	3.4×10^{-5}	3.0×10^{-5}
Little bluestem	5.2×10^{-4}	4.6×10^{-4}	2.5×10^{-4}	2.1×10^{-4}	5.9×10^{-5}	5.5×10^{-5}
Live oak	3.5×10^{-4}	2.9×10^{-4}	2.3×10^{-4}	1.8×10^{-4}	4.4×10^{-5}	4.0×10^{-5}
Longleaf pine foliage	4.1×10^{-4}	3.4×10^{-4}	3.0×10^{-4}	2.1×10^{-4}	5.9×10^{-5}	5.5×10^{-5}
Saw palmetto	4.8×10^{-4}	3.7×10^{-4}	2.9×10^{-4}	2.5×10^{-4}	4.8×10^{-5}	4.0×10^{-5}
Sparkleberry	3.7×10^{-4}	3.1×10^{-4}	1.9×10^{-4}	1.7×10^{-4}	3.4×10^{-5}	3.0×10^{-5}
Swamp bay	3.9×10^{-4}	2.9×10^{-4}	2.4×10^{-4}	1.6×10^{-4}	3.8×10^{-5}	3.3×10^{-5}
Water oak	3.9×10^{-4}	3.2×10^{-4}	2.3×10^{-4}	1.8×10^{-4}	4.6×10^{-5}	4.4×10^{-5}
Wax myrtle	3.8×10^{-4}	3.2×10^{-4}	2.7×10^{-4}	2.1×10^{-4}	2.3×10^{-5}	1.6×10^{-5}
Wiregrass	6.4×10^{-4}	4.3×10^{-4}	4.5×10^{-4}	3.3×10^{-4}	9.6×10^{-5}	8.5×10^{-5}
Yaupon	4.2×10^{-4}	3.6×10^{-4}	3.1×10^{-4}	2.7×10^{-4}	4.8×10^{-5}	4.3×10^{-5}

Table I-2: The RMSE and MAE values corresponding to the DTG curves for dead plant species at heating rate of 30 °C min⁻¹

plant	Simple One-Step Model		Single-Reaction DAEM Model		Multiple-Reaction DAEM Model	
	RMSE	MAE	RMSE	MAE	RMSE	MAE
Darrow's blueberry	4.6×10^{-4}	3.7×10^{-4}	2.7×10^{-4}	2.4×10^{-4}	4.9×10^{-5}	4.6×10^{-5}
Dwarf palmetto	4.9×10^{-4}	3.8×10^{-4}	2.4×10^{-4}	2.0×10^{-4}	5.0×10^{-5}	4.7×10^{-5}
Fetterbush	4.5×10^{-4}	3.8×10^{-4}	2.9×10^{-4}	2.4×10^{-4}	4.9×10^{-5}	4.6×10^{-5}
Inkberry	5.1×10^{-4}	4.4×10^{-4}	2.8×10^{-4}	2.3×10^{-4}	3.3×10^{-5}	3.1×10^{-5}
Little bluestem	6.2×10^{-4}	5.6×10^{-4}	2.6×10^{-4}	2.2×10^{-4}	6.0×10^{-5}	5.5×10^{-5}
Live oak	3.4×10^{-4}	2.9×10^{-4}	2.2×10^{-4}	1.6×10^{-4}	3.7×10^{-5}	3.0×10^{-5}
Longleaf pine foliage	3.6×10^{-4}	3.0×10^{-4}	3.0×10^{-4}	2.7×10^{-4}	6.3×10^{-5}	5.8×10^{-5}
Pine straw	3.9×10^{-4}	2.9×10^{-4}	2.0×10^{-4}	1.6×10^{-4}	5.9×10^{-5}	5.0×10^{-5}
Saw palmetto	4.4×10^{-4}	4.1×10^{-4}	2.8×10^{-4}	2.4×10^{-4}	4.2×10^{-5}	3.9×10^{-5}
Sparkleberry	3.6×10^{-4}	3.0×10^{-4}	2.2×10^{-4}	1.9×10^{-4}	3.5×10^{-5}	3.0×10^{-5}
Swamp bay	4.1×10^{-4}	3.8×10^{-4}	2.1×10^{-4}	1.8×10^{-4}	5.1×10^{-5}	4.6×10^{-5}
Water oak	3.9×10^{-4}	3.5×10^{-4}	3.1×10^{-4}	2.6×10^{-4}	5.5×10^{-5}	5.0×10^{-5}
Wax myrtle	3.5×10^{-4}	2.8×10^{-4}	2.3×10^{-4}	2.0×10^{-4}	2.3×10^{-5}	1.9×10^{-5}
Wiregrass	4.2×10^{-4}	3.9×10^{-4}	3.2×10^{-4}	2.7×10^{-4}	6.6×10^{-5}	5.8×10^{-5}
Yaupon	4.3×10^{-4}	3.8×10^{-4}	3.0×10^{-4}	2.8×10^{-4}	4.7×10^{-5}	4.2×10^{-5}